



HAL
open science

Experimental determination of F partitioning between fluid and hydrous minerals in subduction zones

Jia Wu

► **To cite this version:**

Jia Wu. Experimental determination of F partitioning between fluid and hydrous minerals in subduction zones. Earth Sciences. Université Blaise Pascal - Clermont-Ferrand II, 2013. English. NNT : 2013CLF22351 . tel-01555846

HAL Id: tel-01555846

<https://theses.hal.science/tel-01555846>

Submitted on 4 Jul 2017

HAL is a multi-disciplinary open access archive for the deposit and dissemination of scientific research documents, whether they are published or not. The documents may come from teaching and research institutions in France or abroad, or from public or private research centers.

L'archive ouverte pluridisciplinaire **HAL**, est destinée au dépôt et à la diffusion de documents scientifiques de niveau recherche, publiés ou non, émanant des établissements d'enseignement et de recherche français ou étrangers, des laboratoires publics ou privés.

N_d'Ordre : D.U. 2351

UNIVERSITÉ BLAISE PASCAL – CLERMONT–FERRAND II

(U. F. R. Scientifique et Technique)

ÉCOLE DOCTORALE DES SCIENCES FONDAMENTALES

N °747

THÈSE

Présentée pour obtenir le grade de

DOCTEUR D'UNIVERSITÉ

Spécialité Pétrologie expérimentale – Géochimie

par

Jia WU

**Experimental determination of F partitioning between fluid and
hydrous minerals in subduction zones**

Soutenue publiquement le 30 April 2013, devant la commission d'examen :

Carmen Sanchez-Valle	Professor, ETH Zurich, Switzerland	Rapporteur
Hans Keppler	Professor, BGI, Bayreuth, Germany	Rapporteur
Didier Laporte	Directeur de Recherche, LMV, Clermont-Ferrand	Président
Fabrice Brunet	Directeur de Recherche, CNRS-ISTerre, Grenoble	Examineur
Etienne Médard	Maître de Conférence, LMV, Clermont-Ferrand	Examineur
Kenneth T. Koga	Maître de Conférence, LMV, Clermont-Ferrand	Directeur de thèse

N_d'Ordre : D.U. 2351

UNIVERSITÉ BLAISE PASCAL – CLERMONT–FERRAND II

(U. F. R. Scientifique et Technique)

ÉCOLE DOCTORALE DES SCIENCES FONDAMENTALES

N °747

THÈSE

Présentée pour obtenir le grade de

DOCTEUR D'UNIVERSITÉ

Spécialité Pétrologie expérimentale – Géochimie

par

Jia WU

**Experimental determination of F partitioning between fluid and
hydrous minerals in subduction zones**

Soutenue publiquement le 30 April 2013, devant la commission d'examen :

Carmen Sanchez-Valle	Professor, ETH Zurich, Switzerland	Rapporteur
Hans Keppler	Professor, BGI, Bayreuth, Germany	Rapporteur
Didier Laporte	Directeur de Recherche, LMV, Clermont-Ferrand	Président
Fabrice Brunet	Directeur de Recherche, CNRS-ISTerre, Grenoble	Examineur
Etienne Médard	Maître de Conférence, LMV, Clermont-Ferrand	Examineur
Kenneth T. Koga	Maître de Conférence, LMV, Clermont-Ferrand	Directeur de thèse

Abstract

Mechanisms of volatile transfer from subducting slab to the melting region beneath arc volcanoes are probably the least understood process of arc magma genesis. Fluorine, which suffers minimum degassing in arc primitive melt inclusions, retains the information about the role of volatiles during magma genesis at depth. Experimentally determined solubility of F in aqueous fluid, and partition coefficients of F between fluid and minerals provide first order geochemical constraints about the volatile-transporting agent.

My thesis experimentally determined F solubility in fluid and its partition coefficients among several phases. The systems are in equilibrium with hornblende and a humite group mineral (some contain melt or pyroxene) at 1 – 2 GPa, from 770 to 1047 °C, or equilibrium with hydrogrossular, pyroxene and norbergite or chondrodite at 2.5 – 3 GPa and 877 °C. The experiments were conducted with piston cylinder and cold sealing technique. The oxygen fugacity conditions were controlled by NNO buffer, while some were unbuffered. The fluids were extracted into volumetric flasks, and their compositions were determined by mass balance calculations. Moreover, the consistency was verified by HPLC for fluorine ion, and ICP-MS or ICP-AES for major cations of the quenched fluids.

In 1 GPa experiments, the quench phases are so rare that the majority of the fluid compositions from direct analyses are consistent with mass balance results in their uncertainties. Moreover, my mass balance procedure takes into account all the measurements errors, which leads to large uncertainties on fluid compositions. The consistency demonstrates that most of fluorine after annealing in the capsule is present as fluorine ion. Furthermore, increases of the masses of starting materials, fluid proportions and analytical precisions will improve the uncertainties performances.

$D_F^{Fl/Hb}$ can be represented by a single value 0.135 ± 0.036 , which is independent of temperature, bulk composition and buffer conditions at 1 GPa. D_F between fluid and humite group minerals is much less. X_F of hornblende and norbergite decrease from 1 to 2 GPa, while F partitioning between them doesn't change much. It indicates that F partitioning between

fluid and minerals increases. Moreover, F concentrations in norbergite between NNO buffered and unbuffered experiments are significantly different. Meanwhile, Fe concentration variations of norbergite indicate that unbuffered experiments have higher oxygen fugacity than the NNO buffered ones. According to high temperature improves the free radical exchange reactions, $H_2O + 0.5O_2 \rightleftharpoons 2OH$. It indicates that both water fugacity and oxygen fugacity contribute to OH fugacity in fluid. I developed a simple model in which X_F in humite group minerals are correlated to the ratio between F and OH. It is successfully applied to estimate the F concentration in the fluid, which co-exists with clinohumite, using X_F value.

With the knowledge of my study, a new constraint can be framed on slab flux. The average F concentration in the fluid is 2700 ppm for F-rich experiments and it constrains the maximum amount of F carried by fluid in the presence of amphibole. Using partition coefficient of F to estimate F abundance in subducting slab, one can conclude that the increase of F concentration in the subarc mantle by fluid, in equilibrium with hornblende, to be less than 5 ppm. Significant F enrichments found in arc lavas cannot be derived from aqueous fluid of subducting slab in the presence of amphibole. Therefore, this result highlights the role either 1) slab melt, 2) fluid in equilibrium with eclogite, or perhaps 3) supercritical fluid for the element transfer from slab to mantle wedge.

Keywords: subduction zone, fluorine, solubility, high temperature and high pressure experiment, piston cylinder, oxygen fugacity

Résumé

Les mécanismes de transfert des éléments volatils depuis la plaque plongeante jusqu'au coin mantellique, en dessous des volcans d'arcs, sont un des problèmes fondamentaux, et probablement un des moins bien compris, liés à la genèse des magmas d'arc. Le fluor (F), qui est peu dégazé dans les inclusions primaires des magmas d'arc, peut renseigner sur le rôle des volatiles lors de la genèse des magmas en profondeur. La détermination de la solubilité du F dans les fluides aqueux et du coefficient de partage du F entre un fluide et des minéraux permet dans un premier temps de contraindre l'agent de transport des volatiles lors de la subduction.

Ma thèse en pétrologie expérimentale a permis de déterminer la solubilité du F dans les fluides et son coefficient de partage entre divers phases. Ces systèmes sont à l'équilibre avec des minéraux tel que les hornblendes ou les humites pour des pressions de 1 – 2 GPa et des températures de 770 – 1047 °C. Les expériences ont été menées par piston cylindre et une technique de «soudure à froid ». La fugacité en oxygène a été contrôlée soit par le tampon NNO soit sans tampon. Les fluides ont été extraits dans des fioles jaugées puis leur composition a été déterminée par des calculs de bilan de masse. De plus, le bon accord de ces résultats a été vérifié par HPLC pour les ions fluor et ICP-MS ou ICP-AES pour les cations majeurs des liquides trempés.

Dans les expériences à 1GPa, les phases trempées sont rares et la composition du fluide par analyse direct est en bon accord avec les résultats des bilans de masse. En effet, les résultats obtenus par bilan de masse prennent en compte toutes les incertitudes sur chaque mesure ce qui entraîne des larges barres d'erreurs finales sur les compositions des fluides. Nos résultats montrent que la majeure partie du fluor après chauffage de la capsule est présent sous forme d'ion fluor. De plus, l'augmentation de la quantité de matériaux de départ et de fluide, ainsi qu'une meilleure sensibilité d'analyse permettrait d'améliorer ces résultats.

Le $D_F^{Fl/Hb}$ peut être représenté par une valeur de 0.135 ± 0.036 , qui est indépendante de la température, de la composition en roche totale et de la fugacité en oxygène. Le D_F entre le fluide et les humites est un peu plus bas. Le X_F de la hornblende et la norbergite décroît

depuis 1 à 2 GPa, alors que le partage du F ne change que peu. Ceci indique que le partage du F entre le fluide et les minéraux augmente. De plus, les concentrations en F dans la norbergite avec le tampon NNO ou sans tampon est différent. D'autre part, les variations de concentration en fer de la norbergite indiquent que les expériences sans tampon ont des fugacités en oxygène plus élevées que celles menées avec tampon NNO. Lors du passage à des températures plus hautes la réaction de substitution $H_2O + 0.5O_2 \rightleftharpoons 2OH$ indique que la fugacité en eau et en oxygène influence la fugacité en OH du fluide. J'ai développé un modèle simple pour que le X_F dans les humites soit corrélé avec le F et le OH. En utilisant les valeurs de X_F , ceci a permis d'estimer la concentration en F dans le fluide qui coexiste avec les clinohumite.

Mon étude apporte de nouvelles contraintes sur le fluide sortant de la plaque plongeante en subduction. La concentration maximum en fluor de ce fluide est de 2700 ppm pour des expériences riches en F et en présence d'amphibole. En utilisant le coefficient de partage du F pour estimer l'abondance de F dans la plaque plongeante, on peut déduire que l'augmentation de la concentration de F dans le coin mantellique lié à la circulation de fluide, en équilibre avec la hornblende, est de moins de 5 ppm. Ainsi, les enrichissements significatifs trouvés dans les magmas d'arc ne peuvent pas résulter de la contamination du coin mantellique par des fluides aqueux en présence d'amphibole. Ce résultat implique soit 1) une fusion de la plaque plongeante, soit 2) l'existence d'un fluide en équilibre avec des éclogites, ou soit 3) l'existence de fluides supercritiques pour transférer les éléments vers le coin mantellique.

Mots clés: zone de subduction, fluor, solubilité expérience haute température et haute pression, piston cylindre, fugacité en oxygène.

Acknowledgements

The French spring is magnificent and gratifying. And what is even more gratifying is that I have finally completed my Ph.D. dissertation, entitled *Experimental determination of F partitioning between fluid and hydrous minerals in subduction zone*, in the midst of the magnificent spring in Clermont-Ferrand.

This thesis is a summary of my project in the latest four years with the guidance of my advisor Kenneth T. Koga, from background knowledge introduction, references searches, to conducting experiments, and dealing with the results. It contains my comprehension on the high temperature and high pressure experimental methods and my exploration of the volatile element F transporting in subduction zone, and the ideas and efforts of my advisor Ken, as well as the helps from many teachers, colleagues, classmates in Universite Blaise Pascal, and Laboratoire Magmas et Volcans.

This project led me to the subject of the unclear process in the upper mantle. The strong curiousness inspires me to study and explore the unknown area in earth sciences. According to the time constraint, some recent experimental samples have not been analyzed yet. They are not reported in this thesis.

During these four years, the laboratory supervisors, technical assistants, and colleagues helped me overcome the difficulties of the lingual communication, living, learning, and working in Clermont-Ferrand from the class, access to information, experiments. Thus, I can complete the project research and thesis writing.

I will never forget the period that I lived in France, although it is hard, and sometimes painful. However, this experience also promoted myself to mature as an independent human being. I have acquired a lot, not only knowledge and skills on the earth science, but also

friendship with various people. I sincerely thank everyone for their care and help, which supported me to go through this period.

First of all thank my advisor Ken. I can clearly recall the scene that he met me at the train station. Ken supplied me a platform to study earth sciences. On the academic ideas, he gave me the profound enlightenment. For the experimental techniques, he guided me with patience and carefulness. Moreover, Ken and Estelle helped me in every possible aspect as parents in the everyday life. All of those provided excellent conditions for my research. Ken is a cheerful, open-minded advisor with rigorous scholarship. This is my pleasure to encounter this good advisor.

I am grateful for Hans Kepler and Carmen Sanchez-Valle as reporters to assess my thesis before my thesis defense, as well as Fabrice Brunet, Didier Laporte, Etienne Medard, and Ken Koga to give valuable comments for not only improving my manuscript, but also developing my view of corresponding subjects.

I would like to thank Jean-Luc Devidal (LMV) for his help with the electron microprobe analysis, and Agnès Michel and Caroline Gorge (IPGP) for their help with the high pressure liquid chromatography analysis, as well as Jean-Marc Hénot for his guide on SEM operation. I also acknowledge advices on HPLC from Aurelie Colomb during the early stage of this study, and a mass-balance calculation suggestion for fluid compositions from John Ayers. I also would like to thank Franck Pointud and Fabrice Doré for their work on the piston-cylinder apparatus, and Jean-Louis Fruquiere for disciplined machining on the piston-cylinder assemblages. I appreciate Mhammed Benbakkar (LMV) for ICP-AES measurements, and Frederic Candaudap (Geosciences Environnement Toulouse) for ICP-MS analyses on my fluid samples. Thank Jean-Luc Piro for providing suggestions on fluid analyses with ICP-MS, as well as Eric Brut for helping me to test the circuit design of the combination of an ultrasonic generator and a piston cylinder.

I also extend my gratitude to Nobu. He spent a lot of efforts on SIMS setting for my

volatile element analyses in Woods Hole, US, and taught me to mount my crystals in indium. It is a pity that these series experiments did not finish, and no results can be shown in my thesis, but I still appreciate this ion-probe experience under his guidance.

Thanks Ken, Didier, Nicolas, Etienne, Cécilia, Greg, Pierre, and Manon for sharing many comments and ideas on experiments with piston-cylinder. Thank my master advisor Zheng Haifei in Peking University, and Chen Yang in U.S. for the discussions on some new progress or basic knowledge of geology research via Email. Thank Baptiste Debret for translating my thesis abstract into French, as well as Ken and Estelle for revising and polishing the expressions. I am appreciative for Chantal Bosq, Ivan Vlastelic, Hanika Rizo Garza, Oscar Laurent, Gabrielle Menard, Nina Bellot-Coignus to get the deionized water from the clean chemical lab.

I acknowledge the colleagues Nicolas Cluzel, Marion Le Voyer, Sarah, Ann ï, Thomas, Yann, and Chen Yang, as well as Zhao Zhiyong, Han Junnan, Liang Shichao, Guo Huanxiu and other Chinese friends. I have been able to solve the inconveniences by the French communication in my daily life, with their selfless help. I appreciate my college classmate Zhang Keya, Yang Rong, Liang Hailin, Tian Feng (F), Tian Feng (M), Zhou Minghui, and others gave me some suggestions from their specialized chemistry subject. Particularly I am indebted to Zhang Keya for proofreading and polishing my dissertation draft on instrumental analysis principle.

At last, I felicitate myself that I was born in the peaceful period of China and France. It is possible for me to receive a good education, instead of the hard period that my grandparents and parents suffered during their studies. I will dedicate myself to the social progress and peaceful development with my skills and knowledge, and requite my parents.

The cenarios in France, Clermont-Ferrand, Universite Blaise Pascal, and Laboratoire Magmas et Volcans are important milestones in my life. In the future, wherever I go, they will always remain in my memory.

Contents

Abstract	i
R ésum é.....	iii
Acknowledgements	v
Contents.....	ix
Preface	1
1. Introduction	5
1.1 Subduction zone	6
1.2 Magma Genesis	8
1.3 Volatile Elements.....	12
1.4 Main Aim of Thesis	14
2. Methods.....	17
2.1 Starting Materials	17
2.1.1 Expected Minerals in Experiments.....	17
2.1.2 First Order Investigation from Database	18
2.1.3 Starting Powder Compositions	21
2.2 Experimental Strategy	23
2.2.1 Sealing technique.....	23
2.2.2 Capsule Materials and Buffers	24
2.2.3 High Pressure Apparatus – Piston Cylinder	25
2.2.3.1 Dimension of Assemblies	27
2.2.3.2 Temperature Calibration	27
2.2.3.3 Heating and Pressurization	29
2.2.4 Experimental Conditions	30
2.3 Post-quench Fluid Extraction	33
2.3.1 Aim of the Extraction of Fluid.....	33
2.3.2 Preparation for Opening Capsules.....	33

Contents

2.3.3 Two Ways for Opening	34
2.3.3.1 From the Top	35
2.3.3.2 From the Vertical Side	35
2.3.3.3 Comparisons of these two methods	36
2.3.4 Transfer the Fluid into Volumetric Flasks	37
2.4 Electron Microprobe Analyses for Solid Phases	37
2.4.1 Samples Preparation	37
2.4.2 Principle of the analysis.....	38
2.4.3 Analytical Parameters.....	39
2.4.4 Stoichiometry Calculations	40
2.4.4.1 Hornblende	40
2.4.4.2 Hydrogrossular	41
2.4.4.3 Spinel.....	41
2.5 Analytical Technique for Solutions	42
2.5.1 Potential Candidates Technique.....	42
2.5.2 High Performance Liquid Chromatography	44
2.5.2.1 HPLC Principle and Operation.....	44
2.5.2.2 Tests on HPLC Analysis.....	45
2.5.2.3 Current Setting for HPLC Analysis.....	47
2.5.2.3.1 Basic Parameters.....	47
2.5.2.3.2 Calibrations.....	47
2.5.2.3.3 Measurements.....	48
2.5.3 ICP-AES	49
2.5.3.1 Principle.....	49
2.5.3.2 Calibration Parameters	51
2.5.4 ICP-MS.....	51
2.5.4.1 Components	52
2.5.4.2 Sample Preparation and Introduction	52
2.5.4.3 Elemental Analysis	53
2.5.4.4 Analytical Procedure	54

2.6 Mass Balance Calculation	54
2.6.1 Strategies	54
2.6.2 Conservative Elements Set	56
2.6.3 Determination of Fluid Composition Uncertainties	57
3. Results	59
3.1 Phase Assembly and Texture Description.....	59
3.1.1 SP1 Experiments	59
3.1.2 SP2 Experiments	63
3.1.2.1 Experiments Under 1 GPa	64
3.1.2.2 Experiments at Higher Pressure	72
3.1.3 SP3 Series Experiments.....	74
3.1.4 SP4 Series Experiments.....	76
3.1.5 Excess Doped Experiments	78
3.2 Attainment of Equilibrium.....	80
3.3 Solid Phases Compositions.....	84
3.3.1 Hornblendes.....	84
3.3.2 Humite Group Minerals.....	89
3.3.2.1 Determination of Humite Minerals Species	89
3.3.2.2 Humite Minerals Species.....	90
3.3.3 Hydrogrossular	94
3.3.4 Nominally Anhydrous Minerals	97
3.3.4.1 Olivine	97
3.3.4.2 Pyroxene	98
3.3.4.3 Spinel.....	99
3.3.5 Melt	101
3.3.5.1 1-SP2-18 & 19 experiments	102
3.3.5.2 1-SP2-20 experiment	103
3.3.5.3 1-SP2-21 experiment	106
3.3.5.4 1-(SP1+MgF ₂) experiment	107
3.3.5.5 1-(SP2+Qtz) experiment.....	108

3.4 Fluid Compositions	109
3.4.1 Mass Balance Calculation	110
3.4.1.1 Traditional Method	110
3.4.1.1.1 Experiments without melt.....	110
3.4.1.1.2 Experiments with Melt	116
3.4.1.2 Some Confirmations	118
3.4.2 Direct Measurements.....	120
3.4.2.1 HPLC.....	121
3.4.2.2 ICP-AES	125
3.4.2.3 ICP-MS.....	125
3.5 Partition Coefficients of F and X_F	129
3.5.1 F Partitioning of Minerals	129
3.5.1.1 D_F between Hornblende and Humite Group Minerals.....	130
3.5.1.2 D_F between Hydrogrossular and Humite Group Minerals.....	132
3.5.2 D_F Between Fluid and Hydrous Minerals or Melt.....	133
3.5.3 D_F Between Hornblende and Hydrous Melt.....	136
4. Discussion	137
4.1 F Incorporation of Hydrous Minerals.....	137
4.1.1 Proportion of F in OH sites (X_F).....	137
4.1.1.1 X_F of Hornblende.....	138
4.1.1.2 X_F of Humite Group Minerals	139
4.1.1.2.1 X_F Comparison among Humite Group Minerals	139
4.1.1.2.2 Corrected X_F with TiO_2 Number by Stoichiometry	140
4.1.1.3 X_F at Higher Pressure (>1 GPa).....	141
4.1.2 Parameters Controlling F Incorporation.....	142
4.1.2.1 Oxygen Fugacity Effects on F Incorporation	143
4.1.2.2 Oxygen Fugacity during Annealing.....	146
4.1.3 Stability of Humite Group Minerals with F.....	149
4.2 Fluid Composition Comparison	152
4.2.1 Comparisons between Mass Balance and Direct Analysis.....	152

4.2.1.1 F Concentration Comparison	152
4.2.1.2 Major Elements Concentrations Comparisons	156
4.2.1.3 Indications of the Differences.....	160
4.2.2 Influences of Temperature and F concentration	161
4.2.2.1 Na ₂ O	161
4.2.2.2 SiO ₂	164
4.2.2.3 Al ₂ O ₃	167
4.2.2.4 MgO.....	170
4.2.2.5 CaO.....	173
4.2.2.6 FeO	175
4.2.3 Influences of Pressure.....	176
4.2.4 Summary	177
4.3 Fluorine Preferential Phase.....	179
4.3.1 Fluorine Incorporation of Minerals	180
4.3.1.1 D _F between Hornblende and Humite Group Minerals.....	180
4.3.1.2 D _F between Hydrogrossular and Humite Group Minerals.....	181
4.3.1.3 Additional Results	183
4.3.2 Fluorin Distribution in Minerals and Fluids	183
4.3.2.1 D _F between Fluid and Hornblende.....	184
4.3.2.2 D _F between Fluid and Humite Group Minerals	185
4.3.2.3 D _F between Fluid and Hydrogrossular.....	186
4.3.2.4 D _F between Fluid and Melt	186
4.3.3 Summary	187
4.4 F Transport Budget from Subducting Slab at Amphibolite Facies	187
4.4.1 F Saturation Constraint in Fluid	187
4.4.2 Constraint with X _F Model.....	188
4.4.2.1 X _F Model Suitability.....	189
4.4.2.2 Equilibrium with Clinohumite.....	193
4.4.3 Non-modal Melting Model.....	194
5. Technical Problems.....	199

Contents

5.1 Sealing Technique for High P - T Experiments	199
5.2 Crystal Growth	201
5.3 Advantages and Limitations of Mass Balance and Direct Analysis	202
5.3.1 Differences and Similarities of Fluid Components of Different Methods....	203
5.3.2 Limitations of Mass Balance	204
5.3.3 Post-Quench Procedure	205
5.3.4 Limitations of Direct Analytical Techniques	207
5.4 Standards for High F-bearing Minerals	209
6. Outlooks	211
6.1 Oxygen Fugacity In and Out of Capsules.....	211
6.2 F and Cl Partitioning between Other Minerals and Fluid.....	214
6.3 Improvements on Determination of Fluid Compositions	214
6.4 F Incorporation and Melt Compositions.....	215
References	217
Appendixes.....	227
Appendix I Student's t-test for Grouping D_F	227
Appendix II Expansion Coefficient of Pyrophyllite	229
Appendix III Original Data of ICP-MS Analyses	231

Preface

The plate tectonics revolutionized geology after it was founded in 1960s. It gave some elementary explanations on the distribution of earthquakes, mid-ocean ridges, deep-sea trenches, and mountain chains, and provided a basis to the theory of continental drift, which revealed a new page on the knowledge of the Earth interior structure. Meanwhile, more and more observations encouraged geologists to explore more detailed information on the behavior of the Earth lithosphere, with the technique developments of the space, analyses, and experiments.

Island arcs are the most active areas on the Earth. Subduction zone volcanisms and earthquakes always influence the human living directly. It is important to understand their derivations with investigations on the subduction zone structures and its evolutions. Indeed, they have attracted lots of interests from earth scientists in last few decades. To track the arc magma genesis source is one of the most difficult problems. Several models and hypotheses are created and developed, and influential improvements were made for almost each decade. However, because of the constraints of the current techniques, people cannot get the rock samples directly from the 100-km depth in a subduction zone. The observations from the lavas after eruptions in the volcanic front are the unique potential way.

Different from mid-oceanic basalt or oceanic island basalt, the composition of arc lavas are generally called calc-alkaline andesites. Their compositional differences (major, trace and volatile elements) indicate that some additional water-rich components, which move basaltic incompatible elements, were introduced into sub-arc mantle to involve with the magma genesis process. It is reasonable for scientists to consider these fluids are from the hydrous subducting slab, because the fluids are released from the dehydration process with the increase of pressure and temperature. This so-called “slab flux” transfer the chemical characteristic from slab to arc magma.

However, the nature, the composition, and the sources of this slab flux are ambiguous. There are three possibilities on its nature: aqueous fluids, melts, or supercritical fluids. And

for the sources, it may be derived from the sediments, the slab, or the hydrated metamorphosed phase in the mantle wedge. With traditional trace element behaviors, geochemists cannot solve these problems perfectly. With the developments of the micro-analytical techniques on trace and volatile elements measurements in melt inclusions, some volatile elements like F and Cl attract more interests. The F and Cl suffered less degassing and may retain the information before the entrapment of the melt inclusion. They probably reveal the magma sources as a new tracer (e.g. Le Voyer et al. 2010).

Several researches suggest that F is enriched from subducting slab to sub-arc mantle. To investigate a potential aspect of this process, I focus on the fluorine transport behaviors by aqueous fluids in subduction zones. Two other colleagues (Celia and Greg) focus on the aspect of transporting by silicate melt. The aim of this study is experimental determination of the partitioning of F between fluid and hydrous minerals, and to estimate F quantity transported by aqueous fluids. I performed large quantity fluid-bearing experiments with piston cylinder at P - T conditions of the upper mantle. Hornblende group minerals are chosen as target minerals for its wide distribution in amphibolite of the subducting slab. During this period, I cost lots of time on some technical problems of this study:

1) The low experimental success rate. The large quantity fluid experiment with Ayers' cold sealing technique is still a challenge for experimental geologists. Involved the poor understanding on piston-cylinder, the initial success rate is around 25 %. After summarizing the indications of the failed ones, I made some detailed improvements, such as heating the inner gold layer before tapping, polishing the surfaces of the capsule open end and the lid, leaving enough space in the sample room for preventing leaking by deformation, and using harder holder for the capsule in the piston cylinder assemblage. Currently, the success rate reaches 60 %, and I also would like to improve it with some detailed developments.

2) The fluid extraction. Without knowing the success or failure of an experiment and the dimension of the inner sample room, it is a tedious procedure to challenge one's patience for digging the gold lid by each 0.1 mm depth, in order to avoid any contamination and fluid loss. After opening the capsule, I still need to pay attention on the extraction process in ultrasonic water bath, to prevent the incomplete retrieving fluid (this cannot be confirmed if failed) or mineral loss. Within several tests, another style to open the capsule succeeds – from its

vertical side. It makes this procedure much easier. Both opening styles are introduced and compared in the method section. I would like to employ the leaching technique (Koga et al., 2005) for the higher pressure experiments in the future to decrease the uncertainties from the presence of quench phases.

3) The direct analyses of fluid compositions. At the beginning of the third year, Ken and I found a suitable HPLC lab for F analysis in IPGP with Estelle's help, and got the desired fluoroine chromatography spectrum signal. Before that we have tested this method at OPGC, which is introduced in the method section. Afterwards, the measurements with ICP-AES and ICP-MS were carried out. The comparisons of different element concentrations from these techniques are discussed in this study.

4) The mass balance strategy and error propagation. Before I analyze F concentrations in fluids with HPLC, they are calculated with mass balance approach. In method section, I only introduce the final version of the mass balance with the conservative element set, and just mentioned the tests of the convergent recursion algorithm, which might be an ideal approach to estimate the fluid compositions. However, the convergence of this strategy is monotonic, and its end point is totally determined by the convergent condition. Because this condition cannot be constant for all the experiments, I decide to a traditional way to solve this problem. Moreover, the corresponding uncertainties of fluid compositions are calculated from the mass balance equation. The final error propagation equation is determined after a long time discussion and deduction. It contains all the independent error sources – starting material mass, the solid phase compositions analyzed by electron microprobe, and the aqueous fluid mass after the quench.

5) The precipitates of big crystals ($> 100 \mu\text{m}$) for the volatile element analyses with SIMS. The mineral sizes are usually small. In the experiments conducted with temperature below $800 \text{ }^\circ\text{C}$, the minerals are small and distribute evenly. The increase of temperature promotes the mineral size more efficiently than longer experimental duration. While for hornblende, it is difficult to increase its width, but is easy to elongate it. To solve this problem, I tried two methods. The first method is using mineral seeds. In the latest experiments for ionprobe analyses, this technique works well. The second method is the combination with the ultrasonic sounds. This idea is suggested by Ken. The detailed discussion is in section 5.2.

In order to avoid influencing the integrality of this thesis, most processes above for experimental tests will be not introduced in details. In this study, I will present the most significant original work and results. The structure of this thesis is shown as follows:

1) Introduction. Briefly introduce the background of the subduction zone researches and the reason I am interested in the F behavior between aqueous fluids and hydrous minerals.

2) Methods. Describe the experimental techniques of piston cylinder, and direct analytical techniques of electron microprobe, HPLC, ICP-AES and ICP-MS. The original considerations are the mass balance strategy, the fluid extraction procedure, and the direct analyses on fluid compositions, especially for the fluorine ion.

3) Results. Introduce the experiment results from texture, mineral compositions, and F proportions in OH site (X_F) of the hydrous minerals, to the fluid compositions by mass balance calculations or direct analyses, and the F partitioning between different phases.

4) Discussion. This section is divided into four parts. The first part focuses on the F incorporation of hydrous minerals under different conditions. The X_F of norbergite and chondrodite is significantly various with different buffer conditions, for the reaction of $H_2O + 0.5O_2 \rightleftharpoons 2OH$. The second part compares the fluid compositions from mass balance and direct analyses. The influences of P , T , and fluorine concentrations on major element solubility are investigated. The F partitioning between fluids and hydrous minerals or melt demonstrates the fluorine preferential phase under high P - T conditions, which is shown in the third subsection. In the forth part, the F quantities in the aqueous fluid slab flux are estimated by three ways, which concludes that the aqueous fluid cannot transport significant F from subducting slab to sub-arc mantle at the amphibolite facies.

5) Technical problems. This section discusses some technique problems I met during this study, and lists some potential ways for solving these problems.

6) Outlooks. Some ambiguous aspects of both technique and science problems from this study are expected to be improved in the future.

1. Introduction

A volcano is an opening on a planet's crust that can eject hot magma, volcanic ash and gases originating from the subterranean magma chamber underneath. Volcanic eruptions can give rise to a diverse range of environmental and geological consequences. Sub-oceanic volcanic activities provide the driving force for island formation, and can create hydrothermal vents that sustain deep-sea ecosystems. Intense eruptions occurring on a grand scale can often fundamentally shift the climate pattern as the release of huge volumes of ashes and sulfuric acid droplets has the ability to block the sunlight and cool the Earth's lower atmosphere. From an anthropologic perspective, volcanic eruptions are often found in historical accounts across the world and associated to significant human events such as mass population displacements and widespread famines. Because of these climatic, environmental and socioeconomic impacts volcanoes can exert through their eruptions, the study of volcanism and origin of magma has been considered important by many.

Three types of magmatic or volcanic activities are found on the Earth, and their origins are closely connected to their tectonic context. A predominant majority of volcanoes are distributed along the edges of tectonic plates and are often considered to be the direct products of plate movement. For instance, the Mid-Atlantic Ridge features a concentration of volcanoes resulting from divergence of Eurasian Plate and North American Plate in the north, as well as African Plate and South American Plate in the south. In contrast, the Pacific Ring of Fire, prominent for its high level of volcanic and seismic activities, coincides with a vast stretch of converging plate boundaries. On the contrary, volcanoes are usually not present around transform boundaries, where two neighboring plates laterally grind past each other without generating significant ripping or colliding forces. Volcanoes can also be found within the plate interiors. Experimental observations and analyses revealed that these intraplate volcanoes, while often distanced from the limits of tectonic boundaries, appear to sit on top of hyperactive regions that are commonly referred to as "hot spots". The current prevailing hypothesis suggests that the irregular thermal profile of the earth's mantle creates locales with

anomalously high temperatures, which results in anomalous magmatic activities. The hypothesis provides a satisfactory explanation of volcano chains, a geological phenomenon that is commonly observed around the world (i.e. Hawaiian volcanoes), as the natural outcome of the continuous movement of the crust over the stationary hot spot. This thesis studies the magma genesis hypotheses from the subduction zone.

1.1 Subduction zone

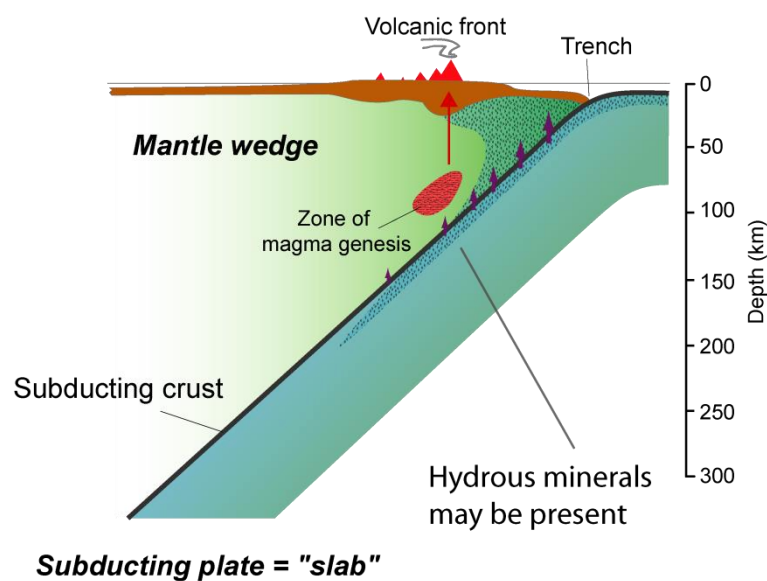


Fig. 1.1 An illustration of the cross-section of a subduction zone. A mantle wedge is a triangular cross-section of mantle that lies above a subducting tectonic plate and below the overriding crust. The subducting slab is overridden by the leading edge of the other plate. During the subducting, the hydrous minerals break down and release water progressively, and the fluid transports from the slab to sub-arc mantle (e.g. Peacock, 1996). The introduction of slab flux decreases the partial melt point of mantle basalt, and creates magma, which is finally erupted from volcanoes to the surface of the Earth.

The Earth's surface has three plate tectonic environments: divergent, convergent, and transform fault plate boundaries (Gill, 1981). The word "subduction" was created by the Swiss geologist André Amstutz (1951) to describe the tectonic convergence of crust and mantle (Roeder, 2009). At the boundary of these two convergent plates, the heavier plate is squeezed (subducted) below its lighter counterpart (e.g. White et al., 1970). Moreover, the subducting plate contains sediment, oceanic crust and mantle lithosphere. For most of the subduction zones, of which the thickness of sediment ranges from 50-500 m to several

kilometers, their sediment has on average 76% terrigenous materials, 7% calcium carbonate and 17% hydrous minerals (Plank and Langmuir, 1998). The average thickness of the normal oceanic crust is reported as 7.1 ± 0.8 km with the seismic results (White et al., 1992), and the oceanic crust is igneous rock (e.g, mid-ocean ridge basalt or MORB). The oceanic mantle lithosphere (peridotites) is typically 50-100 km thick, which relates with the isotherm of cooling lithosphere (Parsons and Sclater, 1977; Turcotte and Schubert, 1982; Hirth and Kohlstedt, 1996), but it is no thicker than the crust beneath the mid-ocean ridges (Parsons, 1982; Anderson, 1995).

Furthermore, the descent of the subducting plate (the “slab”) into the upper mantle is met with increasing temperature and pressure, resulting a series of metamorphic transformations. Because of the presence of accretion prism, the quantity of sediments subducted into mantle is considered to be smaller than its initial thickness (~500m, von Huene and Scholl, 1991; Plank and Langmuir, 1998; Poli and Schmidt, 2002). Oceanic basalt, a major component of the crust, subducts and transforms into greenschist, amphibolite, blueschist, and/or eclogite (e.g. Wyllie and Sekine, 1982; Wyllie, 1988). This conversion simultaneously produces several effects below, respectively. First, the crystal waters entrapped in basalt are released, and rapidly transformed to a supercritical state if it meets the extreme local environment. Second, the generation of eclogite, which is denser compared to basalt, further increases the density of the slab and accelerates its submergence. Third, the continuous plunge of the slab all the way through the asthenosphere into the deep mantle below also generates an opulent amount of supercritical water. Lastly, oceanic mantle lithosphere also undergoes transformations from hydrated peridotite (i.e. serpentinite) to dehydrated peridotite. However, estimates show that only top 5-7 km of oceanic mantle lithosphere is serpentinitized (Reynard, in press). In this thesis research I consider that the basaltic crust provides the primary source of water during arc magma genesis (Schmidt and Poli, 1998).

The water released through these geological changes, driven by buoyancy, leaves the sinking slab and flow through the overlaying mantle wedge, where it has the ability to lower the melting point of the mantle rocks. The resulting melts (magmas) continue to ascend and eventually accumulate in the magma chambers. The buildup of magma and pressurized steam ultimately cause volcanic eruptions, which could bring some materials from subducting slab

to the volcanic front (VF). The observations of erupted products from VF provide primary data to interpret this magma genesis process.

1.2 Magma Genesis

As Fig. 1.1 shows, the depth to the top of the slab from the volcanic front ranges from 72 to 173 km with a global average of 105 km, and the distance of the volcanic front away from the trench depends

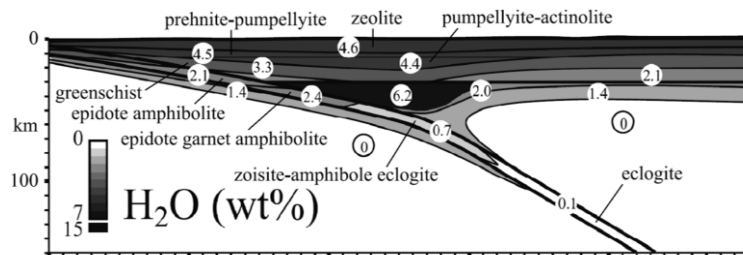


Fig. 1.2a Calculated phase relations in mafic crust and maximum H₂O contents. Anhydrous eclogite formation is predicted to occur at 80 – 90 km depth in the slab. Downgoing, hot slab mantle is nearly anhydrous, and only the tip of the mantle wedge can contain substantial H₂O (modified from Hacker et al., 2003).

on the slab dip (Syracuse and Abers, 2006; Grove et al., 2009). Thus, the normal magma genesis hypothesis is similar, although their exact depths depend on the different subduction zone parameters. The basaltic ocean crust contains hydrous minerals (like amphiboles, chlorite, Peacock, 1996), some of which were formed by hydrothermal alteration as seawater infiltrated into hot, fractured, young ocean crust at the mid-ocean ridge (Gill, 1981). As deep as the slab reaches approximately 100 km beneath the surface, the pressure transforms the slab crust into the anhydrous eclogite, of which water content is close to zero (Fig.1.2a). Above that depth, the aqueous fluids are released from the oceanic crust with progressively increasing pressure, therefore water content of the subducting slab decreases significantly. The oceanic crust is an important water source of arc magma genesis. Furthermore, the slab flux from the subducting slab to sub-arc mantle as aqueous fluids should mainly exist in the amphibolite facies.

The water (i.e. hydrogen) content in the mantle wedge peridotite is crucial for the magma genesis (partial melting). There are two hypotheses. First, the melting induced by the addition of aqueous fluid (this includes fluid rich in silicate-solute such as supercritical fluid) is called flux melting, because the flux is derived from slab. Ringwood (1974) suggested

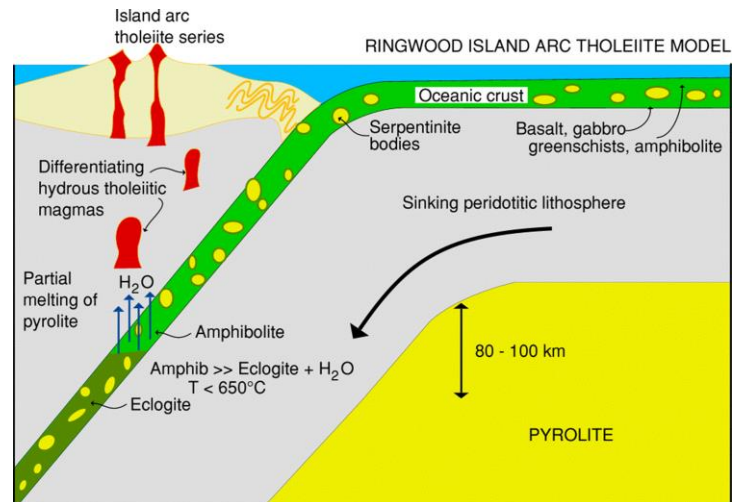


Fig. 1.2b The early tholeiite phase of development of an island-arc (modified from Ringwood, 1974, cited from the lecture of Prof. J. Tarney from University of Leicester, <http://www.le.ac.uk/gl/art/gl209/lecture6/lecture6.html>). The fluids transferred from the slab to subarc mantle is from the breakdown of amphibolite.

the introduction of aqueous fluid to the present hot mantle rocks lowers their melting point resulting in partial melting of ultramafic mantle rocks to yield mafic magma (Fig. 1.2b). However, this general model has progressed to include detailed process of magma genesis in subduction zone. For example, the trace element observations at the Mariana arc by Elliott et al. (1997) demonstrates the systematic variations between islands. It indicates that their magmas sources were suffered different metasomatism reaction with different fluid sources. This strengthens the earlier two-process models, of which fluid materials are from subducted sediment and the dehydrated event in the slab. Moreover, Iwamori (1998) presents a model. The water released from the lower subducting slab is brought down by hosted with serpentine and chlorite. As their breakdown, the aqueous fluid is transported upwards by the slab flux into mantle wedge, and creates partial melting with peridotite (minimum at 2.5 GPa). Furthermore, Straub et al. (2004) utilize their investigations of the trace elements from tephra glass along with other researches to reveal the mantle source is the slab flux under Izu VF. Their model confirms the strong relationship between the arc chemistry and the trench sediment components, which indicates that the slab fluid is composited with ~95% metabasalt fluid and ~5% metasediment fluid. Although the proportion of sediment fluid overall is low, its contribution is revealed in certain aspects of the volcanics composition.

Alternatively, the partial melting of slab which occurs in the depth greater than 100 km is called slab melting. At the deeper depth of slab (the 100 – 150 km depth interval), most oceanic crust is converted into quartz eclogite. While, the high pressure serpentinite can keep the water of its dehydration down through the crust from 100 to 300 km. This water will result in the partial melt of quartz eclogite and the development of rhyodacite-rhyolite magmas when the temperature is higher than 750 °C (Ringwood, 1974). Furthermore, the presence of slab melting is also certified by some studies. For example, in rare locations where the descending plate is very young and hot, the arc rock (adakite) compositions indicate that the magma was produced, to certain extent, by melting of the subducting oceanic crust. Defant and Drummond (1990) suggest that only oceanic basaltic crust younger than 25 Ma is hot enough to initiate melting of the slab at the depth from 60 - 80 km (2.0 - 2.5 GPa). And in the following partial melting experimental studies (10 - 40% metamorphosed basalt melting), some silicate melts (similar to the adakite composition, except lower MgO, Cr and Ni) were produced in the amphibolite to eclogite facies (Rapp et al., 1991; Sen and Dunn,

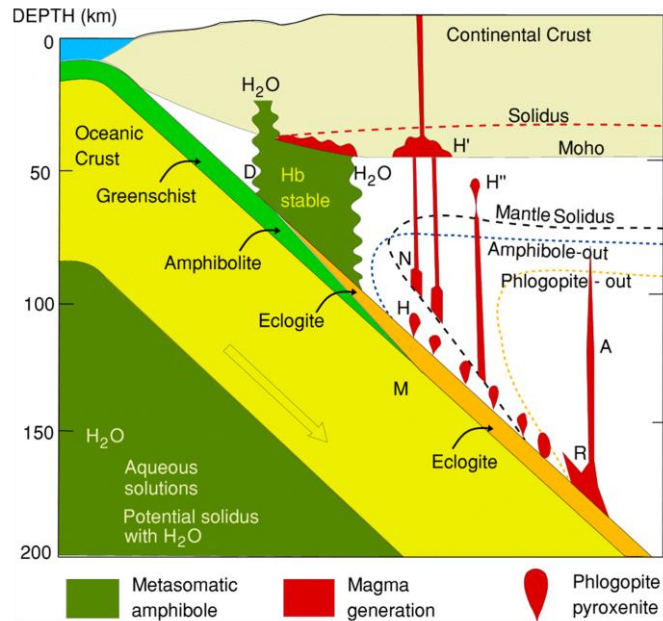


Fig. 1.2c A simple thermal structure model for idealized petrological cross-section through subducted oceanic lithosphere (modified from Wyllie and Sekine, 1982, cited from the lecture of Prof. J. Tarney from University of Leicester, same as the Fig. 1.2c).

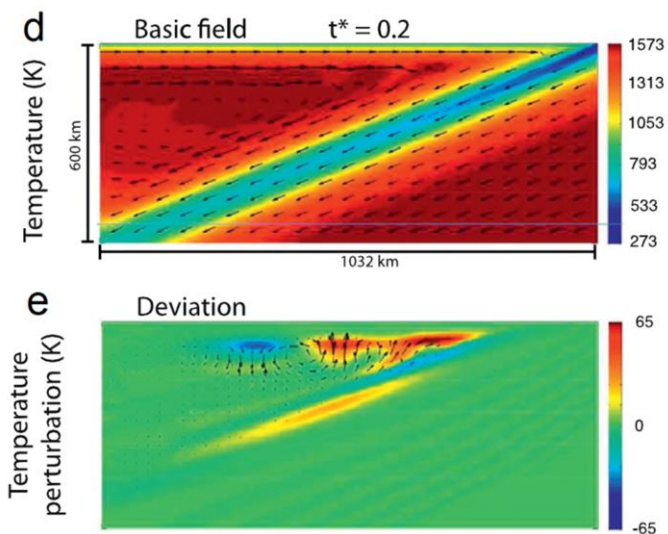


Fig. 1.2 A model run result modified from Wirth and Korenaga (2012). d) Mean temperature and velocity field. e) out-of-plane perturbation temperature and velocity.

1994; Rapp and Watson, 1995). However, Peacock et al. (1994) utilize their numerical model to demonstrate that adakite may be present as the result of not only partial melting of oceanic basalt crust, but also other possibilities like lower arc crust (Atherton and Petford, 1993; Kay and Kay, 1993). They also consider that it is important to identify the exact depth of melting occurrences with the temperature distribution of subduction zones.

Based on both of flux melting and slab melting models, the researches above suggest that the magma geneses can occur in the slab (basaltic crust or sediment) and the mantle wedge. Temperature is another key parameter for partial melting, so the thermal condition underneath the arc is indispensable for creating melt in subduction zone. For instance, Anderson et al. (1978, 1980) demonstrate that the thermal structure corresponds to a subducted crust cooled by endothermic dehydration reactions. They also constructed a numerical program to model the thermal structure of a subduction zone, but they include the effects of frictional heating as an important source. Wyllie and Sekine (1982) use their petrological investigations on the locations of dehydration fronts, solidus boundaries, areas of potential melting, and the variations of their positions to display their potential thermal structures (Fig. 1.2c), and demonstrate that some possible reactions would be more effectively recognized if they are plotted suitably. Moreover, Peacock (2003) suggests that three important and well constrained parameters, which control the thermal structure of a subduction zone, are convergence rate, thermal structure of the incoming lithosphere, and the geometry of the subducting slab. His models are in two-dimension scale, while some current studies illustrate that it is necessary to simulate the model in 3D scale. For example, Wirth and Korenaga (2012) develop numerical models to reveal the possibilities of small-scale convection in the mantle wedge. One of their results demonstrates that the temperature distribution of out-of-plane perturbation temperature is different from that of 2D models (Fig. 1.2d & e). And their model results probably interpret the presence of the “hot fingers” (e.g., Honda et al., 2002). Therefore, the thermal structure of the subduction zone indicates the potential locations for melting, while we still do not know the exact temperature of the melting position in the subduction zone. Turning the problem around, if we can find the nature of the slab flux, we can get more constraints on the thermal structure of the subduction zone.

In summary, the models above have described and simulated the partial melting

processes in the sub-arc mantle and/or in the subducting slab, and indicate that the magma geneses in nature are more complicated than Ringwood's models. However, dehydration of subducting crust and flux melting in the mantle wedge appear to account for most magma genesis possibilities. Thus, more interests are attracted by the slab flux sources and components. This thesis project focuses on the process of slab flux from flux melting aspect, with the presence of the aqueous fluids. Moreover, instead of the traditional trace elements, I study the new tracer behaviors, i.e, volatile tracers F and Cl in this project.

1.3 Volatile Elements

With the compositions of the lava in the volcanic front, scientists found some indications of the variations of the magma compositions. Furthermore, the first crystallized olivines can trap some magma information in the melt inclusions. During the eruption, most of the elements are kept in the lava, while volatile elements are degassed and separated from magmas. In subduction zone, the volatile species in sub-arc lavas are H₂O, CO₂, SO₂, H₂S, HCl and HF. Although other halogen elements Br and I (Baker and Balcone-Boissard, 2009) or noble gases and N₂ (Carroll and Webster, 1994) can be present in the arc magmas, their abundances in the subduction zone are much lower than the former group, even before the degassing. These volatile species were dissolved into magmas during the magma geneses. While the solubility of the major volatile elements decrease and suffer exsolution progressively in the process of magma ascent (e.g. Dixon et al., 1991; Wallace and Anderson, 1998; Sparks, 2003).

In magmatic systems, the volatiles with the highest concentrations are water, carbon dioxide and molecular species of sulfur. H₂O is the dominant volatile species in arc magmas, of which concentrations range from 0.5 to 8 wt%, and CO₂ is the second abundant volatile species with the concentration probably larger than 1 wt% in the primary magma (Symonds et al., 1994; Wallace, 2005). Water exsolution can lead to an increase of the magma viscosity, and subsequent fragmentation process control the dynamic of magma ascent and form the driving force of arc volcanic eruptions (e.g. Anderson, 1975; Tait et al., 1998; Zhang, 2000).

Thus, the investigations on water solubility are crucial for understanding the magma genesis in sub-arc mantle. Generally, these water concentrations in the natural sample were collected from melt inclusions in olivine. However, H₂O not only suffered degassing in melt inclusions before eruptions (e.g. Dixon and Stolper, 1995), but also during an extended experimental heating to make a homogeneous phase (e.g. Chen et al., 2011). So it is difficult to represent their abundances at the moment of entrapment in the magma source with reliable values. McMillan (1994) review the studies on water solubility in many natural or synthetic melt compositions within a wide pressure and temperature condition in last few decades, and conclude that H₂O concentrations in primary magmas must be always equal or higher than the measured water content in magmas.

However, other volatile elements are potential tracers to study the flux-melting magma genesis. If these trace volatile elements degas much during the magma ascent, they cannot keep the information of the sub-arc mantle as well. Nevertheless, fluorine is the last volatile element to be exsolved during magma ascent (Cl at 100MPa and F at <20 MPa, Spilliaert et al., 2006). Its content in melt inclusions is certainly less affected by degassing than H₂O, CO₂ and S. Thus, fluorine is the volatile element that best retains the information of magma genesis (Villemant and Boudon, 1999).

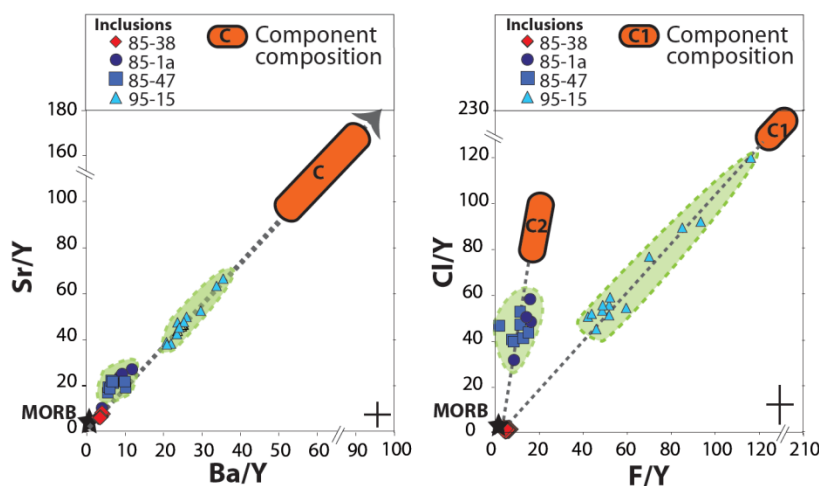


Fig. 1.3 (left) Ba/Y versus Sr/Y, (right) Cl/Y versus F/Y for the Shasta melt inclusions. Cross in the right-bottom of each figure represents the typical analytical error on each ratio. Dashed line represents a mixture between the average melt inclusion

compositions and one H₂O-rich component (C1 or C2). On the right graph, the basaltic andesites melt inclusions compositions can be reproduced by mixing between a depleted mantle and one of two H₂O-rich component (C1 for the 95-15 melt inclusions and C2 for 85-1a and 85-47 melt inclusions). (Simplified after Le Voyer et al., 2010; and cited from Dalou, 2011)

Le Voyer et al. (2010) measured F, Cl and other trace element concentrations in olivine-host melt inclusions from Mount Shasta volcanic front, and utilize F and Cl ratio to reveal the mantle wedge melting sources which were intruded from different slab component. They find the various relationships between concentration ratios of the fluid-mobile element (F, Cl, Ba and Sr) over fluid-immobile element Y, which has the small analysis uncertainty (Fig. 1.3). Apparently, using regular trace elements, Shasta melt inclusion compositions were illustrated with one trend (Fig. 1.3 left), while using F and Cl, they identified two trends, and divide Mount Shasta melt inclusions in two groups, which indicate two water-rich components C1 (95-15 melt inclusions), and C2 (85-1a and 85-47) (Fig. 1.3 right). Furthermore, they compare melt inclusion compositions in volatile and trace elements of subduction zones from United States (Mount Shasta), Italy (Sommatà) and Ecuador (Pichincha and Pan de Azucar), and then find consistent behavior on Cl/F ratio, which also separated the observations from Italy and Ecuador into 2 groups as found in Mount Shasta. It indicates Cl/F ratio variations can be treated as independent with the melting and crystallization processes. Therefore, this work manages to explain the source of magma genesis using F and Cl concentrations in the melt inclusion, along with other traditional trace elements. It is of importance to investigate more knowledge on the F and Cl behavior in the P-T condition of the subduction zone in this study.

1.4 Main Aim of Thesis

The average F content of the pristine sub-arc mantle (*i.e.* not metasomatized) is 14 ± 4 ppm, based on the dry tholeiitic arc-basalt melt inclusions from Mt. Shasta, which is considered as a melt derived from non-metasomatized sub-arc mantle (Baker et al., 1994; Le Voyer et al., 2010). This value is close to that of the depleted source of primitive MORB (16 ± 3 ppm of F, Saal et al., 2002). However, from the available melt inclusion data of primitive arc basalts and basaltic andesites, F concentrations are generally 1 to 16 times higher in comparison to N-MORB (e.g. an average is N-MORB concentration of F is 89 ppm, F concentrations in primitive arc basalts ranges from approximately 100 to 1400 ppm, Bouvier

et al., 2008; Le Voyer et al., 2010; Rose-Koga et al., 2012). Another observation from the Izu volcanic front is that F is enriched relative to the middle rare earth elements (Sm, Nd) by up to 4 times (Straub and Layne, 2003). Clearly, metasomatized sub-arc mantle is enriched in F compared to MORB source mantle.

As shown by many previous studies, a slab flux transports some elements to sub-arc mantle and enriches their abundances (Gill, 1981; Tatsumi and Eggins, 1995), and the enrichment of F is consistent with such standard models (Straub and Layne, 2003; Le Voyer et al., 2010). However, the exact nature of this slab flux is ambiguous; it could be fluid, melt, and/or supercritical fluid. For example, under upper-mantle P-T conditions, F-partitioning experiments show $D_F^{\text{melt/min}}$ (basaltic melt; lherzolite minerals are olivine, orthopyroxene, clinopyroxene, plagioclase and garnet) are more than 10 (Dalou et al., 2012). Since silicate melt is richer in F than residual solids, it is possible to enrich sub-arc mantle with an F-rich silicate melt derived from the slab. On the contrary, Straub and Layne (2003) suggested that aqueous fluid is a potential carrier of F from subducted slab to mantle wedge. Unfortunately, $D_F^{\text{Fluid/Minerals}}$ is poorly known, or rather has not previously been experimentally constrained. Therefore, it has been impossible to quantitatively assess whether a fluid could transport F from the slab to sub-arc mantle.

The experimental study of this thesis reports that F partitioning between an aqueous fluid and hornblende and/or humite group minerals at pressures and temperatures comparable to subduction zone settings. These minerals are chosen because they are probably the main carriers of F, and to a lesser extent of water, in the crustal part of the slab. F concentrations in aqueous fluids were calculated by mass-balance calculations, and confirmed by high pressure liquid chromatography (HPLC), as well as some major elements analyzed by HPLC, ICP-AES and ICP-MS. Finally, we quantify F transported out of the slab by fluid in the presence of hornblende.

1. Introduction

2. Methods

Scientists developed the techniques of high pressure and high temperature experiments. Their purposes are to simulate the conditions in depths of the Earth to observe the chemical reactions among different phases (e.g., mineral, melt, and fluid). In nature, the system is often too complicated to simulate its reactions totally. Therefore, it is important to choose suitable starting compositions and experimental strategies for research subjects. In this section, I will explain how I have selected the suitable methods for my thesis.

2.1 Starting Materials

Starting materials are chosen to reproduce equilibria of natural reactions in a laboratory. However, experiments cannot reproduce every aspect of natural phase equilibria at the same time. Generally speaking, scientists would simplify the experimental system for their targets, at the same time the chemical composition of the starting material should representable the natural samples as close as possible.

2.1.1 Expected Minerals in Experiments

Because F is enriched in subducting slab and sub-arc mantle, the experimental system should be similar to the composition of subducting slab and/or sub-arc mantle. Generally, because F can replace OH in the OH site in many hydrous minerals, these (e.g., mica, humite, and amphibole) are the obvious candidates for my study. Since amphiboles widely exist in subduction zones, I choose amphibole minerals as my target mineral. I have found several amphibole minerals in mafic and ultramafic rocks which are mostly from mantle xenolith (the online database Georoc <http://georoc.mpch-mainz.gwdg.de/georoc/>).

2.1.2 First Order Investigation from Database

The minerals in mantle xenolith may retain the information of chemical composition at the depth of upper mantle (Table 2.1.2a). The compilation shows the amphibole component from different arcs: Banda arc, Central Honshu, Izu-bonin arc, Lesser Antilles, Kamchatka arc, Mexican volcanic belts, Kurile arc, Luzon arc and Northeastern Honshu arc. These regions have volcanic eruptions, and the amphiboles are brought from the underneath.

Table 2.1.2a Amphibole compositions in peridotite (mantle xenolith) of different subduction zone. Data are from Georoc database. The values are in wt%.

Location	Citation	SiO ₂	TiO ₂	Al ₂ O ₃	Cr ₂ O ₃	FeO	CaO	MgO	MnO	K ₂ O	Na ₂ O	H ₂ O
Banda Arc	Linhout K.(1994)	44.40	1.96	10.80		11.72	10.60	14.70	0.18	0.08	1.99	
	Berry R. F.(1981)	53.00		6.67	0.86	2.66	12.90	21.00			0.46	2.00
		51.00	0.28	9.23	0.88	3.06	12.70	20.40			1.00	2.00
Central Honshu	Inomata M.(1974)	40.97	3.61	11.11		8.89	10.19	16.52	0.21	0.19	3.10	
		43.02	5.31	10.85		8.61	10.31	14.85	0.16	0.28	4.22	
		45.66	4.73	10.94		9.51	10.99	14.50	0.16	0.52	2.84	
		45.16	3.72	9.27		8.10	9.66	17.20	0.17	0.20	3.55	
		46.26	3.57	9.92		7.51	9.86	16.82	0.15	0.32	3.48	
		43.20	4.34	11.08		7.63	11.37	16.31	0.41	0.27	3.14	
Izu-Bonin Arc	Parkinson I. J.(1998)	53.74	0.00	4.83	0.89	2.13	12.89	21.75	0	0	0.35	
		51.44	0.00	6.59	1.13	2.65	12.04	21.80	0	0	0.79	
	Arai S.(1990)	41.91	5.10	11.65	0.43	9.14	11.13	15.18	0.10	0.25	2.99	
		45.03	2.23	12.19	2.31	3.29	11.48	18.50	0.02	0.42	2.35	
		48.77	2.04	8.71	0.59	4.28	12.01	19.61	0	0.10	1.80	
	Arai S.(1987)	45.41	0.38	13.62	1.75	3.03	12.05	19.36	0.05	0	3.01	
46.31		0.44	12.85	1.94	2.92	12.49	18.62	0.10	0	2.90		
Lesser Antilles	Coulon C.(1984)	48.84	0.72	7.85	0.14	14.03	10.02	14.43	0.81	0.16	1.25	
		47.40	1.10	9.65	0.00	12.83	11.69	15.07	0.36	0.20	1.49	
		42.36	1.62	13.82	0.07	9.82	11.91	14.83	0.24	0.46	2.19	
		40.17	1.44	16.08	0.08	11.20	11.01	15.64	0.16	0.21	2.69	
		41.22	1.41	15.01	0.03	10.34	11.18	16.05	0.14	0.28	2.76	
		39.75	1.71	16.12	0.00	8.52	12.69	16.07	0.05	0.60	2.54	
Kamchatka Arc	Kepezhinskas P. K.(1995)	43.11	2.11	12.18	0.01	10.97	10.40	14.77	0.13	0.51	3.08	
		42.86	2.1	12.83	0.02	10.13	10.77	15.29	0.11	0.45	3.49	
		42.96	2.91	11.44	0	11.62	11.38	14.81	0.11	0.66	2.47	
	Ishimaru S.(2007)	45.91	0.47	11.44	2.17	3.85	11.83	19.51	0.06	0.19	2.34	
		46.83	0.32	11.04	1.64	3.95	11.62	19.26	0.06	0.18	2.37	

2. Methods

Location	Citation	SiO ₂	TiO ₂	Al ₂ O ₃	Cr ₂ O ₃	FeO	CaO	MgO	MnO	K ₂ O	Na ₂ O	H ₂ O
		49.58	0.06	9.56	1.46	3.45	12.16	19.96	0.05	0.23	1.85	
		49.41	0.02	8.69	1.58	3.27	11.84	20.56	0.06	0.20	2.01	
		46.63	0.33	11.03	2.27	3.95	11.68	19.29	0.05	0.31	2.29	
		47.90	0.82	9.93	1.33	4.59	10.87	19.17	0.07	0.26	2.33	
		47.60	0.16	11.12	0.78	3.79	11.23	19.48	0.05	0.25	2.41	
	Bryant J. A.(2007)	53.39	0.04	5.15	0.01	3.76	11.91	22.34		0.19	1.14	
		56.54	0.05	1.39	0.04	2.88	12.32	23.40		0	0.43	
		54.21	0	4.54	0	3.48	11.62	22.53		0.10	1.02	
		42.12	1.07	12.18	0	12.74	11.26	13.99		0.74	2.13	
		44.77	2.16	9.63	0.10	12.71	11.18	14.40		0.46	2.06	
	Ishimaru S.(2008)	59.34		0.44		1.62	13.08	23.84	0.03		0.11	
		58.22	0.03	1.06	0.35	1.76	13.09	23.47	0.03		0.15	
		51.74	0.05	7.19	0.80	2.89	12.52	21.28	0.06	0.12	1.15	
	Halama R.(2009)	48.91	0.10	9.43	1.30	3.47	12.36	20.17	0.03	0.31	1.71	
		48.14	0.12	9.77	2.38	3.26	12.37	19.62	0.02	0.41	1.80	
Mexican Volcanic Belts	Blatter D. L.(1998)	43.45	0.64	14.16	1.20	4.49	11.70	17.75	0.06	0.22	2.46	
		44.44	1.13	11.56	1.63	5.20	10.87	18.14	0.11	0.68	2.99	
		43.69	0.70	14.22	1.04	4.39	11.80	18.17	0.06	0.22	2.53	
Kurile Arc	Volynets O. N.(1990)	45.84	0.79	12.03	1.47	4.54	12.97	17.18	0.08	0.10	2.36	2.11
		44.26	0.93	12.94	1.41	4.44	12.31	16.92	0.08	0.13	2.26	2.07
		44.72	0.38	14.05	1.46	4.50	12.09	16.90	0.05	0.64	2.02	2.10
		44.22	0.77	13.24	1.65	4.80	12.09	16.82	0.07	0.71	2.10	2.08
		42.50	0.40	13.81	0.39	8.21	11.66	15.75	0.08	0.55	2.03	2.03
		44.22	1.54	11.27	0.19	8.72	12.41	15.63	0.14	0.53	1.94	2.05
		45.56	0.58	8.56	0.18	11.60	10.94	15.34	0.26	0.62	1.62	
		42.54	1.63	10.71	0.17	12.00	10.53	15.25	0.26	0.77	1.94	
Luzon Arc	Arai S.(2000)	48.58	0.30	10.26	0.21	4.84	11.84	19.90	0.09	0.44	2.04	
	Gregoire M.(2008)	46.13	0.51	13.02	0.16	4.24	11.18	19.47	0.10	0.23	2.38	
Northeastern Honshu Arc	Takahashi E.(1980)	44.36	0.41	12.26	1.08	4.74	12.69	18.18	0.10	0.10	2.01	
		41.76	1.54	14.92	1.06	4.51	11.64	17.86	0.09	0.06	2.96	
		44.54	0.53	12.98	1.12	4.00	12.53	18.37	0.05	0.07	2.34	
	Abe N.(1998)	43.80	0.85	14.67	0.15	6.89	11.50	16.48	0.21	0.65	2.17	
		44.44	0.79	12.63	1.09	6.79	11.49	16.55	0.12	0.78	2.25	
	Yamamoto Masatsugu(1984)	42.76	1.63	11.87	1.37	6.17	12.11	16.67	0.14	0.85	2.32	
		43.99	1.31	12.37	1.19	6.71	11.69	17.42	0.09	1.01	2.17	
		41.92	2.17	13.05	1.32	6.34	12.44	16.27	0.07	1.06	2.35	
		44.12	2.24	10.90		8.74	11.55	16.64	0.11	0.87	2.21	
		43.28	2.50	11.97		8.98	11.87	15.76	0.09	1.02	2.16	
		42.64	2.68	12.20		9.14	12.03	15.25	0.10	1.15	2.30	
		42.72	1.86	12.96		9.48	11.78	15.64	0.13	0.82	2.31	
		41.55	1.72	13.77		9.53	12.62	15.21	0.12	1.10	2.07	
		41.98	2.00	13.84		9.86	11.86	14.88	0.13	1.13	2.14	
	Abe N.(1995)	43.31	1.07	15.51	1.13	4.26	11.06	17.42	0.04	0.03	3.19	

2. Methods

Location	Citation	SiO ₂	TiO ₂	Al ₂ O ₃	Cr ₂ O ₃	FeO	CaO	MgO	MnO	K ₂ O	Na ₂ O	H ₂ O
		44.37	1.28	14.59	1.33	4.21	12.12	17.25	0.09	0	1.79	
	Abe N.(1992)	42.98	1.29	15.22	0.15	6.85	11.41	16.00	0.10	1.29	1.47	
		44.19	0.79	12.56	1.08	6.75	11.43	16.46	0.12	0.78	2.24	
		46.76	0.57	11.64	1.23	3.76	12.01	18.75	0.20	0.12	1.25	
		45.45	0.36	14.85	0.70	3.92	12.77	17.7	0.04	0.04	2.27	
	Abe S.(1999)	44.76	1.24	15.69	1.18	4.02	11.96	17.85	0.01	0.65	2.24	
		44.35	1.51	12.41	1.44	3.89	11.59	18.46	0.06	0.40	2.53	
		44.43	1.53	12.61	1.50	4.03	11.49	18.43	0.07	0.34	2.47	

All of these amphibole mineral compositions have significant CaO (from 9.3 to 13.1 wt%), which suggests that they are calcic amphiboles (B site contains 2 Ca). Their various SiO₂, Al₂O₃ and Na₂O concentrations indicate that most of them are not end-member species, while they belong to the hornblende group. Fig. 2.1.2a illustrates the relationship between Al₂O₃, FeO (total) or CaO concentrations vs SiO₂ concentrations. Obviously, CaO is constant, but Al₂O₃ and FeO changes with SiO₂. I use the data plotted in the densest area to represent my target mineral composition. First, I exclude some data of which Al₂O₃ concentration is less than 11 wt%, and this will constrain SiO₂ concentration around 43-48 wt%. Second, the FeO concentration can be separated into two groups. One contains more than 8 wt% FeO, and the other only has approximately 4 wt%. I chose the latter group, because of the low Fe concentration from my natural minerals (cpx and opx). The final starting material composition is close to magnesiohornblende (Table 2.1.2b).

Table 2.1.2b Amphibole compositions in peridotite (mantle xenolith) of different subduction zone after excluding high Al₂O₃ and FeO concentration minerals. The average composition is close to a mineral magnesiohornblende.

Citation	SiO ₂	TiO ₂	Al ₂ O ₃	Cr ₂ O ₃	FeO	CaO	MgO	MnO	K ₂ O	Na ₂ O	H ₂ O
Arai S.(1987)	45.41	0.38	13.62	1.75	3.03	12.05	19.36	0.05	0	3.01	
	46.31	0.44	12.85	1.94	2.92	12.49	18.62	0.10	0	2.90	
Ishimaru S.(2007a)	45.91	0.47	11.44	2.17	3.85	11.83	19.51	0.06	0.19	2.34	
	46.83	0.32	11.04	1.64	3.95	11.62	19.26	0.06	0.18	2.37	
Ishimaru S.(2007b)	46.63	0.33	11.03	2.27	3.95	11.68	19.29	0.05	0.31	2.29	
Blatter D. L.(1998)	43.45	0.64	14.16	1.20	4.49	11.70	17.75	0.06	0.22	2.46	
	44.44	1.13	11.56	1.63	5.20	10.87	18.14	0.11	0.68	2.99	
	43.69	0.70	14.22	1.04	4.39	11.80	18.17	0.06	0.22	2.53	
Volynets O. N.(1990)	45.84	0.79	12.03	1.47	4.54	12.97	17.18	0.08	0.10	2.36	2.11
	44.26	0.93	12.94	1.41	4.44	12.31	16.92	0.08	0.13	2.26	2.07

2. Methods

Citation	SiO ₂	TiO ₂	Al ₂ O ₃	Cr ₂ O ₃	FeO	CaO	MgO	MnO	K ₂ O	Na ₂ O	H ₂ O
Takahashi E.(1980)	44.72	0.38	14.05	1.46	4.50	12.09	16.90	0.05	0.64	2.02	2.10
	44.22	0.77	13.24	1.65	4.80	12.09	16.82	0.07	0.71	2.10	2.08
	44.36	0.41	12.26	1.08	4.74	12.69	18.18	0.10	0.10	2.01	
	44.54	0.53	12.98	1.12	4.00	12.53	18.37	0.05	0.07	2.34	
Abe N.(1995)	43.31	1.07	15.51	1.13	4.26	11.06	17.42	0.04	0.03	3.19	
Abe S.(1999)	44.37	1.28	14.59	1.33	4.21	12.12	17.25	0.09	0	1.79	
	44.76	1.24	15.69	1.18	4.02	11.96	17.85	0.01	0.65	2.24	
	44.35	1.51	12.41	1.44	3.89	11.59	18.46	0.06	0.40	2.53	
	44.43	1.53	12.61	1.50	4.03	11.49	18.43	0.07	0.34	2.47	
Average	44.83	0.78	13.06	1.50	3.85	11.94	18.50	0.07	0.26	2.43	2.09
Std (2σ)	1.03	0.41	1.39	0.35	0.55	0.53	0.87	0.02	0.24	0.37	0.02

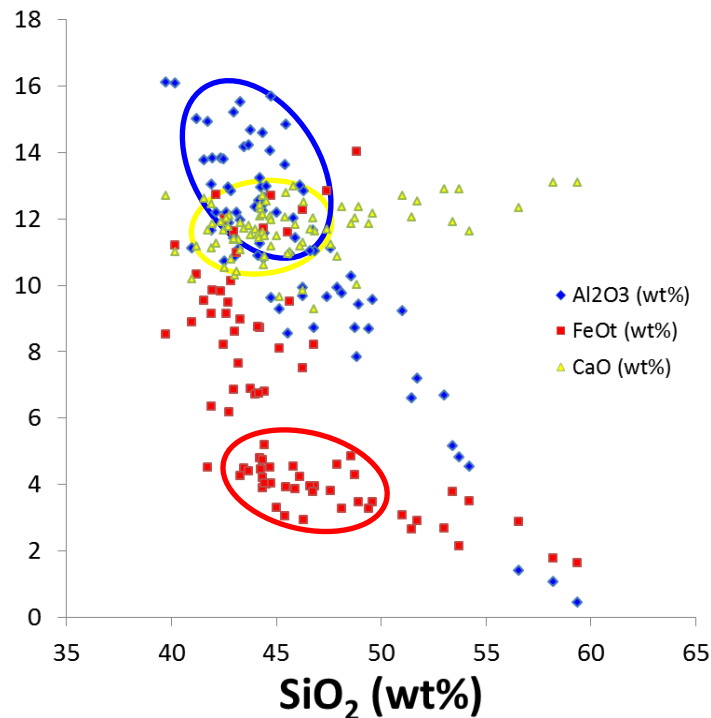


Fig. 2.1.2 Three oxide concentrations vs. SiO₂ concentrations of all the amphibole minerals. Three circles represent the chosen data area with corresponding colors.

2.1.3 Starting Powder Compositions

The experiments were conducted in a predominantly FeO–CaO–MgO–Al₂O₃–SiO₂–H₂O (FCMAS+H₂O) system (also contains minor TiO₂, Cr₂O₃, and MnO). The compositions of the starting mixtures are chosen to promote the growth of a hornblende (Table 2.1.3). Here, anhydrous solid mixtures were first prepared, and then pure water (H₂O) was added before the

experiments.

For the solid part, natural opx, natural cpx, and Al₂O₃ powder were mixed to obtain hornblende stoichiometry. The natural opx and cpx are handpicked from a coarse granular garnet lherzolite xenolith from Pali Aike, Chile (Stern et al., 1986). The compositions determined by electron microprobe are reported in Table 2.1.3. The alumina powder is from Fluka with >99.7% purity. Four starting mixtures (SP1, 2, 3 and 4) were prepared with a varying degree of F doping. For SP1, powders of opx, cpx and alumina were ground in an agate mortar with ethanol (opx:cpx:Al₂O₃ = 96.5:209.9:31.8 in mg). MgF₂ powder was then added to form SP2 and SP3 (for SP2, SP1:MgF₂ = 100:8.9 and for SP3, SP1:SP2=3:5). And SP4 is a mixture of SP1, SP3 and MgO powder. The mixtures contain approximately 0, 5, 2, and 0.5 wt% F by weight from SP1 to SP4, respectively. The compositions of the mixtures were determined by an electron microprobe on the synthesized homogeneous glasses, annealed at 1550 °C and 1 GPa (Table 2.1.3). For the water part, first the solid starting material was weighted in, and Milli-Q water was introduced into a capsule by a pipette. The masses of the solid and the water introduced in the capsule were measured and noted. Approximately equal quantities of water and mixed powder were introduced into the capsule. Therefore, an amphibole-fluid equilibrium was promoted during the experiment.

Table 2.1.3 Compositions of starting materials

	CPX	OPX	SP1	SP2	SP3	SP4
SiO ₂	53.2(6)	56.1(5)	47.5(4)	43.1(6)	47.3(2)	37.5(1.0)
TiO ₂	0.57(6)	0.15(6)	0.42(6)	0.36(4)	0.38(3)	0.3(2)
Al ₂ O ₃	5.62(30)	3.40(13)	13.43(15)	12.11(24)	12.90(11)	10.1(5)
Cr ₂ O ₃	1.07(20)	0.42(6)	0.72(6)	0.67(8)	0.71(5)	0.60(24)
FeO	3.12(11)	6.32(23)	3.60(12)	3.13(16)	3.57(8)	2.88(39)
MgO	15.6(3)	33.9(4)	20.4(1)	24.0(3)	20.4(2)	36.96(93)
MnO	0.07(6)	0.11(5)	0.09(4)	0.09(4)	0.07(3)	0.07(15)
CaO	19.2(4)	0.66(5)	11.7(2)	10.6(2)	11.4(1)	8.97(62)
Na ₂ O	2.11(13)	0.14(4)	1.44(7)	2.14(10)	1.36(5)	2.09(29)
F	n.d.	n.d.	0.02(2)	4.81(7)	1.88(5)	0.51(24)
Total	100.56	101.20	99.34	101.62	99.98	100.00

n.d. indicates “not determined”.

2.2 Experimental Strategy

The aim of my thesis project is to study the behavior of elements under the condition of lower crust and upper mantle. Generally, its pressure ranges from 0.8 to 2.0 GPa and the temperature ranges from 700 to 1200 °C. The high pressure and high temperature experimental technique is a key for these experiments, especially the sealing technique. In this section, I will express the principles for selecting the suitable sealing technique for my study and its working process.

2.2.1 Sealing technique

For high pressure and high temperature experiments, people generally use arc-welding technique to seal metal capsules. However, it is not convenient for experiments with large quantity water, because such experiment makes the welding more difficult that water can be boiled, or we have to leave an enough space between the fluid and welding spots resulting in a bigger capsule (e.g. some solubility experiments, Newton and Manning, 2000, 2002; Manning et al., 2010). If the experiments are conducted with a buffer mixture, double capsule technique should be applied (e.g. Molina and Poli, 2000). This will also create a big capsule with a large temperature gradient during anneal, and that brings one advantage that it can convect the fluid perhaps more effectively than smaller gradient experiments and the movement of fluid may help precipitate large minerals.

Another sealing technique, which is developed by Ayers et al. (1992), solved some disadvantages of arc-welding technique for a large quantity water experiment. It is called cold-sealing technique, because the system is sealed by the inner capsule, which is made by soft noble metal, during initial compression at 0.5 GPa under room temperature, and subsequent annealing. The buffer compounds were prepared by oxidizing the outer chamber to form metal/metal oxides redox pair.

2.2.2 Capsule Materials and Buffers

The sample container of my study was designed by the above mentioned cold-sealing technique, with some modifications. First, the capsule was smaller than those of Ayers et al. (1992) to reduce temperature gradients. Nickel, titanium, or molybdenum were used as the outer chamber material. The dimensions of capsules were as follows: The small capsule chamber is with 4.0 outer diameter (od, all in mm hereinafter in this section), 4.0 height (h), and a 3.2 long (l) central hole with a 2.1 inner diameter (id). The large capsule chamber has the same dimensions except for the central hole with a 3.1 id. Ni capsules were heated from 900 to 1100 °C in an oven for 12-24 hours to make a layer of NiO forming a Ni/NiO (NNO) buffer. The Ni oxides layer formed under 1100 °C can reduce Ni contamination into inner capsule when experimental temperature is higher than 900 °C. Ti and Mo capsules were not oxidized, so the experiments in Ti and Mo chambers were unbuffered.

Gold tubes (small capsule: od=2.0, id=1.6, l=5.0; large capsule: od=3.0, id=2.6, l=5.0) were welded shut at one end, and tapped into the outer capsule. The open end of the inner gold capsule was ground until the sleeve was flush with the outer metal capsule, and then a 2400 mesh SiC paper was used to smooth the ground surface. Every gold lid is approximately 100 mg. Weigh the clean gold, and then melt it to form a sphere. Press the gold spheres with two hard cubes until their thicknesses are in the range 0.3-0.5. Cut them to a fit size before setup into the piston-cylinder.

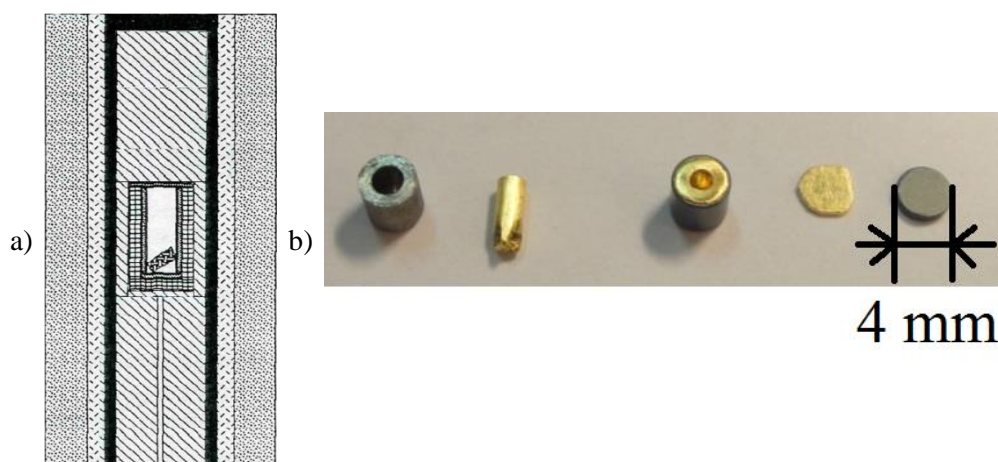


Fig. 2.2.2 a) the cross-section of the assemblies for a 3/4" piston-cylinder. Its outer diameter is 19.1mm. b) sample chamber materials, from left to right, they are nickel chamber without oxide layer, gold tube, prepared capsule with NNO buffer, gold lid, nickel lid, respectively.

2.2.3 High Pressure Apparatus – Piston Cylinder

Piston cylinder is a suitable apparatus for the experiments from 1 to 3 GPa, with a good pressure precision. The temperature can be controlled within the precision of ± 3 °C (e.g. Manning, 1994). The diameter dimensions of piston cylinder assemblage are 1/2 or 3/4 inch. Its capsule diameter can reach 5 mm, which is the largest in all the high-pressure experimental techniques (e.g. Manning, 1994).

The principle for acquiring high pressure is to increase enough force on a small area. The smaller the cross-section area, the higher pressure is gained with the same stress. In the piston cylinder apparatus, an experimental piston assemblage is placed in a vertical tungsten carbide piston (Fig. 2.2.3b and 2.2.3c). Thus, the pressure is created from the vertical orientation, which is uniaxial and non-isotropic, at ambient temperature. However, the NaCl external cell will become ductile and mobile when temperature is higher than 600 °C. It develops a quasi-hydrostatic stress field to reduce the previous uniaxial strain. With the known cross-section surface areas of ram and piston, the pressure in the sample room can be estimated by the equation: $P_{sample} = P_{oil} \cdot S_{ram}/S_{piston}$ (2.2.3). In my lab, the pressure of the piston cylinder is shown in the pressure indicator.

The high experimental temperature is supplied by the graphite furnace. With Joule effect, the graphite with large electric current (300 ~ 400 A, 4 ~ 5 V) can produce abundant heat. Moreover, the temperature is measured by a combined thermocouple, and controlled by a program, which was set manually in the Eurotherm controller. And the cooling water is kept running during the heating. It makes the heating in a stable equilibrium. It should be noted that the electric isolation of the assembly is crucial during the annealing. A pyrex cylinder is placed between the NaCl cell and the furnace, and another isolation sliver (phlogopite is the most suitable, between 1 and 2 in Fig. 2.2.3a) is under the base stopper. This will isolate from short-circuits (between 1 and 3 in Fig. 2.2.3a), and assure that most current will go through via the graphite furnace, and make the heating as effective as possible. However, it is easy to image that a significant thermal gradient will be present in the assemblage, so the dimensions of the MgO parts and capsules should be the same, which could make sure that experiments reproducibility on temperature control. Otherwise, every new set assemblage should be

calibrated with their sizes. Furthermore, I also put an MgO or alumina slice between the thermocouple and the capsule to avoid a potential contamination by the metal capsule. In this study, my experiments were conducted in both scaled piston-cylinder apparatuses available in Laboratoire Magmas et Volcans (LMV), Clermont-Ferrand, France: the 3/4 inch piston cylinder (Figure 2.2.3b) without end-load (Holloway and Wood, 1988) for experiments from 1 to 1.5 GPa, and the 1/2 inch piston cylinder (Figure 2.2.3c) with end-load (Boyd and England, 1960) for experiments from 2 to 3 GPa.

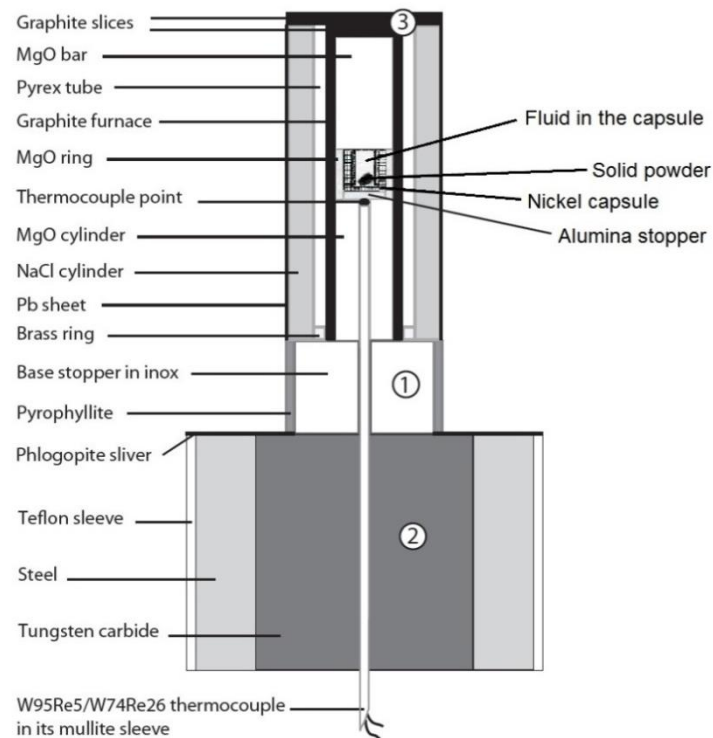


Fig. 2.2.3a Non-scaled schematic sketch of the core cross-section for 3/4 inch piston cylinder. 1, 2, and 3 represent the relevant parts used for short in the text (modified from Dalou, 2011).

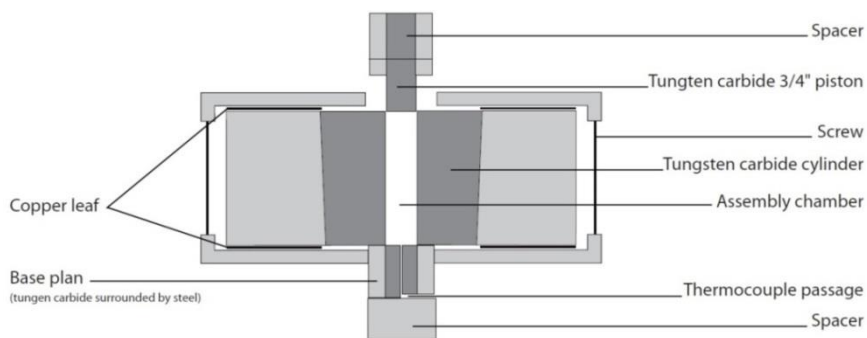


Fig. 2.2.3b Non-scaled drawing of one piston-cylinder 3/4 inch without end-load of the LMV (modified from Dalou, 2011). Assembly is in the tungsten carbide cylinder (i.d is 19.1mm) . Pressure is applied to the assembly between the piston and the base plan.

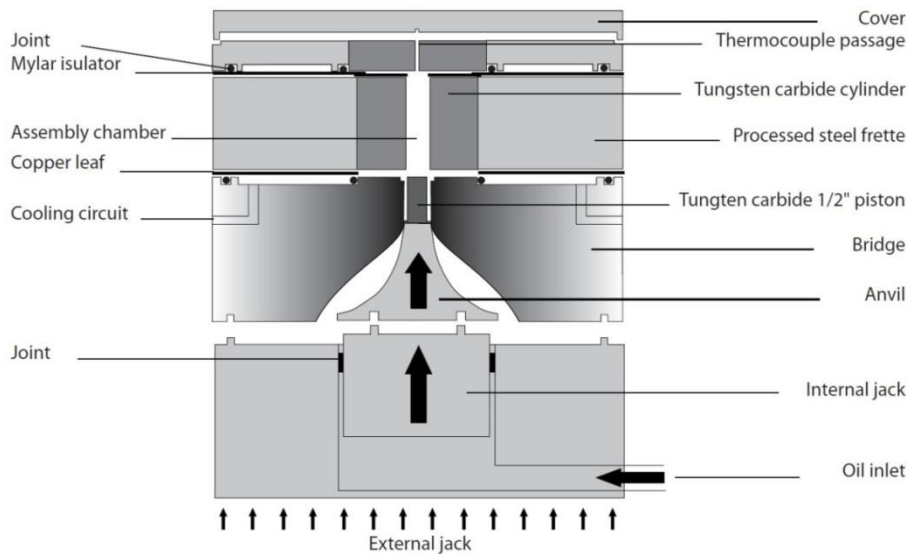


Fig. 2.2.3c Non-scaled drawing of the 1/2 inch piston-cylinder with back pressure of the LMV (cited from Dalou, 2011). Big arrows represent the pressure applied by the internal ram on the piston. Little arrows represent the end-load applied by the external ram on the tungsten carbide cylinder.

2.2.3.1 Dimension of Assemblies

As Fig. 2.2.2a shown, a NaCl-Pyrex composite cylinder was used as pressure medium, and a graphite cylinder serves as furnace. Between the graphite furnace and the metal capsule, crushable magnesia rods were placed as an insulator. The dimensions of magnesia parts were designed to position the capsule at the hot-spot of the assembly.

The details, such as the friction loss and temperature gradient, of the standard assembly used at LMV are found in the paper of Laporte et al. (2004). The sample capsule was surrounded by following materials: a magnesia ring ($h=5.1\text{mm}$) around the capsule, a gold lid (0.5 mm thick, well-polished) and a Ni lid (1.0 mm thick, with oxide layer) above the open end of the capsule. An alumina disk (0.8 mm thick) was placed between the thermocouple and the capsule to protect the thermocouple from contamination.

2.2.3.2 Temperature Calibration

With the knowledge of the cooling system structure in a piston cylinder, it is easy to realize that the temperature close to the cooling water is lower than other areas. Therefore, the

temperature inside the assemblage distributes differently in both horizontal and vertical gradient. It was strictly certified by Watson et al. (2002) with spinel which was formed by reactions between MgO (periclase) and Al₂O₃ (corundum). Meanwhile, they also showed that the temperature in the center is lower than close to the furnace in 3/4 inch piston cylinder. Moreover, the 1/2 inch piston assemblies are narrower, so its lateral temperature gradient is less. On the contrary, more significant temperature gradient is present in the longitudinal profiles, which have a parabolic tendency. The highest temperature area is defined as the hot spot. Temperature decreases dramatically from the hot spot to the end of the furnace (Watson et al., 2002).

Generally, the design of the assemblage should locate the sample room on the hot spot in the graphite furnace, within the most effective zone of 5 to 10 mm where temperature decrease less than 20 °C. The dimensions of my capsule and assemblies constrain the sample room away from the steep lateral gradient area, because they are perfectly centered with the concentric assemblies. Therefore, it is important to find the temperature gradient for each piston cylinder, and then one can calibrate the temperature offset caused by his assemblies.

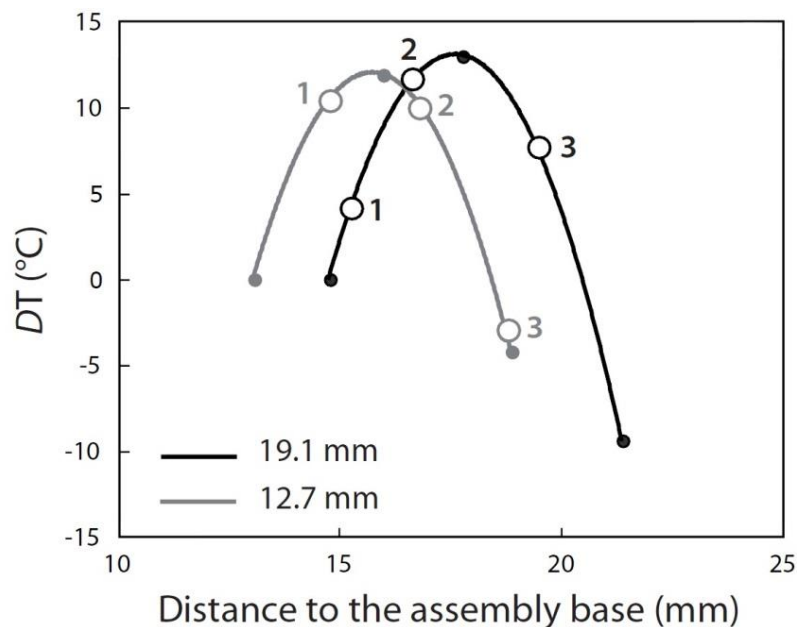


Fig. 2.2.3.2 Temperature calibration curves for both types assemblies: 19.1 mm (3/4", black curve) and 12.7 mm (1/2", gray curve) piston cylinders (cited from Celia, 2011). Measurements (solid symbols) were done at 900 °C and 1 GPa on the 3/4" (black points, Laporte et al., 2004) and at 1000 °C and 1 GPa on the 1/2" (grey points, Laporte, calibration for

group work). DT indicates the temperature difference between the measured position to the base of the assemblies (at 14.8 mm in the 3/4" and 13.1 mm in the 1/2"). Positions of points 1, 2, 3 are from Laporte et al. (2004): 1) the thermocouple tip, 2) the sample base and 3) the sample top.

In my study, I chose the calibrations of Laporte et al. (2004). Thermal profiles of Fig. 2.2.3.2 are applied to estimate temperature variations inside experimental assemblage. In my experiments, the height of inner capsule is maximally 4 mm, and is set on the hot stop of the furnace. Both in 3/4" and 1/2" assemblies, thermal gradient inside the sample room is maximally 2 °C. Because of the effective thermal conductivity of the metal capsules and the fluid convection in the sample room, I estimate that the temperature gradient in my sample room might be less than 2 °C, even if the assemblies are set within a little offset.

Temperature was measured and controlled by W₅Re₉₅-W₂₆Re₇₄ thermocouples. The deviation of the temperature calibration reported by the manufacturer (Concept Alloys, Inc.) is less than 3 °C when temperature is between 700 to 1000 °C. The temperature gradient between thermocouples and the hot spot is from 7 to 20 °C depending on the assembly used. The reported temperatures (Table 2.2.4) were adjusted accounting for these systematic offsets.

2.2.3.3 Heating and Pressurization

The solid mixture and the pure water were loaded into the capsule. Within 2 hours, the capsule was placed in the piston cylinder assembly.

The assemblies in the piston-cylinder without end-load were pressed cold to a pressure of approximately 0.50 to 0.65 GPa at ambient temperature. The temperature was raised to 650 °C at a rate of 50 °C /min. When the temperature reached 650 °C, the experiment was held at the condition for 8 minutes, and the pressure was kept constant. Then, the temperature was increased to the target temperature at a rate of 50 °C /min. During the temperature increasing process, the pressure was increased simultaneously until the desired value.

In the piston-cylinder with end-load, all the 2-3 GPa experiments were conducted. Generally, the end-load is applied once at room condition, to 3750 psi (Pound per Square Inch, 1 psi = 6894.8 Pa), then 0.50 – 0.65 GPa was manually reached by the raising internal ram and then heated to 650 °C. During this process, the pressure was raised continuously to reach 1 GPa. If the target experimental pressure is higher, e.g. 3 GPa, increase the end-load pressure by 1500 psi each time and then raise the internal pressure to corresponding value, which is shown in the Table 2.2.3.3. Repeat this step till the target pressure is reached.

Table 2.2.3.3 The inner pressure values versus the end-load pressure values.

P / GPa	PSI	P / GPa	PSI	P / GPa	PSI
0.6	2012	1.8	6036	3.0	10059
0.8	2682	2.0	6706	3.2	10730
1.0	3353	2.2	7377	3.4	11400
1.2	4024	2.4	8047	3.6	12071
1.4	4694	2.6	8718	3.8	12742
1.6	5365	2.8	9389	4.0	13412

During the experiments, a Eurotherm controller automatically controls temperature. Pressure is manually adjusted twice every 24 hours, and increases excess 0.02 GPa for overnight.

The experiment is terminated with cutting electric current supplied to the assembly. The water circuit accelerates the cooling of the assembly. Quench rate was fast; temperatures decreased 300 °C within the first two seconds of the quench, and fell below 200 °C within less than 12 seconds for ¾ inch piston cylinder and 10 seconds for ½ inch piston cylinder. After temperature is below 50 °C, release the pressure at a rate 0.001 GPa per 3-5 seconds till the pressure is decreased to 0.3 GPa. After that, it is feasible to decompress the assemblage quickly to the room pressure.

2.2.4 Experimental Conditions

The experiments were conducted at a pressure of 1 GPa and temperatures ranging from 750 to 1057 °C, for the duration of 34 to 330 hours. Higher pressure experiments are conducted with a 1/2" piston cylinder, every 0.5 GPa, from 1 to 3 GPa with SP2 starting material at 877 °C, for the duration from 94 to 191 hours. The conditions are reported in Table 2.2.4, except for some experiments in which samples were lost.

Experiments in small capsules above 900 °C were conducted with Mo outer capsules, because Mo did not contaminate the sample inside their Au inner capsules below 1050 °C, while significant amounts of Ni were found in crystalline phases formed in Ni/NiO capsules above 900 °C. With oxidizing the Ni capsule at 1100 °C, the Ni contamination was reduced with Au-Pd inner capsule. Thus, I form oxides layer with this method for the large Ni capsules.

However, the use of Mo capsules imposes a different oxygen fugacity.

The starting material was melted to a homogenous phase in graphite capsules. First, melting SP1 and SP2 were conducted at 1400 °C, but their products are not homogenous. It created melt and olivine. I increased temperature to 1550 °C, under 1 GPa and kept for 2 hours in the following melting experiment. This strategy made homogenous glass for SP1 to SP3 powders. However, SP4 is an MgO-rich powder. It was difficult to quench without quench growth phases, even at 1600 °C. I then mixed 40 % LiBO₂ with SP4 to decrease its melt point and managed to get a homogeneous phase. But the renormalized procedure led to its larger composition uncertainties. The conditions for these melt experiments are not shown in the table below.

Table 2.2.4 The experimental conditions and fluid mass after quench.

Expt. ID	Capsule Materials		Starting Material		Experimental Conditions			Fluid / mg
	Outer	Inner	Solid / mg	H ₂ O / mg	P _i / kbar	T / °C	Duration / h	
1-SP1-1	Ni/NiO	gold	3.1(1)	none	6.5	870	258	none
1-SP1-2	Ni/NiO	gold	1.9(1)	1.0(1)	6.0	955	119	0.0(1)
1-SP1-3	Ni/NiO	gold	1.2(1)	1.4(1)	6.5	955	70	0.3(1)
1-SP1-4	Ni/NiO	gold	2.0(1)	2.0(1)	6.5	900	94	0.9(1)
1-SP1-5	Ni/NiO	gold	1.5(1)	2.9(1)	6.5	877	242	1.6(1)
1-SP1-6	Ni/NiO	gold	1.4(1)	1.8(1)	5.0	827	330	0.6(1)
1-SP1-7	Ni/NiO	gold	3.1(1)	1.7(1)	5.5	857	278	1.0(1)
1-SP1-8	Ni/NiO	gold	1.91(1)	2.96(4)	6.0	807	114	1.21(4)
1-SP2-1	Ni/NiO	gold	9.7(1)	10.0(1)	5.0	770	113	4.5(1)
1-SP2-2	Ni/NiO	Au-Pd	4.4(1)	6.1(1)	5.3	1120	144	n.d
1-SP2-4	Ni/NiO	gold	1.3(1)	1.6(1)	6.5	870	77	1.6(1)
1-SP2-5	Ni/NiO	gold	1.1(1)	1.3(1)	6.0	955	72	0.1(1)
1-SP2-6	Ni/NiO	gold	1.6(1)	2.5(1)	6.5	900	94	n.d
1-SP2-7	Ni/NiO	gold	2.5(1)	3.4(1)	6.5	930	123	n.d
1-SP2-8	Ni/NiO	gold	2.0(1)	3.0(1)	6.5	827	312	1.8(1)
1-SP2-10	Ni/NiO	gold	1.5(1)	2.6(1)	6.5	787	117	n.d
1-SP2-12	Ni/NiO	gold	1.6(1)	3.4(1)	5.5	777	320	0.7(1)
1-SP2-13		Au-Pd	n.d	n.d	5.5	877	144	7.4(1)
1-SP2-14	Ti	gold	1.5(1)	2.6(1)	5.5	877	120	0.6(1)
1-SP2-15	Ti	gold	1.4(1)	2.2(1)	5.5	907	91	1.27(8)
1-SP2-16	Ti	gold	1.31(8)	3.65(5)	6.5	927	34	2.77(5)
1-SP2-17	Mo	gold	1.64(5)	3.3(1)	6.5	917	100	2.66(3)
1-SP2-18	Mo	gold	1.80(2)	2.03(2)	6.0	947	117	0.73(1)
1-SP2-19	Mo	gold	1.35(2)	n.d	6.0	977	94	1.00(4)
1-SP2-20	Mo	gold	1.53(3)	3.05(1)	6.5	1007	74	0.30(1)

2. Methods

Expt. ID	Capsule Materials		Starting Material		Experimental Conditions			Fluid / mg
	Outer	Inner	Solid / mg	H ₂ O / mg	P _i / kbar	T / °C	Duration / h	
1-SP2-21	Mo	gold	1.86(2)	1.38(5)	6.5	1057	73	0.84(1)
1-SP2-22	Ni/NiO	gold	1.46(1)	2.1(1)	5.0	850	123	n.d
1-SP2-23	Ni/NiO	gold	4.78(2)	5.3(1)	5.3	800	143	0.45(1)
1-SP2-24	Ni/NiO	gold	3.27(1)	5.9(1)	5.5	750	215	0.71(1)
2-SP2-1	Ni/NiO	gold	1.57(3)	2.08(4)	6.5	877	120	n.d
2-SP2-2	Ni/NiO	gold	1.68(3)	2.31(3)	6.0	857	118	n.d
2-SP2-3	Ni/NiO	gold	1.73(3)	2.17(3)	6.1	837	100	n.d
3-SP2-1	Ni/NiO	gold	1.44(3)	5.15(3)	6.0	877	96	0.94(3)
4-SP2-1	Ni/NiO	gold	1.64(2)	3.72(2)	6.2	877	95	0.49(4)
4-SP2-2	Ni/NiO	gold	2.04(3)	n.d	6.2	877	191	1.62(6)
5-SP2-1	Ni/NiO	gold	1.42(2)	1.93(7)	6.1	877	94	0.08(4)
1-SP3-1	Ni/NiO	gold	1.3(1)	2.1(1)	6.7	877	160	1.09(5)
1-SP3-2	Ni/NiO	gold	1.7(1)	2.3(1)	5.5	857	120	n.d
1-SP3-3	Ni/NiO	gold	1.4(1)	1.7(1)	6.0	857	119	0.28(5)
1-SP3-4	Ni/NiO	gold	1.7(1)	2.3(1)	6.0	837	169	1.76(4)
1-SP3-5	Ni/NiO	gold	1.4(1)	2.2(1)	5.8	887	117	n.d
1-SP3-6	Ni/NiO	gold	1.6(1)	2.1(1)	6.0	897	72	n.d
1-SP3-7	Ni/NiO	gold	1.66(3)	1.88(1)	5.5	817	162	n.d
1-SP3-8	Mo	gold	1.64(4)	2.34(6)	5.0	957	96	1.91(2)
1-SP4-1	Ni/NiO	gold	1.57(4)	n.d	6.5	877	188	n.d
1-SP4-2	Ni/NiO	gold	1.55(5)	1.7(1)	6.0	857	202	n.d
1-SP4-3	Ni/NiO	gold	2.13(3)	3.03(5)	5.5	890	>68	1.43(1)
1-SP4-4	Ni/NiO	gold	1.50(2)	2.59(2)	5.0	843	143	0.85(2)
1-(SP1+MgF ₂)	Ni/NiO	AuPd	6.37(2) SP1 0.77(1) MgF ₂	8.2(1)	5.5	965	118	1.25(2)
1-(SP1+CaF ₂)	Ni/NiO	gold	2.98(1) SP1 1.12(1) CaF ₂	7.6(1)	5.5	950	116	0.49(1)
1-(SP2+MgF ₂)	Ni/NiO	gold	1.8(1) SP2 1.1(1) MgF ₂	2.7(1)	5.5	877	190	n.d
1-(SP2+Qtz)	Ni/NiO	gold	4.28(1) SP2 6.63(1) Qtz	6.1(1)	5.0	950	94	4.53(1)

n.d indicates “not determined”. The first numbers of Expt. ID indicate the experimental pressure during annealing: from 1 to 5 represents 1.0, 1.5, 2.0, 2.5, and 3.0 GPa, respectively.

2.3 Post-quench Fluid Extraction

Different from anhydrous melt experiments, fluid is an important phase present in a large quantity water-bearing experiment. Fluid reacted with minerals or melt during anneal. It supplied OH for hydrous mineral precipitates. Moreover, it is able to dissolve some elements, e.g. Si, and Ti, under high temperature and high pressure conditions (Ayers and Watson, 1993; Manning, 1994). The fluid composition is key information for understanding the element behaviors between minerals and fluid. Unfortunately, fluid, unlike the solid phases, is difficult to analyze when it is kept in the capsule under room temperature. Generally, people use mass balance calculation to speculate the fluid composition (e.g., Molina and Poli, 2000). It is a big challenge to analyze the fluid composition with analytical apparatuses, but scientists expect the results from this manner. Some elements may precipitate during the quench and reduce their concentration in fluid, and it will lead to some uncertainties for collecting the fluid component. However, the results are important observations, which improve the knowledge about high-pressure fluid composition using direct measurement techniques.

2.3.1 Aim of the Extraction of Fluid

Under general analytical temperature, fluid is a liquid solution. It was not able to fix in epoxy for a solid state analysis. On the other hand, the solution analytical technique is quite different from minerals or melts. The ideal solution for this large quantity water-bearing experiment is *in-suit* observation of the fluid, but it is impossible for the samples with piston-cylinder apparatus. I want to extract the fluid from the capsule and then try to analyze it with different techniques. It should be noted to avoid any contamination from other sources. Generally, the procedure for opening a capsule follows next three steps.

2.3.2 Preparation for Opening Capsules

After quenching, assemblies were removed from the piston cylinder. The retrieved capsules were cut through perpendicularly at approximately 2 mm from the top with a lathe to

uncover the inner gold layer (Fig. 2.3.2b).

The surfaces of the capsules were cleaned of any adhering magnesia and NiO by means of a diamond drill. In order to avoid any contamination, I followed a 3-step procedure to clean charges, volumetric flasks and piercing tools (blade and tweezers): each was washed one time in detergent solution, followed by three times in tap water, and finally three times in deionized water, with each time lasting 5 minutes in an ultrasonic water bath.

All of the operations were done while wearing a pair of rubber gloves to prevent potential contaminations.

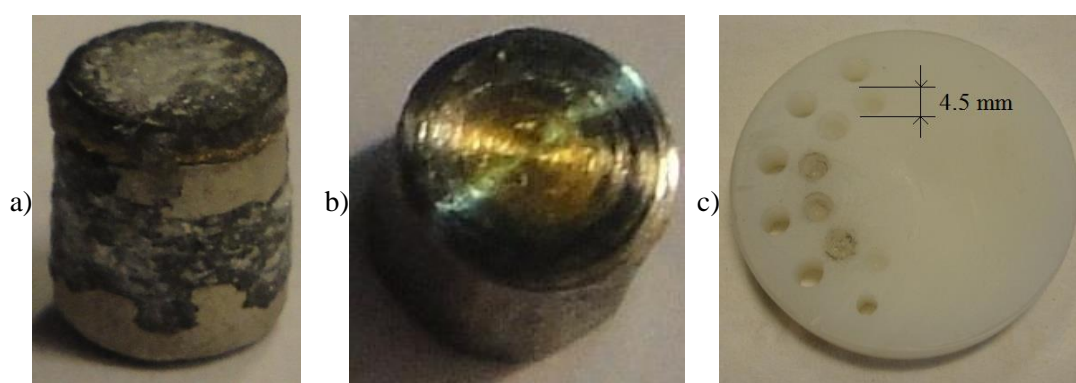


Fig. 2.3.2 The charges after the high pressure and high temperature experiments, and the tool made in house. a) right after taken out from piston-cylinder; b) after cleaning the surface with a diamond drill and a lathe. The diameter of the charge is around 4 mm. c) The holder for the charges after experiments. Five holes with i.d. range from 4.1 to 4.5 mm. Because of the high pressure during anneal, the capsules will be deformed to be wider. And a layer aluminum paper separated the charges and the holder to prevent contamination.

2.3.3 Two Ways for Opening

After cleaning all the tools and the charge, I manage to open the charge with two ways. One is to pierce the top of the inner capsule with a blade. The other is polishing from a side of a charge and to pierce from there. Every cleaned capsule was weighted before piercing the capsule with a blade in the revealed gold area.

2.3.3.1 From the Top

In this case, I put an unopened charge in the holder (Fig. 2.3.2c), and I operated under a binocular. Because the thinnest part on the top of inner capsule is the inner edge, it is the easiest to pierce from there. However, it is difficult to estimate how long should be cut from the top of the charge, because the capsule suffered deformation during the experiment. It is normal that I cannot pierce the capsule to reach the sample room in one operation. Then I have to cut the charge more with the lathe and repeat this post-quench procedure several times until I open the capsule or find the fluid come out from the capsule.

It is indispensable to assure that the capsule opened totally, because gold is soft enough to deform easily and close the gap with repeating piercing. For example, the fluids from experiments 1-SP2-15 and 1-SP3-4 were not collected in once, but twice. To avoid this situation, I improved it as two steps: retrieve the fluid as soon as it comes out, and then pierce deeper to open the capsule totally and retrieve the fluid for the second time. It should be noted that the cutting should not lose any capsule material, since it will influence the result of fluid quantity.

2.3.3.2 From the Vertical Side

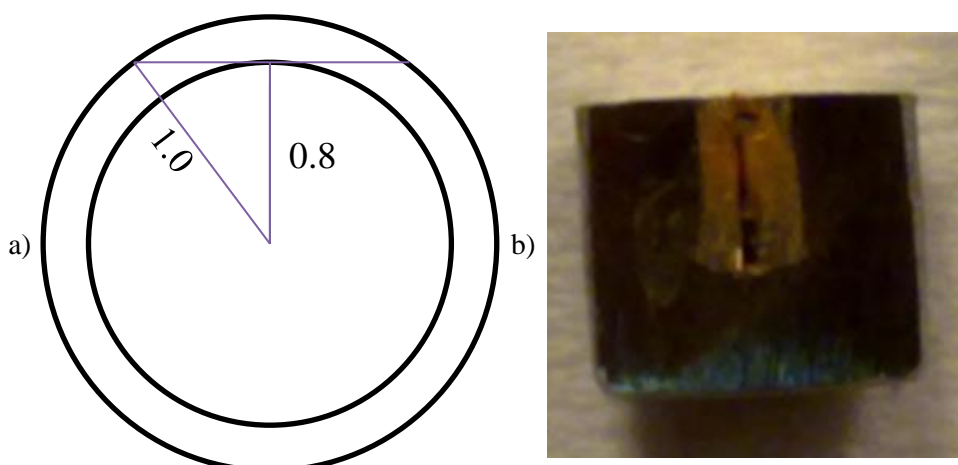


Fig. 2.3.3.2 a) An sketch example to calculate the width of the cross-section in the small gold tube. b) A charge opened from a side. The width of its gold layer is approximately 1.2 mm. It is easier to pierce the gold layer from the bottom than from the top. It indicates more empty space inside can make pierce easier.

To avoid the uncertainty of the cutting from the top, opening the capsule from its vertical side is another way. With the help of a polishing belt apparatus, it is quick to reduce the distance from the edge of the charge. In order to ease the polishing and placement of the sample: 1) I polished the charge from any side until the inner layer appeared; 2) from its opposite side, I polished the charge to the inner gold layer as thin as possible.

I have two ways to identify the end of polishing.

1) By measuring the width of the cross-section of the inner layer. The dimensions of inner gold tube are known. With its id and od value, it is able to calculate the exposed width of the section of inner gold layer. For example, as Fig. 2.3.3.2a shown, the smaller size gold tube has 2.0 mm od and 1.6 mm id, then its widest section is $2 \times \sqrt{1.0^2 - 0.8^2} = 1.2mm$.

2) By the color of the gold layer. Gold is soft and ductile. It is transparent when it is thin enough. When the gold section exposes during the polishing, its color of this region is homogeneous. After the width of gold section reaches around 1 mm, slow down the rate of polishing and check its color. If some parts become darker than others, it indicates that it is thin enough to display the inside dark of the charge. In this case, it is easy to pierce the gold layer.

Generally speaking, opening from the vertical side is not difficult if there is space occupied by fluid. As Fig. 2.3.3.2b shown, it is easier to open the charge from the vertical side than from the top. But when experiments failed and lost almost all of water, the sample room would be pressed to a volume as tight as possible. In that case, it is hard to tell whether it is opened or not only by eyes' observation, while it is possible to watch the sample inside with a microscope.

2.3.3.3 Comparisons of these two methods

Two methods above for opening the charges have advantages and disadvantages of themselves. The same points are piercing from the soft area and cutting or polishing the charges to make the opening as easy as possible.

Obviously, the latter method is more efficient than the former. It shortens the whole duration of the post-quench sample preparation. But a shortcoming is that it is not able to

observe the inside of the capsule after opening it, because the cross-section area too small to gash a large window for observations. The most bothering disadvantage of the first method is that it is impossible to determine how much should be cut from the top. Sometimes, the cutting is perfect by chance that I can pierce the charge very easily. Even once, when I just push the cover slightly, the cover will drop into the capsule and I am able to observe the minerals inside and to pick up some big crystals from the charges.

2.3.4 Transfer the Fluid into Volumetric Flasks

Once the fluid part in the capsule came out, the opened capsule was submerged into deionized water in a beaker. Retrieve the fluid with an ultrasonic water bath for 2 minutes. Then the fluid was transported into a 10 to 50 mL volumetric flask. This resulted in dilutions varying of approximately from 3600 to 36000 times. The opened capsules were then dried for one day in an oven (120 °C) and reweighed. The difference in weight represents the fluid mass present after the experiment.

2.4 Electron Microprobe Analyses for Solid Phases

The solid phases in the capsules could be fixed in the epoxy mount. The electron microprobe technique is convenient to analyze the compositions of solid phases. For major elements besides F, I analyzed them with electron microprobe. It is important to get precise mineral compositions, so I will introduce the procedure of solid phase analyses in this section.

2.4.1 Samples Preparation

After retrieving the fluid of the charges and drying in the oven overnight, the charge was embedded in epoxy with a mold. Samples were then polished with different grade of silicon carbide grinding paper (from 220 to 2400 grid) and following polishing discs with fluid suspended diamonds (6, 3 and 1/4 μm). For every step, the polished surface of the sample was cleaned with ethanol in an ultrasonic water bath. The surface of the sample was then dried and

coated with a layer of carbon for the electron microprobe analyses.

2.4.2 Principle of the analysis

The electron microprobe primarily contains one electron gun and four wavelength dispersive spectrometers (WDS, Fig. 2.4.2). The sample room will be vacuumed after loading samples. The electron gun bombards the sample with an electron beam, and its beam size or focus is controlled by several electromagnetic lenses. The emitted X-rays with characteristic wavelength of elements will be received by a detector, after the element electron was excited by the high energy electrons. The detected intensity generally is proportional to the element concentration. Each detector with different specifically orientated monochromatic single crystal will obtain various sensitive regions. However, it should be noted that the X-ray may excite the nearby atoms to create the secondary X-ray, which can affect the signal intensities. With the standard calibrations, and comparing the wavelengths and the X-ray intensity, the composition can be determined quantitatively, as well as corrected the matrix effects by the software automatically.

Electron microscopy is an *in-situ* non-destructive analytical technique. The compositions of solid phases in all experimental run products were analyzed using a CAMECA SX 100 electron microprobe at Laboratoire Magmas et Volcans.

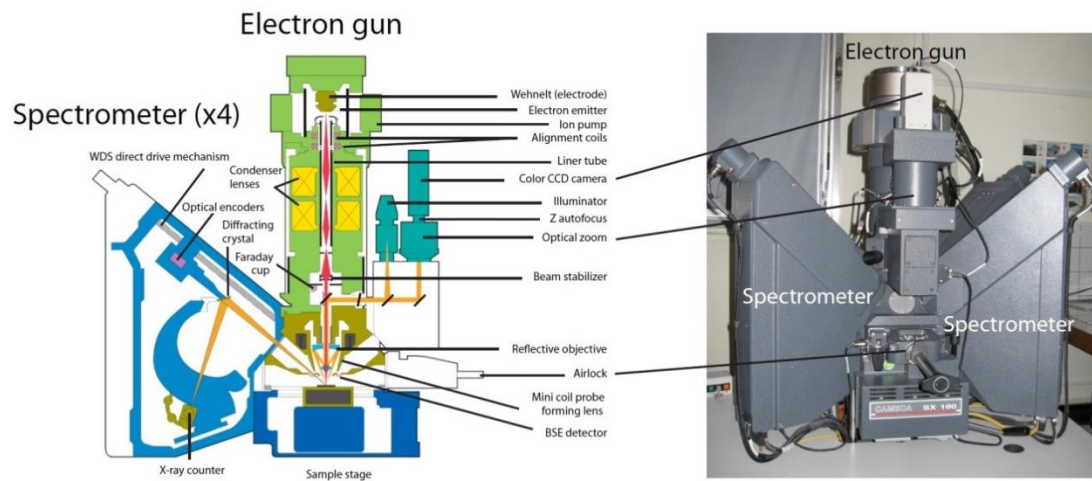


Fig. 2.4.2 Captioned drawing (left) and object picture (right) of the electron microprobe CAMECA SX 100 at Laboratoire Magmas et Volcans (cited from Celia, 2011).

2.4.3 Analytical Parameters

A 10 nA beam current, 15 kV accelerating potential and 10-second peak counting time were used for major elements in minerals and glasses. Beam diameters were 10-100 μm for glasses, and 0 μm for crystalline phases. Calibrations of major elements were carried out using: wollastonite (Si, Ca), MnTiO_3 (Mn, Ti), Cr_2O_3 (Cr), Al_2O_3 (Al), forsterite (Mg), fayalite (Fe), NiO/ olivine (Ni), and albite (Na). To measure the F concentration, a 40 nA beam current, 15 kV accelerating potential, and 30-second peak counting time were employed. The standard for F calibration was crystalline CaF_2 . All backgrounds were measured for the same time periods. Because of high F concentrations in minerals, instead of the analytical method by Witter and Kuehner (2004), I used an interference-free TAP detector method used in our group (Moune et al., 2007).

Generally, I did not measure oxygen concentration for routine analyses, and the compositions were reported as oxides. The valid totals of anhydrous minerals are between 99 to 101 wt%, except spinel, because the total values of olivine and pyroxene fit for this range well. But spinel with high Fe^{3+} concentration can miss total, because electron microprobe counts all iron as FeO. And its total cannot even reach 98 wt% with stoichiometry calculations, which indicates the oxygen loss might influence the matrix effect correction of the software. On the other hand, the totals of hydrous minerals, especially F-rich hornblende, are always lower than 99 wt% after excluding the oxygen substituted by F. It is possible to tell their validities, after I calculate their water concentrations by stoichiometry calculations. Because the total missing for hornblende is always present and most of the total is approximately 99.5 wt%, I normally set the valid interval as 98.5 to 100.5 wt%. However, when I measure some melt compositions with degassed bubbles, of which total is much lower than 100 wt%, it is impossible to treat the missing part as water. In order to determine the water content in these melt, I measure their oxygen concentration, and then it is possible to estimate the water concentration by charge balance.

2.4.4 Stoichiometry Calculations

In my experiments, I created several hydrous minerals, such as hornblende, humite group minerals and hydrogrossular, and some anhydrous minerals, e.g., pyroxene, olivine, and spinel. Because hornblende and hydrogrossular are mixture of different end-members, their chemical formulas are complicated and not easy to calculate their stoichiometry. In the subsection, I will introduce the details of stoichiometry calculations for hornblende, hydrogrossular and spinel. On the contrary, other simple structure minerals are easy to get their formulas. For example, when I calculate with pyroxene composition, I set its oxygen number as 6, and then I will get the total number of cations as 4. It fits pyroxene chemical formula very well. The same situations happen to olivine and humite group minerals.

It should be noted that I count every 2F and/or 2OH as O for hydrous minerals. For instance, the chemical formula of norbergite has 4 O and 2 OH. When I play its stoichiometry calculation, I set there are 5 O (or divalent anions), then I will get 4 cations in total number. The concentrations of H₂O in hydrous minerals were estimated by stoichiometry. Because F substitutes into the hydroxyl site, the remainders of the OH sites are OH. Once the OH concentration had been determined, the water concentration was calculated by multiplying by a factor of 18/34, which is molar mass ratio of H₂O/2OH. The resulting data are used in the mass balance calculations.

Moreover, it is possible to analyze the water and F concentration with SIMS more precisely. But the dimensions of the crystals are too small to analyze with SIMS, especially hornblende. It is always easy to become longer but not wider. Without seed, the crystals in the low temperature experiments cannot grow large enough for the analysis.

2.4.4.1 Hornblende

Hornblende is a mineral subgroup of the amphibole group. It is a hydrous chain silicate, which has a complicated structure. Its chemical formula is $(\text{Na}, \text{K})_{0-1}\text{Ca}_2(\text{Mg}, \text{Fe}^{2+}, \text{Fe}^{3+}, \text{Al})_5\text{Si}_{6-7.5}\text{Al}_{2-0.5}\text{O}_{22}(\text{OH})_2$. In its T site, Al can substitute Si site. In order to balance the charges, Al can enter C site and Na/K can enter A site. The total number of its cations will not be an

integer, when the hornblende is not an end-member.

Iron can exist in hornblende as both Fe^{2+} and Fe^{3+} . While electron microprobe results only report the iron concentration as FeO, it makes the divalent anion number, 23, with a large uncertainty. Even if I measure the oxygen concentrations of hornblendes, I cannot calculate its exact chemical formula. Therefore, instead of assuming an initial oxygen number to follow normal calculating strategy, I prefer to start this stoichiometry calculation from the total cation number, because its chemical formula shows its total cation number is fixed as 15 (exclude A-site number). Moreover, there are 2OH per formula unit in hornblende, so it is feasible to calculate OH number from its F number in the stoichiometry and the water concentration in hornblende.

2.4.4.2 Hydrogrossular

Garnet grains appear in the experiments at 2.5 and 3.0 GPa. Their F concentrations are more than 1 wt%, so there are substantial hydroxyl sites in the mineral. Hydrogrossular, $\text{Ca}_3\text{Al}_2\text{Si}_2\text{O}_8(\text{SiO}_4)_{1-m}(\text{OH})_{4m}$, contains 3 divalent metal cations and 2 trivalent metal cations. It is the unique garnet species with hydroxyl sites. I have verified the presence of hydrogrossular by assuming the divalent anion number in garnet as 12; the number of ferric ions (a) is determined by the sum of Fe, Mg, and Ca minus 3. On the other hand, a part of SiO_2 is replaced by $2\text{H}_2\text{O}$. If I want to calculate its water concentration, I should know its m value, while this may be different among the garnet grains. Following the principle above, m is equal to $3-n(\text{Si})$. Then the divalent anion number is corrected by m and ferric ions values: $12-a/2-2m$. Use this value as the total divalent anions number of hydrogrossular, the values of a and m are revised. Repeat this process iteratively until the corrected oxygen number is convergent. I can then calculate the water concentration and the F proportion in OH site.

2.4.4.3 Spinel

Spinel is a non-silicate mineral. Generally, its chemical formula contains one divalent cation, two trivalent cations and four oxygen ions. It is an anhydrous mineral and simple

structure, so its stoichiometry calculation is much easier than hornblende and hydrogrossular. The unique problem is to determine the abundance of ferric ion, because electron microprobe gives the Fe concentration as FeO. If ferric ion concentration is high, the oxygen number will be less than 4 and the total cannot reach to 100 wt%.

The strategy assumes the cation number is 3 for the stoichiometry calculation. For example, 1-SP2-20 experiment created some spinel. Following the strategy above, the spinel average oxygen number is 3.70. It indicates a part of iron should be present as ferric ion. Excluding Fe^{2+} , the total number of other divalent ions is 0.84, so $n(\text{Fe}^{2+})$ is 0.16. Remaining Fe must be $n(\text{Fe}^{3+})$, which is equal to 0.60. With both proportions of ferrous and ferric ions, I recalculate the concentration of Fe_2O_3 and FeO. Then the total is closer to 100 wt%. The missing part is considered as derived from the oxygen number differences, which lead to the difference of the matrix correction of electron microprobe. However, given the total is within an acceptable range, I did not recalculate the matrix corrections with correct oxygen abundance.

2.5 Analytical Technique for Solutions

Generally, if I know the composition of each solid phase, starting material and their proportions, I could use mass balance to calculate the fluid compositions. It will be discussed in section 2.6. However, it would be necessary to develop some analytical methods for direct measurement for the confirmation of these mass balance calculations.

2.5.1 Potential Candidates Technique

There are many methods for analyzing the compositions of solution samples. Chemical titration usually is a precise way to determine the concentration of a certain ion. Its procedure is complicated but its precision and accuracy is better than calibration-dependent instrument analyses. On the contrary, there are instruments adapted to measure liquid compositions, such as chromatography (GC or LC), mass spectrometer (MS), and atomic emission and absorption

spectra (AES, AAS). Their advantages are their rapid analyses and easy procedures. Normally, after a calibration, these instruments can analyze the sample semi-automatically. However, each technique can only analyze specific elements or ions, which is constrained by their characteristics. For example, AES and AAS are applied to analyze the metallic elements, no matter the element species in the solution, such as cation and/or complex ion.

In this study, measurement of F concentration in the solutions is the main target. Fluorine ion is the most likely species of F in the solution. While F^- is also a strong electronegative coordination anion, it perhaps reacts with Si under high pressure and high temperature in the fluid, to form some complex ion, e.g., SiF_6^{2-} in basic condition or SiF_4 in weak acid condition. The activity of H and OH increases under high pressure and high temperature, so it is hard to determine what exactly happened in such situation. Moreover, the fluorine complexes with Fe, Ca and Mg have been reported by chemists. Thus, F exists in these various ions, the best method to analyze it with MS. Because MS could break molecular ions as elemental particles, and then measure them quantitatively, the most suitable instrument probably is ICP-MS. However, ICP-MS is not a suitable approach for F analysis, and many ICP-MS applied in geology were contaminated by F due to the use of HF in rock digestion. This makes the background for F measurement high and is impossible to analyze F concentration in such an ICP-MS instrument. And ICP-MS is not sensitive for the light anion analysis, so it is not suitable for F.

Considering that the most of F is present in the solution as monatomic anion, two standard methods for analyzing it in solution have been used widely in environmental researches. One is high performance liquid chromatography, the other is selective electrode.

Both of them are mature and suitable techniques for the fluorine ion analysis in principle, but it is necessary to check the feasibility for my lab condition. With a guidebook of a combination fluoride electrode (Mettler Toledo company), I primarily understood that there are a few problems for our measurements:

- 1) For a low level measurement, I must stir the solution at a uniform rate. To put a stirring bar and the electrode in the fluid at the same time, at least 30 mL solution is required. Normally, the dilute solution is only 10 mL with unknown F concentration.

- 2) This measurement requires a certain total ionic strength in all standards and samples.

My solution samples are diluted at least 3600 times. They are nearly pure water with low ionic strength. In this case, a total ionic strength adjustment buffer should be added, which provides a constant background ionic strength, decomposes fluoride complexes ions and adjusts the solution pH. After this measurement, my sample is not available for any other analyses.

3) I did not find this kind of selective electrode for testing and develop a procedure for my aims.

Based on these reasons above, I decide to analyze the solutions with high performance liquid chromatography.

2.5.2 High Performance Liquid Chromatography

High performance liquid chromatography (also named high pressure liquid chromatography; HPLC) is a chromatographic technique used to separate a mixture of compounds in analytical chemistry. It can be used for quantitatively analysis of the specific components. With modern computer technique, its automatic measurements are much more efficient than traditional manual chromatography operation.

2.5.2.1 HPLC Principle and Operation

HPLC contains three main parts: a column, a pump, and a detector (Fig.2.5.2.1). A sample for analysis is introduced with an injector in a discrete small chamber. It will be mixed with the mobile phase and go through the column. In the column, the velocity of each component of the sample is different. The time, when a specific analyte emerges from the column, is called the retention time. With a specific condition, the retention time of a given analyte can be considered as an identifying characteristic.

The column is filled with the stationary phases, which is specially chosen for the species of the analytes. It is very important to choose the suitable stationary phase and mobile phase to separate the target species in the mixture solution, because the retention time is resulted from interactions between the solution species and the stationary phase or mobile phase, flow

rate of mobile phase, and the column dimensions. Moreover, because the packed column is dense, the high pressure is necessary to move the mobile phase and sample efficiently. Thus, a pump is utilized to increase this pressure, which will significant to improve chromatographic resolution.

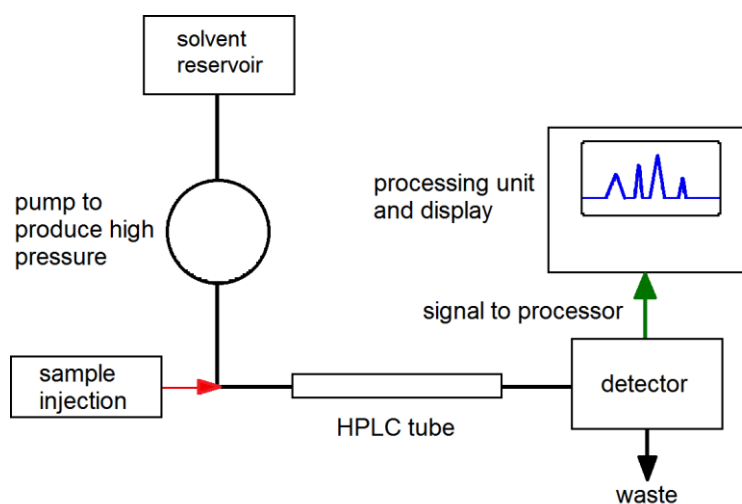


Fig. 2.5.2.1 A sketch map of a HPLC instrument.

The pump supplies enough pressure to move the mobile phase and sample solution through the column. The detector can display the signals when each analyte passes through. The corresponding characteristic retention time and area counts of the sample components will be noted.

Nowadays, HPLC is a mature analytical technique for detecting many normal species. For the normal cations and anions, several columns are available supplied by some companies. It is feasible to find a suitable one for general analysis following their introduction (the correlative mobile phase and parameter information).

2.5.2.2 Tests on HPLC Analysis

I tested the measurements with HPLC, in OPGC, Cezeaux, Aubiere. The first fluid sample from 1-SP2-4 was analyzed by DIONEX ISCI-1500 Ion Chromatograph. The chromatographic solution is 15% KOH solution and deionized water. The column is AS11-HC. This column is for resolving a large number of inorganic anions and organic acid anions in

complex matrices. Each measurement uses 5 mL fluid sample. This ion chromatograph can analyze anions and cations at the same time.

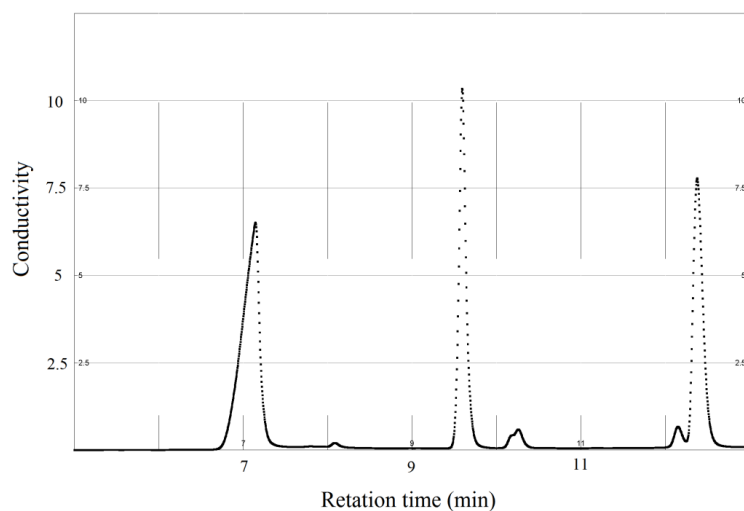


Fig. 2.5.2.2a The chromatogram of the first analysis (a fluid solution of 1-SP2-4) with HPLC, at OPGC, in Mar. 2010.

From 6 to 13 minutes retention time, fluorine ion, acetate, formate, methylsulfonate, chloride, nitrate peaks will occur. The retention times of three largest peaks are 7.1, 9.6 and 12.4 minutes (Fig. 2.5.2.2a). I thought they are F^- , Cl^- and NO_3^- , and it was surprised that there are so much chloride and nitrate anion in my sample. I suspected that they come from the background of our laboratory environment. After this test, I have tried to measure another set samples and the deionized water kept in flasks for different durations. For these low concentration solutions, I cannot identify their exact F peaks in a series of peaks from 6 to 8 minutes retention time of the chromatogram, because of the lack of the coincident standard F solution analysis. I then run the standard solution to determine the position (retention time) of fluorine ion peak. Unfortunately, the HPLC instrument in OPGC seems to be contaminated by unknown organic materials. Most of the samples have a complex peak around 6 minutes (Fig.2.5.2.2b). It is impossible to tell fluorine ion peak from another. I have to stop passing my samples at OPGC. In the end I found another group who studied fluorine and chlorine with HPLC. They use a special column for separating them and all the problems have disappeared.

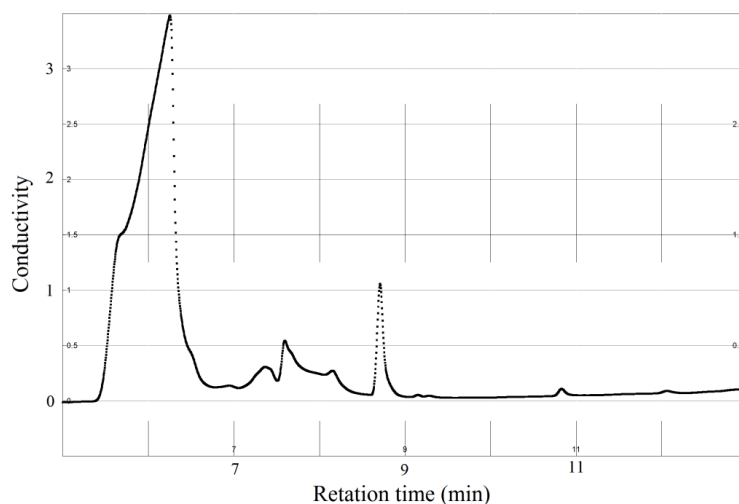


Fig. 2.5.2.2b A chromatogram of a fluorine standard solution. This measurement was conducted on Feb. 8th 2011. There are too much complex peaks in this chromatogram. It indicates HPLC instrument was contaminated.

2.5.2.3 Current Setting for HPLC Analysis

2.5.2.3.1 Basic Parameters

The current HPLC analyses were conducted with DIONEX DX-120 Ion Chromatograph at Institute de Physique du Globe de Paris. For anion analysis, AS9-HC column is employed, as it is suited to quantify F^- , Cl^- and SO_4^{2-} . The eluent is 9 mmol/L Na_2CO_3 (calculated pH is ~12.4) and the flow rate is 0.85 mL/min. Each measurement requires approximately 1 mL fluid sample. For cations, a CS12A column is suitable for quantifying Na^+ , Mg^{2+} , Ca^{2+} and K^+ . Its eluent is 20 mmol/L CH_4O_3S , and the flow rate is 0.98 mL/min. A measurement requires at most 2.5 mL fluid. All anion analyses were repeated twice. The results are accurate within 2% uncertainty.

2.5.2.3.2 Calibrations

The calibrations are conducted before our sample measurements. For fluorine ion, six different concentration standard solutions and a blank solution are analyzed (from 0.102 to 19.99 ppm). F concentration in our sample is from 20 ppb to 1 ppm, so I only use 4 calibration data points (0.102 to 4.902 ppm) to fit the work linear. The blank solution shows no fluorine ion peak. The function intercept is forced to 0. The linear function below could be

used to $y=1.5643x$, $R^2=0.9992$, where y is F concentration (ppm) and x is F peak area ($\mu\text{S}\cdot\text{min}$). The same calibrations are conducted for Na^+ , K^+ , Mg^{2+} and Ca^{2+} .

Table 2.5.2.3.2 The calibration parameters for Na^+ , K^+ , Mg^{2+} and Ca^{2+} concentrations.

Peak Name	Slope	Offset	R^2
Na^+	0.1909	-0.0425	0.9998
K^+	0.1205	-0.0056	0.9998
Mg^{2+}	0.3606	-0.0093	0.9998
Ca^{2+}	0.235	0.0019	0.9999

2.5.2.3.3 Measurements

Generally, after finishing the calibration and inputting these parameters into the software, I can get the concentration by reading its integrated area with the software directly. Unfortunately, two samples have a double peak when F peak appears.

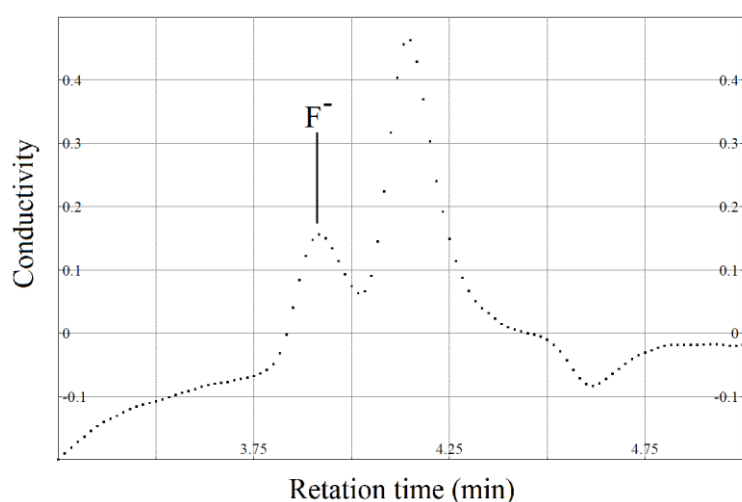


Fig. 2.5.2.3.3 The chromatogram of the 1-SP2-14 solution. It is a rare example of the double peaks measurement. With the coincident standard F solution, it is easy to tell the first peak is F, and the latter represents an organic contamination.

Because two peaks in the double peak are of different height, it is not precise to read the area from the software directly. I decided to separate the peaks and calculate all the F peak areas with PeakFit4. The parameters for peak fitting are below: 1) Baseline: Best, D2; 2) Smoothing: Savitsky-Golay; 3) Peak type: chromatography – GMG. 4) AutoScan: Amp% number is depended on different situations. Select ‘vary widths’ and ‘vary shape’. Then run the PeakFit until no changes. Two data in the results should be noticed: area and center. The

center value means the retention time. Generally it is very close to the value read by software with an uncertainty 0.1 min. The area values are used to determine F concentration, and then correct it by a dilution factor. It is able to get the F concentration of fluid in the capsule.

The concentrations of Na^+ , K^+ , Mg^{2+} and Ca^{2+} in my samples are calculated by the software automatically. This work was performed by Caroline Gorge (IPGP).

2.5.3 ICP-AES

Inductively coupled plasma atomic emission spectroscopy (ICP-AES), which also referred to as inductively coupled plasma optical emission spectrometry (ICP-OES), is an analytical technique used to analyze cations. It is an emission spectroscopy, which uses ICP to excite atoms and ions, and then emit electromagnetic radiation at wavelengths characteristic to a particular element. The intensity of this emission signal is proportional with the concentration of the element within the sample. After I finished HPLC measurement, some samples have approximately 4 mL left, which is enough for ICP-AES analyses. ICP-AES measurements were performed by Mhammed Benbakkar at Laboratoire Magmas et Volcans.

2.5.3.1 Principle

Any ICP-AES instrument, by its operation principle described above, must incorporate a mechanism that transforms the test sample into incandescent plasma and a device that measures the absorbance of the plasma at the specified wavelength. As shown in Figure 2.5.3.1, the plasma-generating unit of the instrument can be further dissected into three components: the radio-frequency (RF) induction coil, the plasma torch and the nebulizer. After uptake or injection, the sample is first transported through the assistance of a peristaltic pump into the nebulizer, where it is converted to aerosol by an intense inflow of humidified argon and continuously injected into the spray chamber. Accumulation of the sample aerosol in the chamber drives a small portion of it vertically up into the torch, whereas a vast majority of the aerosol settles down and eventually drains through the waste outlet.

The torch features 3 concentric layers of quartz glass tubes that are all filled with argon,

but for different purposes. While in the outer sheath it serves as the cooling gas to shield the torch from the extreme temperature inside, the argon in the middle layer of tube follows a tangential path that spirals up the torch and is crucial for the generation and maintenance of the plasma. This argon is first ionized by a brief discharge arc, creating charged particles that, at a sufficient concentration, to ignite the plasma. The inner quartz glass tube is the path for solution sample introduced into the plasma flame. The sample should be an aqueous solution, which is transport in the spray chamber under the help of a peristaltic pump and a nebulizer. As soon as reaching the plasma area, the analytes break down into charged ions, and then to the respective atoms. In the plasma, the loss and gain of the electrons on each atom repeatedly occur, giving off its characteristic wavelength radiation.

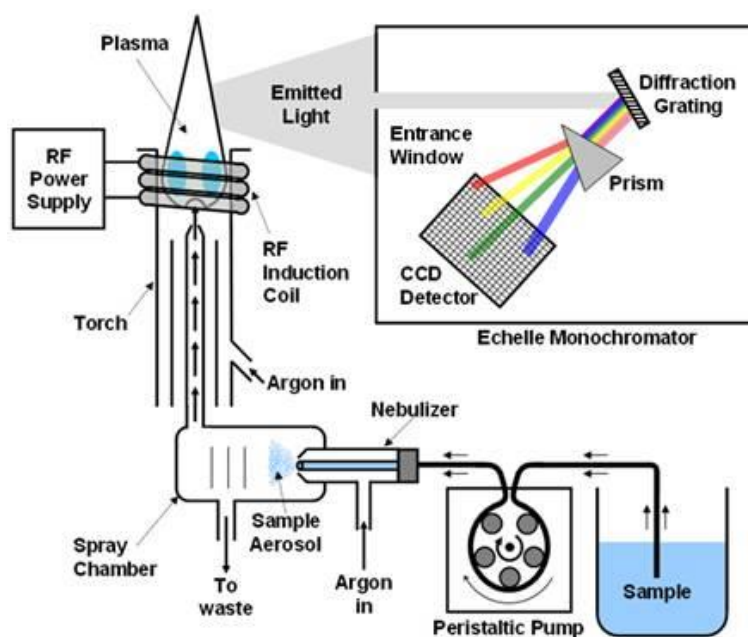


Fig. 2.5.3.1 A sketch figure of ICP-AES structure and working mechanism.

The photoemission of the plasma then passes the narrow slit of the monochromator and is separated into single-color beams on a diffraction grating. These monochromatic beams are diverged onto different locations of the CCD detector to enable simultaneous absorbance measurements at multiple wavelengths. To find out the abundance of an element in the sample, the absorbance at its peculiar wavelength is then interpolated from the calibration curve plotted beforehand using linear regression from a series of standard solution whose concentrations are known. During data processing, computer-assisted data analysis and

refining can often be necessary to resolve interferences that stem from element emitting at wavelengths close to each other.

2.5.3.2 Calibration Parameters

Major element compositions (e.g. Ca, K, Mg, Na and Si) were measured on ULTIMA C Horiba-Jobin-Yvon ICP-AES. The ICP-AES analytical conditions are: Incident power is 1050 W, reflected power is less than 15 W. Plasma gas flow rate is 14 L/min, permanent gas flow rate is 0.2 L/min, and carrier gas flow rate is 0.8 L/min. Solution uptake is 0.8 L/min.

The first order analyses are semi-quantitative measurements, because we only use one blank solution and one 10 ppm standard solution for calibration. These information are input into the software and then it can give the concentration of the unknown samples directly.

Table 2.5.3.2 ICP-AES Calibration parameters of five major elements

Elements	Detect Wavelength	Intensity of Calibration Solution	
	nm	Blank	10 ppm
Ca	317.933	70382.97	1018919.4
K	766.490	12021.38	65917.00
Mg	279.553	111814.97	864833.23
Na	589.592	3038.91	105241.40
Si	288.158	175699.41	2507716.0

2.5.4 ICP-MS

Inductively coupled plasma mass spectrometry (ICP-MS) is a powerful tool for detecting trace amounts of elements (typically metals) from various samples of complex composition, often at abundances as low as 10^{-12} . The method employs roughly the same technique to generate sample plasma, whose ions are then separated through a quadrupole mass filter according to their respective mass-to-charge ratios. ICP-MS offers advantages in the areas of faster measurement, higher precision and lower detection limit over AAS. However, its extreme sensitivity renders it susceptible to trace amount of environmental contaminants, as well as false positives resulting from ions that have near-identical mass-to-charge ratios as the one tested.

2.5.4.1 Components

As mentioned earlier, the plasma-inducing unit in ICP-MS is largely identical to what has been elucidated in 2.5.3.1. Once the plasma is generated and stabilized, the ions are drawn by pressure gradient into the mass spectrometer, through an intermediate vacuum region flanked between a skimmer and a sampler cone. The cones use their central orifices, which align with each other, to filter the plasma so that only those ions traveling in parallel with the orientation of the quadrupole can enter the detection chamber. The ions are then separated by the quadrupole and counted by the detector based on their mass-to-charge ratios.

ICP-MS can also prove useful in quantitative analysis of environmental samples. In this case, various chemicals that comprise the sample are fragmented into isotopes of different elements, from which isotopes of the target element can be identified and their intensities can be compared to the calibration curve created from prepared standard solutions. Alternatively, a single standard enriched with a predetermined quantity of one isotope of the target element can be used to enable single-point measurement.

2.5.4.2 Sample Preparation and Introduction

The common practice of sample preparation in geological analysis using ICP-MS is a process typically referred to as “digestion”, in which the solid sample is dissolved in a suitable solvent to enable subsequent pipetting and injection. HF and HNO₃ are often the solvents of choice as geological samples are generally composed of silicates. However, my extraction fluid does not need to go through this digestion process, while the solution has to be pre-analyzed for its pH and the rough concentration of the target component. With these values determined, the sample solution is then adjusted, usually by dilution and acidification, to a pH and concentration that fall within the range necessitated by the instrument to achieve acceptable accuracy. An internal standard, which often contains indium and/or rhenium, can be added to the sample solution for the purpose of minimizing systematic bias and simplifying measuring procedures.

Once the sample solution is prepared, it is introduced into the measuring body of the

ICP-MS instrument either through a nebulizer or by laser ablation. The nebulizer converts minuscule sample droplets to aerosol by a rapid, continuous stream of a carrier gas of choice. The aerosol is then swept into the plasma to generate ions that are charged and detected. The nebulizer often incorporates a double pass or cyclonic spray chamber to filter off most of the droplets that comprise the aerosol, allowing only the smallest among them to enter the plasma. This sample introduction method generally works best with the solutions as my diluted fluids.

Since a wide range of geological samples are in the form of solid that cannot be readily digested, especially for the experimental synthesized phases, the alternative strategy of laser ablation is employed in these situations. When the laser focuses tuned levels of energy on the surface of the solid sample, it ablates its materials and creates a sample “plume” that can then be directed into the plasma. The laser ablation method proves particularly useful for detecting trace elements in minerals and melts, but it can be difficult to perform quantitative analysis due to the lack of internal standard. Moreover, the destructive nature of laser ablation means that it is commonly reserved as a last resort in sample analysis.

2.5.4.3 Elemental Analysis

The ICP-MS allows determination of elements whose atomic masses range from 7 through 250, which essentially include metals from Li to U. However, the permeation of argon inside the instrument’s measuring chamber inevitably saturates the system with its derivatives that interfere with detection at a number of mass values, such as 40 (coinciding with the mass of Ar), 80 (Ar dimer) and 56 (ArO⁺). ArO interference can be particularly undesirable as its mass is almost identical to that of any simple Fe ion. Therefore, to analysis Fe content, the instrument has to be fitted with a reaction chamber, which is utilized to convert the interferent ion to a neutral atom by reacting with an active gas (e.g., ammonia).

A noticeable advantage of ICP-MS over atomic absorption spectroscopy consists in its ability to scan the sample for all its elements simultaneously, making it a powerful high-throughput analytic method.

2.5.4.4 Analytical Procedure

My solutions are sent to Toulouse for ICP-MS analyses. All the operations are conducted by Frederic Candaudap. The solution samples are mixed with nitric acid solution and standard In/Re solution as internal standard. The calibration is carried out with three different concentration standard solutions (1, 30 and 60 ppb), which contain most elements of positive ions from Be to U. These standard solutions, the nitric acid and In/Re solutions are all analyzed with ICP-MS. All the samples are analyzed for twice with different dilute factor. The details will be introduced in the result section.

2.6 Mass Balance Calculation

The mass balance is a useful theoretical calculation. Usually, it is used to estimate the phase proportions. With some special conditions, it is improved to calculate the unknown composition of a phase, e.g. a melt or fluid phase. Because the high-pressure experimental fluid was unquenchable in large quantity fluid-bearing experiments, the F concentrations in the fluids also could be derived from mass-balance calculations accounting for uncertainties of compositions used. The program script is written in R, translated from a published FORTRAN program (Albarede and Provost, 1977). Several parameters are required: the mass of solid starting material, the fluid mass left in the capsule after quench, compositions of mineral phases and starting material and their errors.

2.6.1 Strategies

The aim of the mass balance is to calculate the fluid composition. The basic strategy is following: 1) With the compositions of solid phases and starting materials, I can get the proportions of different phases; 2) Find the residual composition in the system with their proportions, which should be attributed to the fluid, and hence it is able to acquire the fluid composition.

The first strategy is a so-called convergent recursion algorithm. Its idea is shown as

follows: 1) use the calculated fluid composition and minerals composition to re-estimate the proportion of each phase; 2) renormalize the proportions and get a new fluid composition; 3) repeat these two steps until the result is of convergence (e.g. the difference of SiO₂ between the new and the last composition is less than 0.01 wt%). The calculated results of this strategy will be in a balance with the minerals compositions and its starting material. The ideal composition will appear like an oscillatory convergence. However, in fact, the fluid composition showed a monotonically decreasing convergence, which makes it difficult to determine its end, for different convergent condition giving different fluid compositions. Moreover, the calculated fluid proportion is beyond its uncertainty of the actual proportion.

Although no mistake was found on this strategy, I still cannot get the suitable results for the aim with any unreasonable error. Even if I tried various adjustments for the calculations, such as renormalize the phase proportions with the fixed fluid proportion, or exclude Na and F to determine the initial minerals proportions, or replacing water content in starting materials by summing up water concentration from all the phases, the result always shown the monotonically decreasing convergence. Perhaps, the large errors of some elements, e.g. Si and Al, especially in hornblende compositions result in this situation. Finally, I decided to employ the traditional way to estimate the fluid composition. There are other problems need to be solved. With Prof. John Ayers' advice, I employed a concept of selecting conservative elements to develop another strategy for fluid composition calculation.

High-temperature, high-pressure fluid compositions were determined by a modified mass-balance equation below, because they are unquenchable in fluid-bearing experiment.

$$x_{Flu}^i = \frac{100 \cdot x_{bulk}^i - x_{Hb}^i \cdot \varphi_{Hb} - x_{Nb}^i \cdot \varphi_{Nb}}{\varphi_{Flu}} \quad (2.6.1),$$

where $\varphi_{Flu} = 100 - \varphi_{Hb} - \varphi_{Nb}$ (Hb: hornblende; Nb: norbergite; Flu: fluid). x_j^i (unit: wt%) is the concentration of element i in phase j . φ_j (unit: %, and hereinafter) is the proportion of phase j ($0 < \varphi_j < 100$).

2.6.2 Conservative Elements Set

In this study, the compositions of the minerals were measured. The bulk composition was derived from the masses of the water and anhydrous powder, and their respective compositions. The post-quench fluid mass was measured, and it represents the mass of H₂O in the system at this point, following some water loss during the experiment. Knowing the phase proportions, the fluid composition was determined using Eq. (2.6.1).

In the experiments with more than one crystalline phase, the mineral proportions had to be independently determined. The result was calculated with a normal mass-balance approach, applied to a subset of measured oxides. Certain oxides were then chosen to make up a conservative oxide set; these elements were assumed to be insoluble. The mass-balance calculations were performed with an initial conservative oxide set of SiO₂, TiO₂, Al₂O₃, Cr₂O₃, CaO, MgO, MnO, and FeO, with no renormalization. Thus, whether or not the system lost H₂O, the proportions of these elements were assumed to remain constant. On the contrary, Na₂O and F were readily dissolved into the fluid (our preliminary HPLC measurements of fluid composition showed that Na made up approximately 2 wt%, and F was from 0.05 to 0.5 wt%). Once mineral proportions were determined, the fluid composition was calculated.

To verify the initial conservative oxide set, we examined the fluid composition. I found certain inconsistencies, for example, the fluid in experiment 1-SP2-1 (Table 2.6.2) contained a significant quantity of Al₂O₃ and Cr₂O₃ in addition to Na₂O and F, whereas the Initial Set assumed Al₂O₃ and Cr₂O₃ to be conservative oxides. To resolve this inconsistency, another mass-balance calculation was performed in which Al₂O₃ and Cr₂O₃ were excluded (Second Set). When the mass of one oxide in the fluid was more than 3 % of the bulk composition, I selectively dropped it from the conservative set. Elements with less than 1 wt% (TiO₂, Cr₂O₃ and MnO) had very little effect on the mineral proportions. In summary, the final conservative set generally contained FeO, MgO, CaO, MnO, TiO₂, Al₂O₃, and Cr₂O₃, which were determined by the above procedure and provided the internally consistent oxides for the mass-balance calculations. However, this procedure was result-dependent, and occasionally MgO and/or CaO were also selectively excluded from the above-mentioned oxides.

Table 2.6.2 Results of the conservative elements setting for 1-SP2-1 from mass balance

Proportion	Initial Set	2 nd Set
Hb	57.74(1.15)	57.23(1.07)
Nb	9.70(80)	9.95(80)
Composition of Fluid		
SiO ₂	0.0(2.0)	0.2(2.0)
TiO ₂	0.0(1)	0.0(1)
Al ₂ O ₃	1.9(1.5)	2.1(1.5)
Cr ₂ O ₃	0.3(6)	0.4(6)
FeO	0.0(6)	0.0(6)
MgO	0.2(1.3)	0.0(1.3)
CaO	0.0(9)	0.0(9)
MnO	0.01(9)	0.01(9)
Na ₂ O	2.5(2)	2.5(2)
F	0.35(62)	0.24(62)
H ₂ O	94.7(1.6)	94.6(1.6)

SiO₂ concentration in the fluid ranged from 0 ± 2 % to 5 ± 3 % in my mass balance results, so it was generally excluded from the conservative oxides set. This value is lower than the dissolved SiO₂ concentration in equilibrium with pure quartz (from 7.0 wt% to 12.6 wt% at 1 GPa and from 800 to 900 °C, respectively, Newton and Manning, 2000), but is in the same range as those in fluid-forsterite-enstatite systems (from 0.4 to 2.9 % at 1 GPa from 600 to 900 °C, Newton and Manning, 2002). In the albite-paragonite-quartz system, SiO₂ solubility is 1.7 % at 1 GPa and 500 °C, and 5.4 % at 1.2 GPa and 600 °C (Wohlert et al., 2011). The results are mostly consistent with these previous studies. However, when the concentration of SiO₂ in fluid was effectively zero, I treated SiO₂ as a conservative oxide.

2.6.3 Determination of Fluid Composition Uncertainties

The absolute uncertainty for the fluid composition is determined using the equation:

$$\delta_{Flu}^i{}^2 = \left(\frac{\partial (x_{Flu}^i)}{\partial (x_{bulk}^i)} \cdot \delta_{bulk}^i \right)^2 + \left(\frac{\partial (x_{Flu}^i)}{\partial (x_{Hb}^i)} \cdot \delta_{Hb}^i \right)^2 + \left(\frac{\partial (x_{Flu}^i)}{\partial (x_{Nb}^i)} \cdot \delta_{Nb}^i \right)^2 \quad (2.6.3a).$$

Here, δ_j^i indicates the uncertainty of element i in phase j . Note that the cross-term of error propagation is not included here, because δ_{bulk} does not correlate with either δ_{Hb} or δ_{Nb} .

The bulk composition is calculated from the composition of the starting material and the H₂O proportions, so the bulk composition uncertainties are derived from those of the anhydrous starting composition, and their weight fraction uncertainties. The uncertainty of proportion (δ_{φ_j}) is derived from mass balance results, and is ultimately derived from the uncertainty of the bulk composition. Error propagations of phase proportions are therefore redundant, and excluded from equation (2.6.3a).

The uncertainty of fluid composition is derived from the following equation (unit: wt%):

$$\delta_{Flu}^i = \sqrt{\left(\frac{100 \cdot \delta_{bulk}^i}{\varphi_{Flu}}\right)^2 + \left(-\frac{\varphi_{Hb}}{\varphi_{Flu}} \cdot \delta_{Hb}^i\right)^2 + \left(-\frac{\varphi_{Nb}}{\varphi_{Flu}} \cdot \delta_{Nb}^i\right)^2} \quad (2.6.3b).$$

Thus, using the mass balance procedure above, I can calculate the mineral proportions, and using equations (2.6.1) and (2.6.3b), it is possible to calculate the fluid compositions and their uncertainties (Table 3.4.1.1.1e and Table 3.4.1.1.2).

3. Results

This section presents the experimental results, e.g, phase assemblies, mineral and/or melt structure and compositions, calculated and direct measured fluid compositions and the fluorine partitioning between different phases. Because the success rate of experiments is less than 50 %, of which criterion is given by the presence of water after experiments, I must describe some experiments' texture and phase compositions carefully and decide whether it is able to have comparison with others.

3.1 Phase Assembly and Texture Description

For experiments with large quantity water, the presence of ample fluid in a capsule can be confirmed by visual observation upon the piercing of the capsule. Meanwhile, the empty space between the crystalline phases in the capsule indicates that there was abundant fluid during the high pressure and high temperature experiments.

Generally, four different starting materials create changes in phase assemblages. F-free SP1 experiments only create hornblende. F-rich SP2 experiments crystallize hornblende and norbergite. Intermediate F SP3 experiments yield hornblende and humite. Low F SP4 experiments precipitate mica/amphibole, clinohumite and augite. Moreover, I also conducted some SP2 experiments with higher temperature and pressure, which made melt and other minerals, like pyroxene and garnet. Furthermore, four experiments with excess other powder (MgF_2 or SiO_2) as starting material. In this section, I will talk about the assemblies and texture of all my experiments.

3.1.1 SP1 Experiments

SP1 powder is F-free. The experiments with SP1 provide comparisons against F-doped systems. Also it confirms that the powder I designed precipitate the predicted mineral species.

The 1-SP1-1 sample of the anhydrous SP1 experiment is shown in Fig. 3.1.1a. There is

no empty space in the capsule. Among the minerals, the white area indicates high atomic density, just as the area corresponding metal capsule. It indicates that it is high conductivity melt. The minerals are two species pyroxene. The lighter one is Ca-bearing pyroxene and the darker is orthopyroxene (Table 3.1.1). The largest mineral reaches approximately 100 μm length and 30 μm width. The temperature 877 $^{\circ}\text{C}$ is not high enough to create abundance partial melt in this low silicate system. The absence of the initial fluid prevented the effective convection in the capsule. Most of minerals are small.

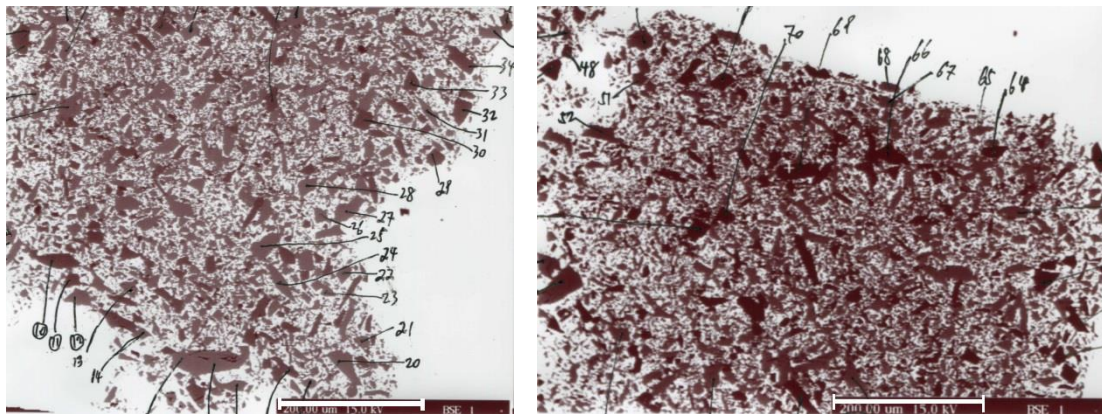


Fig. 3.1.1a 1-SP1-1 experiment, conducted without water. The scale bars are 200 μm .

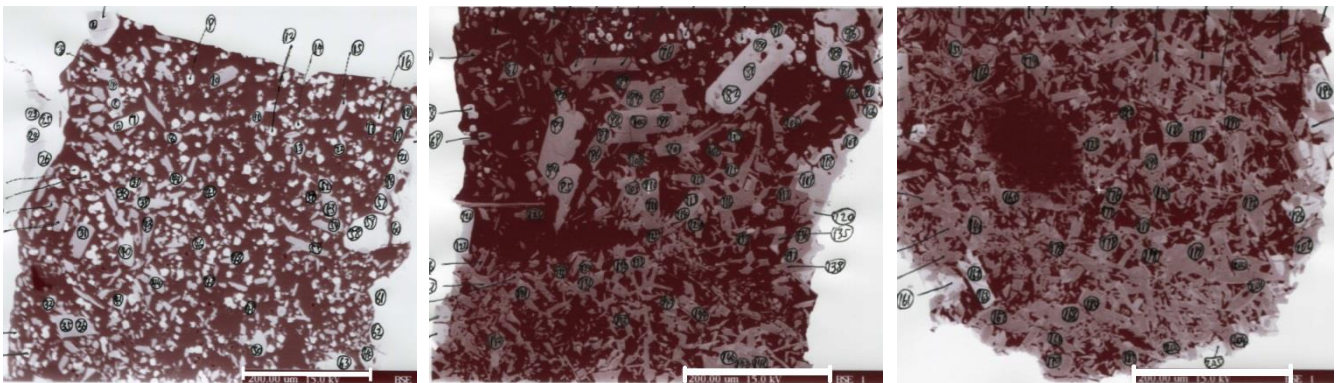


Fig. 3.1.1b The images of 1-SP1-2 capsule (top, middle and bottom portions, respectively from left to right). The scale bars are 200 μm .

The experiment 1-SP1-2 is conducted with 1.0 mg water. An obvious difference with 1-SP1-1 experiment is abundance of empty space in the capsule. After opening this charge, its phase assemblage is olivine, pyroxene, hornblende and spinel (Table 3.1.1). Because of the gravity, the assemblages of minerals at the bottom are denser than those on the top. The biggest pyroxene and hornblende appear in the middle of capsule (Fig. 3.1.1b). Their lengths are more than 100 μm and widths reach 50 μm . It indicates that the fluid convection helps the

precipitation and growth of minerals. The zoning occurs in the big crystals. For example, the biggest pyroxene has a darker core, but it is too small to be analyzed by electron microprobe separately without pyroxene background.

Although no fluid was left after the experiment, the porosity indicates there was fluid during the annealing. In high temperature, the diffusivity of hydrogen is higher than that in lower temperature. The loss of all the water is likely due to its long duration (119 hours). Except some hornblende minerals, most other minerals are Ni rich, which indicate that the sample was contaminated by nickel capsule during the experiment under 955 °C. Thus, the formations of anhydrous minerals are probably derived from either the water exhaustion in the capsule, which made hornblendes break down, or the nickel contaminations. Olivines mostly contact to the capsule wall, especially bigger ones, and this indicates that the nickel introduction is probably the main reason for the presences of anhydrous minerals.

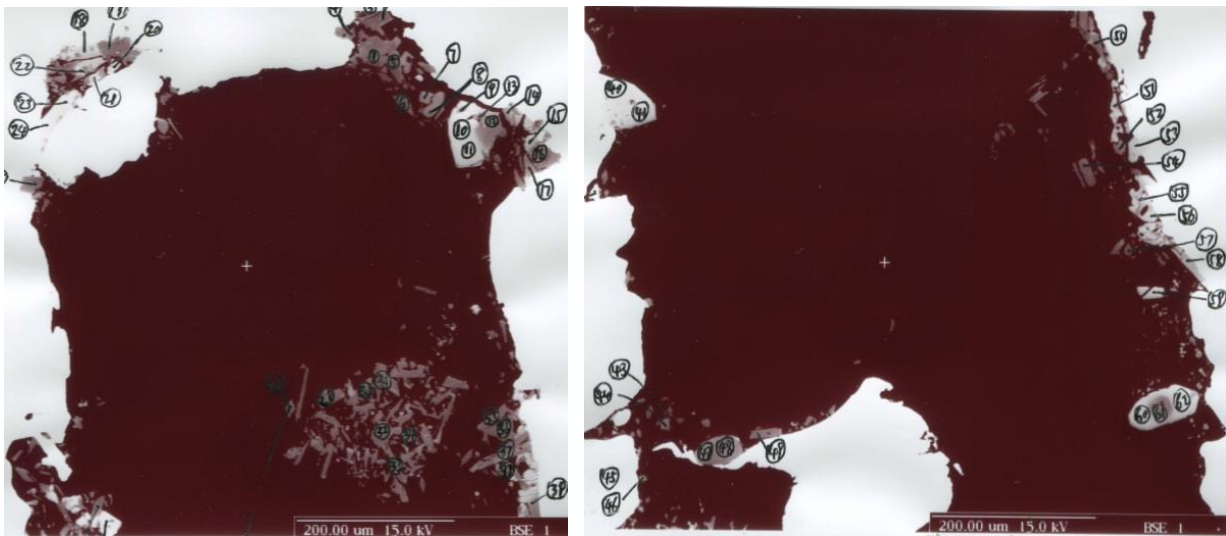


Fig. 3.1.1c Images for 1-SP1-3 experiment sample.

I repeated this experiment at the same conditions, with shorter duration. 1-SP1-3 experiment has 0.3 mg mass difference between before and after the fluid retrieving. Its SEM images showed that its mineral particles are less than those in other experiments. There are three possibilities: 1) Before I mounted the capsule into the epoxy, I deformed and opened the capsule totally. The epoxy flow into the charge easily and fill up the gaps among minerals. It is also possible to lose some samples and create empty space in the charge. 2) Some micro minerals can go out of the capsule when I retrieve the fluid with ultrasonic bathe. In this case,

3. Results

the fluid mass may contain some minerals quantity. 3) The presence of anhydrous minerals in the capsule (olivine and pyroxene) indicates that 1-SP1-3 also lost water as 1-SP1-2. Because all the minerals in the center are hornblende, it is reasonable to treat the system as fluid-bearing after the quench. Moreover, it should be noticed that big crystals (olivine or pyroxene) are zoned and distribute around the capsule walls. With the presence of fluid, it probably confirms that nickel contamination results in the precipitates of olivine and/or pyroxene. Furthermore, from the MgO-rich (SP4) experiments, which created olivine and hornblende, I prefer the nickel contamination increasing local divalent cation concentration led to the precipitation of olivine or pyroxene.

After these three experiments, I conducted five more experiments under lower temperature (from 807 to 900 °C) and different durations (94 to 330 hours). Their pictures are shown below, and their phase assemblages and mineral formulas are shown in Table 3.1.1.

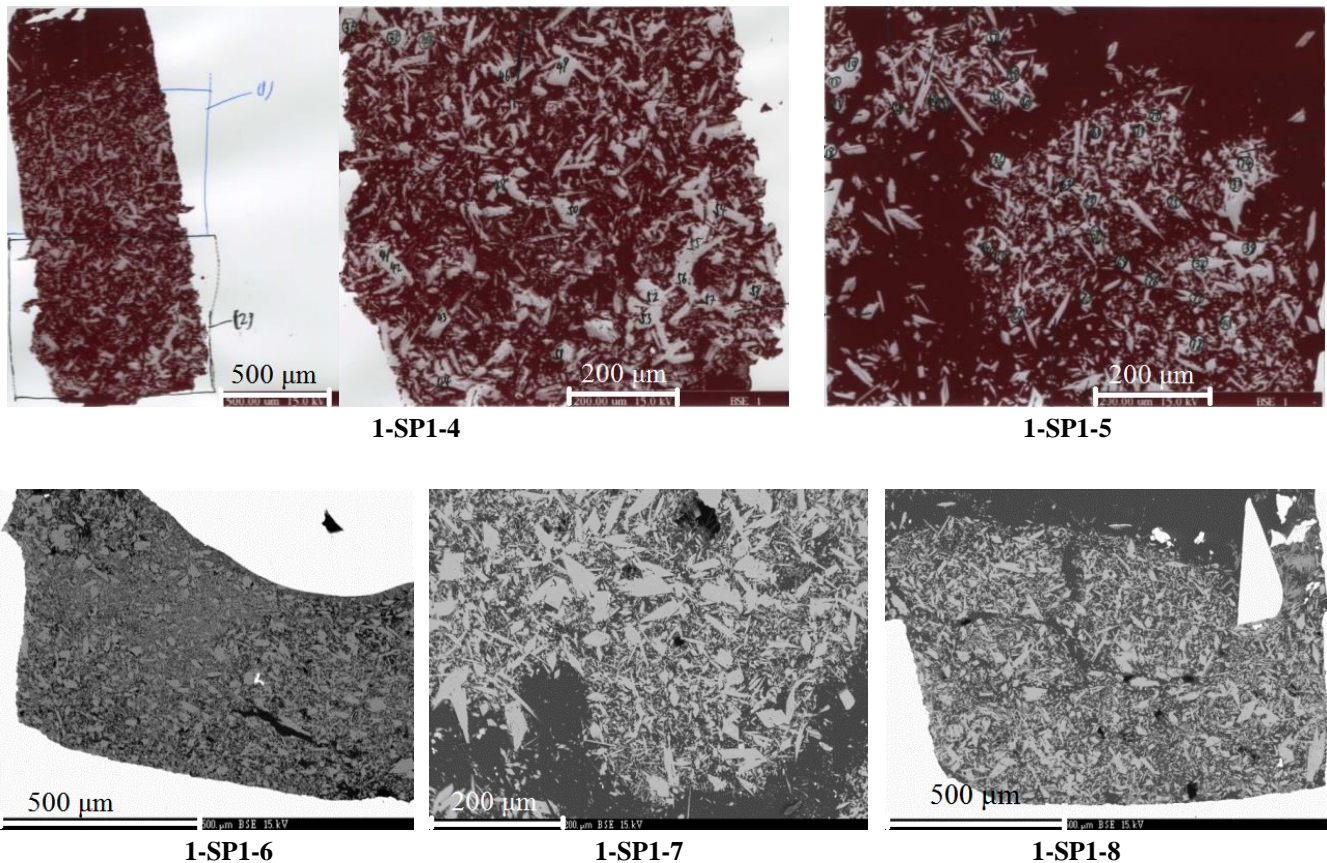


Fig. 3.1.1d Images for the latest 5 SP1 experiments.

These experiments have fluids left after the quench. For most of them, the fluid came out with some bubbles when I pierced the capsules. The minimum fluid mass is 0.6 mg. In the

temperature range, their phase assemble are constant. All these five experiments only create hornblendes and no nickel contamination happened. It indicates that 900 °C is an upper temperature limit of nickel capsule for preventing contamination, if the oxidize layer is formed under 1000 °C. The mineral size is smaller than those from higher temperature experiments. Generally, the widest hornblende crystal only reaches 40 µm, and amphibole is easy to become long, but not wide. In order to increase the mineral size, I managed to run the experiments with longer duration (up to 330 hours), but the results showed that it did not help us and make the water loss more.

Table 3.1.1 Phase mineral formulas of SP1 experiments.

Expt. ID	T / °C	Hornblende	Olivine	Pyroxene	Spinel
1-SP1-1	870			Mg _{1.70} Fe _{0.18} Si _{1.93} Al _{0.14} O ₆ or (Ca _{0.74} Mg _{0.07} Na _{0.14}) (Mg _{0.76} Fe _{0.09} Al _{0.15}) (Si _{1.91} Al _{0.09}) O ₆	
1-SP1-2	955	Na _{0.35} (Ca _{1.83} Mg _{0.03}) (Mg _{3.85} Fe _{0.42} Al _{0.67} Ni _{0.06}) (Si _{6.45} Al _{1.55}) O ₂₂ (OH) ₂ or Na _{0.33} Ca _{1.91} (Mg _{2.93} Fe _{0.29} Al _{0.52} Ni _{1.25}) (Si _{6.69} Al _{1.31}) O ₂₂ (OH) ₂	(Mg, Ni) ₂ SiO ₄	(Ca _{0.94} Mg _{0.67} Fe _{0.05} Al _{0.08} Ni _{0.24}) (Si _{1.89} Al _{0.11}) O ₆	(Mg _{0.37} Ni _{0.60} [Fe ²⁺] _{0.02}) (Al _{1.37} Cr _{0.12} [Fe ³⁺] _{0.49}) O ₄
1-SP1-3	955	Na _{0.33} (Ca _{1.82} Mg _{0.18}) (Mg _{3.84} Fe _{0.40} Ni 0.16 Al _{0.53}) (Si _{6.60} Al _{1.40}) O ₂₂ (OH) ₂	(Mg, Ni) ₂ SiO ₄	(Mg _{0.77} Ca _{0.94} Fe _{0.07} Ni _{0.11} Al _{0.09}) (Si _{1.88} Al _{0.12}) O ₆	
1-SP1-4	900	Na _{0.30} (Ca _{1.85} Mg _{0.11}) (Fe _{0.44} Mg _{3.82} Al _{0.68}) (Si _{6.56} Al _{1.44}) O ₂₂ (OH) ₂			
1-SP1-5	877	Na _{0.29} (Ca _{1.84} Mg _{0.16}) (Mg _{3.82} Fe _{0.42} Al _{0.67}) (Si _{6.64} Al _{1.36}) O ₂₂ (OH) ₂	Mg _{1.7} Ni _{0.3} SiO ₄	(Mg _{1.12} Ca _{0.49} Fe _{0.11} Al _{0.17}) (Si _{1.87} Al _{0.13}) O ₆	
1-SP1-6	827	Na _{0.34} Ca _{1.89} (Fe _{0.42} Al _{0.44} Mg _{4.07}) (Si _{6.70} Al _{1.30}) O ₂₂ (OH) ₂			
1-SP1-7	857	Na _{0.30} (Ca _{1.83} Mg _{0.12}) (Fe _{0.42} Mg _{3.80} Al _{0.71}) (Si _{6.61} Al _{1.39}) O ₂₂ (OH) ₂			(Mg _{0.92} Ni _{0.03} [Fe ²⁺] _{0.04}) (Al _{1.56} Cr _{0.20} [Fe ³⁺] _{0.23}) O ₄
1-SP1-8	807	Na _{0.26} (Ca _{1.87} Mg _{0.07}) (Fe _{0.50} Mg _{3.64} Al _{0.79}) (Si _{6.47} Al _{1.53}) O ₂₂ (OH) ₂			

3.1.2 SP2 Experiments

F concentration of SP2 powder is around 5 wt%, quite higher than the typical abundance in the nature. I would study the mineral or fluid saturation of the hornblende-bearing system with this starting material.

3.1.2.1 Experiments Under 1 GPa

The first SP2 experiment (1-SP2-1) was conducted in a large capsule (id > 2 mm) with 3/4" piston-cylinder under 770 °C for 113 hours. It is a test for this cold-sealing technique. This experiment is successful to keep some fluid left, which indicates I can follow this technique correctly and it is suitable for the fluid bearing experiments.

In 1-SP2-1 capsule, there are two phases in this experiment (Fig. 3.1.2.1a), of which the white part (1) is hornblende and the darker one (2) is norbergite. This phase assembly is constant for the experiments under 950 °C. The minerals distribute evenly in the capsule and most of them contact close to each other. The minerals are small, and only reach up to 15 μm. Their small areas make their measurement a little difficult.

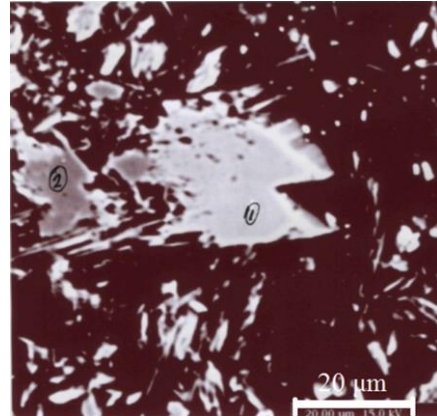


Fig. 3.1.2.1a The image of 1-SP2-1 experiment.

The second SP2 experiment (1-SP2-2) was conducted at 1120 °C. The inner capsule was Au-Pd tube, which has higher melt point than pure gold tube. Its duration is 144 hours, which is too long to remain the water in the capsule. From the electron microprobe data, F-free pyroxene and F-bearing melt are present in the capsule. Their totals are close to 100 wt%. It indicates that melt and minerals do not contain water.

1-SP2-3 is an experiment at 870 °C for 137 hours. No fluid left and I lost the sample for I over-polished it. Then I repeated this experiment (1-SP2-4) at same condition with shorter duration. All the fluid of 1-SP2-4 was kept after the annealing within its uncertainty. The sizes of its biggest hornblende and norbergite are much larger than 1-SP2-1. Its hornblende width reaches 40 μm and norbergite is beyond 100 μm (Fig. 3.1.2.1b). While, the gravity distribution remains. In the bottom of the capsule, the minerals are much narrower and smaller than those big crystals at the top portion. Again, the mineral distribution shows that the fluid convection improves the growth of minerals.

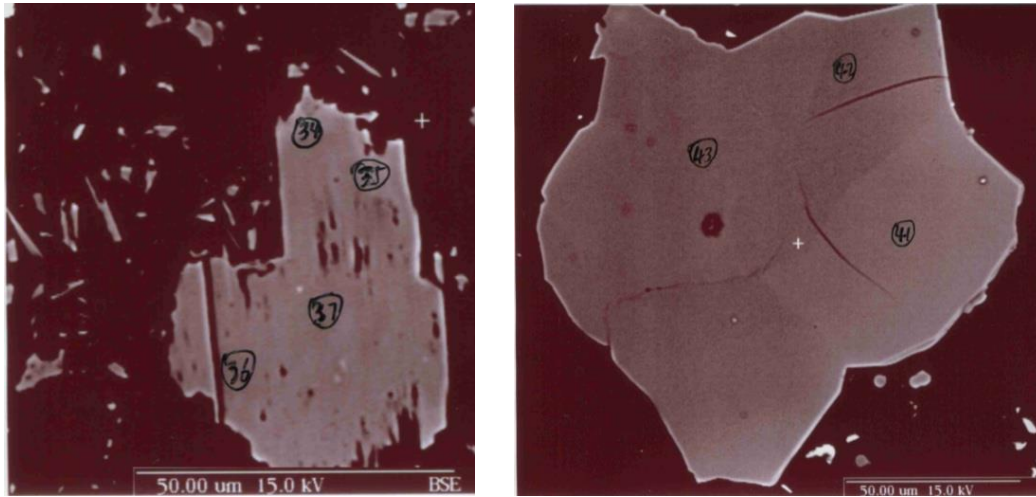


Fig. 3.1.2.1b Minerals from 1-SP2-4 experiment. Hornblende (left) and norbergite (right) are much bigger than those in 1-SP2-1 experiment.

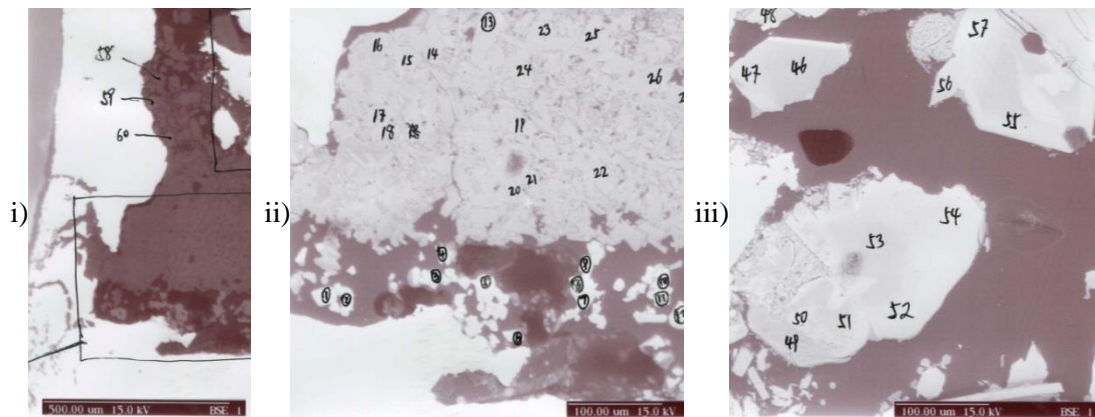


Fig. 3.1.2.1c Images from 1-SP2-5. i) the left-bottom of the capsule, where the significant cracks are present. ii) the hornblende block and the spinel at the bottom. iii) the zoning chondrodite.

1-SP2-5 experiment is a typical failed one. Its assemblies are hornblende (Fig. 3.1.2.1c-ii, in its top portion), chondrodite (Fig. 3.1.2.1c-iii), spinel (Fig. 3.1.2.1c-ii, the white minerals at the bottom) and melt. High temperature indeed helps to increase the minerals size. Three reasons led to this failure. First, its inner gold capsule was leaking. In Fig. 3.1.2.1c-i, some gaps connected inside and outside the inner capsule. It led to the partial loss of starting material. Second, within the uncertainty, there was almost no fluid left, but no pyroxene or olivine is present in the capsule. Third, nickel contaminated the inner capsule. However, the results revealed that too much nickel contamination changed anhydrous mineral to spinel and the hydrous minerals can remain in the capsule after the water exhaustion.

1-SP2-6 experiment lost its fluid. There are hornblende, chondrodite and spinel in this capsule. Chondrodite and spinel minerals are in the upper half of the capsule (Fig. 3.1.2.1d-i),

and their high nickel concentrations indicate the contamination from the outer capsule. It is possible to find the zoning of the chondrodite. Most hornblendes are in the lower half capsule. Nickel concentrations in hornblendes decrease from the boundary to the center, which shows the diffusion gradient.

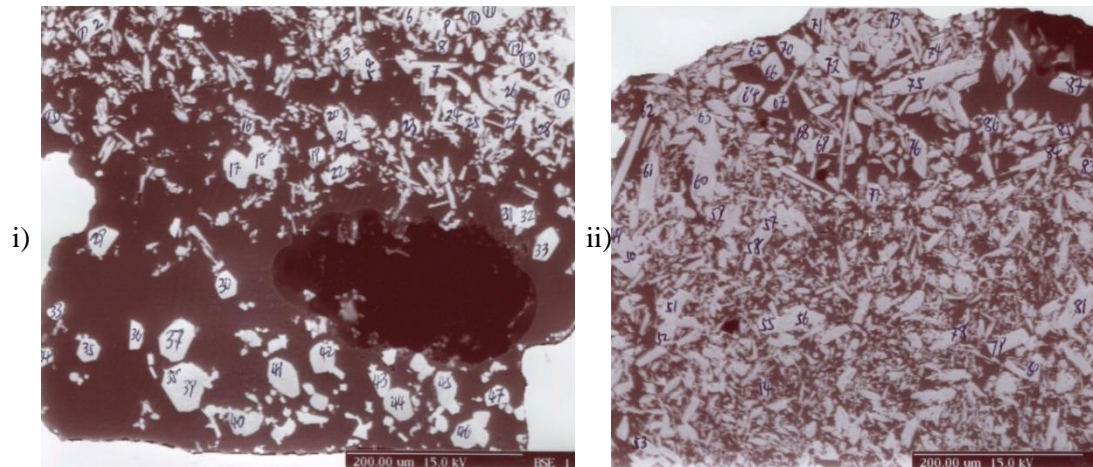


Fig. 3.1.2.1d Images from 1-SP2-6. i) the top portion of the capsule. ii) the bottom portion.

1-SP2-7 experiment is abnormal, which is quite different from the experiments with large quantity water left. There is not a lot of space among the minerals, which indicates that the water proportion is quite low during the experiment and probably no hydrous fluid was left after annealing. Under microscope, it is hard to tell the minerals boundary. The sample looks like an entire glass. Electron microprobe analyses showed that the mineral are hornblende and norbergite. While some abnormal EMPA results report SiO_2 concentrations are less than 50 wt%, of which compositions are between hornblende and norbergite. However, even if abundance of water is present, SP2 powder cannot create melt at 930 °C. Because of the vague mineral boundaries of the sample, it is possible to analyze points plotted on the boundary. Therefore, electron microprobe measurements report these points as mixture compositions.

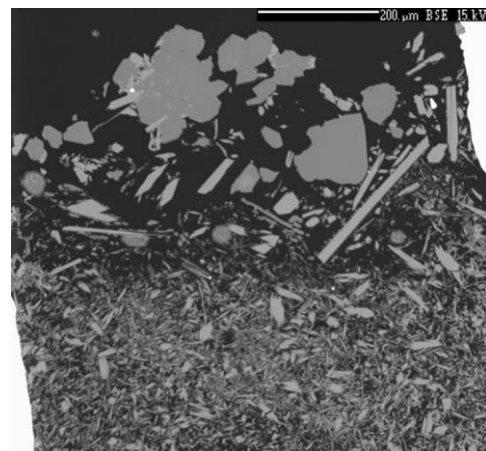


Fig. 3.1.2.1e Images from 1-SP2-8.

1-SP2-8 is another typical successful experiment and has the biggest crystals in melt-free

system (Fig. 3.1.2.1e). Its phase assembly is the same with 1-SP2-4. Two mineral phases are apparent. The bright elongated mineral is hornblende. The darker grey lumpish crystal is norbergite.

In next successful experiments, 1-SP2-12, 13, 15, 16, 17, 23 & 24 have the same hornblende-norbergite-fluid system, while 1-SP2-10 & 22 did not have fluid left. Their images are shown in Fig. 3.1.2.1f. Experiments 1-SP2-13 to 17 were conducted without buffer, but its phase assemblies are not influenced. However, experiment 1-SP2-14 has an excess phase – chondrodite, and its proportion is more than norbergite. Its hornblende has the maximum Ca concentration and relatively low SiO₂ to other SP2 experiments, which indicates a potential bulk material loss during the experiment. The chemical formulas of all the minerals in melt-free systems are shown in Table 3.1.2.1a.

In conclusion, the polished sections of experiments show crystalline phases, and no melt is found in the experiments above. Hornblendes are needle-shaped crystals with a length up to 200 µm. The size of norbergite ranges from 15 to 150 µm. Bigger crystals are always present in the top portion of the charges in the experiments with temperature higher than 800 °C. In the lower portion of the charges hornblendes are short and narrow (width 5 ~ 10 µm), and humite group minerals are smaller (10 µm). The wider spacing between minerals in the upper portion indicates higher fluid contents, which supply more dissolved elements to allow bigger crystals to form. While, for experiments conducted at temperatures lower than 800 °C, their hornblende and norbergite are small and distributed evenly through the charge. Generally speaking, higher temperature (> 800 °C) and longer run duration improve grain growth. However, longer duration (up to 320 hours) in low temperature experiments (< 800 °C) causes no obvious increase in crystal size; instead, this longer duration brings about water loss during the experiments.

3. Results

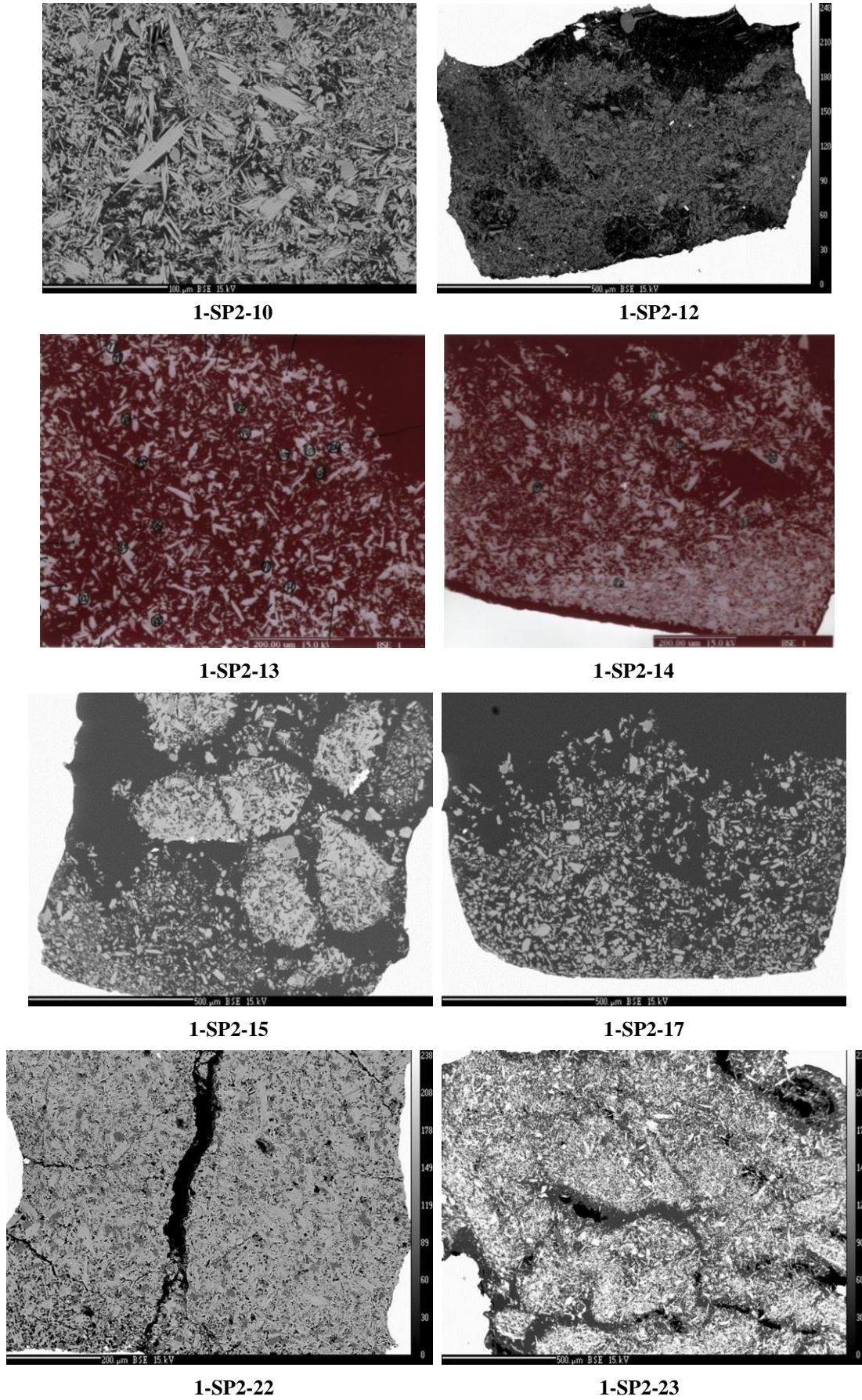


Fig. 3.1.2.1f Images from mineral-fluid system SP2 experiments.

3. Results

1-SP2-9 and 1-SP2-11 experiments happened to meet some problems of thermocouple during anneal. Their target temperature is 827 and 967 °C. When I polished the samples, no minerals left in the chamber and the inner gold layer melt. It indicates that the temperatures for these two experiments are over the gold melt point 1064 °C. The reason for these accidents is unclear. I use an alumina disk instead of MgO disk between thermocouple and the capsule to prevent the contamination of the thermocouple in subsequent experiments.

Table 3.1.2.1a Phase chemical formulas of SP2 experiments (without melt ones) at 1 GPa.

Expt. ID	T / °C	Hornblende	Norbergite	Chondrodite	Spinel
1-SP2-1	770	Na _{0.30} (Ca _{1.89} Mg _{0.05}) (Mg _{3.85} Fe _{0.41} Al _{0.70}) (Si _{6.52} Al _{1.48}) O ₂₂ (F _{0.52} OH _{0.48}) ₂	Mg _{2.96} Si _{0.95} O ₄ (F _{0.98} OH _{0.02}) ₂		
1-SP2-4	870	Na _{0.30} Ca _{2.07} (Mg _{3.79} Fe _{0.45} Al _{0.50}) (Si _{6.21} Al _{1.79}) O ₂₂ (F _{0.49} OH _{0.51}) ₂	Mg _{2.98} Si _{0.98} O ₄ (F _{0.96} OH _{0.04}) ₂		
1-SP2-5	955	Na _{0.38} Ca _{1.93} (Mg _{4.08} Fe _{0.42} Al _{0.35}) (Si _{6.51} Al _{1.49}) (F _{0.54} OH _{0.46}) ₂		(Mg _{4.40} Ni _{0.53}) Si _{1.97} O ₈ (F _{0.79} OH _{0.21}) ₂	(Mg _{0.43} Ni _{0.50} [Fe ²⁺] _{0.06}) (Al _{0.75} Cr _{0.27} [Fe ³⁺] _{0.96}) O ₄
1-SP2-6	900	Na _{0.27} Ca _{2.04} (Mg _{3.70} Fe _{0.41} Al _{0.44} Ni _{0.30}) (Si _{6.28} Al _{1.72}) O ₂₂ (F _{0.48} OH _{0.52}) ₂		(Mg _{4.31} Ni _{0.66}) Si _{1.95} O ₈ (F _{0.85} OH _{0.15}) ₂	(Mg _{0.43} Ni _{0.50} [Fe ²⁺] _{0.06}) (Al _{1.17} Cr _{0.20} [Fe ³⁺] _{0.56}) O ₄
1-SP2-7	930	Na _{0.33} (Ca _{1.79} Mg _{0.12}) (Fe _{0.42} Mg _{3.92} Al _{0.67}) (Si _{6.46} Al _{1.54}) O ₂₂ (F _{0.73} OH _{0.27}) ₂	Mg _{2.95} Si _{0.97} O ₄ F _{2.14}		
1-SP2-8	827	Na _{0.30} Ca _{2.01} (Mg _{3.81} Fe _{0.44} Al _{0.59}) (Si _{6.28} Al _{1.72}) O ₂₂ (F _{0.47} OH _{0.53}) ₂	Mg _{3.02} Si _{0.96} O ₄ (F _{0.98} OH _{0.02}) ₂		
1-SP2-10	787	Na _{0.24} Ca _{1.95} (Fe _{0.49} Mg _{3.84} Al _{0.61}) (Si _{6.47} Al _{1.53}) O ₂₂ (F _{0.55} OH _{0.45}) ₂	Mg _{2.91} Si _{0.97} O ₄ (F _{0.92} OH _{0.08}) ₂		
1-SP2-12	777	Na _{0.30} Ca _{1.91} (Mg _{3.82} Fe _{0.45} Al _{0.58}) (Si _{6.62} Al _{1.38}) O ₂₂ (F _{0.47} OH _{0.53}) ₂	Mg _{2.92} Si _{0.95} O ₄ F _{2.10}		
1-SP2-13	877	Na _{0.28} Ca _{2.09} (Fe _{0.48} Al _{0.34} Mg _{3.94}) (Si _{6.01} Al _{1.99}) O ₂₂ (F _{0.53} OH _{0.47}) ₂	Mg _{2.91} Si _{0.98} O ₄ (F _{0.87} OH _{0.13}) ₂		
1-SP2-14	877	Na _{0.31} Ca _{2.23} (Fe _{0.49} Mg _{3.89} Al _{0.29}) (Si _{5.84} Al _{2.16}) O ₂₂ (F _{0.46} OH _{0.54}) ₂	Mg _{2.94} Si _{0.99} O ₄ (F _{0.81} OH _{0.19}) ₂	Mg _{4.95} Si _{1.97} O ₈ (F _{0.83} OH _{0.17}) ₂	
1-SP2-15	907	Na _{0.27} Ca _{2.04} (Fe _{0.47} Al _{0.45} Mg _{3.92}) (Si _{6.00} Al _{2.00}) O ₂₂ (F _{0.49} OH _{0.51}) ₂	Mg _{2.91} Si _{0.99} O ₄ (F _{0.80} OH _{0.20}) ₂		
1-SP2-16	927	Na _{0.24} Ca _{2.15} (Fe _{0.47} Mg _{3.88} Al _{0.34}) (Si _{5.91} Al _{2.09}) O ₂₂ (F _{0.50} OH _{0.50}) ₂	Mg _{2.91} Si _{0.99} O ₄ (F _{0.79} OH _{0.21}) ₂		
1-SP2-17	917	Na _{0.24} Ca _{2.17} (Fe _{0.44} Mg _{3.89} Al _{0.34}) (Si _{5.96} Al _{2.04}) O ₂₂ (F _{0.46} OH _{0.54}) ₂	Mg _{2.94} Si _{0.99} O ₄ (F _{0.85} OH _{0.15}) ₂		

Some elements, such as Si and/or Ti, become soluble under my experimental conditions. New quench phases are formed due to the solubility decreasing upon quenching. Some little spheres, which are quench phases, attached to the surface of a hornblende (Fig. 3.1.2.1g).

However, they are too small to be measured with electron microprobe. Nevertheless, the fluid compositions calculated by the mass balance procedure cover the components of the quench phases.

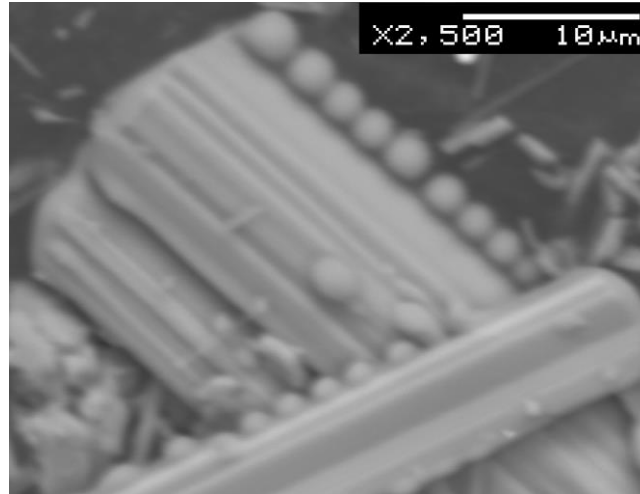


Fig. 3.1.2.1g A SEM image of 1-SP2-10 quench phase.

Ti and Mo capsules were utilized for the experiments over 900 °C (1-SP2-15 to 18), and Mo capsule would not contaminate the mineral composition. I conducted four higher temperature experiments from 947 to 1057 °C. Because of their partial melting, their phase assemblies changed. The mineral chemical formulas of these four melt-bearing experiments are shown in Table 3.1.2.1b.

1-SP2-18 is similar to normal SP2 experiments. It contains hornblende and norbergite, besides a small quantity of melt. 1-SP2-19 changed a little. It contains no norbergite but chondrodite. Their melt phases are at the bottom of the capsules (Fig. 3.1.2.1h). The shape is close to sphere. There are many bubbles in the melt, which indicates that the melt suffered degassing during the quench. It makes electron microprobe analyses difficult. It is hard to estimate its water content with its missing total.

1-SP2-20 created more melt. From its picture (Fig. 3.1.2.1h), the proportion of melt probably reaches 60%. Its phase assemblies are hornblende, humite, spinel, pyroxene, Si-rich melt and Mg-rich melt. 1-SP2-21 has more than 80% melt because of the highest temperature. For minerals, it has clinohumite and spinel. However, the melts from these two experiments have two formations. One is bubbled melt as those from 1-SP2-18 and 1-SP2-19. The other is triangle shape glasses, and obvious precipitates are present among the gaps. The latter is more

in the center of the capsule than at the edge. It fits that the temperature decreases more rapidly around the capsule wall than in the center. Therefore, this is a quenched melt, because the temperature decreases not quickly enough to keep the original structure of melts during anneal.

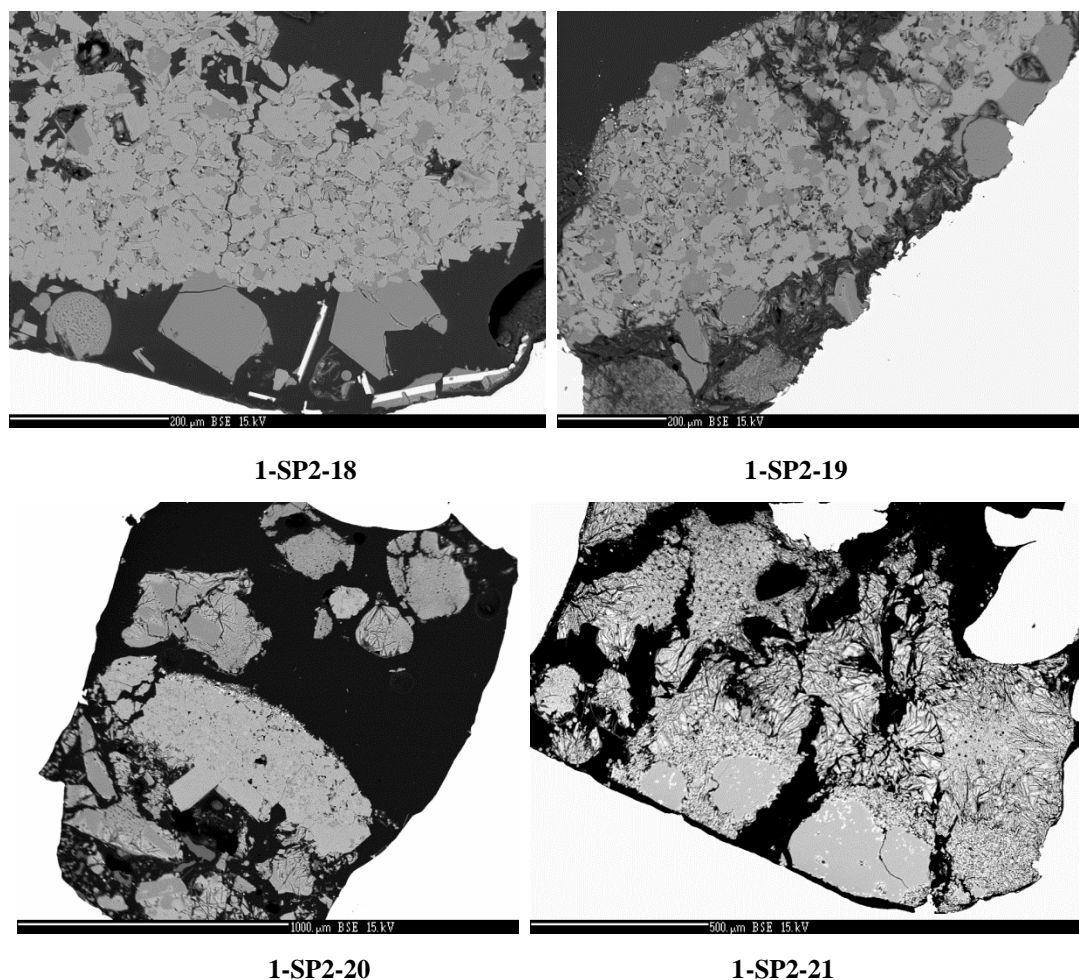


Fig. 3.1.2.1h Four experiments with melt phase, conducted in unbuffered capsules.

Table 3.1.2.1b Phase chemical formulas of SP2 experiments (with melt) at 1 GPa.

Expt. ID	T / °C	Hornblende	Humite Group	Spinel	Pyroxene
1-SP2-18	947	$\text{Na}_{0.35} \text{Ca}_{2.03} (\text{Fe}_{0.51} \text{Mg}_{3.98} \text{Al}_{0.35})$ $(\text{Si}_{6.14} \text{Al}_{1.86}) \text{O}_{22} (\text{F}_{0.50} \text{OH}_{0.50})_2$	$\text{Mg}_{2.93} \text{Si}_{0.99} \text{O}_4$ $(\text{F}_{0.83} \text{OH}_{0.17})_2$		
1-SP2-19	977	$\text{Na}_{0.39} \text{Ca}_{2.05} (\text{Mg}_{4.08} \text{Fe}_{0.50} \text{Al}_{0.24})$ $(\text{Si}_{6.18} \text{Al}_{1.82}) \text{O}_{22} (\text{F}_{0.47} \text{OH}_{0.53})_2$	$\text{Mg}_{4.86} \text{Si}_{2.00} \text{O}_8$ $(\text{F}_{0.73} \text{OH}_{0.27})_2$		
1-SP2-20	1007	$\text{Na}_{0.29} \text{Ca}_{2.16} (\text{Fe}_{0.50} \text{Mg}_{4.00} \text{Al}_{0.23})$ $(\text{Si}_{6.03} \text{Al}_{1.97}) \text{O}_{22} (\text{F}_{0.44} \text{OH}_{0.56})_2$	$\text{Mg}_{4.80} \text{Si}_{2.00} \text{O}_8$ $(\text{F}_{0.68} \text{OH}_{0.32})_2$	$(\text{Mg}_{0.80} [\text{Fe}^{2+}]_{0.16}) (\text{Al}_{0.94})$ $\text{Cr}_{0.45} [\text{Fe}^{3+}]_{0.60} \text{O}_4$	$(\text{Ca}_{0.95} \text{Mg}_{0.81} \text{Fe}_{0.14})$ $\text{Al}_{0.10} (\text{Si}_{1.78} \text{Al}_{0.22}) \text{O}_6$
1-SP2-21	1057		$\text{Mg}_{6.83} \text{Si}_{3.01} \text{O}_{12}$ $(\text{F}_{0.66} \text{OH}_{0.34})_2$	$(\text{Mg}_{0.96} [\text{Fe}^{2+}]_{0.01}) (\text{Al}_{0.54})$ $\text{Cr}_{0.82} [\text{Fe}^{3+}]_{0.62} \text{O}_4$	

3.1.2.2 Experiments at Higher Pressure

Some experiments are conducted at the conditions from 1.5 to 3.0 GPa at 877 °C, with NNO buffer capsules. 1-SP2-4 is conducted at 870 °C, of which temperature is close, so they are the comparable data for the investigation of the systematic changes from 1.0 to 3.0 GPa. Unfortunately, only three experiments have fluid left and two of them (3-SP2-1 and 4-SP2-2) were retrieved fluid into flasks. The others do not have obvious fluid when I opened the capsules.

2-SP2-1, 2-SP2-2 and 3-SP2-1 have crystallized hornblende and norbergite. Besides these, 2-SP2-1 contains spinel as well. 2-SP2-3 is a failed experiment. It is similar to the phase structure of the failed experiment 1-SP2-7, which has no obvious grain boundary as well. With its electron microprobe analyses, there are MgF₂ and hornblende via their stoichiometry calculations. The bright nubs may be spinel, but it is too small to analyze. The biggest white stuff in 3-SP2-1 is a broken piece of blade. The phase assemblies and the mineral chemical formulas are shown in Table 3.1.2.2a.

Table 3.1.2.2a Phase chemical formulas of SP2 experiments from 1.5 to 2.0 GPa

Expt. ID	T / °C	Hornblende	Norbergite	Spinel
2-SP2-1	877	Na _{0.28} Ca _{2.09} (Fe _{0.45} Al _{0.45} Mg _{3.89}) (Si _{6.20} Al _{1.80}) O ₂₂ (F _{0.39} OH _{0.61}) ₂	Mg _{2.94} Si _{0.99} O ₄ (F _{0.78} OH _{0.22}) ₂	(Mg _{0.67} Ni _{0.25} [Fe ²⁺] _{0.07}) (Al _{1.31} Cr _{0.24} [Fe ³⁺] _{0.44}) O ₄
2-SP2-2	857	Na _{0.32} Ca _{1.97} (Mg _{3.85} Fe _{0.43} Al _{0.61}) (Si _{6.48} Al _{1.52}) O ₂₂ (F _{0.42} OH _{0.58}) ₂	Mg _{2.97} Si _{0.97} O ₄ (F _{0.92} OH _{0.08}) ₂	
3-SP2-1	877	Na _{0.30} Ca _{2.02} (Mg _{3.82} Al _{0.54} Fe _{0.45}) (Si _{6.32} Al _{1.68}) O ₂₂ (F _{0.36} OH _{0.64}) ₂	Mg _{2.88} Si _{0.99} O ₄ (F _{0.75} OH _{0.25}) ₂	

Table 3.1.2.2b Phase chemical formulas of SP2 experiments from 2.5 to 3.0 GPa

Expt. ID	T / °C	Norbergite	Chondrodite	Pyroxene	Hydrogrossular
4-SP2-1	877		Mg _{4.78} Si _{1.97} O ₈ (F _{0.74} OH _{0.26}) ₂	(Ca _{0.94} Mg _{0.93} Fe _{0.06}) (Si _{1.96} Al _{0.08}) O ₆	([Fe ²⁺] _{0.36} Mg _{1.39} Ca _{1.23}) (Al _{1.91} [Fe ³⁺] _{0.03} Cr _{0.03}) (SiO ₄) _{2.79} (F _{0.38} OH _{0.46})
4-SP2-2	877	Mg _{2.85} Si _{0.99} O ₄ (F _{0.72} OH _{0.28}) ₂	Mg _{4.69} Fe _{0.11} Si _{1.98} O ₈ (F _{0.73} OH _{0.27}) ₂	(Ca _{0.94} Mg _{0.89} Fe _{0.06}) (Si _{1.95} Al _{0.11}) O ₆	([Fe ²⁺] _{0.29} Mg _{1.64} Ca _{1.07}) (Al _{1.88} [Fe ³⁺] _{0.05} Cr _{0.06}) (SiO ₄) _{2.85} (F _{0.26} OH _{0.34})
5-SP2-1	877	Mg _{2.91} Si _{0.98} O ₄ (F _{0.76} OH _{0.24}) ₂		(Ca _{0.94} Mg _{0.92} Fe _{0.06}) (Si _{1.97} Al _{0.07}) O ₆	([Fe ²⁺] _{0.27} Mg _{1.80} Ca _{0.92}) (Al _{1.92} [Fe ³⁺] _{0.04} Cr _{0.04}) (SiO ₄) _{2.78} (F _{0.34} OH _{0.54})

3. Results

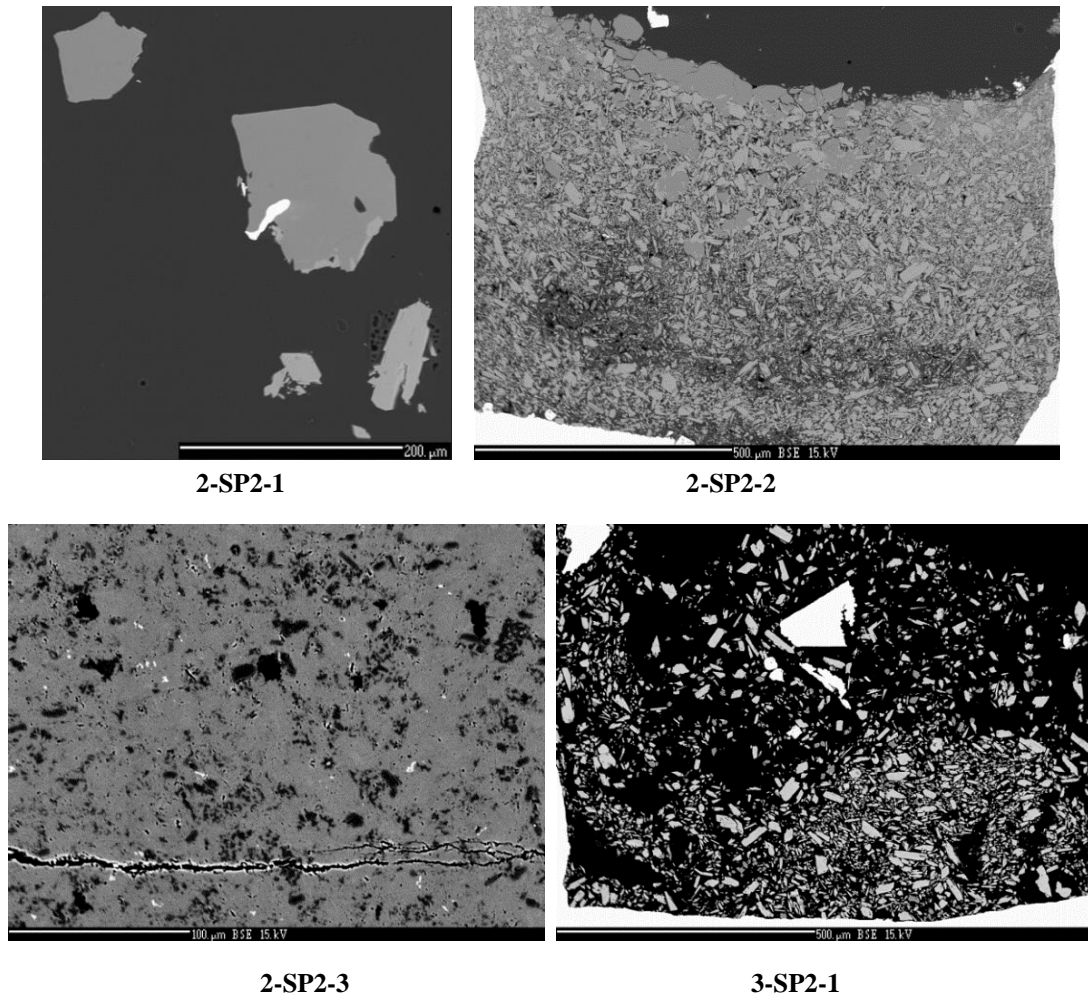


Fig. 3.1.2.2a SP2 experiments from 1.5 to 2.0 GPa. Their temperature is around 877 °C.

SP2 experiments at 2.5 and 3.0 GPa have totally different assemblies. Their biggest crystals are at the bottom of the capsules, which is different from the crystals distributions of the lower pressure experiments. Their sizes are larger than 100 µm and they are humite group minerals (norbergite and/or chondrodite). Instead of hornblende, garnet and pyroxene appear in these experiments. The quench phases are obvious in the capsules. They contact with the minerals or the capsule wall in the space occupied by fluid. Their phase assemblies and the mineral chemical formulas are shown in Table 3.1.2.2b.

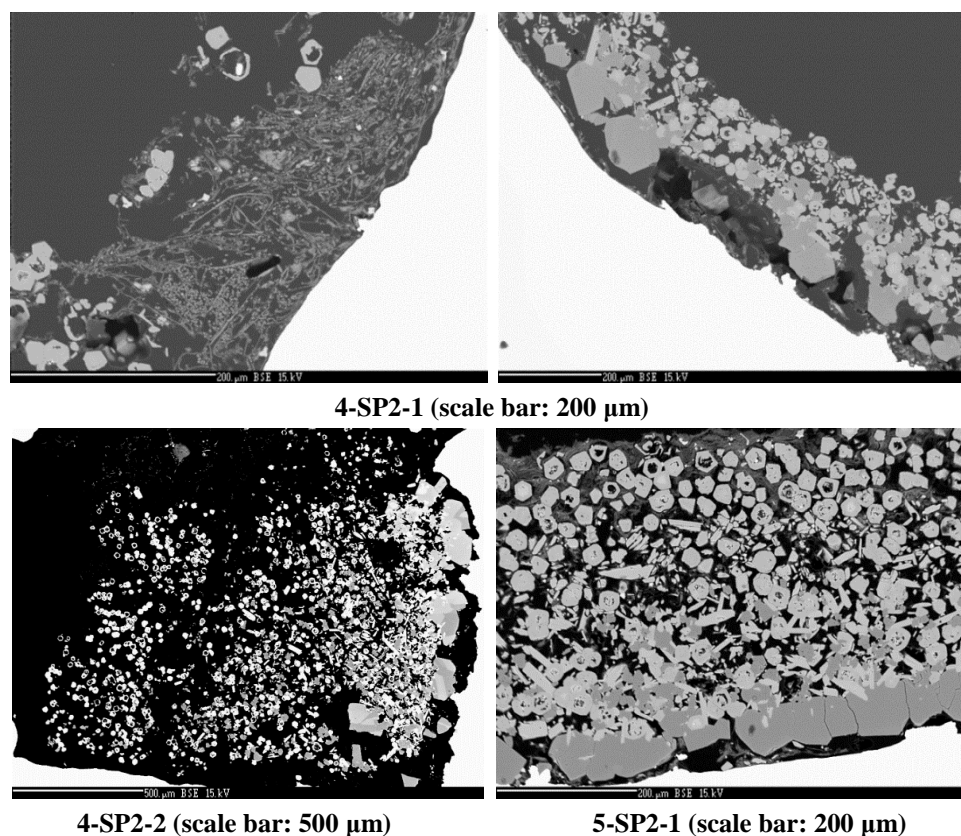


Fig. 3.1.2.2b SP2 experiments from 2.5 to 3.0 GPa. Their temperature is at 877 °C.

3.1.3 SP3 Series Experiments

Most SP3 experiments were conducted in nickel capsules with NNO buffer. The experiment at 957 °C was conducted with Mo capsules. Their phase assemblages are almost the same, hornblende and/or chondrodite (Table 3.1.3).

Table 3.1.3 Phase chemical formulas of SP3 experiments at 1.0GPa

Expt. ID	T / °C	Hornblende	Chondrodite
1-SP3-1	877	$\text{Na}_{0.30} (\text{Ca}_{1.91} \text{Mg}_{0.05}) (\text{Fe}_{0.45} \text{Mg}_{3.92} \text{Al}_{0.50}) (\text{Si}_{6.32} \text{Al}_{1.68}) \text{O}_{22} (\text{F}_{0.31} \text{OH}_{0.69})_2$	
1-SP3-2	857	$\text{Na}_{0.29} (\text{Ca}_{1.95} \text{Mg}_{0.12}) (\text{Fe}_{0.49} \text{Al}_{0.41} \text{Mg}_{4.03}) (\text{Si}_{6.45} \text{Al}_{1.55}) \text{O}_{22} (\text{F}_{0.29} \text{OH}_{0.71})_2$	$\text{Mg}_{4.84} \text{Si}_{1.99} \text{O}_8 (\text{F}_{0.62} \text{OH}_{0.38})_2$
1-SP3-3	857	$\text{Na}_{0.33} (\text{Ca}_{1.91} \text{Mg}_{0.05}) (\text{Fe}_{0.43} \text{Al}_{0.57} \text{Mg}_{3.92}) (\text{Si}_{6.32} \text{Al}_{1.68}) \text{O}_{22} (\text{F}_{0.33} \text{OH}_{0.67})_2$	$\text{Mg}_{4.84} \text{Si}_{1.99} \text{O}_8 (\text{F}_{0.69} \text{OH}_{0.31})_2$
1-SP3-4	837	$\text{Na}_{0.30} (\text{Ca}_{1.91} \text{Mg}_{0.04}) (\text{Fe}_{0.44} \text{Mg}_{3.91} \text{Al}_{0.56}) (\text{Si}_{6.42} \text{Al}_{1.58}) \text{O}_{22} (\text{F}_{0.31} \text{OH}_{0.69})_2$	$\text{Mg}_{4.87} \text{Si}_{1.99} \text{O}_8 (\text{F}_{0.69} \text{OH}_{0.31})_2$
1-SP3-5	887	$\text{Na}_{0.28} \text{Ca}_{1.95} (\text{Fe}_{0.43} \text{Al}_{0.50} \text{Mg}_{3.99}) (\text{Si}_{6.40} \text{Al}_{1.60}) \text{O}_{22} (\text{F}_{0.28} \text{OH}_{0.72})_2$	$\text{Mg}_{4.82} \text{Si}_{1.99} \text{O}_8 (\text{F}_{0.62} \text{OH}_{0.38})_2$
1-SP3-6	897	$\text{Na}_{0.28} (\text{Ca}_{1.92} \text{Mg}_{0.04}) (\text{Fe}_{0.45} \text{Mg}_{3.98} \text{Al}_{0.51}) (\text{Si}_{6.34} \text{Al}_{1.66}) \text{O}_{22} (\text{F}_{0.32} \text{OH}_{0.68})_2$	$\text{Mg}_{4.76} \text{Si}_{2.00} \text{O}_8 (\text{F}_{0.62} \text{OH}_{0.38})_2$
1-SP3-7	817	$\text{Na}_{0.32} (\text{Ca}_{1.88} \text{Mg}_{0.07}) (\text{Fe}_{0.44} \text{Mg}_{3.94} \text{Al}_{0.54}) (\text{Si}_{6.45} \text{Al}_{1.55}) \text{O}_{22} (\text{F}_{0.35} \text{OH}_{0.65})_2$	
1-SP3-8	957	$\text{Na}_{0.25} \text{Ca}_{1.94} (\text{Fe}_{0.45} \text{Mg}_{4.02} \text{Al}_{0.48}) (\text{Si}_{6.15} \text{Al}_{1.85}) \text{O}_{22} (\text{F}_{0.33} \text{OH}_{0.67})_2$	$\text{Mg}_{4.75} \text{Fe}_{0.06} \text{Si}_{2.01} \text{O}_8 (\text{F}_{0.60} \text{OH}_{0.40})_2$

3. Results

The pictures in Fig 3.1.3 show that the phase assemblies of SP3 experiments are quite similar. However, no chondrodite are found in 1-SP3-1 and 1-SP3-7 experiments. They only have hornblende. I re-polished 1-SP3-1 sample for three times and looked for chondrodite with electron microprobe and still cannot find any chondrodite minerals. However, most SP3 experiments have two minerals, so it is reasonable to treat two phase assemblies as a normal situation. For the mass balance calculation, I employed chondrodite composition from other SP3 experiments.

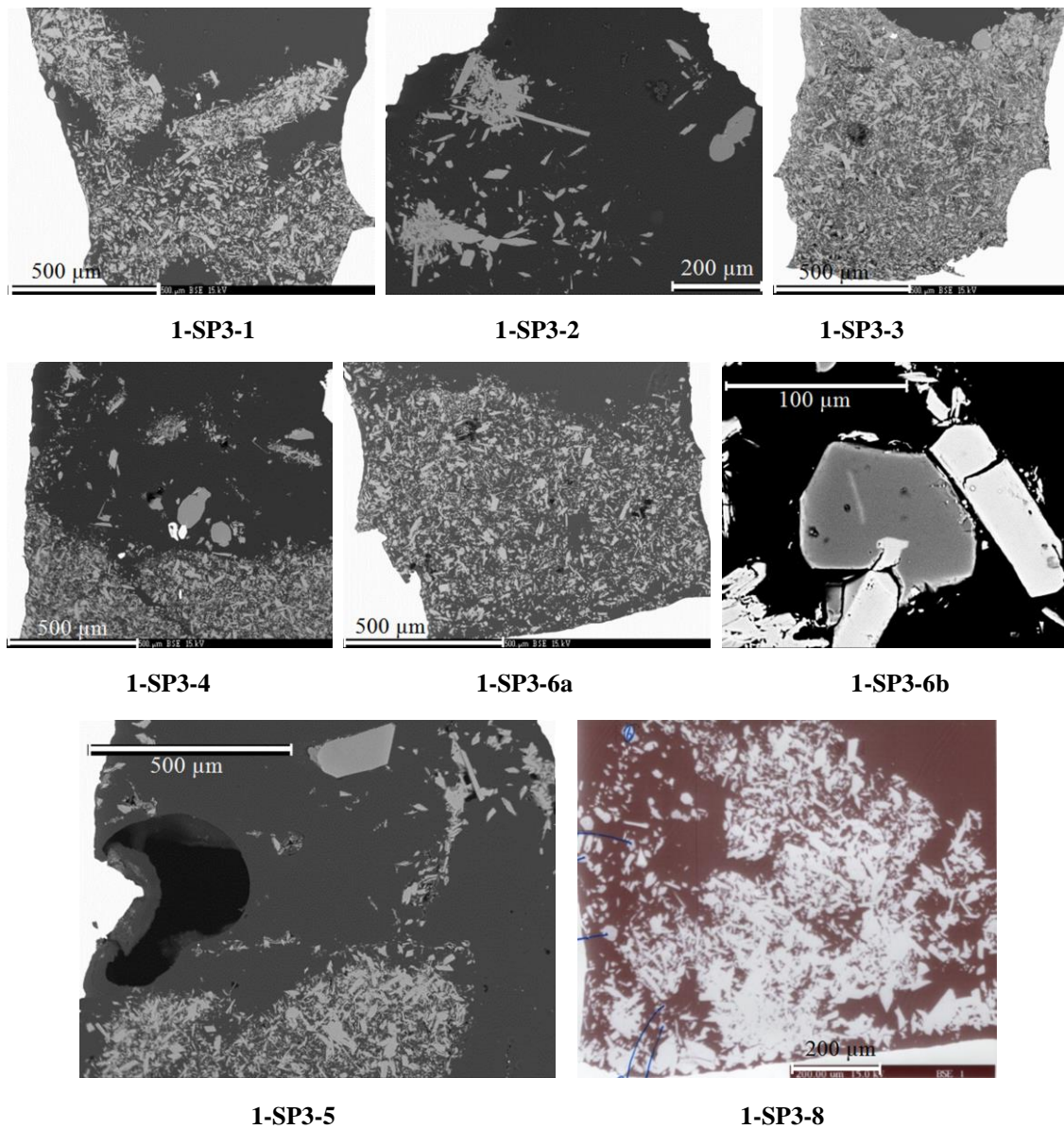


Fig. 3.1.3 The images of SP3 experiments. Except 1-SP3-6b, all of them are the cross-section of their capsules. 6b is some big crystal taken out of its capsule and fixed in epoxy.

In 1-SP3-5, the biggest chondrodite (~150 μm) in SP3 series experiments as Fig 3.1.3 shown. Figure 1-SP3-6b shows the biggest crystals of 1-SP3-6 experiment. When I opened the capsule, they are at the top of the minerals. I picked them up under microscope and mounted them in epoxy separately. The chondrodite size reaches 100 μm and the width of hornblende reaches approximately 40 μm . For the 1-SP3-7 experiments, I failed to open the capsule with the new method, and lost half capsule. Thus, I also mounted its rest minerals into epoxy in the same manner, and no capsule picture was taken.

3.1.4 SP4 Series Experiments

SP4 powder has the lowest F concentration (0.5 wt%). It is a mixture of SP1, SP3 and MgO powder. It is MgO richer than SP1 to SP3 starting materials, so it creates minerals with higher MgO concentrations.

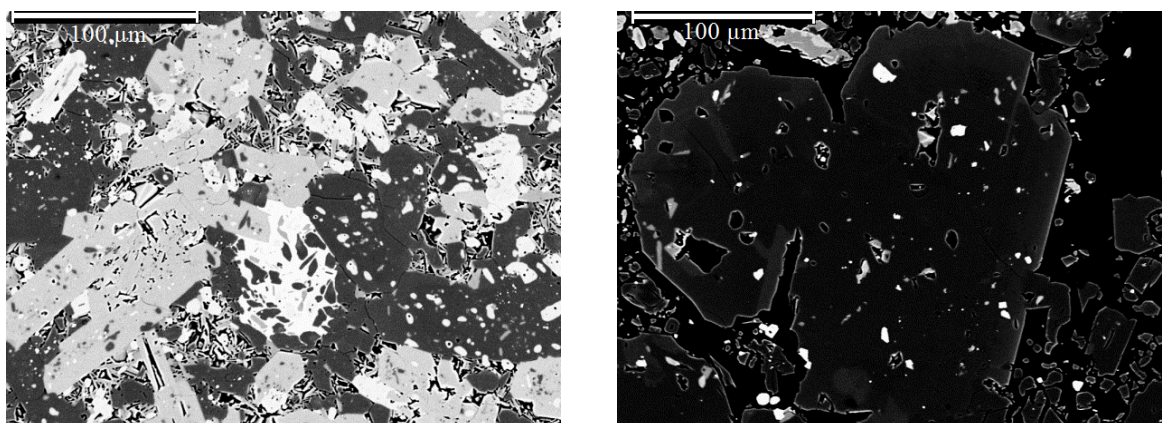


Fig. 3.1.4a The images of 1-SP4-1 (left) and 1-SP4-2 (right).

The initial two SP4 experiments were kept for too long durations (188 and 202 hours, respectively) to keep fluid. From Fig. 3.1.4a, their crystals are zoned. 1-SP4-1 contains hornblende, clinohumite, augite and a whit Ca-rich melt (in the center of the picture Fig. 3.1.4a left, surround some smaller minerals). 1-SP4-2 contains hornblende, clinohumite and augite. The biggest crystal in Fig. 3.1.4a right is clinohumite, and it is zoning. Its rim is brighter than its center. I measured two points at the edge of this crystal, which shows that the rim contains more MgO, SiO₂ and less F than the core. For stoichiometry calculation, it is like olivine, but olivine cannot have F more than 1 wt%. It perhaps indicates the breakdown

product of clinohumite. The size of clinohumite is over 100 μm in 1-SP4-2 and reaches 50 μm in 1-SP4-1. The width of hornblende obviously increases, comparing with those in SP1 to SP3 experiments. Augite width is approximately the same as hornblende. All the phase assemblies and the mineral chemical formulas are shown in Table 3.1.4.

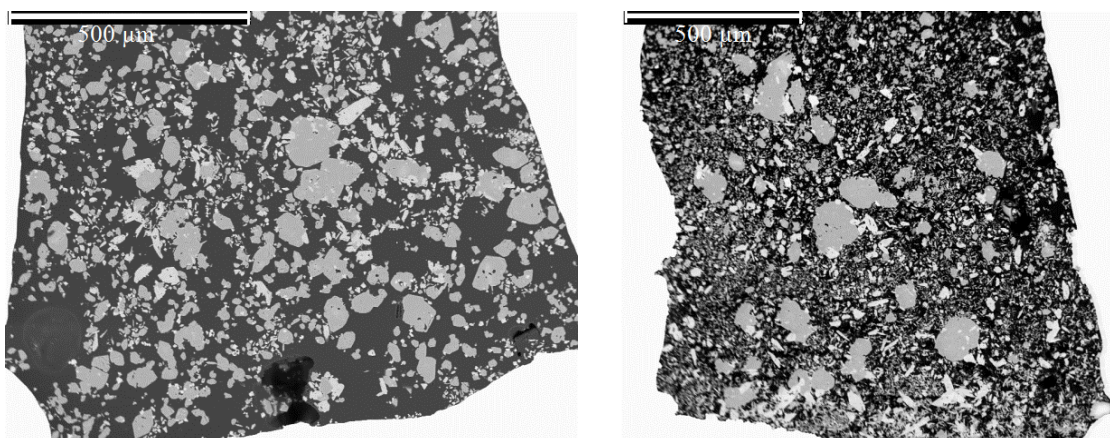


Fig. 3.1.4b The images of 1-SP4-3 (left) and 1-SP4-4 (right).

Table 3.1.4 Phase assemblies and their chemical formulas of SP4 experiments at 1.0 GPa

Expt. ID	T/ $^{\circ}\text{C}$	Hornblende	Clinohumite	Pyroxene	Clintonite
1-SP4-1	877	$\text{Na}_{0.81} \text{Ca}_{2.06} (\text{Fe}_{0.51} \text{Mg}_{3.92} \text{Al}_{0.36})$ $(\text{Si}_{5.53} \text{Al}_{2.47}) \text{O}_{22} (\text{F}_{0.12} \text{OH}_{0.88})_2$	$\text{Mg}_{8.70} \text{Si}_{4.02} \text{O}_{16}$ $(\text{F}_{0.34} \text{OH}_{0.66})_2$	$(\text{Mg}_{0.84} \text{Ca}_{0.98} \text{Al}_{0.08})$ $\text{Fe}_{0.07} (\text{Si}_{1.79} \text{Al}_{0.21}) \text{O}_6$	
1-SP4-2	857	$\text{Na}_{0.88} \text{Ca}_{2.02} (\text{Fe}_{0.53} \text{Mg}_{3.85} \text{Al}_{0.45})$ $(\text{Si}_{5.82} \text{Al}_{2.18}) \text{O}_{22} (\text{F}_{0.12} \text{OH}_{0.88})_2$	$\text{Mg}_{8.62} \text{Si}_{4.03} \text{O}_{16}$ $(\text{F}_{0.36} \text{OH}_{0.64})_2$	$(\text{Mg}_{0.83} \text{Ca}_{0.97} \text{Al}_{0.08})$ $\text{Fe}_{0.08} (\text{Si}_{1.83} \text{Al}_{0.17}) \text{O}_6$	
1-SP4-3	890		$\text{Mg}_{8.70} \text{Si}_{4.01} \text{O}_{16}$ $(\text{F}_{0.39} \text{OH}_{0.61})_2$	$(\text{Ca}_{1.00} \text{Mg}_{0.83} \text{Fe}_{0.11})$ $\text{Al}_{0.07} (\text{Si}_{1.81} \text{Al}_{0.19}) \text{O}_6$	$\text{Ca}_{1.96} (\text{Mg}_{4.61} \text{Fe}_{0.51} \text{Al}_{0.88})$ $(\text{Si}_{2.89} \text{Al}_{5.11}) \text{O}_{20} (\text{F}_{0.07} \text{OH}_{0.93})_4$
1-SP4-4	843	$\text{Na}_{0.88} \text{Ca}_{2.07} (\text{Fe}_{0.54} \text{Mg}_{3.95} \text{Al}_{0.35})$ $(\text{Si}_{5.85} \text{Al}_{2.15}) \text{O}_{22} (\text{F}_{0.13} \text{OH}_{0.87})_2$	$\text{Mg}_{8.78} \text{Si}_{4.00} \text{O}_{16}$ $(\text{F}_{0.39} \text{OH}_{0.61})_2$	$(\text{Ca}_{0.96} \text{Mg}_{0.85} \text{Fe}_{0.09})$ $\text{Al}_{0.06} (\text{Si}_{1.81} \text{Al}_{0.19}) \text{O}_6$	

1-SP4-3 contains augite, clinohumite and clintonite, while 1-SP4-4 has hornblende, clinohumite and augite. Both of them have fluid left and their durations are longer than 72 hours. However, 1-SP4-3 met some apparatus problems. The heating system of piston-cylinder stopped for a few times, and I restarted the program for a few times. Its abnormal phase assembly might be caused by the accident or Ni contamination. Nevertheless, 1-SP4-4 is a successful one, of which phase assembly should be standard for SP4 experiments. More successful SP4 experiments are needed to confirm it. But it is no doubt that clinohumite and augite must be created in SP4 experiments, because they exist in all four SP4

experiments.

The biggest crystals in these two experiments are clinohumite. They reach 100 μm . Their augites are wider than 50 μm . The proportions of hornblende or clintonite are small, and their mineral sizes are small as well. Their widths only reach approximately 20 μm .

3.1.5 Excess Doped Experiments

I conducted four SP1 or SP2 experiments with some excess in chemical components, such as MgF_2 , CaF_2 or quartz. The aim is to investigate how the mineral assembly (paragenesis) changes, if I change $\text{MgO-SiO}_2\text{-F}$ proportion of the starting materials. They are conducted at 1 GPa and different temperatures. The masses of each doped powder are shown in Table 2.2.4. The bulk compositions of these four experiments are listed below.

Table 3.1.5 The bulk compositions of each excess doped experiment at 1 GPa

Oxides	1-(SP1+ MgF_2)	2σ	1-(SP1+ CaF_2)	2σ	1-(SP2+Qtz)	2σ	1-(SP2+ MgF_2)	2σ
SiO_2	42.38	0.49	34.52	0.29	77.67	0.67	26.55	0.36
TiO_2	0.38	0.05	0.31	0.04	0.14	0.02	0.22	0.02
Al_2O_3	11.98	0.17	9.76	0.11	4.75	0.1	7.46	0.15
Cr_2O_3	0.64	0.06	0.52	0.05	0.26	0.03	0.42	0.05
FeO	3.21	0.12	2.62	0.09	1.23	0.07	1.93	0.10
MgO	25.13	0.31	14.79	0.08	9.41	0.16	14.78	0.21
CaO	10.48	0.23	28.15	0.16	4.15	0.07	34.06	0.10
MnO	0.08	0.04	0.07	0.03	0.03	0.02	0.05	0.02
Na_2O	1.29	0.07	1.05	0.05	0.84	0.04	1.32	0.06
F	6.58	0.15	13.32	0.01	1.89	0.03	21.65	0.04

1-(SP2+ MgF_2) was doped with absolute excess MgF_2 into SP2 powder (Fig. 3.1.5a right), and its F concentration reached 21 wt% (Table 3.1.5). It has fluid left, but I missed it by failed operation. Its solid phase assemblies are MgF_2 , norbergite and silicate melts (among minerals, e.g. in the center of the capsule), as well as some precipitates and little spheres of melt in very small quantities. The sizes of its MgF_2 phase (50 μm) and norbergite (200 μm) are quite large.

1-(SP1+ MgF_2) has less F concentration (6.58 wt%) than 1-(SP2+ MgF_2), and more than SP2. Its experimental temperature is 965 $^\circ\text{C}$, much higher than 1-(SP2+ MgF_2). 1.25 mg fluid has been retrieved from its capsule into a flask for HPLC analysis. Its phase assemblies are

melt, chondrodite and spinel. Because these spinels are small and only present in the melt, it was perhaps formed during the quench. There is a gray layer attached to the melt on the top portion of this charge (Fig. 3.1.5a left). It could be a precipitate phase or a part of the melt, for it is underneath the surface. However, the obvious precipitates are present at the edge of the capsule at the right portion of the picture.

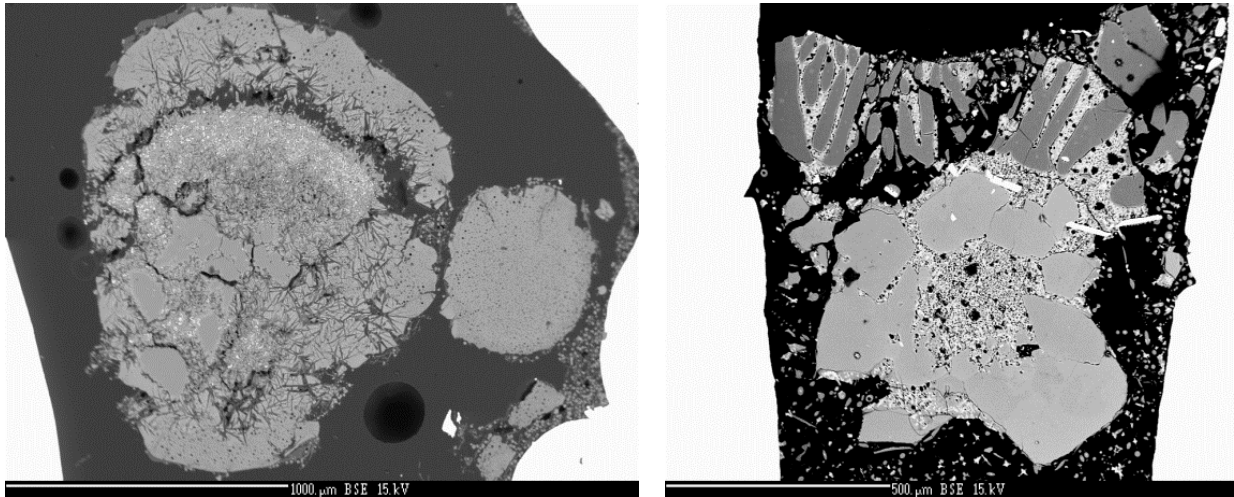


Fig. 3.1.5a The images of experiment 1-(SP1+MgF₂) (left) and 1-(SP2+MgF₂) (right)

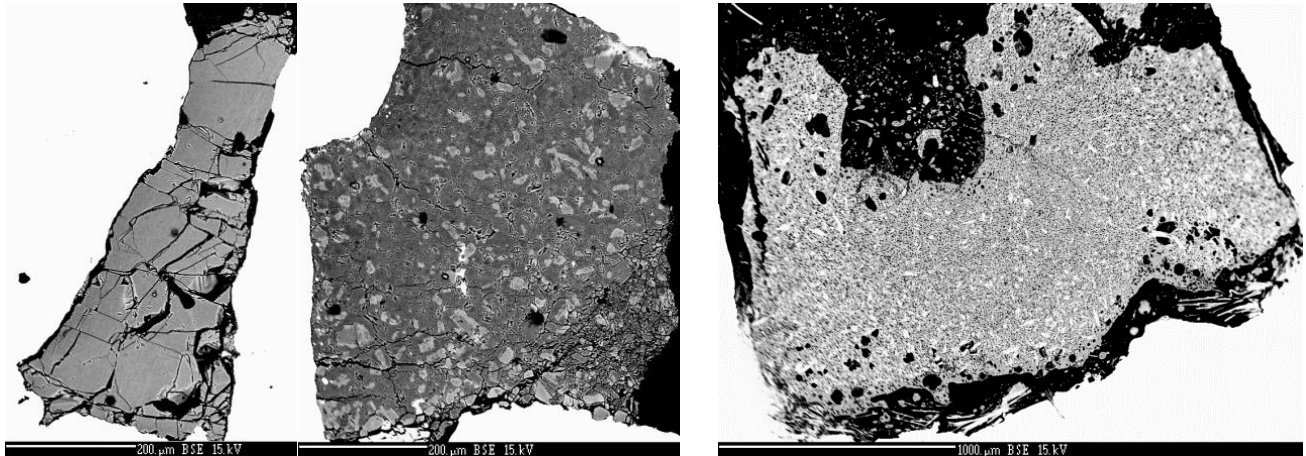


Fig. 3.1.5b The images of experiments 1-(SP1+CaF₂) (left) and 1-(SP2+Qtz) (right)

In order to keep MgO-SiO₂ ratio in the bulk composition, I introduced CaF₂ into SP1 to investigate the phase assemblies. While, this experiment 1-(SP1+CaF₂) is failed (Fig. 3.1.5b, left), for it lost most of its water and remained a separate CaF₂ phase and no obvious space among minerals. It indicates this experiment failed to convert the fluid inside. This experiment failed to get a mineral-fluid system. Nevertheless, augite is present in the capsule and surrounded by F-bearing melt surrounding. The fluid mass (mass difference) may be

derived from the losses of some micro mineral crystals and soluble precipitate.

In experiment 1-(SP2+Qtz), the starting material composition moves to SiO₂-rich side, by adding a quartz crystal with SP2 powder into the capsule. This experiment is conducted at 950 °C, and melts is the dominant phase in the capsule, and some anthophyllite [(Fe_{0.26} Mg_{5.10} Ca_{1.33} Ni_{0.16}) Si_{7.94} O₂₂ (F_{0.47} OH_{0.53})₂], hornblende [Na_{0.09} (Ca_{1.67} Mg_{0.31}) (Mg_{4.27} Fe_{0.33} Ni_{0.07} Al_{0.20} Cr_{0.13}) (Si_{7.45} Al_{0.55}) O₂₂ (F_{0.48} OH_{0.52})₂] and talc [Mg_{3.96} Ni_{1.83} Si_{8.01} O₂₀ (F_{0.27} OH_{0.73})₄] are present in the melt, as well as some isolated spheric melt in the empty space of the bottom portion. The sizes of these minerals and spheric melts are small. Generally, their widths only reach around 20 μm. The obvious nickel contamination happened at the bottom portion of the capsule, where talc was found. Mass balance calculation will not work when the sample has melt and contaminations. Fortunately, I managed to collect its fluid for HPLC measurement.

3.2 Attainment of Equilibrium

The temperatures of the successful SP1 experiments range from 807 to 900 °C, and the duration varies from 94 to 330 hours. The width of hornblende ranges from 35 to 60 μm with a median of approximately 40 μm. An increase of temperature influences the size of hornblendes crystals more effectively than an increase of run duration; higher the run temperature crystallizes larger hornblende than longer run duration at low temperature runs.

In the structures of hornblendes, T sites are shared by SiO₂ and Al₂O₃. Comparisons of their concentrations distinguish hornblende species, by the T site exchange tendency in the case of SP1 experiments. Fig. 3.2a illustrates that most of points distribute along single exchange vector, except a part of 1-SP1-2. Hornblendes from 1-SP1-2 experiment are obviously separated into 2 groups, and their chemical formulas are shown in Table 3.1.1. The reason led to this separation was probably that the group with lower slope is significantly contaminated by Ni, as well as exhausted its water during annealing. Moreover, hornblende is the dominant phase in the successful SP1 runs (1-SP1-3 to 8), which is reproducible. Their stoichiometry calculations (Table 3.1.1) also indicate that their Na, Ca and Si number in the chemical formula are constant. In section 3.1.1, the textures show the crystals are euhedral

3. Results

and not zoned, excluding the experiments with the Ni contamination. And the phase assemblies from the different duration experiments are similar. Therefore, I conclude that SP1 experiments reached near equilibrium conditions during their temperature region with the existence of water.

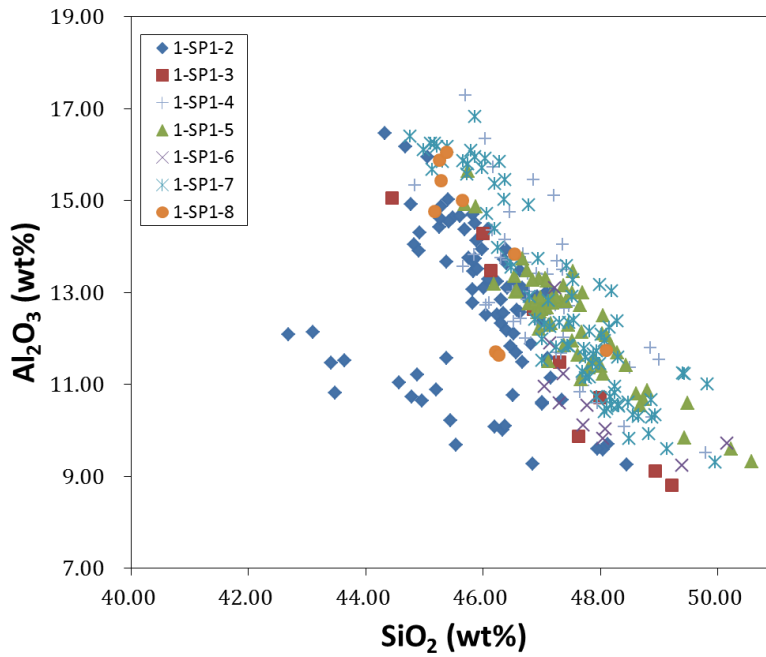


Fig. 3.2a SiO₂ vs. Al₂O₃ concentration in hornblendes from SP1 experiments.

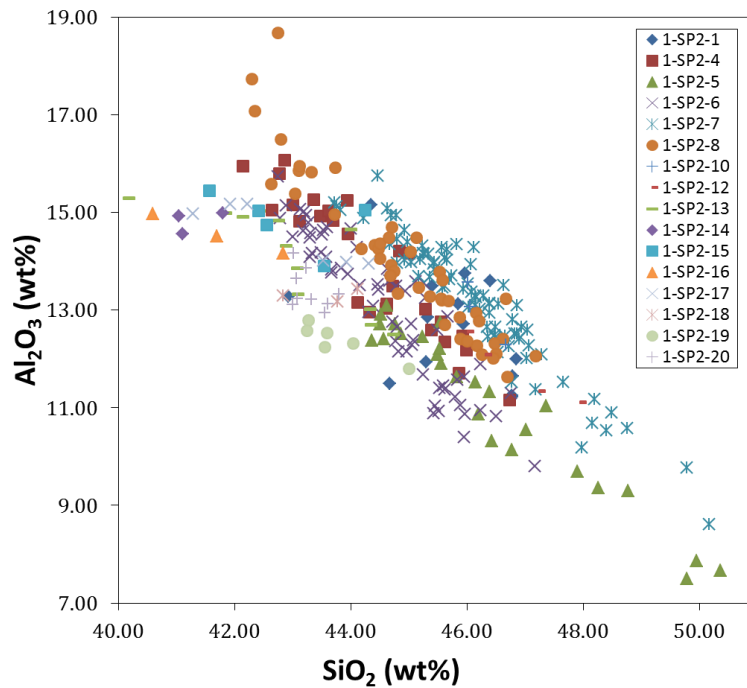


Fig. 3.2b SiO₂ vs. Al₂O₃ concentration in hornblendes from SP2 experiments.

3. Results

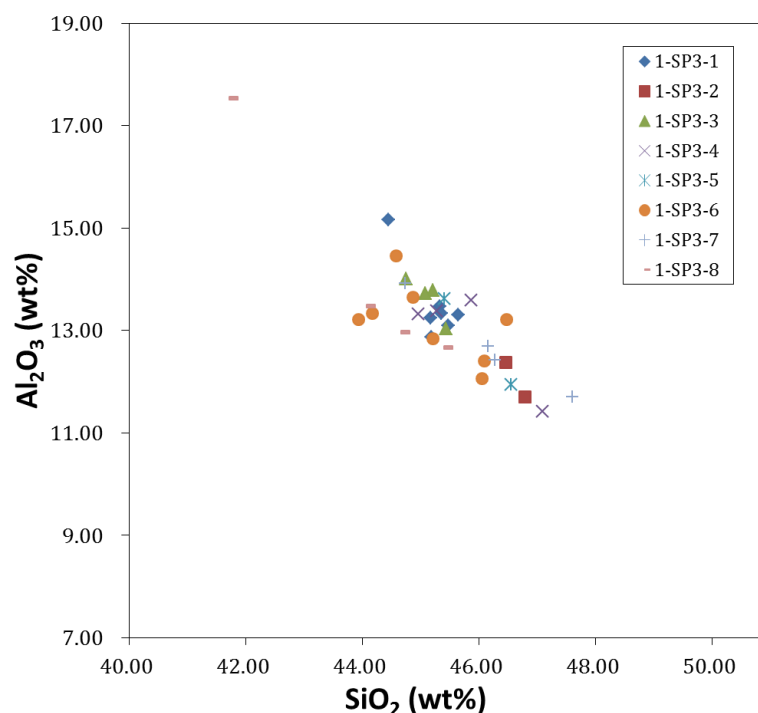


Fig. 3.2c SiO₂ vs. Al₂O₃ concentration in hornblendes from SP3 experiments.

The hornblendes in SP2 and SP3 experiments are approximately the same size as those found in SP1 ones, regardless of changes in the temperature or the duration. The maximum size of humite group minerals in each experiment ranges from approximately 20 to 150 μm. For comparison, an unbuffered experiment in an Au-Pd capsule, sealed by arc welding, was conducted with the SP2 powder and water, and its norbergite crystals reached only 20 μm. Moreover, the hornblende and norbergite compositions of SP2 experiments are quite similar, although F is affected by oxygen fugacity. All the analysis points of SP2 hornblendes are plotted around the same area in Fig. 3.2b. Comparing their chemical formulas with SP1 hornblendes (Table 3.1.1 and Table 3.1.2.1a), it is feasible to classify them to the hornblendes. But their SiO₂ concentrations are a little offset, which indicates perhaps different subgroup minerals. The duration of 1-SP2-16 is only 34 hours and it has the same mineral compositions. In a large water quantity experiment, the fluid convection helps the system reach equilibrium in a short time. Therefore, the SP2 experiments with a hornblende-norbergite-fluid system reached near equilibrium. Some experiments, which were conducted with temperature higher than 940 °C, created melt. Because they have fluid left after the quench, and their experimental durations are longer than 72 hours, and always crystallized humite group

minerals. Although the partial melt happens, it is reasonable to conclude that they reached the equilibrium during annealing. However, experiment 1-SP2-14 has an abnormal phase assemblage: hornblende-norbergite-chondrodite-fluid. Although its phase assemblage and hornblende composition indicate a potential material loss and/or Ti contamination, its fluid mass (0.6 mg) demonstrates that the system was closed during the annealing. Thus, it is reasonable to treat this experiment as an equilibrium one, but it is not comparable with other SP2 experiments for its changed bulk composition.

For SP3 experiments, their phase assemblage is hornblende and chondrodite, which is independent of experimental conditions, as the same for SP2 experiments. Although I failed to sample chondrodite in 1-SP3-1 capsule, its hornblende composition is close to other SP3 experiments. Because the absence of chondrodite would indicate a decrease in F concentration in the bulk composition, it is reasonable to infer the presence of chondrodite in 1-SP3-1. All SP3 minerals show euhedral faceted shapes, and the chondrodite compositions are nearly constant. Fig. 3.2c illustrates that SiO_2 and Al_2O_3 concentration from SP3 experiments are in the similar area with SP2, and it is reasonable to classify them as hornblendes. Moreover, SP3 hornblendes have similar concentrations on other major elements (Na, Ca, Mg, and F). Based on these criteria, I conclude that all the successful SP3 experiments reached near equilibrium.

The phase assemblies of SP4 experiments are quite different, but hornblendes and clinohumite are present. The decreasing of SiO_2 concentrations in starting material resulted in low SiO_2 concentration hornblende, and its high MgO promotes to the presence of augite. The proportions of hornblendes in SP4 experiments are less than those from SP1 to SP3 experiments. Instead of hornblendes, clinohumite is a dominant mineral, of which sizes reached over 100 μm . Augite and hornblende dimensions are in the similar level comparing to SP2 experiments. The same mineral assembly for three experiments indicates that 1-SP4-4 reached a near equilibrium. 1-SP4-3 experiment is an exception, which crystallized clintonite. However, its big clinohumite crystals are not zoned, and 1.43 mg fluid was kept in its charge. Thus, the abnormal phase assembly might be caused by the Ni contamination, and the system perhaps reached the near equilibrium as well.

In summary, the experiments, which kept the fluid after quenching, were successfully

sealed as semi-close systems. Their reproducible phase assemblies demonstrate that the experiments reach the near equilibrium. Thus, the experiment duration over 48 hours and the presence of its fluid indicate the near equilibrium. Therefore, it is reasonable to treat some experiments (excess dope, or melt-bearing SP2 experiments) as close equilibrium runs.

3.3 Solid Phases Compositions

Solid phases (melt and minerals) stay in the charges after the post-quench procedure. I will introduce their compositions from electron microprobe analyses in this section and compare with some natural samples. I will introduce a method to decide the composition of degassed melt. For hydrous minerals, I would like to talk about the stoichiometry calculation for F proportion in OH site.

3.3.1 Hornblendes

All starting materials (from SP1 to SP4) all create hornblendes, though those from SP4 experiments are different from others. The excess SiO₂-dope experiment, 1-(SP2+Qtz), created a mineral-melt-fluid system. It is different from other mineral-fluid system experiments. Its amphibole minerals are hornblende and anthophyllite.

As the stoichiometry calculations shown (Table 3.3.1), the ratio $n(\text{Mg})/n(\text{Mg}+\text{Fe})$ (Mg#) of the hornblendes from SP1 to SP3 experiments are quite constant (0.90 ± 0.01 ; Some minerals are contaminated by nickel. Their Mg# counts their Ni number in formula). The number of Na on the basis of 24 oxygen atoms is 0.31(3), 0.30(5) and 0.29(3) for SP1, SP2 and SP3 experiments, respectively, but 0.86(4) for SP4 experiments. For the higher initial F concentration, F in hornblendes is higher. For SP2 runs with 5 wt% F, their hornblendes have approximately 2.2wt% F. Hornblendes from SP3 experiments only contain 1.4 wt% F, and from SP4 ones only have 0.5 wt% F. These general tendencies are deduced from results excluding failed experiment, which lost water during runs.

The ratio $n(\text{Al})/n(\text{Al}+\text{Si})$ (Al#) ranges from 0.21 to 0.30. The average values of Al# in

successful experiments with different starting powders are 0.24, 0.27, 0.26 and 0.30, from SP1 to SP4 respectively. The ratios between Al_2O_3 and SiO_2 in hornblendes and their compositions are close to those of starting materials from SP1 to SP3, but different for SP4 experiments. It indicates the introduction of too much MgO makes SP4 a different system. The Al# of the hornblendes from SP1 to SP3 experiments correlate with the F concentration of each starting material. The hornblendes of MgO-rich SP4 experiments have higher Al# than other three starting powder experiments. It demonstrates that the alumina concentration of hornblende can be influenced by MgO concentration of starting materials in aqueous hydrous experiments. Moreover, the abundances of Ca (CaO from 12.17 to 14.96 wt%) also behave similarly with alumina. These hornblendes have some subtle differences, but the ranges of compositional variation of hornblendes are independent of temperature conditions.

Table 3.3.1a Atomic abundance of some major elements of hornblendes in formula unit.

Expt. ID	Na	Ca	Fe	Si	Mg(+Ni)	Al	Mg#	Al#
1-SP1-2	0.35	1.87	0.38	6.52	4.02	2.11	0.91	0.24
1-SP1-3	0.33	1.82	0.40	6.60	4.18	3.41	0.91	0.34
1-SP1-4	0.30	1.85	0.44	6.56	3.93	2.12	0.90	0.24
1-SP1-5	0.29	1.84	0.42	6.64	3.98	2.03	0.90	0.23
1-SP1-6	0.34	1.89	0.42	6.70	4.07	1.74	0.91	0.21
1-SP1-7	0.30	1.83	0.42	6.61	3.92	2.10	0.90	0.24
1-SP1-8	0.26	1.87	0.50	6.47	3.71	2.32	0.88	0.26
1-SP2-1	0.30	1.89	0.41	6.52	3.90	2.18	0.90	0.25
1-SP2-4	0.30	2.07	0.45	6.21	3.79	2.29	0.89	0.27
1-SP2-5	0.38	1.93	0.42	6.51	4.08	1.84	0.91	0.22
1-SP2-6	0.27	2.04	0.41	6.28	4.00	2.16	0.91	0.26
1-SP2-7	0.33	1.79	0.42	6.46	4.04	2.21	0.91	0.25
1-SP2-8	0.30	2.01	0.44	6.28	3.81	2.31	0.90	0.27
1-SP2-10	0.24	1.95	0.49	6.47	3.84	2.14	0.89	0.25
1-SP2-12	0.30	1.91	0.45	6.62	3.82	1.96	0.89	0.23
1-SP2-13	0.28	2.09	0.48	6.01	3.94	2.33	0.89	0.28
1-SP2-14	0.31	2.23	0.49	5.84	3.89	2.16	0.89	0.27
1-SP2-15	0.27	2.04	0.47	6.00	3.92	2.45	0.89	0.29
1-SP2-16	0.24	2.15	0.47	5.91	3.88	2.43	0.89	0.29
1-SP2-17	0.24	2.17	0.44	5.96	3.89	2.38	0.90	0.29
1-SP2-18	0.35	2.03	0.51	6.14	3.98	2.21	0.89	0.26
1-SP2-19	0.39	2.05	0.50	6.18	4.08	2.06	0.89	0.25
1-SP2-20	0.29	2.16	0.50	6.03	4.00	2.20	0.89	0.27
1-SP2-22	0.20	1.83	0.42	7.22	4.24	1.13	0.91	0.14

3. Results

Expt. ID	Na	Ca	Fe	Si	Mg(+Ni)	Al	Mg#	Al#
1-SP2-23	0.33	2.00	0.39	6.58	3.96	1.88	0.91	0.22
2-SP2-1	0.28	2.09	0.45	6.20	3.89	2.25	0.90	0.27
2-SP2-2	0.32	1.97	0.43	6.48	3.85	2.13	0.90	0.25
3-SP2-1	0.30	2.20	0.45	6.32	3.82	2.22	0.89	0.26
1-SP3-1	0.30	1.91	0.45	6.32	3.97	2.18	0.90	0.26
1-SP3-2	0.29	1.95	0.49	6.45	4.15	1.96	0.89	0.23
1-SP3-3	0.33	1.91	0.43	6.32	3.97	2.25	0.90	0.26
1-SP3-4	0.30	1.91	0.44	6.42	3.95	2.14	0.90	0.25
1-SP3-5	0.28	1.95	0.43	6.40	3.99	2.10	0.90	0.25
1-SP3-6	0.28	1.92	0.45	6.34	4.02	2.17	0.90	0.25
1-SP3-7	0.32	1.88	0.44	6.45	4.01	2.09	0.90	0.24
1-SP3-8	0.25	1.94	0.45	6.15	4.02	2.33	0.90	0.27
1-SP4-1	0.81	2.06	0.51	5.53	3.92	2.83	0.88	0.34
1-SP4-2	0.88	2.02	0.53	5.82	3.85	2.63	0.88	0.31
1-SP4-4	0.88	2.07	0.54	5.85	3.95	2.50	0.88	0.30
1-(SP2+Qtz)	0.00	1.33	0.26	7.94	5.26	0.07	0.95	0.01
	0.09	1.67	0.33	7.45	4.65	0.75	0.93	0.09

SP4 hornblendes have higher Al#, NaO concentrations. Because more Si is substituted by Al in T site, charge balance requires trivalent in C site or Na^+/K^+ in A site. And its similar Mg# and Ca compositions with SP1 to SP3 hornblende, indicates their cations in B and C sites do not differ much. The Mg abundance of hornblendes in SP2 and SP3 experiments is somewhat similar to amphiboles found in sub-arc mantle peridotites (e.g. Abe et al., 1998; Ionov, 2010). Ca, Na, and Al are within compositional range for amphiboles in metamorphosed oceanic crusts (e.g. Mevel et al., 1978). This compositional variation of SiO_2 and Al_2O_3 does not correlate with F in the OH-site. It should also be noted that the standard deviations of SiO_2 and Al_2O_3 are larger than for the other oxides in all hornblendes. However, the variation follows the exchange relationship of Si and Al in the T site. This variation is perhaps due to nucleation kinetics and potential compositional stratification in the charge.

In conclusion, all the amphiboles are of the hornblende group (a calc-amphibole), while the variations of some elements can divide these amphibole into different subgroup: magnesiohornblende (SP1, Table 3.1.1), magnesiohornblende or tschermakite (SP2 at 1 GPa, Table 3.1.2.1a & b), tschermakite (SP2 at 1.5~2.0 GPa, Table 3.1.2.2a and SP3, Table 3.1.3), pargasite (SP4, Table 3.1.4). By far my experimental results show that F concentration in

3. Results

every hornblende crystal in the same capsule is not influenced by the subtle variations (such as Si concentration differences in T site, Ni contaminations). While some divalent cation concentrations are constant, they perhaps can affect potentially F behaviors.

Table 3.3.1b The average compositions of hornblende group minerals (unit: wt%).

Expt. ID	T/ °C	SiO ₂	TiO ₂	Al ₂ O ₃	Cr ₂ O ₃	FeO	MgO	CaO	MnO	NiO	Na ₂ O	F	H ₂ O	Total
1-SP1-2	995	45.96	0.44	12.61	0.53	3.24	17.10	12.21	0.08	3.47	1.26		2.10	99.01
		1.07	0.08	1.68	0.23	0.68	2.91	0.70	0.04	5.19	0.17		0.05	0.39
1-SP1-3	995	47.17	0.46	11.71		3.42	19.29	12.15	0.08	1.44	1.22		2.14	99.09
		1.51	0.10	2.28		0.42	2.20	2.00	0.02	2.08	0.14		0.02	0.55
1-SP1-4	900	47.06	0.41	12.92	0.50	3.79	18.94	12.32	0.08		1.11		2.15	99.30
		0.94	0.06	1.62	0.24	0.26	0.53	0.71	0.03		0.16		0.02	0.55
1-SP1-5	877	47.51	0.45	12.33		3.64	19.09	12.28	0.08	0.36	1.09		2.14	98.98
		0.95	0.09	1.19		0.21	0.64	0.51	0.03	0.35	0.16		0.01	0.34
1-SP1-6	827	47.54	0.40	10.47	0.97	3.69	19.38	12.41	0.07	0.16	1.26		2.13	98.49
		0.62	0.12	0.48	0.23	0.26	0.39	0.46	0.09	0.08	0.14		0.01	0.34
1-SP1-7	857	47.32	0.42	12.78	0.50	3.64	18.84	12.17	0.08	0.14	1.11		2.13	99.14
		1.23	0.06	2.12	0.23	0.25	0.74	0.50	0.03	0.25	0.10		0.01	0.38
1-SP1-8	807	45.98	0.45	14.00	0.47	4.23	17.67	12.40	0.12	0.14	0.95		2.13	98.50
		0.94	0.12	1.85	0.30	0.56	0.91	0.53	0.09	0.10	0.27		0.01	0.52
1-SP2-1	770	46.56	0.39	13.20	0.58	3.47	18.69	12.57	0.08	0.07	1.09	2.33	1.04	99.08
		0.33	0.05	0.75	0.33	0.23	0.33	0.39	0.02	0.08	0.04	0.18	0.08	0.67
1-SP2-4	870	44.34	0.33	13.89	0.79	3.89	18.18	13.57	0.08	0.66	1.10	2.17	1.11	99.21
		1.19	0.08	1.36	0.26	0.35	0.66	0.25	0.03	1.03	0.08	0.12	0.06	0.41
1-SP2-5	955	46.41	0.29	11.11	0.93	3.54	19.50	12.87	0.09	0.70	1.40	2.42	0.96	99.22
		1.79	0.08	1.69	0.35	0.59	0.57	0.22	0.03	0.77	0.18	0.16	0.08	0.40
1-SP2-6	900	44.61	0.29	13.04	0.58	3.52	17.64	13.51	0.08	2.64	0.98	2.16	1.11	99.26
		1.11	0.06	1.46	0.29	0.73	1.11	0.26	0.03	2.70	0.07	0.24	0.10	0.42
1-SP2-7	930	46.14		13.17	0.83	3.57	19.38	11.91	0.05	0.21	1.21	3.30	0.58	98.98
		1.24		1.35	0.14	0.34	0.46	0.24	0.03	0.18	0.13	0.23	0.11	0.35
1-SP2-8	827	44.93	0.35	13.98	0.70	3.73	18.26	13.43	0.08	0.27	1.09	2.11	1.14	99.21
		1.33	0.06	1.61	0.26	0.23	0.50	0.24	0.03	0.18	0.11	0.13	0.06	0.43
1-SP2-10	787	46.25	0.35	12.97	0.33	4.22	18.42	12.99	0.08	0.31	0.90	2.48	0.97	99.22
		0.70	0.12	0.64	0.20	0.80	0.41	0.48	0.09	0.32	0.15	0.27	0.08	0.49
1-SP2-12	777	46.89	0.36	11.78	0.84	3.79	18.17	12.62	0.09	0.84	1.11	2.11	1.12	98.85
		0.88	0.03	0.67	0.22	0.44	0.77	0.33	0.01	0.61	0.08	0.10	0.04	0.29
1-SP2-13	877	42.99	0.36	14.12	0.83	4.08	18.90	13.97	0.10	0.06	1.02	2.33	1.04	98.83
		1.28	0.05	1.00	0.40	0.54	0.33	0.35	0.02	0.03	0.09	0.10	0.05	0.19
1-SP2-14	877	41.97	0.33	14.72	0.66	4.23	18.73	14.96	0.05	0.08	1.16	2.11	1.15	99.30
		0.66	0.12	0.48	0.15	0.28	0.38	0.49	0.09	0.07	0.14	0.22	0.03	0.26
1-SP2-15	907	42.86	0.47	14.84	0.57	3.98	18.79	13.63	0.09	0.06	1.01	2.22	1.09	98.69
		1.04	0.17	0.58	0.19	0.27	0.39	0.45	0.09	0.08	0.13	0.26	0.05	0.36

3. Results

Expt. ID	T/ °C	SiO ₂	TiO ₂	Al ₂ O ₃	Cr ₂ O ₃	FeO	MgO	CaO	MnO	NiO	Na ₂ O	F	H ₂ O	Total
1-SP2-16	927	41.71	0.42	14.55	0.96	3.97	18.37	14.18	0.07	0.03	0.88	2.21	1.07	97.49
		1.13	0.12	0.41	0.26	0.65	0.38	0.49	0.09	0.07	0.12	0.27	0.03	0.56
1-SP2-17	917	42.87	0.32	14.54	0.92	3.81	18.78	14.57	0.07	0.10	0.87	2.11	1.15	99.26
		1.22	0.11	0.62	0.21	0.73	0.43	0.50	0.09	0.07	0.12	0.26	0.05	0.88
1-SP2-18	947	43.58	0.23	13.30	0.92	4.31	18.96	13.44	0.06		1.30	2.22	1.07	98.49
		0.69	0.11	0.33	0.16	0.30	0.41	0.45	0.09		0.14	0.33	0.05	0.68
1-SP2-19	977	43.79	0.20	12.37	0.97	4.21	19.40	13.54	0.05	0.08	1.42	2.07	1.14	98.39
		0.82	0.11	0.34	0.16	0.28	0.44	0.50	0.09	0.11	0.15	0.16	0.02	0.37
1-SP2-20	1007	43.30	0.22	13.40	0.71	4.28	19.26	14.48	0.06	0.12	1.07	2.02	1.20	99.27
		0.67	0.11	0.40	0.15	0.28	0.39	0.48	0.09	0.08	0.13	0.22	0.05	0.54
1-SP2-22	850	51.99	0.47	6.90	1.01	3.58	20.47	12.31	0.07	0.06	0.76	2.49	0.98	100.06
		1.14	0.09	1.20	0.17	0.35	0.47	0.64	0.09	0.07	0.11	0.38	0.09	0.61
1-SP2-23	800	47.16	0.43	11.43	1.03	3.33	19.03	13.39	0.10	0.18	1.21	2.37	1.02	99.71
		0.81	0.08	0.96	0.23	0.25	0.45	0.44	0.08	0.13	0.15	0.37	0.12	0.66
2-SP2-1	877	43.60	0.27	13.43	0.66	3.76	18.38	13.69	0.08	0.15	1.01	1.75	1.28	97.34
		0.82	0.11	0.94	0.14	0.26	0.38	0.49	0.09	0.12	0.13	0.24	0.06	0.54
2-SP2-2	857	45.85	0.31	12.79	0.68	3.65	18.24	13.00	0.05	0.17	1.16	1.88	1.23	98.24
		0.75	0.11	0.56	0.26	0.26	0.42	0.44	0.09	0.08	0.14	0.15	0.02	0.23
3-SP2-1	877	44.97	0.17	13.39	0.79	3.84	18.23	13.40	0.09	0.59	1.11	1.61	1.37	98.88
		0.70	0.10	0.31	0.15	0.27	0.39	0.48	0.09	0.13	0.13	0.24	0.05	0.25
1-SP3-1	877	45.46	0.36	13.30	0.44	3.85	19.41	12.80	0.09	0.29	1.11	1.40	1.49	99.41
		0.69	0.12	0.33	0.13	0.26	0.39	0.44	0.09	0.09	0.13	0.21	0.03	0.55
1-SP3-2	857	46.63	0.37	12.04	0.12	4.26	20.14	12.57	0.09	0.16	1.09	1.31	1.54	99.78
		0.71	0.11	0.48	0.10	0.28	0.43	0.44	0.09	0.11	0.13	0.20	0.01	0.03
1-SP3-3	857	45.12	0.35	13.63	0.37	3.63	19.01	12.75	0.05	0.30	1.20	1.48	1.43	98.73
		0.69	0.12	0.42	0.13	0.26	0.41	0.44	0.09	0.09	0.14	0.22	0.04	0.28
1-SP3-4	837	45.80	0.40	12.92	0.45	3.73	18.94	12.72	0.09	0.32	1.10	1.42	1.46	98.80
		0.94	0.12	1.01	0.13	0.26	0.39	0.44	0.09	0.09	0.13	0.21	0.04	0.15
1-SP3-5	887	45.98	0.40	12.78	0.77	3.65	19.25	12.92	0.10	0.25	1.03	1.28	1.55	99.42
		0.81	0.12	1.19	0.15	0.26	0.42	0.45	0.09	0.11	0.12	0.20	0.01	0.57
1-SP3-6	897	45.18	0.33	13.15	0.46	3.82	19.22	12.74	0.07	0.10	1.04	1.43	1.46	98.40
		0.95	0.11	0.74	0.19	0.26	0.40	0.47	0.09	0.07	0.13	0.23	0.06	0.99
1-SP3-7	817	46.20	0.37	12.68	0.45	3.75	19.30	12.54	0.09	0.18	1.17	1.57	1.40	99.06
		1.17	0.12	0.93	0.16	0.27	0.52	0.48	0.09	0.12	0.14	0.14	0.04	0.43
1-SP3-8	957	43.97	0.43	14.15	0.37	3.86	19.26	12.95	0.11	0.07	0.92	1.44	1.41	98.36
		1.59	0.12	2.27	0.27	0.29	0.73	0.45	0.09	0.08	0.12	0.20	0.06	0.52
1-SP4-1	877	38.77	0.42	16.85	0.82	4.25	18.46	13.47	0.05	0.07	2.93	0.51	1.86	98.30
		1.73	0.12	1.95	0.15	0.28	0.42	0.45	0.08	0.07	0.24	0.09	0.02	0.41
1-SP4-2	857	40.50	0.63	15.51	0.70	4.38	17.98	13.15	0.01	0.05	3.16	0.55	1.83	98.24
		0.69	0.13	0.36	0.25	0.28	0.42	0.44	0.08	0.07	0.25	0.09	0.02	0.35

Expt. ID	T/ °C	SiO ₂	TiO ₂	Al ₂ O ₃	Cr ₂ O ₃	FeO	MgO	CaO	MnO	NiO	Na ₂ O	F	H ₂ O	Total
1-SP4-4	843	40.63	0.37	14.74	0.41	4.46	18.43	13.40	0.06		3.16	0.59	1.80	97.81
		0.79	0.05	0.96	0.05	0.30	0.43	0.22	0.16		0.22	0.15	0.04	0.33
1-(SP2+Qtz)	950	54.18	0.44	4.63	1.17	2.90	22.35	11.34	0.03	0.61	0.32	2.21	1.13	100.40
		0.90	0.08	0.18	0.17	0.23	0.50	0.41	0.09	0.10	0.08	0.35	0.17	
anthophyllite		58.66	0.06	0.58	0.65	2.28	25.29	9.19	0.07	1.45	0.06	2.20	1.17	100.72
		0.96	0.06	0.18	0.28	0.21	0.58	0.87	0.09	0.13	0.06	0.36	0.16	0.29

3.3.2 Humite Group Minerals

Except SP1, all other F-bearing experiments create humite group minerals independent of temperature and pressure. Because the starting materials did not have much TiO₂ (approximately 0.4 wt%), the TiO₂ concentration of humite minerals are close to zero. Their components are majority of SiO₂, MgO, FeO and F. It is easy to compare humite products in different experiments with their chemical formulas.

3.3.2.1 Determination of Humite Minerals Species

Humite group minerals have similar composition and structure. Their chemical formula is Mg(OH,F)₂ nMg₂SiO₄. Here, n is 1, 2, 3 or 4, and corresponding to norbergite, chondrodite, humite and clinohumite, respectively. The distinction of the humite species is based on the stoichiometry calculation with oxide proportions determined by electron microprobe analysis. The proportion of F in OH site is also based on the stoichiometric calculation.

The X_F values of most F-rich experiments are close to 1. Assuming MgF₂ nMg₂SiO₄ as an F saturated end-member, I calculate its F and SiO₂ concentrations from n=1 to 4.

$$F \text{ (wt\%)} = \frac{38}{62.3 + 140.7 \cdot n} \times 100\%$$

Table 3.3.2.1 Expected F and SiO₂ concentrations of humite minerals

n (species)	62.3+140.7n	F (wt%)	n SiO ₂	SiO ₂ (wt%)
1 norbergite	203.0	18.7	60.1	29.6
2 chondrodite	343.7	11.1	120.2	35.0
3 humite	484.4	7.84	180.3	37.2
4 clinohumite	625.1	6.08	240.4	38.5

Based on the values in Table 3.3.2.1 above, it is possible to distinguish the humite species with F and SiO₂ limitations. For example, no matter I assume its O number as 13 or 17, the mineral formula from 1-SP2-21 is sound. Because its F is 5.14 wt% and SiO₂ is 36.81 wt%, the mineral is humite rather than clinohumite based on the table. The slightly lower SiO₂ is due to incorporation of Fe. Another major element in humite minerals is Mg. However, its concentration is almost constant ranging from 56 to 58 wt%, which is not suitable criterion for humite classification.

3.3.2.2 Humite Minerals Species

SP2 starting powder contains 9 wt% MgF₂ more than SP1 starting powder, which promotes the presence of norbergite. At 1 GPa, the concentrations of F in norbergite fall into two groups: one (NNO buffered experiments) ranges from 17 to 19 wt%, and the other (unbuffered) from 14.5 to 16.1 wt% (Table 3.3.2.2a). In contrast, the concentrations of F in hornblende are nearly constant. Moreover, FeO concentrations of norbergite can also be grouped as F. In unbuffered experiments, FeO concentration is only up to 1.31 wt%. While those conducted with NNO buffer, FeO concentration is higher and maximally 3.13 wt% at the maximum concentration.

Melt-bearing SP2 experiments have different humite mineral compositions, e.g., 1-SP2-18 has norbergite. 1-SP2-19 and 1-SP2-20 created chondrodite (Table 3.3.2.2b). 1-SP2-21 yielded humite (Table 3.3.2.2c). With an increasing of temperature, the melt proportion increases while the F mineral concentrations decrease.

Table 3.3.2.2a The average compositions of norbergite (unit: wt%).

Expt. ID	T/ °C	SiO ₂	TiO ₂	Al ₂ O ₃	Cr ₂ O ₃	FeO	MgO	CaO	MnO	NiO	Na ₂ O	F	H ₂ O	Total
1-SP2-1	770	27.74	0.55	0.40	0.16	2.54	56.52	0.61	0.11		0.03	17.90	0.19	99.22
		0.38	0.07	0.43	0.08	0.48	1.54	0.41	0.04		0.04	0.36	0.13	0.80
1-SP2-4	870	28.23	0.70	0.04	0.05	0.47	58.36	0.21	0.07	0.76	0.01	17.72	0.35	99.52
		0.22	0.14	0.01	0.03	0.03	0.98	0.03	0.03	0.59	0.01	0.39	0.16	0.68
1-SP2-7	930	28.06		0.52	0.07	1.46	57.16	0.64	0.04	0.06	0.04	19.60	0.01	99.43
		0.81		0.89	0.05	0.21	2.05	0.67	0.03	0.04	0.06	0.59	0.06	0.51
1-SP2-8	827	27.85	0.56	0.04	0.05	0.65	58.99	0.16	0.08	0.09	0.01	17.95	0.22	99.10
		0.28	0.07	0.02	0.02	0.23	0.45	0.03	0.02	0.03	0.01	0.31	0.12	0.49

3. Results

Expt. ID	T/ °C	SiO ₂	TiO ₂	Al ₂ O ₃	Cr ₂ O ₃	FeO	MgO	CaO	MnO	NiO	Na ₂ O	F	H ₂ O	Total
1-SP2-10	787	28.02	0.54	0.11	0.09	3.13	56.66	0.46	0.16	0.14	0.01	16.96	0.65	99.81
		0.52	0.12	0.05	0.09	0.45	0.90	0.10	0.13	0.10	0.05	0.65	0.10	0.41
1-SP2-12	777	27.02	0.54	0.49	0.14	2.81	56.07	0.71	0.12	0.25	0.03	18.98	0.02	99.20
		0.58	0.13	0.54	0.08	1.09	1.24	0.41	0.08	0.24	0.05	0.85	0.06	0.44
1-SP2-13	877	28.74	0.66	0.32	0.10	1.31	57.06	0.54	0.10	0.09	0.01	16.09	1.13	99.39
		0.47	0.14	0.40	0.09	0.30	1.03	0.35	0.03	0.07	0.02	0.65	0.34	0.49
1-SP2-14	877	29.44	0.94	0.06	0.04	0.56	58.49	0.29	0.02	0.07	0.00	15.16	1.71	100.42
		0.54	0.15	0.05	0.10	0.13	0.66	0.09	0.08	0.07	0.05	0.58	0.26	0.20
1-SP2-15	907	29.47	1.43	0.05	0.08	0.75	58.12	0.19	0.08	0.04	0.00	15.14	1.74	100.73
		0.54	0.18	0.05	0.10	0.20	0.69	0.07	0.08	0.07	0.05	0.62	0.11	0.41
1-SP2-16	927	28.75	1.24	0.07	0.02	1.08	57.04	0.28	0.10	0.06	0.01	14.52	1.86	98.93
		0.49	0.16	0.05	0.09	0.15	0.68	0.08	0.08	0.07	0.05	0.63	0.05	0.06
1-SP2-17	917	29.48	0.70	0.04	0.06	0.97	59.04	0.29	0.09	0.11	0.00	15.99	1.38	101.45
		0.50	0.13	0.05	0.10	0.15	0.69	0.08	0.08	0.07	0.05	0.64	0.06	0.14
1-SP2-18	947	29.10	0.92	0.03	0.10	0.71	57.63	0.23	0.05		0.02	15.44	1.47	99.22
		0.54	0.15	0.05	0.09	0.13	0.77	0.08	0.08		0.05	0.78	0.16	0.55
1-SP2-22	850	28.08	0.50	0.18	0.14	2.35	57.27	0.47	0.06	0.14	0.01	18.76	0.02	100.09
		0.57	0.08	0.07	0.10	0.44	0.97	0.12	0.08	0.07	0.05	1.02	0.03	0.31
1-SP2-23	800	27.85	0.61	0.15	0.10	3.10	56.31	0.53	0.17	0.25	0.01	18.10	0.11	99.69
		0.72	0.15	0.11	0.11	0.79	0.97	0.11	0.10	0.21	0.05	1.02	0.20	0.24
2-SP2-1	877	28.69	0.95	0.05	0.05	0.65	57.12	0.14	0.06	0.26	0.02	14.33	1.91	98.19
		0.49	0.15	0.05	0.10	0.13	0.68	0.07	0.08	0.11	0.05	0.63	0.12	0.30
2-SP2-2	857	28.21	0.66	0.25	0.05	0.65	57.85	0.45	0.07	0.19	0.02	16.93	0.69	98.90
		0.77	0.13	0.37	0.10	0.13	1.14	0.50	0.08	0.08	0.05	0.42	0.14	0.49
3-SP2-1	877	29.06	1.07	0.03	0.06	1.64	56.72	0.19	0.06	0.65	0.01	13.89	2.20	99.74
		0.54	0.15	0.05	0.10	0.18	0.72	0.07	0.08	0.13	0.05	0.61	0.11	0.02
4-SP2-2	877	28.99	1.17	0.04	0.12	1.57	55.82	0.11	0.01	1.51	0.01	13.24	2.46	99.47
		0.57	0.07	0.05	0.04	0.19	0.86	0.03	0.14	0.13	0.05	0.55	0.19	0.44
5-SP2-1	877	28.88	1.10	0.06	0.07	1.34	57.24	0.07	0.01	0.54	0.01	14.04	2.13	99.59
		0.54	0.16	0.05	0.10	0.17	0.73	0.06	0.08	0.11	0.05	0.61	0.09	0.19
1-(SP2+MgF ₂)	877	26.33	0.24	0.05	0.05	0.50	58.05	0.32	0.06		0.01	20.36	0.00	97.41
		0.35	0.05	0.04	0.04	0.06	0.43	0.04	0.03		0.02	0.28	0.00	0.61

In higher pressure SP2 experiments, norbergite was always precipitated. Its F concentration decreases approximately from 16 to 14 wt% with an increase of pressure from 1 to 2 GPa. In 2.5 and 3 GPa experiments, F concentrations remain about 14 wt%. It shows pressure variations influence the F concentration in norbergite more than temperature increasing in fluid-mineral systems.

The results of SP3 experiments demonstrate that different concentrations of MgF₂ create

different humite group minerals. The lower concentration of Mg and F and higher silicate in the starting material produces a humite group mineral with more SiO₂ similar to norbergite, so SP3 experiments created chondrodite with approximately 7 wt% F (Table 3.3.2.2b). Up to 957 °C, SP3 experiments do not produce obvious melt phase, but a hornblende-chondrodite-fluid system. However, lower MgO concentration leads to lower proportion of chondrodite in the capsule. There are two experiments, in which I did not find any chondrodite minerals, while I believe that SP3 should be present in small quantity.

Table 3.3.2.2b The average compositions of chondrodite (unit: wt%).

Expt. ID	T/ °C	SiO ₂	TiO ₂	Al ₂ O ₃	Cr ₂ O ₃	FeO	MgO	CaO	MnO	NiO	Na ₂ O	F	H ₂ O	Total
1-SP2-5	955	32.51	0.60	0.04	0.03	1.13	48.65	0.10	0.08	10.72	0.02	8.29	1.01	99.69
		0.65	0.08	0.02	0.02	0.10	4.01	0.03	0.03	4.77	0.02	0.52	0.14	0.36
1-SP2-6	900	31.64	0.60	0.05	0.05	0.97	46.93	0.14	0.08	13.22	0.01	8.75	0.71	99.48
		0.46	0.08	0.10	0.03	0.12	2.37	0.05	0.03	2.59	0.01	0.28	0.11	0.48
1-SP2-14	877	34.37	0.48	0.03	0.05	0.74	57.80	0.15	0.10	0.17	0.01	9.14	0.89	100.09
		0.59	0.12	0.05	0.10	0.22	0.69	0.07	0.09	0.08	0.05	0.49	0.23	0.25
1-SP2-19	977	34.77	0.49	0.03	0.08	1.19	56.56	0.16	0.08	0.13	0.00	7.99	1.41	99.52
		0.70	0.12	0.05	0.10	0.16	0.85	0.07	0.09	0.11	0.05	0.29	0.09	0.21
1-SP2-20	1007	34.76	0.57	0.04	0.09	2.19	55.98	0.17	0.11	0.32	0.01	7.51	1.65	100.24
		0.60	0.13	0.05	0.10	0.20	0.64	0.08	0.09	0.08	0.05	0.39	0.09	0.74
1-SP3-2	857	34.86	1.19	0.05	0.06	1.08	57.00	0.03	0.07	0.41	0.00	6.91	1.99	100.72
		0.60	0.16	0.05	0.08	0.24	0.80	0.06	0.09	0.18	0.05	0.42	0.06	0.58
1-SP3-3	857	34.46	1.14	0.03	0.06	0.98	56.34	0.06	0.06	0.60	0.00	7.52	1.63	99.73
		0.59	0.16	0.05	0.10	0.15	0.68	0.06	0.09	0.10	0.05	0.44	0.07	0.62
1-SP3-4	837	34.40	0.90	0.03	0.03	0.76	56.65	0.04	0.11	0.61	0.01	7.59	1.60	99.53
		0.59	0.15	0.05	0.09	0.14	0.68	0.06	0.08	0.10	0.05	0.44	0.06	0.76
1-SP3-5	887	34.86	1.43	0.02	0.06	1.04	56.61	0.05	0.17	0.24	0.00	6.83	2.01	100.44
		0.60	0.17	0.05	0.08	0.15	0.80	0.06	0.09	0.11	0.05	0.42		
1-SP3-6	897	35.32	1.27	0.17	0.11	1.52	56.35	0.19	0.11	0.44	0.01	6.94	2.00	101.51
		0.58	0.17	0.29	0.10	0.64	1.21	0.26	0.09	0.42	0.05	0.44	0.11	0.81
1-SP3-8	957	35.00	1.32	0.24	0.08	1.21	55.59	0.32	0.07	0.19	0.02	6.62	2.09	99.97
		0.60	0.17	0.34	0.10	0.18	1.13	0.44	0.09	0.08	0.05	0.37	0.04	0.77
4-SP2-1	877	33.62	0.60	0.01	0.08	2.58	54.79	0.05	0.04	1.91	0.01	8.03	1.31	99.66
		0.59	0.13	0.05	0.10	0.22	0.71	0.06	0.08	0.38	0.05	0.47	0.02	0.41
4-SP2-2	877	33.47	0.53	0.03	0.09	2.21	53.06	0.05	0.02	3.56	0.01	7.78	1.36	102.45
		0.65	0.09	0.05	0.10	0.20	0.92	0.06	0.08	0.18	0.05	0.62	0.16	0.72
1-(SP1+MgF ₂)	965	33.77	0.34	0.04	0.14	2.54	55.75	0.19	0.08	0.51	0.01	8.64	1.04	99.43
		0.53	0.11	0.05	0.11	0.25	0.77	0.07	0.08	0.13	0.05	0.94	0.17	0.27

With the observations of SP1 to SP3 experiments, it is interesting to study whether Mg or F concentration controls the humite mineral speciation. SP4 starting powder has higher MgO concentration and lower F and SiO₂ concentrations. SP4 phase assemblies show that they produced clinohumite with 2 wt% F, but not norbergite. It indicates that F concentration of the system is crucial to determine the humite mineral species. With a decreasing of F concentration from 5 to 0.5 wt%, the humite mineral species transform from norbergite to clinohumite. The chondrodite and clinohumite from NNO buffered SP3 and SP4 experiments have approximately 1.0 wt% FeO (Table 3.3.2.2c).

Table 3.3.2.2c The average compositions of humite and clinohumite (unit: wt%).

Clinohumite	T/ °C	SiO ₂	TiO ₂	Al ₂ O ₃	Cr ₂ O ₃	FeO	MgO	CaO	MnO	NiO	Na ₂ O	F	H ₂ O	Total
1-SP4-1	877	38.48	0.66	0.04	0.07	0.80	55.79	0.42	0.09	0.15	0.02	2.06	1.89	99.60
		0.67	0.13	0.05	0.10	0.14	0.84	0.10	0.09	0.07	0.05	0.15	0.02	0.39
1-SP4-2	857	38.33	0.77	0.03	0.06	0.76	54.98	0.16	0.09	1.15	0.01	2.14	1.83	99.41
		0.67	0.14	0.05	0.10	0.17	0.84	0.07	0.09	0.63	0.05	0.15	0.01	0.66
1-SP4-3	890	38.09	0.74	0.04	0.06	1.29	55.36	0.22	0.09		0.00	2.32	1.74	98.98
		0.69	0.06	0.05	0.04	0.26	0.84	0.06	0.17		0.05	0.24	0.04	0.18
1-SP4-4	843	38.16	0.70	0.01	0.02	0.88	56.24	0.22	0.07		0.00	2.35	1.75	99.42
		0.68	0.06	0.05	0.04	0.16	0.85	0.03	0.17		0.04	0.24	0.01	0.80
Humite														
1-SP2-21	1057	36.81	0.31	0.03	0.16	0.93	56.09	0.13	0.05	0.32	0.01	5.14	1.23	99.05
		0.64	0.11	0.05	0.11	0.14	0.83	0.07	0.08	0.12	0.05	0.36	0.04	0.28

Excess doping experiment 1-(SP2+MgF₂) creates abnormal norbergite with 19.91 wt% F. Its atomic number from stoichiometry is 2.20 ± 0.17 in its chemical formula. Although its uncertainty reaches 0.17 (based on the standard deviation of F concentration from electron microprobe analysis), its number is still excess to the standard formula of norbergite. I do not push further study on this mineral. However, I have two hypotheses for the abnormality: 1) F could take place of O contact with Si or Si is replaced by 4H, and F can take this OH site; 2) This mineral is a mixture of MgF₂/Mg(OH)₂ and norbergite. If I set cation total number as 4.3, the Mg number is 3.3, Si number is 1.0, and the total O number is 5.3. The aim of this experiment is to study phase assembly variations with absolute excess F. It demonstrates that norbergite is always present in high F concentration experiments. Furthermore, it indicates that norbergite is a saturation phase of F, as well as other SP2 experiments.

3.3.3 Hydrogrossular

In SP2 experiment at 2.5 and 3 GPa, hornblende breaks down. Instead of hornblendes, a hydrous garnet – hydrogrossular appears in the capsule. Its shape is semi-spheric. Their sizes are small, of which average diameters reach 20 μm . But it is interesting that all the hydrous garnets show empty spherical void in their centers (Fig. 3.1.2.2 4-SP2-1 & 2, 5-SP2-1).

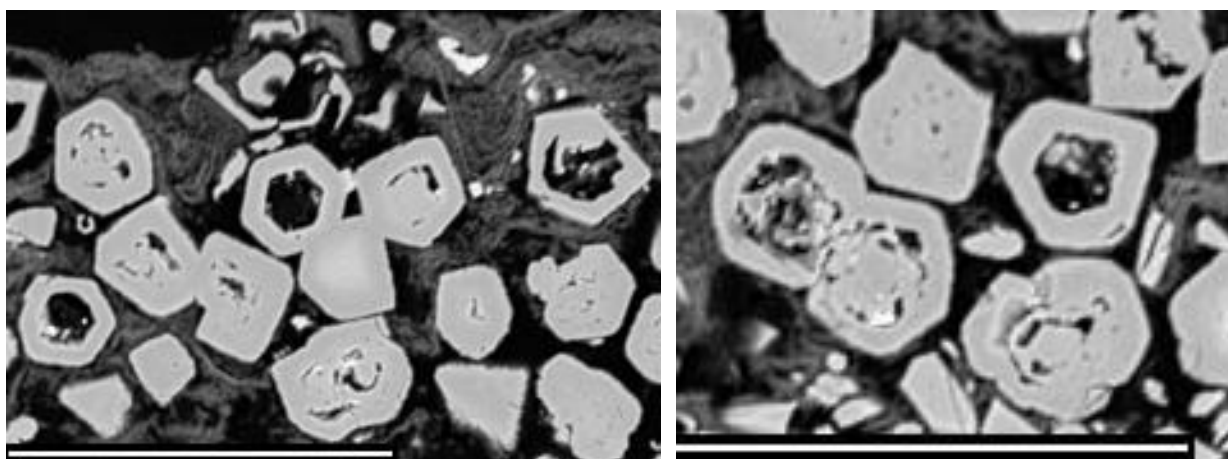


Fig. 3.3.3 The magnified images from 5-SP2-1 experiments. Left: a cross-section of a typical center void hydrogrossular crystal. Right: some empty hydrogrossular crystals with mineral scraps inside. The bar scale is 100 μm .

Table 3.3.3a Individual hydrogrossular compositions from SP2 experiments at 2.5 and 3 GPa (unit: wt%).

Expt.ID	No. Pt.	SiO ₂	TiO ₂	Al ₂ O ₃	Cr ₂ O ₃	FeO	MgO	CaO	MnO	NiO	Na ₂ O	F	Total
4-SP2-1	28	39.61	0.15	22.95	0.55	6.47	13.55	15.88	0.18	0.03	0.00	1.50	100.87
	30	39.04	0.22	22.58	0.66	6.89	12.81	16.30	0.20	0.02	0.03	1.71	100.47
	31	39.03	0.14	22.96	0.57	6.41	13.10	16.21	0.18	0.06	0.00	1.84	100.50
5-SP2-1	38	39.79	0.12	23.19	0.67	5.36	17.29	12.41	0.10	0.02	0.00	1.51	100.46
	41	39.66	0.04	23.25	0.80	5.00	17.28	12.22	0.13	0.02	0.02	1.63	100.06
	39*	34.78	0.85	22.26	0.49	6.76	9.05	20.87	0.20	0.05	0.00	4.41	99.74
	40*	36.81	0.84	22.49	0.64	7.31	11.51	17.93	0.21	0.00	0.00	2.91	100.64
4-SP2-2	2	39.10	0.13	22.56	0.89	5.01	15.98	13.11	0.03		0.00	1.35	98.17
	3	38.25	0.34	22.32	0.81	6.59	12.46	16.76	0.16		0.03	1.82	99.54
	18	41.52	0.17	21.57	1.64	5.25	17.20	11.92	0.35		0.00	0.42	100.05
	20	39.49	0.16	22.17	0.77	6.23	14.40	14.78	0.23		0.00	1.39	99.62
	21	40.24	0.16	22.45	1.28	5.04	16.57	12.81	0.17		0.00	0.96	99.67
	16*	33.82	0.79	21.41	0.47	5.79	7.57	23.69	0.40		0.02	5.59	99.57
	17*	37.52	0.96	20.85	0.45	5.25	9.92	21.71	0.22		0.03	2.75	99.66

No. Pt. indicates the number of different analytical position, and hereinafter. * indicates this analysis point is close to the center of the mineral sphere.

At the beginning of the experiment, I usually spent more than 40 minutes to reach 2.5 or 3 GPa. During the compression process, some hornblendes precipitate. When the pressure is beyond 2 GPa, the amphibole begins to break down and form micro garnet nuclei. Then, the garnet may grow and encircle the pre-existing mineral (hornblendes). If garnet envelops the mineral totally, then the pre-existing mineral cannot dissolve into fluid anymore and remain inside the garnet. While hornblende is no longer stable under the higher pressure, they transfer to some amorphous scraps. This may lead to most hydrogrossulars with mineral scraps in their empty center (Fig. 3.3.3). But the origin of the cavity is not determined, either it is due to amorphous scraps loss during the polishing process, or the breakdown hornblende dissolution during the experiment.

The chemical formula of hydrogrossular is $\text{Ca}_3\text{Al}_2\text{Si}_2\text{O}_8(\text{SiO}_4)_{1-m}(\text{OH})_{4m}$. Its divalent cation can be replaced by Mg, Fe or Mn, and its trivalent cation can be substituted by Fe, Mn and Cr. In hydrous garnet, part of SiO_2 was replaced by $2\text{H}_2\text{O}$. Their OH concentrations were estimated with stoichiometry calculation.

As I described above, all the hydrogrossular do not have homogeneous composition. Some contain exotic mineral inclusions, but they are too small to measure. The core measurements, which are marked star in Table 3.3.3a, have quite different compositions from those on the mineral rims. The core scraps of hydrogrossular are rich in CaO and F, and depleted in SiO_2 and MgO. If these scraps are products from hornblende breakdown, it indicates that the hydrogrossular envelop them in a small quasi-close system to prevent the convection with the fluid system, otherwise they should be dissolved into fluid and precipitate as other crystals. Two possibilities led to the discrepancy between these three major elements dissolutions: 1) A new phase assemblage is determined by the final P-T condition. The consumption of Si and Mg are more than Ca, especially in norbergite or chondrodite; 2) The higher pressure increases the solubility of Si and Mg in fluid, which is helpful to transport them to new crystals via fluid, while Ca do not. Before the hydrogrossular completely enclosed the hornblende scraps, SiO_2 and MgO can be transferred in quicker rate than CaO. Thus, this resulted in the CaO-rich scraps materials in the hydrogrossular void.

Except the four analyses on the hydrogrossular central portion (star-marked compositions in Table 3.3.3a), others have slightly different SiO_2 and F concentrations, so

each crystal may have an m value of itself. It is important to calculate m value in their chemical formulas. However, if this system is in equilibrium, the chemical formula of the same mineral species should be similar. For example, the F proportions of OH site of norbergite or chondrodite in the same experiment are very close.

Normally, other garnet species are anhydrous minerals. F and OH can be only incorporated into the vacancies. While hydrogrossular is different, and two reasons limit its F concentrations: 1) m value. The abundance of SiO_2 , replaced by $2\text{H}_2\text{O}$, determines the upper limit of OH and F in this hydrous garnet; and 2) the activity of F and OH for competing OH site in this mineral. However, in my experiments, the CaO-F rich material in the core leads to the different chemical environment inside and outside the hydrogrossular minerals. This should explain that the F concentrations range from 0.42 to 1.82 wt%. From the hydrogrossular stoichiometry calculations, SiO_2 and F concentrations must constrain the F proportion in its OH site, m value, and oxygen abundance. Therefore, it was not possible to uniquely calculate the garnet stoichiometry.

In conclusion, it is difficult to decide which mineral composition is more reliable among these various hydrogrossular grains with or without cavities. But it is reasonable to treat the rim compositions as the true values. Thus, I choose the points from the analytical points on the edge of hydrogrossular, and report their averages in Table 3.3.3b..

Table 3.3.3b The average hydrogrossular compositions at 2.5 and 3 GPa (unit: wt%).

Expt. ID	SiO_2	TiO_2	Al_2O_3	Cr_2O_3	FeO	MgO	CaO	MnO	NiO	Na_2O	F	H_2O	Total
4-SP2-1	39.23	0.17	22.83	0.59	6.59	13.15	16.13	0.19	0.04	0.01	1.68	0.93	100.84
	0.64	0.10	0.40	0.14	0.34	0.37	0.53	0.10	0.07	0.05	0.25	0.05	0.25
4-SP2-2	39.72	0.19	22.21	1.08	5.62	15.32	13.88	0.19		0.01	1.19	0.73	99.64
	1.24	0.08	0.40	0.37	0.74	1.91	1.92	0.19		0.05	0.52	0.41	0.63
5-SP2-1	39.72	0.08	23.22	0.73	5.18	17.29	12.32	0.12	0.02	0.01	1.57	1.14	100.74
	0.65	0.09	0.41	0.15	0.31	0.38	0.46	0.09	0.07	0.05	0.24	0.08	0.40

3.3.4 Nominally Anhydrous Minerals

Several nominally anhydrous minerals (olivine, pyroxene and spinel) are present in some of my experiments, within a small proportion. At 1-GPa experiments, it is rare to find anhydrous minerals in the capsules. It indicates that these experiments may suffer some abnormal process. In this section, I will introduce their compositions.

3.3.4.1 Olivine

The chemical formula of olivine is $(\text{Mg, Fe})_2[\text{SiO}_4]$. It is an orthosilicate, with a simple structure. In my experiments, olivine was precipitated in some SP1 experiments. Normally, successful SP1 experiments only produce hornblende. And olivine always co-exists with pyroxene in SP1 experiments. If only based on the results of 1-SP1-2 and 1-SP1-3, I concluded olivine and pyroxene are the products of hornblende breakdown, due to the water loss. While there is 1.6 mg fluid left in the 1-SP1-5 experiment, so water exhaustion is not the reason for the presence of olivine.

From their compositions, they all have NiO. This case is not common in the natural minerals. It indicates that nickel contamination happened during the experiments. This kind contamination usually happened in the experimental temperature over 900 °C. 1-SP1-2 and 1-SP1-3 were conducted at 955 °C. Their NiO concentrations of their olivine are more than that from 1-SP1-5, which was conducted at 877 °C. And the proportions of olivine in 1-SP1-2 and 1-SP1-3 are higher than 1-SP1-5 as well. Considering similarity of NiO behavior with MgO, nickel contaminations pull the system composition to richer in MgO. With the phase assemblies of SP4 experiments, I learned that MgO rich starting material will create pyroxene and clinohumite. The absence of F in SP1 powder promotes olivine and pyroxene crystallization, because humite minerals forms need the presence of F by combining mineral components of $\text{Mg}(\text{F, OH})_2$ and olivine.

There is no Ni-free olivine from SP1 experiments so far; the presence of olivine is most-likely derived from nickel contamination from its outer capsule. The compositions of olivine from SP1 experiments are shown in the table below.

Table 3.3.4.1 The average composition of olivine from SP1 experiments (unit: wt%).

Expt. ID	T/ °C	SiO ₂	TiO ₂	Al ₂ O ₃	Cr ₂ O ₃	FeO	MgO	CaO	MnO	NiO	Na ₂ O	Total
1-SP1-2	870	35.03	0.01	0.01	0.05	1.22	24.63	0.10	0.10	38.66	0.02	99.83
		0.87	0.02	0.02	0.04	0.17	3.20	0.04	0.03	3.76	0.02	0.44
		39.91	0.01	0.01	0.03	0.80	43.85	0.06	0.11	15.36	0.01	100.16
		0.35	0.01	0.01	0.04	0.04	0.48	0.01	0.02	0.72	0.01	0.75
1-SP1-3	995	35.73	0.02	0.07		1.13	28.48	0.07	0.11	33.90	0.01	99.52
		1.81	0.03	0.27		0.30	7.68	0.08	0.04	9.10	0.02	0.48
1-SP1-5	877	39.79	0.00	0.03		0.54	44.04	0.08	0.20	15.23	0.00	99.93

3.3.4.2 Pyroxene

1-SP1-1 was conducted without water and 1-SP2-2 exhausted its fluid totally because of its high temperature. The SP1 experiment creates enstatite and augite, while the SP2 only has enstatite. There are two enstatite minerals in 1-SP2-2: Fe-bearing (~5 wt% FeO), and Fe-free. The excess doping experiment, 1-(SP1+CaF₂), created two augite compositions, but only by slight differences. Its phase assembly is similar to the above two experiments: pyroxenes and melt, in addition to CaF₂. However, its fluid mass is 0.49 mg, which derived from mass difference, but the texture of this experiment is similar with those two water-free experiments. It indicates that fluid mass may be not fluid, but micro minerals or precipitates loss during the post-quench procedure. 1-SP1-2, 3 and 5 experiments have augite, accompanying with olivine. The contamination in 1-SP1-5 is so weak that only one olivine and two augite grains. This is micro local nickel enrichment, and the influence can be ignored in mass-balance calculation.

Other augite minerals are present in SP2 melt-bearing experiment (1-SP2-20), SP2 higher pressure experiments, and SP4 experiments with apparent indications of the presence of water during anneal. Their compositions are similar, except subtle some variances. For example, SiO₂ (~54 wt%) and MgO (~17 wt%) concentrations from the experiments at 2.5 and 3 GPa are higher than those at 1 GPa (1-SP2-20, 48 wt% SiO₂ and 14.6 wt% MgO), while Al₂O₃ concentrations are lower (~2 wt% for 2.5 and 3.0 GPa, but 7 wt% at 1 GPa, Table 3.3.4.2). Comparing with the augite compositions from SP4 experiments, that from 1-SP2-20 has more FeO (4.5 wt%) than SP4 (~3 wt%). Although their starting compositions are quite different, the presence of the melt improves 1-SP2-20 to create similar augite to SP4 experiments.

Table 3.3.4.2 The pyroxene compositions from the experiments (unit: wt%).

Expt. ID	T/ °C	SiO ₂	TiO ₂	Al ₂ O ₃	Cr ₂ O ₃	FeO	MgO	CaO	MnO	NiO	Na ₂ O	F	Total	
1-SP1-1	870	55.99	0.17	3.36	0.38	6.17	33.08	0.66	0.13		0.14		100.09	
		0.50	0.03	0.16	0.05	0.10	0.36	0.03	0.03		0.02		0.73	
	870	52.89	0.58	5.66	1.00	3.01	15.35	19.13	0.08		1.99		99.69	
		0.33	0.05	0.13	0.10	0.08	0.19	0.17	0.03		0.07		0.51	
1-SP1-2	995	49.90	0.26	4.35	0.33	1.52	11.84	23.29	0.04	7.85	0.14		99.54	
		0.99	0.10	1.94	0.14	0.41	1.47	1.03	0.03	2.43	0.18		0.51	
1-SP1-3	995	50.48	0.28	4.78		2.15	13.95	23.55	0.08	3.77	0.13		99.18	
		1.25	0.10	1.35		0.69	2.48	0.33	0.05	3.83	0.05		0.40	
1-SP1-5	877	51.69	0.42	7.15		3.60	20.86	12.59	0.08	0.19	1.12		97.71	
		0.45	0.11	1.05		0.80	6.78	8.04	0.04	0.04	0.70		0.58	
1-SP2-2	1120	55.64	0.09	6.06	0.94	0.24	36.53	0.81	0.07		0.02	0.16	100.58	
		0.89	0.04	1.27	0.19	0.11	0.61	0.08	0.04		0.01	0.03	0.23	
	1120	54.54	0.14	5.09	0.54	5.32	32.58	0.99	0.12		0.04	0.19	99.57	
		0.64	0.07	1.18	0.10	0.58	0.43	0.27	0.03		0.04	0.07	0.86	
		1007	48.03	0.22	7.21	0.83	4.51	14.61	23.92	0.06	0.06	0.09	0.22	99.77
		1.28	0.11	0.92	0.22	0.98	0.55	0.62	0.09	0.07	0.07	0.10		
4-SP2-1	877	54.14	0.08	1.96	0.46	1.85	17.24	24.20	0.04	0.27	0.12	0.05	100.42	
		0.79	0.09	0.52	0.17	0.19	0.38	0.68	0.08	0.09	0.07	0.10		
4-SP2-2	877	53.27	0.06	2.53	0.43	2.10	16.35	23.91	0.04	0.84	0.18	0.09	99.81	
		0.88	0.07	0.18	0.14	0.20	0.41	0.59	0.09	0.11	0.07	0.12		
5-SP2-1	877	54.56	0.04	1.54	0.43	1.90	17.15	24.17	0.03	0.33	0.35	0.08	100.59	
		0.79	0.09	0.24	0.13	0.20	0.38	0.68	0.08	0.13	0.09	0.10		
1-SP4-1	877	47.95	0.85	6.65	0.83	2.32	15.13	24.64	0.03	0.01	0.23	0.08	98.74	
		0.80	0.28	0.89	0.16	0.21	0.46	0.61	0.08	0.07	0.08	0.06		
1-SP4-2	857	49.33	0.68	5.63	0.93	2.56	15.07	24.37	0.01	0.07	0.20	0.13	98.99	
		1.00	0.14	0.48	0.16	1.05	0.57	0.61	0.08	0.08	0.07	0.07		
1-SP4-3	890	48.37	0.57	5.91	0.52	3.39	14.84	25.06	0.05		0.05	0.07	98.83	
		1.65	0.23	1.49	0.46	0.78	0.74	0.32	0.16		0.06	0.09		
1-SP4-4	843	48.99	0.69	5.81	0.90	2.94	15.40	24.12	0.08		0.36	0.06	99.35	
		1.00	0.24	1.02	0.26	0.34	0.38	1.56	0.17		0.51	0.09		
1-(SP1+ CaF ₂)	950	50.44	0.31	5.85	1.06	3.25	14.75	23.92	0.06	0.10	0.32	0.10	100.15	
		0.85	0.08	0.62	0.17	0.56	0.44	0.60	0.09	0.08	0.15	0.14		
		53.17	0.61	5.50	1.04	2.99	15.37	19.06	0.07	0.05	1.95	0.05	99.85	
		0.88	0.09	0.20	0.17	0.24	0.40	0.53	0.09	0.07	0.17	0.11		

3.3.4.3 Spinel

Sometimes, a non-silicate mineral (spinel) is present in the capsules. Its normal chemical formula contains one divalent and two trivalent cations with four oxygen atoms. In my experiments, spinel contains Fe, Mg, Ni, Al and Cr. If the sample is contaminated by nickel,

nickel concentration will be higher than 10 wt%. Moreover, because iron can be ferric or ferrous in the spinel, and electron microprobe results count Fe as ferrous, the total of spinel is always less than 100 wt%. However, the chemical formula of spinel is simple. It is possible to estimate its ferric and ferrous concentration respectively via stoichiometry calculation. In Table 3.3.4.3, the last three columns are the concentrations of ferric and ferrous oxides and the new total values. Although some new total values are still much less than 100 wt%, they are usually increased by approximately 2 to 4 wt% and much better than the total values from electron microprobe analysis.

Table 3.3.4.3 The compositions of spinel in the experiments (unit: wt%).

Expt. ID	T/ °C	SiO ₂	TiO ₂	Al ₂ O ₃	Cr ₂ O ₃	FeO	MgO	CaO	MnO	NiO	Na ₂ O	Total	Fe ₂ O ₃	FeO	Total'
1-SP1-2	995	0.64	0.36	38.41	5.26	19.53	8.73	0.13	0.12	23.63	0.02	96.83	21.27	0.82	98.61
		1.19	0.12	4.11	2.65	4.43	3.43	0.12	0.04	6.18	0.06		5.57	0.73	1.16
1-SP1-7	857	0.15	0.07	50.16	9.50	12.05	23.32	0.12	0.16	1.58	0.01	97.14	11.43	1.77	98.28
		0.11	0.03	3.21	2.72	0.82	0.40	0.06	0.04	1.05	0.01		1.62	1.23	0.31
1-SP2-5	955	0.16	0.39	19.28	10.35	36.53	8.71	0.04	0.18	18.71	0.01	94.38	38.17	2.18	98.18
		0.15	0.14	4.54	2.24	5.50	2.65	0.04	0.09	5.74	0.01		5.31	0.99	0.82
1-SP2-6	900	0.55	0.33	32.53	8.36	24.09	9.57	0.11	0.21	20.15	0.02	95.12	24.71	1.85	98.41
		0.50	0.21	5.20	3.68	6.14	4.17	0.07	0.07	7.84	0.02		7.16	1.22	0.94
1-SP2-20	1007	0.08	0.21	26.69	18.81	30.23	17.96	0.19	0.28	1.06	0.02	95.55	26.63	6.27	98.19
		0.06	0.10	1.36	0.57	1.69	0.41	0.08	0.12	0.12	0.07		1.89	0.01	0.20
1-SP2-21	1057	0.26	0.17	14.63	33.00	24.01	20.48	0.02	0.20	0.71	0.01	93.49	26.19	0.44	96.11
		0.21	0.10	0.35	1.58	0.97	0.48	0.06	0.11	0.15	0.07		1.63	0.50	0.35
2-SP2-1	877	0.04	0.12	37.65	10.46	20.77	15.22	0.05	0.24	10.66	0.00	95.23	36.04	5.22	98.84
		0.06	0.10	1.56	0.43	1.26	0.74	0.06	0.11	1.11	0.06		0.28	1.31	0.20
1-SP3-1	877	0.03	0.06	53.90	6.07	11.38	23.68	0.08	0.13	1.90	0.02	97.27	10.87	1.59	98.33
		0.06	0.09	0.75	0.80	1.18	0.44	0.06	0.10	0.37	0.05		1.08	0.21	0.61
1-(SP1+ MgF ₂)	965	0.39	0.17	17.34	31.49	27.74	15.61	0.57	0.28	1.68	0.01	95.28	22.84	7.18	97.56
		0.65	0.10	2.38	3.05	3.31	0.67	0.44	0.12	0.28	0.07		4.24	0.58	0.93

The last three columns are calculated from stoichiometry results. Others are analyzed by electron microprobe.

In these experiments, the proportion and the size of spinel minerals are small. Generally, the biggest size just enough for electron microprobe analysis. Based on its presence in the capsules and its small size and proportions, it is impossible to tell whether spinel is present in all the experiments or not.

In SP1 experiments, their hornblende contains approximately 12 wt% Al₂O₃. Any other

silicate minerals do not have so much Al_2O_3 concentration. Once hornblende breaks down, there is excess alumina dissolved into fluid. When the fluid is saturated with Al, they will precipitate a new phase with higher Al_2O_3 than 12 wt%. Generally spinel plays this role in my experiments, so in the experiments, which have large proportion of melt, they created obvious spinel crystals, e.g. 1-SP2-20, 21 and 1-(SP1+MgF₂).

In F-bearing experiments, humite group minerals were created. They are Al-free minerals, so Al_2O_3 concentrations in hornblende are higher than those in SP1 experiments. Up to now, no spinel is found in SP4 experiments, and only one SP3 experiment has spinel. Excluding the melting experiments, spinel is also found in some nickel contaminated experiments. Nickel enriched in the SP1 experiments and lead to hornblende breakdown also precipitated spinel. For SP2 ones (1-SP2-5 & 6), nickel contamination transforms norbergite to chondrodite. This process needs more silica from hornblende, and also releases alumina into fluid and form spinel. Hornblende and pyroxene from SP4 experiments contains Al, so spinel cannot be precipitated in these experiments.

3.3.5 Melt

The experiments with obvious melt phase mostly occurred under the temperature above 940 °C. Two kinds of melt textures are present in these large quantity water-bearing experiments. I use different procedures to estimate the melt compositions in this section.

1) Some melts look like glass without bubble, or quenched melt phases. Because they do not have gaps and have large enough surface for electron microprobe analysis, their compositions could be measured directly. If the results show total missing, the residual part is water.

2) Other melts are quenched with small bubbles. For example, SP2 high temperature experiments, their main melt textures are present with bubbles, which indicate that water was partially exsolved during the quench (Fig. 3.1.2.1h). They do not have a uniform surface large enough for electron microprobe analysis. Thus, the measurements have large total missing (generally larger than 10 wt%). In the hydrous system, the melt generally is saturated by water. It is hard to determine the proportion from water or from bubbles in the total missing. When I

report their compositions, the missing total is normalized to 100 wt% (excluding O substituted with F), which is called as “normalized” in the tables below. For some of them, the compositions were confirmed with re-measuring oxygen concentration. Although the uncertainty of oxygen measurement reaches 1.6 wt%, I can find the water abundance in the melt with charge balance calculation. The precondition is that all the iron cation is Fe^{2+} . This assumption would make some errors, but the low abundance of Fe (approximately 3 wt%) and the high Fe atomic mass (56) will make the errors acceptable. In subsections below, I referred this method as “charge balance”. The details for the melt composition determinations are described below.

3.3.5.1 1-SP2-18 & 19 experiments

The melts in 1-SP2-18 and 19 experiments have same texture, with bubbles inside them. I measured the average composition of the melt in 1-SP2-19, and normalize the composition with the two methods described above.

Table 3.3.5.1 Melt compositions of 1-SP2-19 experiment, with two methods (unit: wt%).

	No. Pt.	SiO ₂	TiO ₂	FeO	MgO	CaO	MnO	NiO	Al ₂ O ₃	Cr ₂ O ₃	Na ₂ O	F	H ₂ O	Total
Charge	36	43.84	0.59	2.54	10.60	13.57	0.06	0.04	17.52	0.03	0.57	6.07	7.01	102.56
balanced	37	44.98	0.52	2.71	11.22	13.17	0.07	0.00	17.32	0.02	0.75	5.27	6.00	102.22
	Aver.	44.41	0.55	2.63	10.91	13.37	0.06	0.02	17.42	0.02	0.66	5.67	6.51	102.39
	StdD	1.01	0.14	0.34	0.47	0.68	0.15	0.11	0.52	0.16	0.16	0.86	0.71	
Normalized	Aver.	45.82	0.56	3.09	12.33	15.22	0.11	0.00	18.86	0.03	0.37	6.10		102.57
	StdD	1.07	0.22	0.37	0.50	0.77	0.15	0.16	0.55	0.18	0.14	0.31		

The total is the sum of all the oxides and F (> 100 wt%). If excluded the oxygen substituted by F, the total will be 100 wt%. In section 3.3.5, all the tables follow this rule.

These two methods have different analytical setting. Their oxygen abundances are different, which causes the matrix effect change, and lead to slightly different compositions, so the measurements for the same melt area are individual. In Table 3.3.5.1, their average compositions are similar, except some subtle inconsistencies (e.g., Na₂O concentration). The concentrations of normalized are slightly larger than that from charge balance, while most elements concentrations are within their uncertainties. Based on melt texture of 1-SP2-18, its composition should be similar with 1-SP2-19.

3.3.5.2 1-SP2-20 experiment

Two kinds of melts (bubbled melt and high silica melt) are present in this experiment (Fig. 3.3.5.2). It is unusual to find the high silica melt in the bottom portion of the capsule, although its proportion is small. Its position indicates that the local environment might be the reason for creating it. In the center of the capsule, a large mineral mixture block may separate the inner capsule into two parts. This structure would prevent the efficient fluid convection in the whole capsule. It is possible to form a local near equilibrium in a small area. However, the bubbled melts are present in the both sides of the block part. Their similar textures and compositions indicate the acquirement of the near equilibrium.

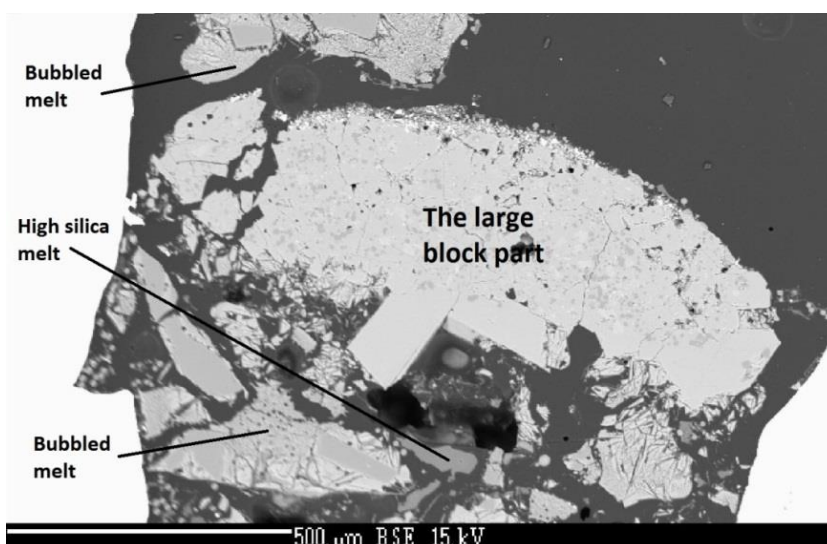


Fig. 3.3.5.2 The magnified image from 1-SP2-20 experiment. In the capsule center, a large mineral mixture separated the capsule as two areas. Two kinds of texture melts (high silica melt and bubbled melt) are present in the bottom portion of the capsule.

Table 3.3.5.2a Compositions of high silica melt (original data; unit: wt%).

No.Pt.	SiO ₂	TiO ₂	Al ₂ O ₃	Cr ₂ O ₃	FeO	MgO	CaO	MnO	NiO	Na ₂ O	F	Total
31	60.72	0.04	3.93	0.00	0.08	0.05	1.24	0.00	0.02	0.18	0.14	66.42
39	57.74	0.01	4.40	0.00	0.12	0.04	2.78	0.02	0.03	0.24	1.51	66.96
42	64.69	0.00	5.28	0.00	0.27	0.07	1.48	0.00	0.00	0.86	0.52	73.21
43	61.47	0.01	5.29	0.04	0.08	0.10	1.50	0.01	0.00	0.93	0.52	70.01
Aver.	61.15	0.02	4.72	0.01	0.13	0.07	1.75	0.01	0.01	0.55	0.67	69.15
StdD	2.85	0.12	0.67	0.13	0.14	0.05	0.70	0.10	0.09	0.40	0.59	

These four points show high silica melt compositions. This melt has no bubble, but their totals are significantly less than 100 wt%. If all the missing part is water, the melt will contain 30 wt% water. It is impossible, because the water mole proportion is over 50%, and under

room temperature, it should be aqueous solution and unquenchable.

Table 3.3.5.2b Compositions of high silica melt (original data) with oxygen (unit: wt%).

No.Pt.	Si	Ti	Al	Cr	Fe	Mg	Ca	Mn	Ni	Na	F	O	Total
23	29.45	0.03	2.85	0.00	0.10	0.08	1.06	0.00	0.02	0.79	0.66	39.90	75.03
24	32.56	0.00	3.21	0.00	0.13	0.11	1.20	0.04	0.00	0.06	0.71	39.97	78.00
25	29.86	0.00	2.87	0.04	0.09	0.07	1.01	0.03	0.00	0.75	0.66	39.04	74.46

The analyses with the oxygen concentration for this melt (with 20 μm beam size) demonstrate that some elements may be overlooked during the measurements. Their total miss more than 20 wt%, which is larger than the uncertainties of oxygen concentrations (~ 1.4 wt%). With SEM images, some metal nubs were found in this melt, and EDS detector certified that they are gold and molybdenum. They are from the capsule. However, the minerals in this experiment do not have so much total missing. This shows Au and Mo can transport into the sample room without contaminating the minerals. For this high silica melt composition determination, I use charge balance methods. Point No. 24 does not have enough anion to balance the cations' charges, so I discard it (Table 3.3.5.2c).

Table 3.3.5.2c Normalized compositions of high silica melt (unit: wt%).

No.Pt.	SiO ₂	TiO ₂	Al ₂ O ₃	Cr ₂ O ₃	FeO	MgO	CaO	MnO	NiO	Na ₂ O	F	H ₂ O	Total
23	83.52	0.08	7.14	0.00	0.16	0.18	1.97	0.00	0.03	1.42	0.87	4.87	100.37
25	85.52	0.01	7.25	0.08	0.15	0.15	1.89	0.05	0.00	1.36	0.88	2.97	100.37
Aver.	84.52	0.04	7.19	0.04	0.16	0.17	1.93	0.02	0.01	1.39	0.88	3.92	100.37
StdD	1.59	0.11	0.34	0.17	0.16	0.09	0.29	0.13	0.06	0.23	0.40	1.34	

I did not measure Au and Mo concentrations of the melt. In the bubbled melt, the total missing may be partially from these two elements as well. But as the high silica melt case, the normalizing gives a correct result.

Actually, two textures of the bubbled melt are present in the capsule (Fig. 3.3.5.2). One texture is melt with bubbles evenly distributed. The other is a texture with cracks, which looks like quenched crystals, and their precipitates in the gaps. The precipitate is too narrow to be analyzed precisely. I only have one suitable measurement (No. Pt. 41). Based on the compositions in Table 3.3.5.2d, the major elements of the average composition of bubbled melt is between that value of melt quenched phase and precipitate, like Mg, Ca, Si and Al. It

acts as the fractionation, which separates the elements into two groups when they cooled down. Therefore, the actual melt are represented by the normalized compositions of the former texture.

Table 3.3.5.2d Compositions of bubbled melt, quench phase and precipitate (original data, unit: wt%).

Phases	No.Pt.	SiO ₂	TiO ₂	Al ₂ O ₃	Cr ₂ O ₃	FeO	MgO	CaO	MnO	NiO	Na ₂ O	F	Total
Quench phase from the melt	8	38.82	0.55	17.51	0.00	2.67	5.02	20.25	0.10	0.00	0.02	8.58	93.54
	9	39.50	0.53	18.51	0.00	2.73	3.60	20.03	0.09	0.02	0.15	7.64	92.82
	10	40.26	0.45	18.62	0.10	2.63	3.76	17.86	0.09	0.00	0.21	5.79	89.78
	44	39.13	0.49	17.07	0.00	2.72	5.41	17.52	0.07	0.00	0.41	5.89	88.75
	47	38.63	0.37	16.99	0.14	2.85	5.79	20.20	0.09	0.04	0.10	6.77	91.98
Aver.		39.27	0.48	17.74	0.05	2.72	4.71	19.17	0.09	0.01	6.93	0.18	91.37
StdD		1.05	0.25	0.78	0.20	0.44	0.99	1.36	0.18	0.13	1.19	0.15	
Bubbled melt	11	34.59	0.35	14.44	0.12	2.72	10.31	11.17	0.13	0.05	0.67	5.64	80.27
	12	37.68	0.51	15.54	0.00	2.81	9.98	12.58	0.19	0.00	0.65	6.05	86.07
	13	37.47	0.47	15.15	0.06	2.95	9.82	12.90	0.09	0.00	0.70	5.16	84.80
	45	37.93	0.49	15.93	0.09	2.87	8.94	12.66	0.16	0.01	0.72	5.07	84.95
	46	36.08	0.44	15.16	0.00	2.73	8.56	12.15	0.13	0.02	0.49	6.45	82.22
	50	33.55	0.39	14.71	0.12	2.56	8.00	12.22	0.10	0.07	0.32	4.40	76.57
	51	36.08	0.57	14.93	0.07	2.97	9.19	12.80	0.23	0.11	0.61	5.82	83.43
	52	35.65	0.42	15.01	0.00	2.76	9.21	11.82	0.12	0.05	0.60	6.09	81.74
53	33.07	0.33	14.05	0.00	2.59	8.34	12.16	0.13	0.06	0.53	5.33	76.69	
Aver.		35.79	0.44	14.99	0.05	2.77	9.15	12.27	0.14	0.04	5.56	0.59	81.86
StdD		1.77	0.24	0.61	0.19	0.44	0.78	0.83	0.18	0.14	0.66	0.20	
Precipitate	41	32.91	0.31	13.11	0.04	3.89	14.67	11.39	0.20	0.02	0.32	6.49	83.41

Table 3.3.5.2e Normalized compositions of bubbled melt (unit: wt%).

No.Pt	SiO ₂	TiO ₂	Al ₂ O ₃	Cr ₂ O ₃	FeO	MgO	CaO	MnO	NiO	Na ₂ O	F	H ₂ O	Total
19	40.83	0.51	16.62	0.00	3.28	10.82	13.14	0.05	0.06	1.00	7.41	9.31	103.12
20	42.87	0.46	17.83	0.03	3.09	10.59	13.23	0.12	0.00	1.31	7.34	6.14	103.09
21	39.83	0.51	16.87	0.09	2.69	7.55	14.07	0.09	0.04	0.68	4.42	14.91	101.86
22	40.44	0.45	16.72	0.08	2.91	8.78	14.60	0.05	0.03	1.04	6.20	11.20	102.61
Aver.	40.99	0.48	17.01	0.05	2.99	9.44	13.76	0.08	0.03	1.01	6.34	10.39	102.67
StdD	1.32	0.13	0.56	0.16	0.36	1.55	0.70	0.14	0.11	0.26	1.40	3.67	

In addition, I do not know whether Au or Mo contaminate the melt or not, but they cannot change the composition too much, even if they contaminate the melt. Nevertheless, I decide to estimate the melt composition by charge balance, to avoid big errors and to estimate water concentration more precisely. In conclusion, two melt compositions are shown in Table

3.3.5.2c & e. And the phase proportion of the bubbled melt is much larger than high silica melt.

3.3.5.3 1-SP2-21 experiment

The bubbled melt is the dominant solid phase in this experiment. The humite and spinel crystals distribute in the bottom of the capsule (Fig. 3.1.2.1h). The sizes of spinel are generally small, and they are present inside humite minerals. It indicates that the crystallization of humite led to the present of spinel, because humite only requires abundances of Si, Mg from melt, and the residual elements are crucial for spinel. Although the high proportion melt exist all around the capsule, they are from the same melt texture, as the section 3.3.5.2 described. I also used large beam size (from 20 to 50 μm) to measure their average compositions.

Table 3.3.5.3 Normalized compositions of bubbled melt without estimated water concentration (unit: wt%).

No. Pt.	SiO ₂	TiO ₂	Al ₂ O ₃	Cr ₂ O ₃	FeO	MgO	CaO	MnO	NiO	Na ₂ O	F	Total
28	45.44	0.43	15.08	0.09	3.59	15.57	15.47	0.06	0.09	0.89	5.68	102.39
29	45.56	0.39	15.38	0.11	3.27	15.25	15.75	0.07	0.00	1.15	5.29	102.23
32	45.44	0.49	15.32	0.07	3.52	14.11	17.13	0.12	0.01	0.71	5.07	102.13
34	50.37	0.44	15.22	0.11	3.03	14.68	11.67	0.05	0.06	1.00	5.61	102.36
37	47.31	0.40	15.57	0.11	3.36	16.56	12.55	0.09	0.09	0.94	5.04	102.12
38	47.01	0.37	15.21	0.12	3.43	16.80	13.14	0.04	0.07	0.79	5.07	102.13
39	46.04	0.41	15.18	0.11	3.52	15.26	15.75	0.04	0.11	0.53	5.24	102.21
Aver.	46.74	0.42	15.28	0.10	3.39	15.46	14.49	0.07	0.06	0.86	5.28	102.22
StdD	1.77	0.14	0.37	0.13	0.28	0.96	2.03	0.10	0.12	0.20	0.44	

In Table 3.3.5.3, two measurements No. 32 & 39 are the average composition of quench phase and precipitates. They have similar composition, which demonstrates that these two formations are from the same derivation. This result does not have water concentration, so the average concentration is higher than real values.

3.3.5.4 1-(SP1+MgF₂) experiment

The phase assembly has been introduced in section 3.1.5. As Fig. 3.1.5a (left) shown, its melt textures are the same with the experiment 1-SP2-21, but it contains more quenched melt phase. The distribution of the quenched melt phase and the bubbled melt indicates that the formation of the quench phase was a result of a slow quench rate, because the bubbled melts are closer to the capsule wall. The parameters of electron microprobe analysis for the melt of this experiment were: the current of 4 nA and the beam size from 20 to 100 μm .

Table 3.3.5.4a Compositions of melt quench phases from 1-(SP1+ MgF₂), by charge balance (unit: wt%).

No.Pt.	SiO ₂	TiO ₂	Al ₂ O ₃	Cr ₂ O ₃	FeO	MgO	CaO	MnO	NiO	Na ₂ O	F	H ₂ O	Total
44	37.12	0.36	16.58	0.00	2.84	10.72	16.14	0.16	0.00	1.23	8.92	9.35	103.76
45	38.80	0.50	17.14	0.00	2.90	8.82	16.73	0.12	0.14	1.47	8.32	8.31	103.50
48	38.58	0.36	16.22	0.03	2.88	8.77	18.66	0.07	0.00	1.11	10.29	7.11	104.33
Aver.	38.17	0.41	16.65	0.01	2.87	9.44	17.17	0.12	0.05	1.27	9.18	8.26	103.86
StdD	1.04	0.24	0.68	0.20	0.45	1.11	1.32	0.18	0.21	0.28	1.90	1.12	

Table 3.3.5.4b Compositions of bubbled melt, from 1-(SP1+ MgF₂), by charge balance (unit: wt%).

No.Pt.	SiO ₂	TiO ₂	Al ₂ O ₃	Cr ₂ O ₃	FeO	MgO	CaO	MnO	NiO	Na ₂ O	F	H ₂ O	Total
40	37.54	0.44	16.35	0.00	2.85	11.25	14.65	0.16	0.15	0.97	8.22	10.84	103.46
41	38.81	0.41	16.46	0.00	2.56	11.74	15.14	0.20	0.05	0.88	8.69	8.64	103.66
42	38.05	0.52	16.09	0.00	2.84	11.68	14.39	0.06	0.06	0.93	8.85	10.26	103.73
43	38.99	0.42	16.40	0.00	2.96	11.74	14.76	0.04	0.05	1.03	8.31	8.72	103.50
46	37.40	0.44	15.83	0.02	2.64	11.34	15.20	0.06	0.10	0.62	8.73	11.10	103.68
47	40.47	0.41	16.79	0.11	2.61	11.40	14.82	0.10	0.08	1.01	8.48	7.16	103.57
Aver.	38.54	0.44	16.32	0.02	2.74	11.53	14.83	0.10	0.08	0.91	8.55	9.45	103.60
StdD	1.14	0.26	0.72	0.23	0.48	0.64	0.95	0.20	0.22	0.26	1.96	1.53	0.11

Nine different melt areas were analyzed. Three of them (44, 45 and 48) are melt quench phase with the area larger than 20 μm . The oxygen concentrations were analyzed in all the measurements, so I use the charge balance to estimate their compositions (Table 3.3.5.4a & b). The compositions of the bubbled melts are shown in Table 3.3.5.4b.

Comparing the compositions of these two melt context, their average compositions are obviously different on MgO and CaO. Furthermore, point 46 is to measure its average

composition of melt quench phase and the precipitates in the same area using 100 μm beam size. Other five points in Table 3.3.5.4b are the average compositions of the bubble melt texture, using 50 to 100 μm beam size. These melt measurements gave a constant melt composition, although their missing total is different. Water concentrations differ much, because they are based on oxygen uncertainties, which is more than 1 wt%. There is not large enough surface of precipitate for electron microprobe analysis. Again, the composition comparisons demonstrate that the melt quench phase is not the real melt composition during annealing, while it is derived from the bubbled melts.

3.3.5.5 1-(SP2+Qtz) experiment

I doped the SP2 powder with excess in quartz, so silica concentration increases much and its melting point decreases. At the experimental temperature 950 $^{\circ}\text{C}$, it is easy to produce melt. Almost all the amphibole minerals are surrounded in the melt. This melt did not create quenched melt phase, because of its high silica nature. The bubbles in the melt indicate that it suffered degassing during the quench, but there is big enough area for electron microprobe analysis. Moreover, some isolated spheric melts reach 20 μm (see 3.1.5 Excess Doped Experiments), and they are able to be analyzed with electron microprobe. With oxygen concentration, it is easy to estimate the water concentration with charge balance. The reported measurements gave good total.

Table 3.3.5.5 Two average melt compositions of 1-(SP2+Qtz) experiment (unit: wt%).

	No. Pt.	SiO ₂	TiO ₂	Al ₂ O ₃	Cr ₂ O ₃	FeO	MgO	CaO	MnO	NiO	Na ₂ O	F	H ₂ O	total
Bubbled melt phase	56	76.84	0.16	6.77	0.09	0.59	1.05	4.26	0.00	0.22	0.33	1.82	8.64	100.76
	57	76.32	0.11	6.85	0.02	0.67	1.22	4.12	0.02	0.06	0.42	1.50	9.32	100.63
	58	77.77	0.21	6.61	0.00	0.69	1.03	4.19	0.05	0.23	0.34	2.28	7.52	100.96
	59	76.62	0.20	6.80	0.07	0.60	0.72	4.46	0.03	0.14	0.31	2.55	8.58	101.07
	Aver.	76.89	0.17	6.76	0.05	0.64	1.00	4.26	0.03	0.16	0.35	2.04	8.51	100.86
	StdD	1.37	0.10	0.29	0.14	0.19	0.21	0.36	0.11	0.11	0.11	0.50	0.74	
Spheric melt	60	80.66	0.09	5.02	0.08	0.51	0.89	2.27	0.00	0.15	0.10	2.67	8.63	101.13
	61	84.32	0.10	4.19	0.05	0.45	0.58	1.72	0.06	0.11	0.16	2.33	6.91	100.98
	Aver.	82.49	0.09	4.61	0.06	0.48	0.74	2.00	0.03	0.13	0.13	2.50	7.77	101.06
	StdD	2.59	0.09	0.59	0.14	0.17	0.22	0.40	0.11	0.11	0.09	0.55	1.22	

There are two kinds melt in this capsule. Their compositions are different (the spheric melts have more silica and less Al and Ca than the bubbled melt phase), but their F concentrations are close.

3.4 Fluid Compositions

In large quantity water-bearing experiment, fluid is an important phase. The fluid proportions of my experiments are normally over 30 wt%. Determination of the fluid composition is important for this study.

In previous studies on the minerals solubility, scientists estimated the values by the mass difference of the mineral crystal between before and after the experiment. For example, Manning (1994) investigate the quartz solubility in water; Newton and Manning (2000) study the quartz solubility in H₂O-NaCl and H₂O-CO₂ solutions; Ayers and Watson (1993) experimentally determine the rutile solubility in supercritical aqueous fluid; Rapp et al. (2010) conduct the experiments to learn the rutile solubility in Cl and F-bearing fluids. Generally, these studies do not try any method to measure the fluid composition directly, because in their experiments, most of the solute in fluid precipitates during the quench. They do not think fluid carries enough information for their results (e.g., Ayers et al., 1997). On the other hand, some studies estimate fluid composition by mass balance calculations. For example, instead of weighting the mineral mass difference, Molina and Poli (2000) estimate the coexisting fluids in their experiments by a mass balance approach.

In my experiments, generally they are conducted at 1 GPa. I do not find obvious precipitates on the surface of the minerals or capsule inner wall. It indicates most fluid solute stays in the fluid after I quenched the experiments. If I ignore the fluid composition of my experiments, the results will be unreliable. The most concerned element of my thesis is fluorine, so I spent much time on the direct analysis of fluorine. For the fluid compositions, I calculated it with a mass balance approach, and also try some direct analysis techniques.

In this section, I will describe all the methods I have tried to determinate the fluid compositions of my samples, and some details of this process.

3.4.1 Mass Balance Calculation

3.4.1.1 Traditional Method

With the concept of conservative elements set (see 2.6.2 Conservative Elements Set), I calculated the fluid composition with a typical mass balance approach. The fluid compositions in the successful experiments are dealt with the mass balance calculation.

Generally, SP1 experiments have one mineral phase, hornblende. SP2 and SP3 experiments without melt have two mineral phases, hornblende and norbergite or chondrodite. SP4, SP2 melt-bearing and SP2 higher pressure experiments have at least three solid phases, and they are the most complicated for mass balance. Meanwhile, their results are not as reliable as the former two group experiments. I will describe the details of some experiments, of which mass balance encounter some problems. I do not calculate the proportion of mineral phases of the fluid exhausted experiments.

3.4.1.1.1 Experiments without melt

When the experimental temperature is below 940 °C, the phase assemblies of each series experiment do not change. It is easy for these experiments to calculate their phase proportions. Once the conservative element set is determined, the result is evident. However, some experiments have abnormal phase assemblies. For example, when spinel is present in the capsule, indicating need adjustment for calculation, I will do the mass balance calculation with spinel composition.

Two successful SP1 experiments (1-SP1-3 & 5, Table 3.1.1) contain olivine and augite, and these are considered as the derivation of nickel contamination. The proportions of olivine and augite in 1-SP1-5 experiment are less than 1%. The same situation occurs for 1-SP1-7 experiment, of which spinel proportion is less than 1%. They are small enough to be ignored in the mass balance calculation. Therefore, it is feasible for 1-SP1-4 to 8 experiments to calculate fluid compositions only with hornblende composition. On the contrary, the proportions of olivine and augite in the 1-SP1-3 experiment are more than 10%, and it was obviously suffered fluid loss and nickel contamination during anneal, while its hornblende

composition is similar to that of other SP1 experiments. For they are F-free experiment, the results are compared to F-bearing experiments.

Few SP2 and SP3 experiments created abnormal phase assembly. In this section, I calculated their fluid compositions with all the reasonable possibilities, and select the most suitable composition for the discussion section.

Table 3.4.1.1.1a 1-SP2-14 mass balance results with different phase assemblies (unit: wt%).

Phases	Prop	StdD	Prop	StdD	Prop	StdD
Hornblende	70.60	2.38	70.59	2.38	70.66	2.38
Norbergite	7.92	20.71	18.37	1.09		
Chondrodite	10.60	29.97			18.60	1.10
Oxide	Fluid composition					
SiO ₂	14.63	5.57	15.81	5.59	13.72	5.55
TiO ₂	0.00	0.20	0.00	0.20	0.06	0.19
Al ₂ O ₃	3.35	1.81	3.36	1.82	3.33	1.80
Cr ₂ O ₃	0.39	0.30	0.40	0.30	0.39	0.30
FeO	0.04	0.74	0.08	0.74	0.00	0.73
MgO	0.00	3.12	0.01	3.14	0.00	3.11
CaO	0.00	1.53	0.00	1.54	0.00	1.53
MnO	0.07	0.15	0.09	0.15	0.06	0.15
Na ₂ O	2.59	0.45	2.60	0.45	2.58	0.45
F	2.25	0.70	1.05	0.73	3.16	0.69
H ₂ O	76.66	10.06	76.59	10.09	76.69	10.03

The phase assembly of 1-SP2-14 experiment is hornblende, norbergite and chondrodite. It has 0.6 mg fluid left after the quench. The presence of chondrodite indicates the bulk composition loss during anneal. Thus, using SP2 starting composition as bulk composition of mass balance calculation, the result is not precise. Nevertheless, I use their mineral compositions to estimate their proportions for different phase assemblies, 1) hornblende, norbergite and chondrodite; 2) hornblende and norbergite; 3) hornblende and chondrodite. The compositions of norbergite and chondrodite are similar after excluding Si and F from conservative element set. The calculated results are shown in Table 3.4.1.1.1a. No matter which phase assemblies I chose, the proportion of hornblende is always around 70.6 wt% and the total proportion of norbergite and chondrodite is approximately 18.5 wt%. Their conservative element set is Fe, Mg, Ca and Ti. In my opinion, the result from hornblende-

norbergite phase assemblies is the most reliable. However, the F concentration in minerals, especially in humite group minerals, is relative with that of starting powder. The loss of starting powder makes F of norbergite lower, which leads to a higher F concentration in fluid from mass balance, so even 1.05 wt% F in fluid is also higher than the expected result. In this case, when partial loss happened during an experiment, the fluid composition from mass balance is not reliable, and the discussion section will not employ this value for comparison. A direct analysis is desired (see Section 3.4.2 Direct Measurements).

Table 3.4.1.1.b 1-SP2-18 mass balance results with different phase assemblies (unit: wt%).

Phases	Prop	StdD	Prop	StdD
Hornblende	69.66	5.97	68.03	10.45
Norbergite	18.71	2.14	18.65	2.16
Melt			3.11	17.00
Oxides	Fluid composition			
SiO ₂	13.84	1.80	12.91	1.84
TiO ₂	0.04	0.17	0.02	0.17
Al ₂ O ₃	5.40	0.72	4.90	0.73
Cr ₂ O ₃	0.02	0.27	0.05	0.27
FeO	0.00	0.52	0.00	0.53
MgO	0.00	1.07	0.00	1.09
CaO	2.25	0.72	1.92	0.73
MnO	0.06	0.14	0.06	0.14
Na ₂ O	2.35	0.28	2.41	0.28
F	0.70	0.55	0.47	0.55
H ₂ O	75.33	0.97	77.26	1.00

1-SP2-18 experiment is the first one with the presence of melt and fluid phase. From Fig. 3.1.2.1h, its melt proportion in the capsule is probably around 5 wt%. The most abundant mineral in this experiment is hornblende. Firstly, I calculate its fluid composition by ignoring its melt composition, for I did not measure its composition. Its conservative element set contains Fe, Mg, Ti and Cr. The F concentration is 0.70 wt%. Owing to a similarity of melt composition between 1-SP2-19 and 20 experiments, I performed mass balance calculation with melt composition from 1-SP2-19. The proportions of hornblende and norbergite are very close to the former, while the uncertainties of the latter are much bigger than those of the former. The proportion of melt is 3.11% with 5 times uncertainty, which indicates that it could

be ignored, although this proportion fits the estimation for its SEM image (Fig. 3.1.2.1h). With their uncertainties, their F concentrations in fluid are the same. The results are shown in Table 3.4.1.1.1b, and I prefer the first result with small proportion uncertainties.

Table 3.4.1.1.1c 4-SP2-2 mass balance results with different phase assemblies (unit: wt%).

Phases	Prop	StdD	Prop	StdD
Norbergite	21.57	10.04	24.06	2.20
Chondrodite	2.88	11.31		
Augite	13.12	4.69	13.38	4.60
Hydrogrossular	52.77	1.67	52.75	1.67
Oxides	Fluid composition			
SiO ₂	8.79	1.68	8.91	1.68
TiO ₂	0.00	0.07	0.00	0.07
Al ₂ O ₃	0.05	0.55	0.05	0.55
Cr ₂ O ₃	0.02	0.24	0.02	0.24
FeO	0.00	0.50	0.00	0.50
MgO	0.20	1.42	0.31	1.42
CaO	0.12	1.19	0.05	1.19
MnO	0.00	0.13	0.00	0.13
Na ₂ O	2.35	0.15	2.35	0.15
F	1.21	0.38	1.09	0.38
H ₂ O	87.25	1.98	87.21	1.98

4-SP2-2 experiment was conducted at 2.5 GPa, and created four minerals: norbergite, chondrodite, augite and hydrogrossular. I exclude Na, F and Si from the conservative element set. Its F concentration is 1.21 wt%. The proportions of norbergite and chondrodite are 21.57 wt% and 2.88 wt%, respectively. From inspection of its SEM image, their proportions seem to reflect what is expected. The compositions of norbergite and chondrodite are similar, except SiO₂ and F. The proportion of chondrodite is small with a large uncertainty. Moreover, in 5-SP2-1 experiment, only norbergite is created. It is more reasonable to estimate the fluid composition without chondrodite. The second mass balance calculation only uses norbergite, pyroxene and garnet. The conservative element set is Fe, Mg, Ca, Ti, Al and Cr. The latter calculation has much smaller uncertainties of phase proportions than the former, which indicates three phases mode is better for the mass balance calculation. Within their uncertainties, the results could be considered as the same.

Generally, SP3 experiments create hornblende and chondrodite minerals. The mass

balance results show that the proportion of chondrodite is less than the proportion of norbergite in SP2 experiment. It is typically less than 6%. In two SP3 experiments (1-SP3-1 and 1-SP3-7), I do not find chondrodite. 1-SP3-7 does not have fluid left, so no mass balance calculation is performed. For 1-SP3-1 experiment, I treat the data with two kinds of phase assembly. First, this experiment creates a hornblende-fluid system, so I calculate the fluid composition only with one mineral. On the other hand, because the F concentration of hornblende is similar to those in other SP3 experiments, it should create chondrodite. I employ the chondrodite composition from 1-SP3-3 to calculate the fluid composition. The result shows the proportions of hornblende and chondrodite are 89.34% and 5.43%, respectively. This is quite close to the results of other SP3 experiments. For this experiment, it is more reasonable to calculate the fluid composition with the second method.

Table 3.4.1.1.1d The results of 1-SP3-1 mass balance with different phase assemblies (unit: wt%).

Phases	Prop	StdD	Prop	StdD
Hornblende	100	0	89.34	3.24
Chondrodite			5.43	1.31
Oxides	Fluid composition			
SiO ₂	2.09	2.64	5.35	2.52
TiO ₂	0.02	0.15	0.00	0.13
Al ₂ O ₃	0.00	0.83	1.14	0.79
Cr ₂ O ₃	0.31	0.18	0.35	0.16
FeO	0.00	0.40	0.09	0.36
MgO	1.15	1.25	0.00	1.19
CaO	0.00	0.86	0.00	0.80
MnO	0.00	0.11	0.00	0.09
Na ₂ O	0.29	0.20	0.41	0.18
F	0.56	0.29	0.25	0.26
H ₂ O	95.58	4.74	92.42	4.57

In SP4 series experiments, only 1-SP4-4 has more than 1.0 mg fluid left and it is in equilibrium for long enough duration. From the cross-section image of this experiment, the proportion of clinohumite is the most of three minerals. The mass balance was calculated with its three mineral phase compositions and its conservative element set (Fe, Mg, Ca, Ti, Si and F). The calculated result shows the proportions of hornblende, clinohumite, and augite are 17.10%, 50.76%, and 24.88 %, respectively, and it is consistent with the observation.

3. Results

The bulk composition of SP4 powder is normalized to 100 wt% after I measure its melt with LiBO₂. Its uncertainties are amplified by ~1.5. For mass balance calculation, the phase uncertainties also influence the result. Instead of the uncertainties after normalized, I employed the uncertainties of bulk composition directly from electron microprobe analysis. The calculation gives the result as 16.88% hornblende, 51.02% clinohumite, and 24.82% augite. The values are very close to the previous one. It indicates that different uncertainties will not change the proportion result too much. The fluid composition does not have any F from the mass balance result.

Table 3.4.1.1.1e Fluid compositions of the experiments without melt (unit: wt%).

Expt. ID	Oxide	SiO ₂	TiO ₂	Al ₂ O ₃	Cr ₂ O ₃	FeO	MgO	CaO	MnO	Na ₂ O	F	H ₂ O
1-SP1-3	Aver.	4.36	0.03	10.65		1.53	1.43	0.88	0.03	1.31		79.78
	stdv	13.39	0.41	7.71		1.77	8.71	6.94	0.18	0.72		23.64
1-SP1-4	Aver.	1.02	0.01	1.12	0.48	0.00	3.31	0.00	0.02	0.72		93.31
	stdv	5.30	0.21	3.90	0.56	0.82	2.38	2.48	0.12	0.45		8.23
1-SP1-5	Aver.	0.08	0.00	1.07		0.00	1.24	0.00	0.01	0.33		97.26
	stdv	2.60	0.10	1.31		0.35	1.15	0.85	0.05	0.20		4.39
1-SP1-6	Aver.	0.00	0.04	6.58	0.00	0.00	2.16	0.00	0.04	0.42		90.76
	stdv	6.79	0.31	2.23	0.56	0.91	2.84	2.18	0.23	0.45		12.12
1-SP1-7	Aver.	0.52	0.02	2.18		0.00	4.54	0.00	0.04	1.03		91.65
	stdv	6.12	0.26	6.54		0.98	2.92	2.19	0.17	0.45		7.79
1-SP1-8	Aver.	2.29	0.00	0.00	0.37	0.00	4.04	0.00	0.00	0.74		92.56
	stdv	2.09	0.20	2.83	0.47	0.88	1.48	0.99	0.15	0.44		1.96
1-SP2-1	Aver.	0.19	0.00	2.08	0.35	0.00	0.02	0.00	0.01	2.54	0.24	94.56
	stdv	2.03	0.12	1.47	0.60	0.58	1.32	0.85	0.09	0.24	0.62	1.62
1-SP2-4	Aver.	2.95	0.00	1.00	0.04	0.02	0.00	0.00	0.01	1.00	0.11	94.87
	stdv	2.40	0.07	1.08	0.18	0.33	1.35	0.59	0.04	0.17	0.27	4.25
1-SP2-8	Aver.	3.29	0.00	1.13	0.12	0.09	0.00	0.00	0.01	1.35	0.24	93.77
	stdv	2.48	0.07	1.51	0.24	0.35	1.32	0.60	0.05	0.20	0.28	3.73
1-SP2-12	Aver.	0.13	0.00	4.95	0.00	0.00	0.14	0.11	0.00	2.61	0.10	91.94
	stdv	5.87	0.14	2.12	0.46	1.09	3.48	1.55	0.10	0.45	0.73	10.19
1-SP2-15	Aver.	5.27	0.00	0.64	0.23	0.00	0.05	0.02	0.00	1.39	0.65	91.75
	stdv	2.73	0.15	0.93	0.19	0.38	1.50	0.75	0.09	0.22	0.37	4.64
1-SP2-16	Aver.	3.12	0.00	0.58	0.00	0.00	0.02	0.00	0.01	0.67	0.25	95.34
	stdv	1.18	0.05	0.37	0.10	0.26	0.64	0.33	0.04	0.09	0.16	1.96
1-SP2-17	Aver.	4.00	0.00	0.92	0.00	0.12	0.00	0.00	0.01	0.88	0.27	93.80
	stdv	0.99	0.06	0.38	0.10	0.34	0.52	0.30	0.04	0.10	0.16	1.17
1-SP2-18	Aver.	13.84	0.04	5.40	0.02	0.00	0.00	2.25	0.06	2.35	0.70	75.33
	stdv	1.80	0.17	0.72	0.27	0.52	1.07	0.72	0.14	0.28	0.55	0.97

3. Results

Expt. ID	Oxide	SiO ₂	TiO ₂	Al ₂ O ₃	Cr ₂ O ₃	FeO	MgO	CaO	MnO	Na ₂ O	F	H ₂ O
1-SP2-23	Aver.	11.86	0.00	21.34	0.00	0.22	0.00	0.39	0.00	8.08	0.15	57.96
	stdv	6.28	0.54	5.36	1.31	1.92	3.68	2.62	0.53	1.05	2.29	1.47
3-SP2-1	Aver.	4.08	0.05	2.29	0.06	0.00	0.00	0.10	0.01	1.80	1.65	89.95
	stdv	1.92	0.13	0.68	0.21	0.41	1.09	0.69	0.12	0.23	0.36	2.12
4-SP2-2	Aver.	8.91	0.00	0.05	0.02	0.00	0.31	0.05	0.00	2.35	1.09	87.21
	stdv	1.68	0.07	0.55	0.24	0.50	1.42	1.19	0.13	0.15	0.38	1.98
1-SP3-1	Aver.	5.35	0.00	1.14	0.35	0.09	0.00	0.00	0.00	0.41	0.25	92.42
	stdv	2.52	0.13	0.79	0.16	0.36	1.19	0.80	0.09	0.18	0.26	4.57
1-SP3-3	Aver.	18.82	0.00	2.64	1.49	1.03	0.02	0.00	0.09	1.11	0.40	74.39
	stdv	7.37	0.45	2.57	0.55	1.19	3.57	2.52	0.33	0.62	0.90	12.73
1-SP3-4	Aver.	3.73	0.00	1.18	0.28	0.16	0.00	0.00	0.00	0.34	0.14	94.17
	stdv	1.79	0.10	0.97	0.13	0.28	0.82	0.59	0.08	0.14	0.21	2.95
1-SP3-8	Aver.	5.04	0.00	0.26	0.31	0.06	0.05	0.00	0.00	0.44	0.18	93.67
	stdv	1.37	0.09	1.66	0.20	0.23	0.65	0.41	0.07	0.11	0.16	1.16
1-SP4-3	Aver.	3.07	0.00	0.00	0.45	0.57	0.65	0.00	0.01	2.82	0.00	92.41
	stdv	1.93	0.30	0.93	0.38	0.67	1.78	0.96	0.26	0.43	0.39	0.89
1-SP4-4	Aver.	0.00	0.00	9.23	0.44	1.42	2.16	0.86	0.00	2.20	0.00	83.68
	stdv	2.19	0.32	0.98	0.39	0.66	2.06	1.22	0.28	0.51	0.42	1.48

3.4.1.1.2 Experiments with Melt

In the large quantity water experiments, the partial melting point is lowered due to the presence of water. When the experiment quenched, the hydrous melt usually degassed. Although I managed to estimate the melt composition in section 3.3.5, mass-balance calculation is unreliable with the given the heterogeneities and uncertainty. In any case, with the estimated melt compositions, I have deduced the fluid composition using mass-balance for some useful information. I describe the details for these calculations below.

1-SP2-19 experiment contains hornblende, chondrodite and melt. The mass balance calculation for this experiment first conducts with these three phase compositions. Following the mass balance procedure (section 2.6.2), Mn, Na and F are excluded from the calculation. The total of the proportions of these three solid phases is more than 100 wt%. Normalize them to estimate the fluid composition. The proportions of hornblende, chondrodite and melt are 46.17%, 19.34% and 34.49%, respectively. These values are in agreement with the qualitative assessment of its capsule cross-section image. The F concentration in fluid is determined as 0.47 wt%.

1-SP2-20 experiment has the most complicated phase assemblies in SP2 series

experiments. If I use normal conservative elements set, mass balance will not work. The total of each phase proportion is above 100 wt%. For this calculation, I only exclude Na from the conservative set and normalize the proportion to 100 wt%. The proportion result for each phase is 38.05% hornblende, 22.32% chondrodite, 0.87% spinel, 34.48% bubbled melt and 4.28% silica melt. In consequence, F concentration of fluid is 0.71 wt%. It demonstrates that if the phase number is larger than the number of major conservative element (> 1 wt% in bulk composition), it is impossible to get a reliable result, and the calculated value can be only treated as a reference.

In 1-SP2-21 experiment, the melt proportion is probably more than 60 wt% from the cross-section picture (Fig. 3.1.2.1h). Its melt composition was normalized to 100 wt% without estimating its water content. Calculate the phase proportions with this melt composition data. After tried several element sets, F concentration of fluid is zero all the same, while the phase proportions are reasonable. One possibility is melt composition is not precise enough, and I should estimate its water concentration. I assume its melt contains 7.0 ± 0.5 wt% water, which is estimated for 1-SP2-19 and 20 experiments. I normalize its composition and run the mass balance program. As expected, the result gives more melt proportion, because the melt content become less after normalizing. However, the fluid composition does not change. It indicates mass balance process is correct, and suggests the fluid composition is F-free. The conservative element set contains Fe, Mg, Ca, Ti, Cr and F. This mass balance approach does not fit with this experiment.

In four excess SiO_2 or MgF_2 experiments, two of them have obvious fluid left when I opened the capsules. In 1-(SP2+Qtz) experiment (Fig. 3.1.5b, right), additional quartz pulls the bulk composition to silica rich side, so it does not create humite group mineral. The obvious nickel contamination would result in larger uncertainties of the fluid composition. I tried mass balance calculation with its three phases, hornblende, talc and melt, ignoring nickel contamination and anthophyllite with little quantity. The result shows Na, Fe and Si are dissolved into the fluid. In the other experiment 1-(SP1+ MgF_2), the bulk composition is similar with SP2 starting material composition, but with more F concentration (approximately 6.6 wt%). Its experimental temperature is high enough to create melt, so only chondrodite, spinel and melt exist in the capsule (Fig. 3.1.5a, left). Within three times calculations, Na, Si

and Al are excluded from the conservative element set. The phase proportions are 29.70% chondrodite, 1.85% spinel and 68.45% melt. The proportions are reasonable by comparing with the capsule cross-section image.

Table 3.4.1.1.2 Fluid compositions of the experiments with melt (unit: wt%).

	Oxide	SiO ₂	TiO ₂	Al ₂ O ₃	Cr ₂ O ₃	FeO	MgO	CaO	MnO	Na ₂ O	F	H ₂ O
1-SP2-19	Aver.	1.09	0.00	0.51	0.27	0.07	0.42	0.00	0.04	1.69	0.47	95.44
	stdv	2.00	0.09	0.67	0.16	0.35	1.14	0.58	0.08	0.21	0.25	2.62
1-SP2-20	Aver.	5.61	0.00	3.08	1.04	0.00	3.80	1.08	0.04	6.88	0.71	77.77
	stdv	5.27	0.41	2.07	0.59	1.27	3.91	1.96	0.38	0.78	2.62	7.32
1-SP2-21	Aver.	2.67	0.00	1.77	0.00	0.15	0.11	0.29	0.05	3.12	0.00	91.86
	stdv	3.10	0.23	0.82	0.26	0.55	1.74	3.01	0.18	0.37	0.69	1.03
1-(SP2+Qtz)	Aver.	19.88	0.00	0.29	0.03	0.56	0.45	0.17	0.03	1.27	0.00	77.32
	stdv	2.43	0.14	0.44	0.21	0.30	0.56	0.50	0.15	0.17	0.68	0.96
1-(SP1+MgF2)	Aver.	32.14	0.00	2.55	0.00	0.36	2.12	1.39	0.00	3.58	0.00	57.85
	stdv	5.36	1.00	2.87	0.96	1.95	3.33	3.76	0.77	1.02	7.44	5.81

On the mass balance results of these melt experiments, it should be noted that the fluid composition is F-free when the proportion of melt is above 50%. It must be correlated with the presence of the melt in the experiments, either the uncertainties of melt composition are large, or the estimated melt composition cannot reflect its actual composition during anneal. Moreover, it led to larger uncertainties of fluid compositions. On the other hand, melt contains much more F than fluid. Melt incorporate F more than fluid, so when melt proportion is large enough, the sensitivity of mass balance calculation cannot satisfy low F concentration of fluid. However, the F concentration of fluid cannot be zero absolutely. The direct analysis technique is also expected for this situation.

3.4.1.2 Some Confirmations

For every large quantity water experiment, I loaded solid powder and deionized water into a capsule, and noted down their masses. The ideal situation is that all the fluid remains after quenching the experiment within its uncertainty (e.g., 1-SP2-4). However, nearly all the successful experiments contain less fluid mass than the initial water quantity after quenching, for the hydrogen can diffuse during anneal. Therefore, the fluid mass is derived from the difference between before and after retrieving the fluid into a flask. This solution is a mixture

with dissolved elements from the solid starting material. Obviously, if I assume the fluid mass as the water quantity, it will introduce systematic errors. It is necessary to confirm this assumption. In this section, I will count the total water quantity for all the sources, and compare to the fluid mass.

From HPLC analyses (IPGP), there are several weight percent solutes in the fluid, such as, Na^+ , K^+ , Ca^{2+} , Mg^{2+} and F. After I exchange their concentration to oxides mass, I can estimate H_2O concentration in fluid. With stoichiometry calculations, hydrous minerals contain approximately 1~2 wt% H_2O . The proportions of minerals in the solid starting material are calculated with mass balance. With all the parameters mentioned above, it is possible to get the quantities of minerals and H_2O .

For example, 1-SP2-15 experiment contains 1.4 ± 0.1 mg SP2 powder and 1.27 ± 0.08 mg fluid. Mass balance showed the proportions of hornblende and norbergite are 77 ± 3 % and 16 ± 1 %, respectively. The compositions of minerals from electron microprobe analyses shows the totals of hornblende and norbergite are 97.6 % and 99.0 %. Based on the stoichiometry calculation, the totals with H_2O are 98.64 % (hornblende) and 100.73 % (norbergite). HPLC measurement shows the total proportion of solutes in the fluid is 6.84 %, so H_2O proportion is 93.2 %.

$$m(\text{hornblende}) = 1.4 \times 77.36\% \times \frac{98.64}{97.60} = 1.09 \text{ (mg)}$$

$$m(\text{norbergite}) = 1.4 \times 16.16\% \times \frac{100.73}{98.98} = 0.23 \text{ (mg)}$$

$$m(\text{H}_2\text{O})^{\text{fluid}} = 1.27 \times 93.16\% = 1.18 \text{ (mg)}$$

$$m(\text{H}_2\text{O})^{\text{total}} = 1.18 + 1.09 \times 1.04\% + 0.23 \times 1.74\% = 1.20 \text{ (mg)}$$

The water quantity is close to the fluid mass and within its uncertainty. The assumption for mass balance calculation is reasonable. Furthermore, I continue to calculate solid mass dissolved into fluid.

$$m(\text{Solute})^{\text{fluid}} = 1.4 - 1.09 \times 97.60\% - 0.23 \times 98.98\% = 0.10 \text{ (mg)}$$

The fluid mass is 1.28 mg from this calculation. It is the same value to that I measured after experiment within their uncertainty. And the solute proportion is 8.07 %, which is very close to the estimated value from HPLC data. All the calculations for the confirmation are show in Table 3.4.1.2. It certifies the assumption for my mass balance calculation.

Table 3.4.1.2 Comparisons of measured fluid mass and calculated water and fluid mass (unit: mg).

Expt.ID	Fluid ^a	H ₂ O ^b	Fluid ^b
1-SP2-14	0.6(1)	0.60(10)	0.74(18)
1-SP2-15	1.27(8)	1.20(7)	1.28(17)
1-SP2-16	2.77(5)	2.76(5)	2.88(14)
1-SP2-17	2.66(3)	2.65(3)	2.80(10)
1-SP2-18	0.73(1)	0.73(1)	0.94(16)
1-SP3-3	0.28(5)	0.29(5)	0.35(18)
1-SP3-4	1.76(4)	1.73(5)	1.80(18)

^a fluid mass by measured different mass.

^b the calculated values with EMP, HPLC and mass balance data.

3.4.2 Direct Measurements

Although mass balance is a reasonable strategy to estimate the fluid composition, it is still a model calculation. In melt-bearing experiments, F concentrations of fluid compositions are reported as zero. It indicates that mass balance does not work for all the experiments. Moreover, as I account all the uncertainty sources, the uncertainties of results are quite large. On the other hand, most of experiments have reliable and reproducible results with mass balance, but it does not work well for some abnormal ones, whose bulk composition changes. For example, some experiments with nickel contaminations, or some might lose fluid part and starting material during anneal. A direct analysis technique for the fluid of these experiments is expected.

It is necessary to know the dilution factor of each retrieved solution. The fluid in the capsule is retrieved into a volumetric flask, of which volume is fixed as 10, 25, or 50 mL. While the calibrations solution for HPLC measurements are diluted by weighted determined quantity deionized water. Their units are ppm ($\mu\text{g/g}$). So, the quantity of the dilute solution is derived from density times its volume. Because the diluted factor is 3600 at least, their solution density could be considered as the same as the pure water. From the Lang's handbook of chemistry (Lange and Speight, 2005), from 14 to 32 °C, the density of water is from 0.99924 to 0.99503 g/mL. My experimental room temperature is in this temperature range, so I use 0.997 g/mL to calculate the fluid quantity in each volumetric flask.

Table 3.4.2 Dilute factor of each retrieved solution

Expt. ID	Fluid / mg	Flask No.	V / mL	Dilute Factor
1-SP1-8	1.21(4)	21	10	8074
1-SP2-14	0.6(1)	12	10	16283
1-SP2-15 ^a	1.27(8)	13	25	19232
		17	10	7693
1-SP2-16	2.77(5)	19	50	17635
1-SP2-17	2.66(3)	22	10	3673
1-SP2-18	0.73(1)	24	10	13384
1-SP2-19	1.00(4)	25	10	9770
1-SP2-20	0.30(1)	27	10	32567
1-SP2-21	0.84(1)	26	10	11631
1-SP2-22 ^b	< d.l.	37	10	-
1-SP2-23	0.45(1)	35	25	54278
1-SP2-24	0.71(1)	36	25	34401
2-SP2-1 ^b	< d.l.	20	25	-
3-SP2-1	0.94(3)	23	10	10394
4-SP2-2	1.62(6)	28	10	6031
1-SP3-1	1.09(5)	14	10	8963
1-SP3-3	0.28(5)	15	10	34893
1-SP3-4 ^a	1.76(4)	16	10	5551
		18	10	5551
1-SP3-8	1.91(2)	29	10	5115
1-SP4-3	1.43(1)	30	10	6832
1-SP4-4	0.85(2)	31	10	11494
1-SP4-5	0.40(1)	38	10	24425
1-(SP1+MgF ₂)	1.25(2)	33	25	19540
1-(SP1+CaF ₂)	0.49(1)	34	25	49847
1-(SP2+Qtz)	4.53(1)	32	10	2157

^a The fluid in the capsule is retrieved twice into two volumetric flasks.

^b The fluid mass is below the detection limit, so the dilute factor is undetermined.

The solutions in Table 3.4.2 are analyzed in IPGP with HPLC for anions and cations. Four of them are analyzed with ICP-AES in LMV. The latest cations analyses are conducted in Toulouse, with ICP-MS fluid mode. In this section, I will report the results after correcting. And the original data are shown in Appendix III .

3.4.2.1 HPLC

Before analyzing the unknown concentration samples, some standard solutions are tested for verifying fluorine peak (retention time). It is an indispensable procedure to identify the F

peak during the measurements. For example, when I analyzed the solution from 1-SP2-14, around retention time 4 minutes, there is a double peak (Fig. 2.5.2.3.3 & Fig. 3.4.2.1). With the signal of standard solutions, the first peak represents F signal due to the same retention time. The same double peak situation happened during the analysis for the fluid from 4-SP2-2 experiment (Fig. 3.4.2.1). I use Peakfit 4 to count the first peak area. Two of the most important parameters are area and center (as explained in 2.5.2.3 Current Setting for HPLC Analysis).

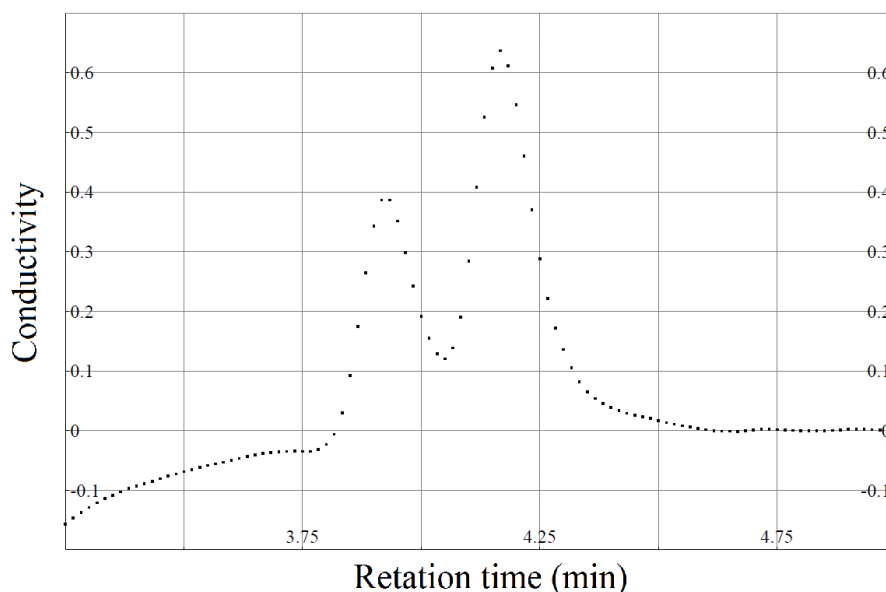


Fig. 3.4.2.1 The chromatogram of 4-SP2-2 fluid solution has a double peak around retention time four minutes.

The original fitting data and relative F concentration are shown in Table 3.4.2.1a. Each retrieved solution is analyzed twice as parallel experiments. The result shows HPLC analyses have a good repeatability. It demonstrates that the uncertainties of F concentrations are much less than the result of mass balance calculations. It also fits a normal regular that the uncertainty of the instrument analysis is approximately 1%. However, the sensitive of HPLC analysis could reach ppb level. If the concentration is just above the detection limit, the errors may reach 15%. Although the F concentrations of my dilute solutions are quite small, it is much higher than the detection limit. The uncertainties of my measurements are around 1%.

Table 3.4.2.1a The F peak area and the center (retention time), and their F concentrations in dilute solutions and fluid in the capsules of each experiment.

Expt. ID	Area	Center	Solution	Fluid	Expt. ID	Area	Center	Solution	Fluid
	$\mu\text{S}^*\text{min}$	min	ppb	wt%		$\mu\text{S}^*\text{min}$	min	ppb	wt%
12 1-SP2-14	0.031	3.912	48.5	0.081	26 1-SP2-21	0.090	3.923	141	0.167
12b 1-SP2-14	0.032	3.910	50.1	0.083	26b 1-SP2-21	0.092	3.923	143	0.170
13 1-SP2-15	0.015	3.914	23.5	0.046	27 1-SP2-20	0.064	3.924	100	0.332
13b 1-SP2-15	0.015	3.915	23.5	0.046	27b 1-SP2-20	0.065	3.924	101	0.336
14 1-SP3-1	0.051	3.907	79.8	0.073	28 4-SP2-2	0.058	3.923	90.5	0.056
14b 1-SP3-1	0.055	3.909	86.0	0.079	28b 4-SP2-2	0.057	3.923	88.6	0.055
15 1-SP3-3	0.018	3.911	28.2	0.100	29 1-SP3-8	0.036	3.923	55.9	0.029
15b 1-SP3-3	0.020	3.913	31.3	0.111	29b 1-SP3-8	0.035	3.937	55.0	0.029
16 1-SP3-4	0.035	3.914	54.8	0.031	30 1-SP4-3	0.015	3.924	24.1	0.017
16b 1-SP3-4	0.040	3.920	62.6	0.035	30b 1-SP4-3	0.016	3.922	24.4	0.017
17 1-SP2-15	0.009	3.927	14.1	0.011	31 1-SP4-4	0.003	3.911	5.21	0.006
17b 1-SP2-15	0.009	3.921	14.1	0.011	31b 1-SP4-4	0.004	3.912	5.49	0.006
18 1-SP3-4	0.052	3.907	81.3	0.046	32 1-(SP2+Qtz)	0.424	3.924	663	0.146
18b 1-SP3-4	0.054	3.927	84.5	0.048	32b 1-(SP2+Qtz)	0.430	3.919	672	0.148
19 1-SP2-16	0.092	4.431	144	0.259	33 1-(SP1+MgF ₂)	0.031	3.918	48.5	0.097
19b 1-SP2-16	0.088	4.035	138	0.248	33b 1-(SP1+MgF ₂)	0.030	3.918	46.8	0.093
20 2-SP2-1	0.118	3.909	185	0.221	34 1-(SP1+CaF ₂)	0.718	3.918	1124	5.716
20b 2-SP2-1	0.118	3.924	185	0.221	34b 1-(SP1+CaF ₂)	0.706	3.918	1104	5.614
22 1-SP2-17	0.334	3.907	522	0.196	35 1-SP2-23	0.114	3.922	178	0.987
22b 1-SP2-17	0.333	3.905	521	0.195	35b 1-SP2-23	0.114	3.922	178	0.984
23 3-SP2-1	0.219	3.961	343	0.363	36 1-SP2-24	0.054	3.922	84.4	0.296
23b 3-SP2-1	0.221	3.914	346	0.367	36b 1-SP2-24	0.053	3.922	83.6	0.293
24 1-SP2-18	0.256	3.917	400	0.547	37 1-SP2-22	0.004	3.922	5.70	0.568
24b 1-SP2-18	0.267	3.918	418	0.570	37b 1-SP2-22	0.004	3.934	5.90	0.588
25 1-SP2-19	0.164	3.917	257	0.256					
25b 1-SP2-19	0.157	3.924	246	0.245					

Table 3.4.2.1b The fluorion concentration of the fluid in the capsule of each capsule.

Expt. ID	[F]/wt%	Expt. ID	[F]/wt%	Expt. ID	[F]/wt%	Expt. ID	[F]/wt%
1-SP2-14	0.082(1)	1-SP2-20	0.334(2)	1-SP3-4	0.080(3)	1-(SP2+Qtz)	0.147(1)
1-SP2-15	0.057(1)	1-SP2-21	0.169(1)	1-SP3-8	0.029	1-(SP1+MgF ₂)	0.095(2)
1-SP2-16	0.253(6)	1-SP2-23	0.985(1)	1-SP4-3	0.017	1-(SP1+CaF ₂)	5.665(51)
1-SP2-17	0.196(1)	1-SP2-24	0.295(1)	1-SP4-4	0.006		
1-SP2-18	0.559(12)	1-SP3-1	0.076(3)	3-SP2-1	0.365(2)		
1-SP2-19	0.251(5)	1-SP3-3	0.106(6)	4-SP2-2	0.055(1)		

The cation species of HPLC analyses contain Li^+ , Na^+ , K^+ , Mg^{2+} and Ca^{2+} . I do not have any data about Li in the solid phases, so I do not report Li^+ concentrations. The HPLC cation

measurements are conducted by the instrument automatically. The concentrations are shown in Table 3.4.2.1c, and the unit is ppm.

In Table 3.4.2.1b, the fluorion concentrations of the fluid in the capsule are calculated, with its dilute factor and the concentration measured by HPLC. It is impossible to calculate the F concentration of 1-SP2-22 and 2-SP2-1, because their fluid mass is below the detection limit.

Table 3.4.2.1c The cation concentrations of dilute solutions with HPLC (unit: ppm).

Expt. ID	Na ⁺	K ⁺	Mg ²⁺	Ca ²⁺	Expt. ID	Na ⁺	K ⁺	Mg ²⁺	Ca ²⁺
12 1-SP2-14	1.18	0.11	0.060	0.016	19 1-SP2-16	0.12	0.01	0.012	0.047
13 1-SP2-15	2.18	0.10	0.007	0.005	20 2-SP2-1	1.55	0.08	0.005	0.007
14 1-SP3-1	0.74	0.14	0.006	0.007	21 1-SP1-8	0.74	0.03	0.005	0.008
15 1-SP3-3	0.24	0.04	0.006	0.008	22 1-SP2-17	1.41	0.10	0.008	0.013
16 1-SP3-4	2.47	0.08	0.003	0.003	23 3-SP2-1	1.04	0.09	0.009	0.015
17 1-SP2-15	0.61	0.08	0.007	0.010	24 1-SP2-18	0.55	0.12	0.08	0.200
18 1-SP3-4	1.25	0.06	0.006	0.020					
24 1-SP2-18	0.55	0.12	0.08	0.200					

Table 3.4.2.1d The cation concentrations in the fluid of the capsules (unit: wt%).

Expt. ID	Na ₂ O	K ₂ O	MgO	CaO	Expt. ID	Na ₂ O	K ₂ O	MgO	CaO
1-SP1-8	0.89	0.03	0.01	0.01	1-SP3-1	0.91	0.15	0.01	0.01
1-SP2-14	2.64	0.22	0.17	0.04	1-SP3-3	1.15	0.17	0.04	0.04
1-SP2-15	6.41	0.31	0.03	0.02	1-SP3-4	2.84	0.10	0.01	0.02
1-SP2-16	0.29	0.02	0.04	0.12	2-SP2-1	2.50	0.12	0.01	0.01
1-SP2-17	0.71	0.05	0.00	0.01	3-SP2-1	1.49	0.11	0.02	0.02
1-SP2-18	1.01	0.20	0.17	0.38					

After timing the dilute factor of each experiment, I calculate these cations concentrations in the fluid of the capsules (Table 3.4.2.1d). Obviously, there is a few weight percent of sodium ion in each fluid, while most magnesium and calcium concentrations are close to zero. Potassium concentration is approximately 0.1 wt%. In the starting materials, potassium concentration is nearly zero (0.02 wt%), so most potassium is dissolved into the fluid during anneal. If the proportion of fluid is less than solid phase, its potassium concentration could be higher than that in the solid phases.

3.4.2.2 ICP-AES

ICP-AES is a sensitive technique for measuring some metal cation concentrations in solution. ICP-AES can measure silicon concentration. As it is a test for analyzing these solutions with ICP-AES, only 10 ppm standard solution is used for its calibration. These results are semi-quantitative data, but they have comparable values with HPLC results (at least in the same magnitude), except Na concentration of 1-SP3-1 is much higher than HPLC result. For most of the data, the data from ICP-AES is higher than those from HPLC.

Table 3.4.2.2 Five cation concentrations of retrieved solution (left) and fluid in the capsule before opening (right) analyzed by ICP-AES.

Expt. ID	Dilute Solution (ppm)					Fluid (wt%)				
	Na ⁺	K ⁺	Mg ²⁺	Ca ²⁺	Si	Na ₂ O	K ₂ O	MgO	CaO	SiO ₂
14 1-SP3-1	1.90	0.04	0.025	0.210	0.36	2.34	0.04	0.04	0.27	0.85
15 1-SP3-3	0.58	0.11	n.d	n.d	n.d	2.78	0.47	n.d	n.d	n.d
19 1-SP2-16	0.11	0.07	<L.D	0.037	0.34	0.26	0.14	<L.D	0.09	1.57
20 2-SP2-1	1.95	0.08	0.010	0.004	1.06	3.15	0.11	0.02	0.01	3.26
22 1-SP2-17	1.59	0.05	0.010	0.010	2.46	0.80	0.02	0.01	0.01	2.37

n.d indicates “not determined”. L.D indicates detect limitation. 1-SP3-3 does not have enough solution to analyze five elements. Mg concentration in 1-SP2-16 is lower than its detection limit.

3.4.2.3 ICP-MS

Fifteen fluid samples are analyzed with ICP-MS, in Toulouse. Before introducing solutions into ICP-MS, the samples are mixed with nitric acid solution to reach a suitable pH condition for measurement. And In/Re solution is also introduced into the mixture as internal standard. All the samples are diluted by two different factors. Different solutions were added into the container as the sequence of sample, nitric acid and InRe solutions. The dilute details are shown in Table 3.4.2.3a & b.

Table 3.4.2.3a Preparation information (unit: mg) and dilute factors (July 19, 2012)

Expt. ID 20120719	m(container)	+m(sample)	+m(HNO ₃)	+m(InRe62)	Dilute Factor
01-blank	5.17	14.82	14.82	14.94	1.01
02-E19 1-SP2-16	5.18	6.38	15.60	15.73	8.84
03-E20 2-SP2-1	5.13	6.61	15.02	15.14	6.79
04-E25 1-SP2-19	5.17	7.04	16.01	16.14	5.86
05-E26 1-SP2-21	5.17	6.28	15.71	15.83	9.58
06-E27 1-SP2-20	5.13	6.04	16.95	17.08	13.18
07-E28 4-SP2-2	5.16	6.48	14.42	14.54	7.13
08-E29B 1-SP3-8	5.26	6.37	15.33	15.46	9.16
09-E30 1-SP4-3	5.15	6.36	15.59	15.72	8.72
10-E31 1-SP4-4	5.06	6.25	16.64	16.76	9.85
11-E32 1-(SP2+Qtz)	5.18	6.73	13.91	14.04	5.73
12-E33 1-(SP1+MgF ₂)	5.25	6.34	14.05	14.18	8.20
13-E34 1-(SP1+CaF ₂)	5.17	7.10	14.55	14.68	4.93
14-E35 1-SP2-23	5.14	6.88	13.92	14.04	5.11
15-E36 1-SP2-24	5.06	7.19	15.37	15.50	4.90
16-E37 1-SP2-22	5.16	6.11	14.61	14.73	10.01

Table 3.4.2.3b Preparation information (unit: mg) and dilute factors (July 24, 2012)

Expt. ID 20120724	m(container)	+m(sample)	+m(HNO ₃)	+m(InRe62)	Dilute Factor
01-blank	5.27	12.68	12.92	13.01	1.05
02-E19 1-SP2-16	5.17	11.68	11.82	11.95	1.04
03-E20 2-SP2-1	5.17	10.54	10.76	10.88	1.06
04-E25 1-SP2-19	5.18	7.62	7.78	7.90	1.11
05-E26 1-SP2-21	5.18	8.23	8.38	8.50	1.09
06-E27 1-SP2-20	5.16	7.77	7.92	8.05	1.11
07-E28 4-SP2-2	5.06	8.44	8.59	8.73	1.08
08-E29 1-SP3-8	5.17	6.87	7.02	7.15	1.16
09-E30 1-SP4-3	5.26	8.05	8.21	8.33	1.10
10-E31 1-SP4-4	5.17	7.52	7.67	7.79	1.12
11-E32 1-(SP2+Qtz)	5.16	7.02	7.17	7.29	1.15
12-E33 1-(SP1+MgF ₂)	5.14	9.43	9.62	9.74	1.07
13-E34 1-(SP1+CaF ₂)	5.09	11.06	11.27	11.39	1.05
14-E35 1-SP2-23	5.16	12.05	12.28	12.40	1.05
15-E36 1-SP2-24	5.41	11.54	11.81	11.92	1.06
16-E37 1-SP2-22	5.17	6.46	6.61	6.74	1.22

However, the fluid masses of two samples are under the detection limit of balance, so only 13 results are shown in Table 3.4.2.3c and 3.4.2.3d. The original elements concentrations (in ppb) and their relative standard deviations are shown in Appendix III .

Table 3.4.2.3c ICP-MS analyses for the samples without dilution (July 24, 2012). Under each Expt. ID, the first column is the composition and the second is its absolute uncertainties (unit: wt%).

Expt. ID	1-SP2-16		1-SP2-19		1-SP2-20		1-SP2-21		1-SP2-23	
Na ₂ O										
MgO	0.017	0.000	0.027	0.001	0.092	0.002	0.103	0.006	0.19	0.05
Al ₂ O ₃	0.154	0.002	0.211	0.004	0.26	0.01	0.42	0.01	0.12	0.02
SiO ₂										
K ₂ O	0.120	0.002	0.057	0.001	0.32	0.03	0.142	0.006	0.551	0.003
CaO	0.067	0.001	0.068	0.002	0.25	0.01	0.245	0.004	0.26	0.07
TiO ₂	0.002	0.000	0.001	0.000	0.002	0.000	0.008	0.000	0.007	0.002
Cr ₂ O ₃	0.000	0.000	0.000	0.000	0.000	0.000	0.002	0.000	0.014	0.009
MnO	0.000	0.000	0.001	0.000	0.001	0.000	0.002	0.000	0.003	0.001
FeO	0.002	0.000	0.035	0.001	0.015	0.001	0.063	0.004	0.069	0.012
NiO	0.002	0.000	0.009	0.000	0.084	0.002	0.001	0.000	0.418	0.001
Expt. ID	1-SP2-24		1-SP3-8		4-SP2-2		1-SP4-3		1-SP4-4	
Na ₂ O										
MgO	2.13	0.59	0.07	0.03	0.221	0.004	0.075	0.004	0.026	0.000
Al ₂ O ₃	1.56	0.42	0.021	0.002	0.013	0.000	0.025	0.001	0.009	0.000
SiO ₂										
K ₂ O	0.417	0.007	0.059	0.001	0.066	0.002	0.060	0.001	0.062	0.002
CaO	0.83	0.1w	0.040	0.001	0.040	0.001	0.029	0.002	0.037	0.000
TiO ₂	0.035	0.002	0.000	0.000	0.000	0.000	0.000	0.000	0.000	0.000
Cr ₂ O ₃	0.078	0.005	0.001	0.001	0.000	0.000	0.001	0.000	0.000	0.000
MnO	0.013	0.001	0.000	0.000	0.000	0.000	0.000	0.000	0.000	0.000
FeO	0.38	0.01	0.004	0.000	0.002	0.000	0.003	0.002	0.001	0.000
NiO	1.12	0.02	0.071	0.005	1.255	0.008	0.144	0.001	0.005	0.000
Expt. ID	1-(SP1+CaF ₂)		1-(SP1+MgF ₂)		1-(SP2+Qtz)					
Na ₂ O										
MgO	0.277	0.007	0.007	0.000	0.014	0.000				
Al ₂ O ₃	0.61	0.10	0.058	0.001	0.048	0.001				
SiO ₂										
K ₂ O	0.867	0.007	0.195	0.007	0.023	0.000				
CaO	4.89	0.04	0.072	0.003	0.015	0.000				
TiO ₂	0.012	0.001	0.002	0.000	0.000	0.000				
Cr ₂ O ₃	0.004	0.002	0.001	0.001	0.000	0.000				
MnO	0.006	0.001	0.001	0.000	0.000	0.000				
FeO	0.048	0.003	0.017	0.004	0.017	0.000				
NiO	1.38	0.03	0.072	0.003	0.128	0.001				

These data are calculated from original data multiplying the dilute factors of retrieving fluid process and ICP-MS sample preparation procedure, and then transform elements masses from cation to oxides formation, and their units from ppb to wt %.

Table 3.4.2.3d ICP-MS analyses for the samples with dilution (July 19, 2012). Under each Expt. ID, the first column is the composition and the second is its absolute uncertainties (unit: wt%).

Expt. ID	1-SP2-16		1-SP2-19		1-SP2-20		1-SP2-21		1-SP2-23	
Na ₂ O	0.53	0.01	0.97	0.04	4.17	0.04	4.44	0.12	8.59	0.10
MgO	0.016	0.000	0.030	0.002	0.096	0.009	0.12	0.02	0.31	0.21
Al ₂ O ₃	0.140	0.003	0.24	0.02	0.37	0.01	0.49	0.01	0.14	0.04
SiO ₂	2.04	0.05	2.21	0.19	1.94	0.41	5.85	0.15	7.86	0.88
K ₂ O	0.31	0.01	0.31	0.05	0.96	0.02	0.28	0.03	0.78	0.03
CaO	0.121	0.007	0.11	0.02	0.373	0.006	0.272	0.007	0.26	0.11
TiO ₂	0.001	0.001	0.001	0.000	0.003	0.001	0.010	0.001	0.010	0.005
Cr ₂ O ₃	0.000	0.000	0.001	0.000	0.001	0.000	0.004	0.004	0.02	0.01
MnO	0.000	0.000	0.001	0.000	0.001	0.000	0.002	0.000	0.003	0.002
FeO	0.005	0.000	0.069	0.005	0.095	0.003	0.162	0.003	0.10	0.09
NiO	0.002	0.000	0.012	0.001	0.008	0.001	0.002	0.000	0.14	0.06
Expt. ID	1-SP2-24		1-SP3-8		4-SP2-2		1-SP4-3		1-SP4-4	
Na ₂ O	5.08	0.08	0.537	0.007	0.735	0.008	1.56	0.02	0.85	0.02
MgO	1.11	0.46	0.049	0.001	0.227	0.001	0.029	0.000	0.026	0.000
Al ₂ O ₃	0.64	0.10	0.015	0.003	0.015	0.000	0.031	0.001	0.009	0.000
SiO ₂	6.67	0.54	0.38	0.07	0.70	0.04	0.352	0.009	2.325	0.009
K ₂ O	0.48	0.04	0.116	0.006	0.120	0.007	0.124	0.003	0.17	0.02
CaO	0.61	0.03	0.036	0.002	0.046	0.002	0.038	0.003	0.028	0.008
TiO ₂	0.025	0.001	0.000	0.000	0.000	0.000	0.000	0.000	0.000	0.000
Cr ₂ O ₃	0.05	0.02	0.000	0.000	0.000	0.000	0.000	0.000	0.000	0.000
MnO	0.020	0.002	0.000	0.000	0.000	0.000	0.000	0.000	0.000	0.000
FeO	0.43	0.06	0.005	0.002	0.001	0.000	0.002	0.000	0.002	0.000
NiO	13.45	0.08	0.107	0.000	0.943	0.006	0.062	0.000	0.328	0.003
Expt. ID	1-(SP1+CaF ₂)		1-(SP1+MgF ₂)		1-(SP2+Qtz)					
Na ₂ O	3.35	0.07	3.49	0.03	0.211	0.003				
MgO	0.25	0.01	0.003	0.000	0.011	0.001				
Al ₂ O ₃	0.513	0.003	0.036	0.002	0.039	0.000				
SiO ₂	1.86	0.06	3.45	0.05	0.27	0.05				
K ₂ O	1.04	0.02	0.35	0.01	0.035	0.001				
CaO	4.45	0.02	0.066	0.007	0.013	0.001				
TiO ₂	0.011	0.001	0.001	0.000	0.000	0.000				
Cr ₂ O ₃	0.001	0.000	0.000	0.000	0.000	0.000				
MnO	0.007	0.000	0.000	0.000	0.000	0.000				
FeO	0.062	0.005	0.010	0.001	0.015	0.000				
NiO	1.595	0.002	0.019	0.001	0.079	0.004				

The ICP-MS measurements for the undiluted samples do not report Na₂O and SiO₂ concentrations, because their concentrations are too high for the same analytical setting. While the measurements for the diluted samples report all other major elements

concentrations. It should be noted that Na₂O and SiO₂ concentrations are indeed the highest level for most of the samples. The second level concentrations are MgO, CaO, K₂O and Al₂O₃. Their oxides concentrations are quite depended on the starting materials, and differ much from experiment to experiment.

Comparing their relative oxides concentrations, most of them are consistent. Although some of them differ much, the values are within the same magnitude order, except NiO concentration of 1-SP2-24. Its diluted fluid has 10 times more Ni than undiluted test. One possibility is that NiO layer chip was mixed in the fluid sample. Although I polished the outer surface of the capsule, the NiO layer between inner capsule and outer chamber cannot be cleaned. Thus, the chips may derive from this part. However, the ICP-MS operator considers the uncertainties are higher than normal analysis with some unknown reason. In consequence, the results from the analyses on July 19, 2012 will be employed in the discussion versus mass balance results.

3.5 Partition Coefficients of F and X_F

The partition coefficient of F (D_F) is a ratio of F concentration between two phases. It is defined as: $D_F^{i/j} = [F]^i/[F]^j$, where $[F]^i$ is F concentration in phase i (unit: wt%, and hereinafter). D_F describes the distribution of F between the two phases i and j .

In hydrous minerals, F generally substitutes into the OH site. Define $X_F^i = \frac{n_F}{n_F+n_{OH}}$, which describes the competitive ability between F and OH for the hydroxyl site in phase i . The hydroxyl site partition coefficient of X_F , $D_{X_F}^{i/j} = X_F^i/X_F^j$ (3.5), reflects the ease of F incorporation in phase i over phase j .

3.5.1 F Partitioning of Minerals

In F-bearing experiments, hornblende and humite group minerals are created. Their compositions are measured with electron microprobe, so the uncertainties are smaller than that of F concentration in fluid. Although some anhydrous minerals were created in my

experiments, e.g., spinel, olivine, and augite, their F concentrations are lower than the detection limit of electron microprobe. Comparing with hydrous minerals, they are not main F carriers, so D_F between anhydrous minerals and hydrous minerals are close to 0. Some experiments did not create hornblende, but hydrogrossular (SP2 experiments under 2.5 or 3.0 GPa) or mica (1-SP4-3 experiment). However, these results are small proportion in my experiments, and I will describe them in another section.

3.5.1.1 D_F between Hornblende and Humite Group Minerals

All the experiments, which contain hornblende and humite group minerals, are listed in Table 3.5.1.1, as well as the failed experiment results. Their results are also consistent with the successful ones. In section 3.1, the texture details of all the experiments are introduced. For example, 1-SP2-7, as a failed experiment, contains hornblende and norbergite. Their abnormal texture and higher F concentration indicates that it is not a comparable experiment with others. A similar situation happened to 2-SP2-3, and its assemblies are totally different from 2-SP2-1 & 2. Thus, its information is not in the result table.

Some experiments lost their water during the experiments, and no obvious fluid was observed at the moment of the capsule piercing. In several latest experiments, I performed the post-quench procedure for all of them, and verified the presence of fluid by mass differences for a few of them. It should be noted that experiments 1-SP2-5, 6, 7, 10 & 22 are failed. After the water in the capsule was exhausted, the hydrous minerals probably become unstable. Some elements (especially F) may become slightly enriched in the minerals. Comparing minerals compositions and species of 1-SP2-5, 7 & 10 with those in successful ones, a higher F abundance is present in their hornblendes. It indicates that hornblendes may be partially dehydrated during anneal or the lower water activity decreased the OH incorporation in minerals. In experiment 1-SP1-2, its products olivine and pyroxene were formed because of nickel contamination. The experiment 1-SP2-2 exhausted water and created melt and pyroxene at 1120 °C, which is too hot for the existence of hornblende. Water loss and nickel contamination improves hornblende breakdown. However, the process of the water loss during the experiment is unknown, so these failed experiments will not be discussed.

3. Results

In 1-SP4-1 & 2 capsules, I did not find fluid left after quench. While comparing with 1-SP4-4, $D_F^{Hb/Chu}$ and X_F^{Hb} are similar, but X_F^{Chu} is slightly smaller. It is necessary to conduct more SP4 experiments, for conforming this difference is happened by chance or not.

Table 3.5.1.1 D_F and X_F between hornblende and humite minerals

Expt. ID	T/ °C	10000/T (1/K)	D_F			X_F			$D(X_F)$			
			Hb/Nb	Hb/Chd	Hb/Chu	Hb	Nb	Chd	Chu	Hb/Nb	Hb/Chd	Hb/Chu
1-SP2-1	770	9.59	0.13(1)			0.52(4)	1.01(9)			0.51(6)		
1-SP2-4	870	8.75	0.12(1)			0.49(3)	0.96(2)			0.51(3)		
1-SP2-5 ^a	955	8.14		0.29(3)		0.55(3)		0.79(3)			0.69(5)	
1-SP2-6 ^a	900	8.52		0.25(3)		0.49(5)		0.85(2)			0.58(6)	
1-SP2-7 ^a	930	8.31	0.17(1)			0.75(6)	1.07(4)			0.70(6)		
1-SP2-8	827	9.09	0.12(1)			0.48(3)	0.97(2)			0.49(3)		
1-SP2-10 ^a	787	9.43	0.15(2)			0.56(4)	0.93(1)			0.60(4)		
1-SP2-12	777	9.52	0.12(1)			0.50(3)	1.03(7)			0.49(4)		
1-SP2-13	877	8.69	0.15(1)			0.54(6)	0.87(4)			0.62(4)		
1-SP2-14	877	8.69	0.14(2)	0.25(3)		0.48(6)	0.81(3)	0.77(3)		0.59(3)	0.62(3)	
1-SP2-15	907	8.47	0.15(2)			0.50(6)	0.80(3)			0.63(3)		
1-SP2-16	927	8.33	0.15(2)			0.51(6)	0.79(3)			0.65(8)		
1-SP2-17	917	8.40	0.13(2)			0.48(6)	0.85(3)			0.57(7)		
1-SP2-18	947	8.20	0.14(2)			0.51(7)	0.83(4)			0.61(9)		
1-SP2-19	977	8.00		0.26(2)		0.46(4)		0.73(3)			0.63(6)	
1-SP2-20	1007	7.81		0.27(3)		0.44(5)		0.68(4)			0.65(8)	
1-SP2-22 ^a	850	8.90	0.13(2)			0.55(8)	1.02(6)			0.54(8)		
1-SP2-23	800	9.32	0.13(2)			0.52(8)	0.99(6)			0.53(9)		
2-SP2-1	877	8.69	0.12(2)			0.39(5)	0.78(3)			0.50(7)		
2-SP2-2	857	8.85	0.11(1)			0.42(3)	0.92(2)			0.46(3)		
3-SP2-1	877	8.69	0.12(2)			0.36(5)	0.75(3)			0.48(7)		
1-SP3-2	857	8.85		0.19(3)		0.29(5)		0.62(4)			0.47(9)	
1-SP3-3	857	8.85		0.20(3)		0.33(5)		0.69(4)			0.48(8)	
1-SP3-4	837	9.01		0.19(3)		0.32(5)		0.69(4)			0.46(8)	
1-SP3-5	887	8.62		0.19(3)		0.29(5)		0.62(4)			0.47(9)	
1-SP3-6	897	8.55		0.21(4)		0.32(5)		0.62(4)			0.52(9)	
1-SP3-8	957	8.13		0.22(3)		0.33(4)		0.60(3)			0.55(7)	
1-SP4-1	877	8.69			0.25(5)	0.12(2)			0.34(2)			0.34(6)
1-SP4-2	857	8.85			0.26(5)	0.12(2)			0.36(3)			0.33(6)
1-SP4-3 ^b	890	8.60			0.25(7)	0.07(2)			0.39(4)			0.18(5)
1-SP4-4	843	8.96			0.25(7)	0.13(3)			0.39(4)			0.33(8)

Hb: hornblende. Nb: norbergite. Chd: chondrodite. Chu: clinohumite. And hereinafter.

^a experiments without fluid left are obviously different from others, and are excluded from discussion section.

^b hornblende is replaced by clintonite.

D_F between hornblende and humite group minerals are constant over the temperature range. $D_F^{Hb/Nb}$ is from 0.12 to 0.15, and its standard deviation is 0.02. $D_F^{Hb/Chd}$ is approximately 0.27 in SP2 experiments or 0.19 in SP3 experiments, and their standard deviation is 0.03.

With the NNO buffer, $D_{X_F}^{Hb/Nb}$ ranges from 0.49 to 0.51, and $D_{X_F}^{Hb/Chd}$ ranges from 0.46 to 0.55, and $D_{X_F}^{Hb/Chu}$ is approximately 0.33. Without the NNO buffer, $D_{X_F}^{Hb/Nb}$ ranges from 0.57 to 0.65. It is concluded that humite group minerals can incorporate the fluorine anion more effectively than hornblende. Different buffer conditions result in different $D_{X_F}^{Hb/Nb}$ values. It is easy to notice that under 1 GPa X_F^{Hb} is almost constant, while X_F^{Nb} decreases from approximately 1 (NNO buffer) to 0.8 (unbuffered). It leads to $D_{X_F}^{Hb/Nb}$ increases.

3.5.1.2 D_F between Hydrogrossular and Humite Group Minerals

SP2 experiments at 2.5 and 3.0 GPa create hydrogrossular, augite and norbergite / chondrodite. The F concentrations of hydrogrossular and norbergite or chondrodite are higher than augite. However, the OH number of hydrogrossular formula is uncertain, which is depended on Si number replaced by H_2O . It is possible that the hydroxyl numbers, even the composition of each hydrogrossular mineral in the same experiment is different. That is why the uncertainties of some elements are quite large. On the other hand, most of the hydrogrossular crystals are empty spheres. The cross-section area of crystal is normally just large enough for electron microprobe analysis, so its uncertainties are larger than humite group minerals.

Table 3.5.1.2 D_F and X_F between hydrogrossular and humite minerals

Expt. ID	T/ °C	10000/T (1/K)	D_F		X_F			$D(X_F)$	
			Hdg/Nb	Hdg/Chd	Hdg	Nb	Chd	Hdg/Nb	Hdg/Chd
4-SP2-1	877	9.59		0.21(3)	0.46(7)			0.74(6)	0.51(6)
4-SP2-2	877	8.75	0.09(4)	0.15(7)	0.48(13)	0.72(4)	0.73(6)	0.51(3)	
5-SP2-1	877	8.14	0.11(2)		0.39(6)	0.76(3)			0.69(5)

F concentration of hydrogrossular is lower than that of hornblende at 1 GPa experiments and 877 °C, and so is F concentration of norbergite or chondrodite. X_F of norbergite decreases from 1 to 0.75 approximately. Although X_F of hydrogrossular does not decrease as much as norbergite does, the hydroxyl site in hydrogrossular is less than norbergite or chondrodite. Consequently, $D_F^{Hdg/Nb}$ and $D_F^{Hdg/Chd}$ decrease as the pressure increases. Since F concentrations in minerals decrease, fluid should contain more F.

3.5.2 D_F Between Fluid and Hydrous Minerals or Melt

Since I assume the total mass of oxides in precipitated quench phases is negligible, and was dissolved into fluid part during high-pressure temperature experiments, the composition of the fluid is calculated by mass balance. The F concentration of fluid is also determined by HPLC, and corresponding D_F values are shown in Table 3.5.2. Because some F concentrations of calculated fluid compositions are zero, it is convenient to express the partition coefficient of F as fluid over minerals.

In mass balance block (Table 3.5.2), the error propagations from mass weighing and mineral or fluid compositions lead to large errors, so D_F between fluid and crystalline phases fluctuates more than D_F between minerals. For example, D_F between fluid and hornblende at 1 GPa varies from 0.05 to 0.35 (exclude 1-SP2-14 result), and its error from 0.08 to 1.30, while D_F between hornblende and norbergite is 0.13 ± 0.02 . Furthermore, since F concentrations in humite group minerals are higher than in hornblendes, D_F between fluid and hornblende is higher than that between fluid and a humite group mineral.

An exception experiment 1-SP2-14 created hornblende, norbergite and chondrodite. As I described in the Section 3.1.2.1, the reason for this mineral assemblage is probably a gradual loss of fluid during annealing. Comparing the composition of hornblende and norbergite with other experiments, which are conducted without the NNO buffer, 1-SP2-14 also reached equilibrium. However, in my experiments lower F concentration in the bulk composition changes norbergite (SP2) into chondrodite (SP3). In experiment 1-SP2-14, most of the humite group minerals are chondrodite. It suggests that obvious F loss occurred during the experiment. Assuming F diffusion across Au capsule is negligibly slow, I speculate the

presence of micro fissures in the gold inner capsule, which allows fluid leakage before the inner capsule was sealed completely. In conclusion, the fluid composition of 1-SP2-14 by mass balance is unreliable. This exception is excluded from the discussion, as its mass balance result, which determined higher F concentration in fluid, is inconsistent with other experiments. F concentration from HPLC analysis for this experiment is more reliable than mass balance.

Table 3.5.2 D_F between fluid (mass balance and HPLC) and minerals or melt

Expt. ID	T/ °C	Mass Balance					HPLC				
		Fl/Hb	Fl/Nb	Fl/Chd	Fl/Chu	Fl/Melt	Fl/Hb	Fl/Nb	Fl/Chd	Fl/Chu	Fl/Melt
1-SP2-1	770	0.10(27)	0.013(34)								
1-SP2-4	870	0.05(13)	0.006(15)								
1-SP2-8	827	0.11(13)	0.013(16)								
1-SP2-12	777	0.05(33)	0.006(39)								
1-SP2-14	877	1.09(36)	0.149(46)	0.25(8)			0.040(5)	0.005	0.009		
1-SP2-15	907	0.29(17)	0.043(25)				0.026(3)	0.004			
1-SP2-16	927	0.11(8)	0.017(11)				0.114(14)	0.017(1)			
1-SP2-17	917	0.13(8)	0.017(10)				0.093(12)	0.012			
1-SP2-18	947	0.32(25)	0.046(36)				0.251(37)	0.036(2)			
1-SP2-19	977	0.23(12)		0.06(3)		0.08(5)	0.121(10)		0.031(1)		0.044(7)
1-SP2-20	1007	0.35(1.30)		0.10(35)		0.11(41)	0.166(18)		0.045(2)		0.053(12)
1-SP2-23	800	0.06(97)	0.008(126)				0.416(64)	0.054(3)			
3-SP2-1	877	1.03(27)	0.119(27)				0.227(34)	0.026(1)			
4-SP2-2	877		0.082(29)	0.14(5)				0.004	0.007(1)		
1-SP3-1	877	0.18(19)		0.03(3)			0.054(9)		0.010(1)		
1-SP3-3	857	0.27(61)		0.05(12)			0.071(11)		0.014(1)		
1-SP3-4	837	0.10(15)		0.02(3)			0.056(9)		0.011(1)		
1-SP3-8	957	0.12(11)		0.03(2)			0.020(3)		0.004		
1-SP4-3	890				0.00(17)					0.007(1)	
1-SP4-4	843	0.00(70)			0.00(18)		0.011(3)		0.003		
1-(SP2+Qtz)	950	0.00(31)				0.00(33)	0.066(11)				0.072(18)
1-(SP1+MgF ₂)	965			0.00(86)		0.00(87)			0.011(1)		0.011(3)

Fl indicates “fluid”.

From mass balance calculation, experiment 3-SP2-1 (2 GPa) contains higher F than those at 1 GPa. Because the F concentration of its hornblende and norbergite decrease and no other F-bearing phase was found, it leads to high F in fluid. However, it is hard to give a partition coefficient as a conclusion without more parallel experiments for comparison. Ayers et al. (1997) conducted experiments at 2-3 GPa between peridotites and water, and significant

quenched solute was collected after experiments. It is reasonable for 3-SP2-1 experiment to contain quench phase, which is not dissolved into deionized water in the post-quench procedure, and cause significant different D_F between HPLC and mass balance approach.

I used a chondrodite composition from 1-SP3-3 to calculate mass balance to obtain the fluid composition of 1-SP3-1. The results of comparisons (with or without chondrodite) are shown in Table 3.4.1.1.1d. In the following section, I will use the result of hornblende-chondrodite-fluid assemblies along with other successful runs for a discussion.

In SP4 and melt-bearing experiments, F concentrations of their fluids are zero from mass balance calculation, so their D_F between fluid and minerals or melt are 0 with big errors. It indicates mass balance is beyond its suitable region, and this should correlate with its phase assembly.

To avoid the large error from mass balance calculations and some infeasible cases, direct analyses of F in the fluid were performed. Fluorine is difficult to precipitate without Mg^{2+} or Ca^{2+} in the fluid at room temperature. Assuming F^- is the only fluorine species, the direct measurement of F by HPLC is a potentially viable method. For example, in 1-SP2-16 or 1-SP2-17 experiments, there is approximately 2.7 mg fluid left after quenching. These experimental samples have the highest fluid quantities and the least fluid composition uncertainties of all the experiments by mass balance. Their fluids were diluted approximately 3700 times when we retrieved them into 10 mL volumetric flasks. The results show that $D_F^{Fl/Hb}$ of 1-SP2-16 (0.114 ± 0.014 from HPLC and 0.11 ± 0.08 from MB) and 1-SP2-17 (0.093 ± 0.012 from HPLC and 0.13 ± 0.08 from MB) by these two methods are consistent (Table 3.5.2).

Comparing D_F values between mass balance and HPLC blocks, most values of SP2 and SP3 experiments in HPLC block are smaller than mass balance, and are plotted in the uncertainties of calculated results. However, there are also some exceptions, e.g. 1-SP2-15, its D_F from HPLC is smaller than its lower limit of uncertainty from mass balance; and 1-SP2-23, its D_F from HPLC is much higher than its mass balance result. The reasons of these inconsistencies are probably derived from the limitation of each method. In consequence, $D_F^{Fl/Hb}$ ranges from 0.011 to 0.416, and $D_F^{Fl/Nb}$, $D_F^{Fl/Chd}$, or $D_F^{Fl/Chu}$ are even smaller. In any case, this demonstrates that fluorine is easier to be incorporated by hydrous minerals than

fluid.

HPLC results give some useful information for SP4 and melt-bearing experiments about $D_F^{Fl/Hb}$, $D_F^{Fl/Chu}$, and $D_F^{Fl/Melt}$. Their values are smaller than 0.1, and comparable to partial corresponding values from SP2 and SP3 experiments. $D_F^{Fl/Melt}$ is close to $D_F^{Fl/Chd}$, because F concentration of melt is close to F concentration of chondrodite.

3.5.3 D_F Between Hornblende and Hydrous Melt

The partition coefficients of F between hornblende and melt reflect the ability of incorporating F between these two phases. The presence of melt phase is not designed for the experimental aim, but by chance, so there is only five $D_F^{Hb/Fl}$ in Table 3.5.3.

Table 3.5.3 D_F between hornblende and melt

Expt. ID	T/ °C	$D_F^{Hb/Fl}$
1-SP2-18	947	0.39(8)
1-SP2-19	977	0.37(6)
1-SP2-20	1007	0.32(8)
1-SP2-20b	1007	2.30(1.08)
1-(SP2+Qtz)	850	1.09(32)

The first three D_F values are averagely 0.36, while the last two are higher than 1. The hornblende compositions are similar with each other, so it indicates that the D_F difference between these two blocks is derived from the melt composition discrepancy. However, due to the degassed and exsolved process during the quench, the quenched melt compositions are different from the actual during anneal. Easy dissolved elements, water, sodium and fluorine should have higher concentration than the analyzed results.

4. Discussion

The main aim of my thesis is to determine the partition coefficient of F among aqueous fluid, minerals and hydrous melt at amphibolite facies in the subduction zone. Meanwhile, some interesting observations, which are worth for further studies, are present in the results. In the first part, fluorine incorporation of hydrous minerals will be presented. The fluid compositions and their relationship with pressure, temperature and F concentrations will be discussed in the second part. In the third subsection, the partition coefficient of F between fluid, minerals and/or melt will be shown. With these data, I manage to calculate F budget transported into subarc mantle by aqueous fluid in subduction zone.

4.1 F Incorporation of Hydrous Minerals

SP1 experiments do not create humite group minerals. After doping MgF_2 into the starting powders, norbergite or chondrodite are present in SP2 or SP3 experiments. Fluorine promotes precipitation of humite group minerals, and different F concentrations create different humite species minerals.

In the experiments with large quantity of water, hydrous minerals are more abundant than anhydrous minerals. Generally, F takes up proportion of the OH site in the hydrous minerals, significantly deviating from molar abundance of F in fluid. The proportions of F in the OH site in hydrous minerals provide an insight to F behavior.

4.1.1 Proportion of F in OH sites (X_F)

In hydrous minerals there are fixed specific sites for OH, while OH in the anhydrous minerals can only exist in vacancies and lattice defects. Moreover, F takes place of OH in OH sites, and X_F represents its proportion in this site (see Section 3.5 Partition Coefficients of F and X_F). In consequence, the proportion of F in OH sites is an interesting parameter for

studying F behavior in precipitating minerals.

4.1.1.1 X_F of Hornblende

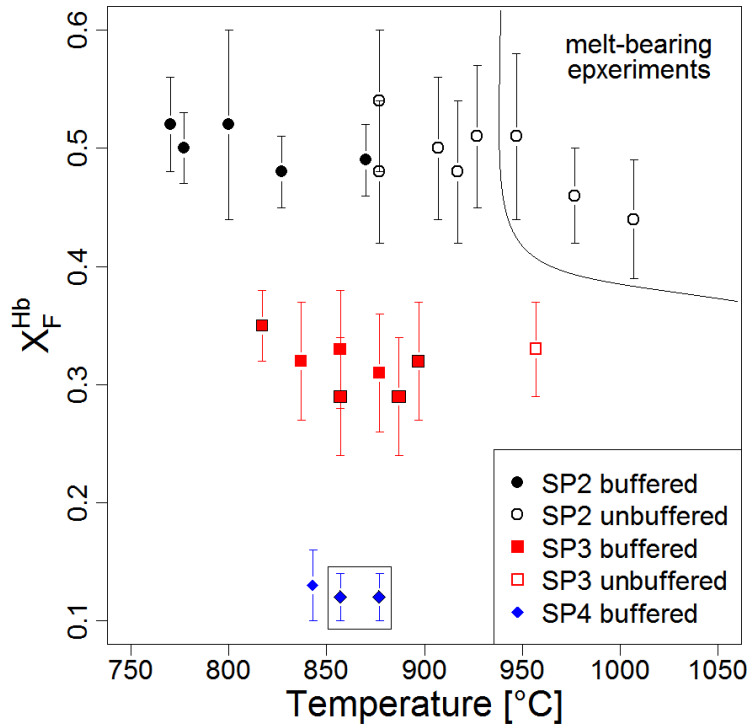


Fig. 4.1.1.1 X_F of hornblende from SP2, SP3 and SP4 experiments. Solid symbols indicate experiments with NNO buffer. Open symbols mean unbuffered ones. With a decrease of F concentration in starting material, X_F in Hb decrease. The black curve separates the three melt-bearing experiments from other melt-free experiments. SP2 data only contain successful results. The symbols for SP3 and SP4 failed experiments are plotted in black frames.

As Fig. 4.1.1.1 shown, each series experiments create hornblendes with different F concentrations. Each group of hornblende has similar X_F value. Up to 950 °C, the X_F value of each group is constant within the uncertainties. With a decrease of F concentration in starting powders (from SP2 to SP4), X_F values of hornblendes decrease.

Some of SP2 experiments are conducted without NNO buffer, but their X_F are almost the same with those conducted with NNO buffer until 950 °C. However, X_F of hornblende at 977 and 1007 °C are 0.46 and 0.44, respectively, and they are slightly lower than other unbuffered experiments. Because of high temperature, the melt is present in these experiments. It indicates that different buffer conditions do not change the X_F values of hornblende in SP2 experiments. The presence of melt decreases the F proportion of OH sites in hornblende. This relates with the melt composition, which has more F than hornblende and fluid.

4.1.1.2 X_F of Humite Group Minerals

4.1.1.2.1 X_F Comparison among Humite Group Minerals

In the chemical formulas of hornblende and humite group minerals, both of them contain 2OH. X_F values of humite group minerals are higher than those of hornblendes. Especially in SP2 experiments with NNO buffer, X_F of norbergite even reach 1. Furthermore, among the experiments conducted with NNO buffer of the same series, X_F values are relatively constant within their uncertainties. However, unbuffered SP2 experiments from 877 to 1057 °C reveal that their X_F are significantly lower than those in NNO buffered ones. Apparently, the oxygen fugacity affects X_F in norbergite, and they are plotted approximately 0.8 (Fig. 4.1.1.2.1).

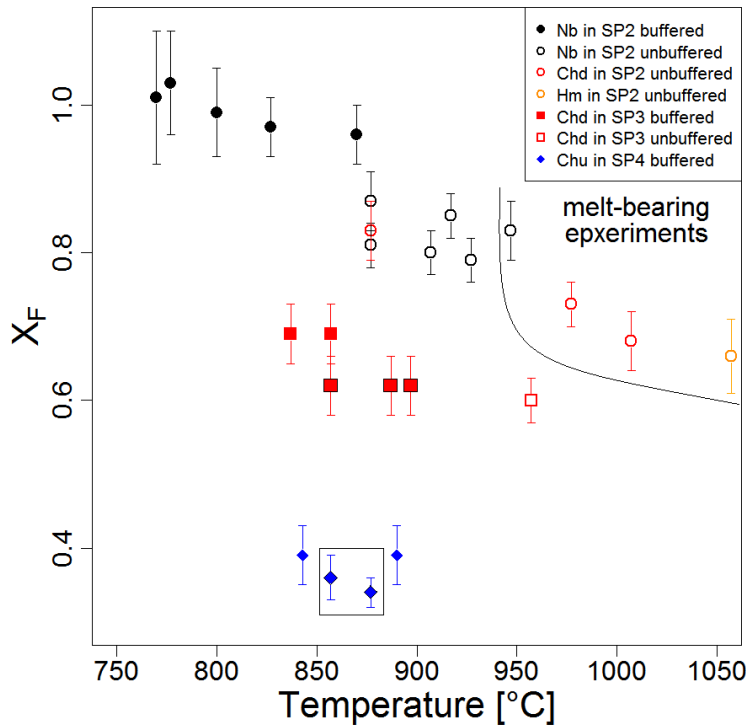


Fig. 4.1.1.2.1 X_F of humite group minerals from SP2 (round), SP3 (square) and SP4 (diamond) experiments. Nb, Chd, Hm and Chu indicate norbergite (black), chondrodite (red), humite (orange) and clinohumite (blue), respectively. Solid symbols mean experiments with NNO buffer. Open symbols mean those without buffer. The black curve separates the four melt-bearing experiments from other melt-free experiments. SP2 data only contain successful results. The symbols for SP3 and SP4 failed experiments are plotted in black frames.

Since the melt is present in the experiments, humite minerals species transform from norbergite to chondrodite, then humite. The X_F decreases from 0.83 to 0.66 with an increase of temperature and the melt proportion in the capsules. The melt contains more F than fluid and hornblende, which lead to F concentrations and X_F of minerals decrease. Moreover, Fig. 4.1.1.2.1 suggests that X_F decreases with temperature increasing. Because water fugacity coefficient increases with temperature, the water content or X_{OH} increases.

The NNO buffered SP3 group experiments illustrates that X_F values are apparently divided as two values: 0.62 and 0.69, of which discrepancy correlate with the presence of the fluid after quench. This observation showed an abnormal tendency that the absence of water after quench resulted in a lower X_F value, i.e., higher OH content in chondrodite. This indicated that the OH concentration is not proportional with water activity. Moreover, the oxygen fugacity of my experiments is controlled by the hydrogen equilibrium, so the water quantity not only contributes to the water fugacity during anneal, but also controlled the oxygen fugacity. Both of them contribute to the OH activity. Furthermore, three SP2 unbuffered experiments in Ti capsules (black open round symbols) have lower X_F values than three others (Table 3.5.1.1, 1-SP2-13 – 18). X_F values of norbergite decrease with temperature increasing, if I separate these black open round points into 2 groups with capsule materials.

4.1.1.2.2 Corrected X_F with TiO_2 Number by Stoichiometry

The unbuffered SP2 norbergite of Ti capsules have obviously higher TiO_2 concentration than the other three points from AuPd or Mo capsules (Table 3.3.2.2a), which indicates Ti capsule may also contaminate the sample slightly. Generally the TiO_2 concentrations of humite group minerals are lower than 1 wt%. Using stoichiometry calculation, the number of Ti in each chemical formula is less than 0.06 (Table 4.1.1.2.2). TiO_2 was ignored for the approximate calculations. Actually, the humite group comprises a polysomatic series of minerals with the general formula $nMg_2SiO_4 \cdot Mg_{1-x}Ti_x(OH,F)_{2-2x}O_{2x}$. If TiO_2 concentration of the minerals cannot be ignored, it will influence the number of OH site. And maybe X_F values will increase slightly.

In unbuffered SP2 experiments, SP3 and SP4 experiments, their Ti number in the chemical formula is close for each group. The Ti number of norbergite in SP2 experiments ranges from 0.02 to 0.04, and that of chondrodite in SP3 experiments are from 0.04 to 0.06. The comparisons of X_F before and after the correction by Ti number show no obvious changes within the uncertainties (Table 4.1.1.2.2). For example, the X_F values of 1-SP3-3 & 4 experiments are 0.07 higher than other SP3 results. After this correction, the differences remain the same. In consequence, TiO_2 concentrations in humite group minerals in these

experiments are not a key reason for the X_F differences.

Table 4.1.1.2.2 Corrected X_F with Ti Number of some SP2, SP3 and SP4 experiments

Expt. ID	T/ °C	Nb	Ti No.	Corrected X_F	Chd	Ti No.	Corrected X_F	Chu	Ti No.	Corrected X_F
1-SP2-13	877	0.87	0.02	0.89						
1-SP2-14	877	0.81	0.02	0.83	0.77	0.02	0.79			
1-SP2-15	907	0.80	0.04	0.84						
1-SP2-16	927	0.79	0.03	0.81						
1-SP2-17	917	0.85	0.02	0.86						
1-SP2-18	947	0.83	0.02	0.85						
1-SP2-19	977				0.73	0.02	0.74			
1-SP2-20	1007				0.68	0.02	0.69			
2-SP2-1	877	0.78	0.02	0.80						
2-SP2-2	857	0.92	0.02	0.94						
3-SP2-1	877	0.75	0.03	0.77						
4-SP2-1	877				0.74	0.03	0.76			
4-SP2-2	877	0.72	0.03	0.74	0.73	0.02	0.74			
5-SP2-1	877	0.76	0.03	0.78						
1-SP3-2	857				0.62	0.05	0.65			
1-SP3-3	857				0.69	0.05	0.73			
1-SP3-4	837				0.69	0.04	0.72			
1-SP3-5	887				0.62	0.06	0.66			
1-SP3-6	897				0.62	0.05	0.65			
1-SP3-8	957				0.60	0.06	0.64			
1-SP4-1	877							0.34	0.05	0.36
1-SP4-2	857							0.36	0.06	0.38
1-SP4-3	890							0.39	0.06	0.41
1-SP4-4	843							0.39	0.06	0.41

4.1.1.3 X_F at Higher Pressure (>1 GPa)

SP2 experiments from 1.5 to 3.0 GPa are conducted at 877 °C. In order to compare with the experiment at 1 GPa, I plot the data from 1-SP2-4 at 870 °C in Fig. 4.1.1.3. Before hornblende breakdown (the pressure is lower than 2.5 GPa), the X_F of hornblende and norbergite decrease with an increasing of pressure. Two X_F values of norbergite at 1.5 GPa differ significantly. Both of these two experiments do not have obvious fluid left, which indicates the fluid loss during anneal. However, the ratios of X_F between hornblende and norbergite are nearly constant with the pressure increase within their uncertainties. It argues that the loss of the bulk starting material do not change the F behaviors between these two

minerals. Moreover, the water exhaustion does not influence mineral compositions. I conclude that 2-SP2-2 experiment, of which minerals has more X_F , suffered less material loss during anneal. Overall, X_F of hornblende and norbergite in SP2 experiments decrease with an increase of pressure until the phase assemblies (hornblende, norbergite and fluid) change. In detail, X_F of hornblende linearly decreases versus the pressure, while that of norbergite decreases along a curve. From 1.5 to 2.0 GPa, its value decreases more than from 1.0 to 1.5 GPa. This indicates that hornblende and norbergite have different response to the compositional changes of fluid with an increase of pressure.

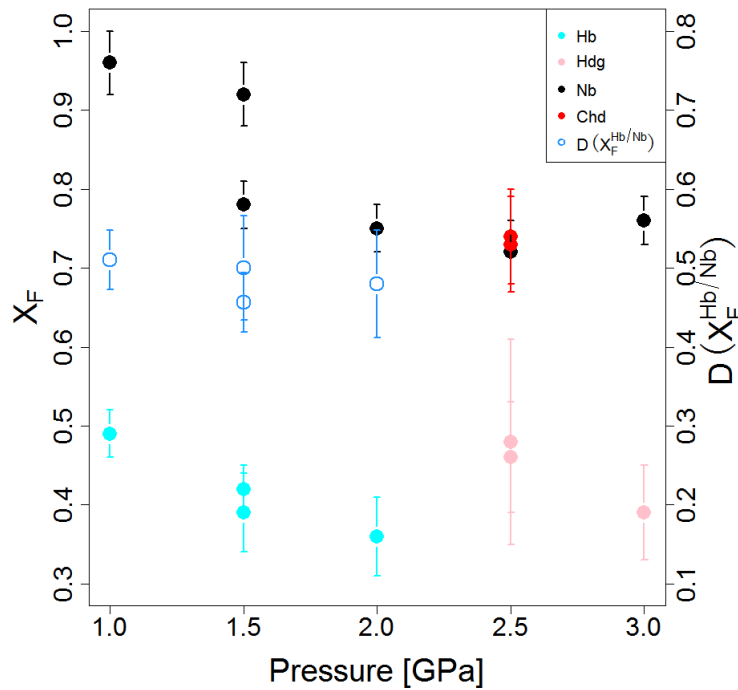


Fig. 4.1.1.3 X_F values of hornblende (cyan), hydrogrossular (pink), norbergite (black) and chondrodite (red) from SP2 experiments at 877 °C, from 1 to 3 GPa. They are solid symbols. The open light blue round symbols are X_F ratio of Hb vs. Nb. The relative label is on the right side of the image.

4.1.2 Parameters Controlling F Incorporation

The ability of F to be incorporated into different minerals is given by D_{X_F} (defined by Eq. 3.5), where $D_{X_F}^{Hb/Nb} = 0.49\sim 0.51$, and $D_{X_F}^{Hb/Nb} = 0.57\sim 0.65$ for the successful experiments with or without NNO buffer, respectively. $D_{X_F}^{Hb/Nb}$ increases, because X_F^{Nb} decreases from almost 1 to 0.8, while $X_F^{Hb} = 0.48\sim 0.54$ is relatively constant in coexistence with norbergite. In contrast, $D_{X_F}^{Hb/Chd}$ (0.45~0.48) decreases with a decrease of F

concentration in the starting powder (Table 3.5.1.1). Because of smaller $X_F^{Chd} = 0.69$ and $X_F^{Hb} = 0.31\sim 0.33$ compared to the norbergite-bearing system, $D_{X_F}^{Hb/Chd}$ is only slightly smaller than $D_{X_F}^{Hb/Nb}$. $D_{X_F}^{Hb/Chu}$ from SP4 experiments is obviously smaller than those from SP2 and SP3 experiments.

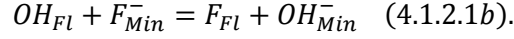
It is obvious to conclude that X_F of hornblende decreases with a decrease of F concentration of starting material. However, the water-free experiments do not create hydrous minerals, which states that water plays an important role in the process of hornblende and humite group minerals precipitate. The aqueous fluid supply OH in the system. OH and F will compete for the OH site of the minerals. Furthermore, Fig. 4.1.1.3 shows that an increase of pressure can decrease X_F significantly at the same temperature. Meanwhile, X_F of norbergite decreases if temperature increases at 1 GPa. Both of them indicate that pressure affect X_F value more efficient than temperature. It is easy to understand P, T, and F concentration effects on F incorporation, so I will discuss the influence from oxygen fugacity in this section.

4.1.2.1 Oxygen Fugacity Effects on F Incorporation

In SP2 norbergite-bearing experiments, the change of F occupancy in the hydroxyl sites depends only on oxygen fugacity changes. Furthermore, this change is due to F in norbergite, because there is no significant change in X_F^{Hb} . Given that the activity of F in solution is unlikely to depend on oxygen fugacity, the activity of OH species must vary with oxygen fugacity. The oxygen fugacity changes the activity of OH in the fluid by the reaction: $H_2O + \frac{1}{2}O_2 \rightleftharpoons 2OH$ (4.1.2.1a). Here, OH is a hydroxyl free radical, with a neutral charge. Thus this is a free radical reaction, which usually happens under high temperature conditions. Otherwise, there is another reaction $2Fe^{2+} + \frac{1}{2}O_2 + H_2O \rightleftharpoons 2Fe^{3+} + 2OH^-$. This is a reaction of third order. It also relates with iron concentration in fluid. Thus, the similar Fe-free experiment should be conducted in the future to distinguish the influence of these two reactions. Since a_{H_2O} is approximately 1 in the experimental conditions, a_{OH} must increase if f_{O_2} increases. This increases the incorporation of OH into the hydroxyl site in minerals. The structures of humite group minerals are simpler than hornblende. In this section, I will set

norbergite as an example for the discussion.

The OH site in humite minerals is always situated next to Mg. X_F probably relates to the ratio between the activities of F and OH, i.e., the following exchange reaction,



Here, OH and F in fluid represent both anion and free radicals species, and they can react with minerals, of which OH and F are of anion formation. To express our model in simple terms, the concentrations of OH and F in the fluid are expressed as the total of both species. The equilibrium constant of this exchange reaction can be written as

$$K = \frac{a_F^{Fl} \cdot a_{OH}^{Min}}{a_{OH}^{Fl} \cdot a_F^{Min}}$$

Replacing activity with the product of concentration and activity coefficients I obtain:

$$K = \gamma \cdot \frac{[F]}{[OH]} \cdot \frac{1 - X_F^{Min}}{X_F^{Min}} \Rightarrow X_F^{Min} = \frac{1}{1 + b/R} \quad (4.1.2.1c),$$

where γ , a constant at given P, T, and bulk composition, is a product of four activity coefficients which correspond to the relative activities of F and OH in fluid and mineral. $b = K/\gamma$ and $R = [F]/[OH]$. It should be noted that the activity of anion and free radical species are much different, so [F] and [OH] here cannot be represented by their total, but need an activity equivalent factor between anion and free radical.

The Eq. 4.1.2.1c demonstrates that at the same pressure and temperature conditions, the essential parameter controlling X_F of minerals is the ratio [F]/[OH]. In principle, any condition which can change the activity ratio of OH and F will change X_F value of hornblende and humite group minerals. The decrease of F concentration of bulk composition remarkably leads to that in fluid lower, so X_F decreases. Buffer conditions can affect X_F values of norbergite in SP2 experiments, and it indicates that the oxygen fugacity also can change the OH activity in fluid.

Many experimental researches on Fe-free system, especially MgO-SiO₂-H₂O (MSH) system, consider that oxygen fugacity is a minor effect for the phase assemblage and mineral compositions. For example, Kohlstedt et al. (1996) and Otsuka and Karato (2011) focus on the water fugacity effect on the water solubility in minerals and melt of their MSH systems. Nevertheless, some experimental results may be interpreted as indications of f_{O_2} influence in MSH system. Rauch and Keppler (2002) find some slight differences in a natural

orthopyroxene between NNO buffered and IW buffered experiments, but they prefer to count it as vacancy by Fe reduction in IW buffer (i.e. Fe exists in these experiments in trace quantity). Moreover, Bai and Kohlstedt (1992) show the water concentration is essentially hydrogen solubility in anhydrous minerals, which correlates with f_{H_2} and f_{O_2} . They conclude that hydrogen ions are associated with either oxygen interstitials or magnesium vacancies. Furthermore, Yang (2012) investigates the relationship between f_{O_2} and H solubility in feldspars. He argues that H incorporation mechanisms in feldspars vacancies is different at reducing condition (IW buffer) and oxidizing condition (NNO, RRO and HM buffers).

However, my experimental system is quite different from the studies mentioned above. First, hydrous minerals have certain OH site, e.g., humite contains 2OH in the chemical formula. F and OH enter OH site, and their proportions make their competition detectable. Some researches on the relationship between f_{O_2} and OH solubility in anhydrous minerals believe that it is dependent on their vacancies. Different mechanisms are employed to interpret the incorporation of H in anhydrous minerals in various redox statuses. Water solubility in anhydrous minerals is dependent on H incorporation, of which mechanism is different from F. If OH and F are independent, their ratios cannot reflect their relationship as hydrous minerals.

Second, F compete the OH sites in hydrous minerals in my experiments. Most previous experiments utilized natural anhydrous crystals as starting materials to study their water solubility, so their fluid proportions are often too small to crystallize hydrous minerals. On the other hand, even if the water is sufficient, the hydrous minerals are pure OH end member. The differences will be invisible, unless the phase assemblage changes. Within the normal experimental oxygen fugacity regions ($\sim \log NNO \pm 4$, at 1000 °C), it is reasonable to display the same phase assemblage. F plays a role to monitor the OH activity.

Third, in successful SP2 experiments, the fluid mass is sufficient enough to treat a_{H_2O} as 1, because H₂O is a dominant phase in fluid (e.g., 1-SP2-4, 16 & 17). While in the same buffered conditions, different fluid proportion in the system will not influence the phase assembly and mineral compositions. Thus, the discrepancy of X_F in norbergite is not determined by water quantity. Furthermore, the temperature only slightly influences the result,

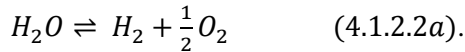
so it is reasonable to think about the effect of oxygen fugacity.

Following Eq. 4.1.2.1a, if a_{H_2O} is assumed as 1, a_{OH} will be proportional to $f_{O_2}^{\frac{1}{2}}$. If oxygen fugacity increases, the activity of OH will increase as well. Because of the increase of OH molecular competitive ability in the fluid, incorporation of OH into the hydroxyl site in minerals is promoted.

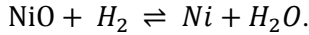
In conclusion, the essential of the F proportion in OH site in hydrous mineral is the competition between F and OH, and find the relationship between OH concentration and the oxygen fugacity.

4.1.2.2 Oxygen Fugacity during Annealing

The f_{O_2} of samples buffered by NNO is considered to function as follows (Ayers et al., 1997), when H_2 is produced by dissociation of H_2O as reaction,



This H_2 diffuses out through the gold capsule, but O_2 remains in the capsule, and when H reaches the NiO layer, a reaction occurs as,



Thus, in the presence of water, the assemblage Ni+NiO fixes f_{O_2} , and assuming $a_{H_2O} \approx 1$, f_{H_2} can be also defined by reaction (4.1.2.2a). Diffusion of H_2 continues until μ_{H_2} and μ_{O_2} (μ is chemical potential) are in equilibrium inside and outside of the gold layer, therefore $\mu_{O_2}^{inside} = \mu_{O_2}^{buffer}$. At the same P-T condition, $f_{O_2}^{inside} = f_{O_2}^{buffer}$. With this buffer arrangement, nickel powder can be oxidized to NiO, and hematite can be reduced to magnetite (Ayers et al., 1997). They demonstrate that this NNO buffer of this cold-sealing technique can control the oxygen fugacity very well. Generally, when NiO layer and water in sample room were present during the experiments, the buffer will work well and control the oxygen fugacity approximate NNO level, while the detailed process may not behave ideally as Ayers described. Jakobsson (2012) described that carbon permeation will change the oxygen fugacity by creating CO, CO₂ and CH₄, of which increasing proportions can result in the decrease of hydrogen and water fugacity. However, most successful buffered experiments,

which has fluid left in the capsule, indicates the buffer works well. In the NNO buffered experiments, it is feasible to consider the oxygen fugacity is equal to that of NNO buffer.

When the NNO buffer is exhausted by consumption of NiO, diffusive loss of H₂ is expected to continue throughout the experiment duration, since hydrogen cannot be sealed inside any metal capsule. It is expected that the oxygen fugacity would be higher in unbuffered experiments than in NNO buffered experiments. For example, in Ayers' experiments (1997), which were conducted without buffer during anneal, he found the evidence of the presence of hematite inclusions in olivine. It indicates that his olivine (Fo98) and orthopyroxene become unstable.

I also find some indications of an increase of ferric ion in the unbuffered experiments. Normally, iron in norbergite is Fe²⁺. In SP2 experiments with an NNO buffer, the Fe concentration in norbergite is approximately 3 wt%. In contrast, in unbuffered experiments, the Fe concentration is no higher than 1.3 wt%. Meanwhile, the iron concentrations of hornblende in unbuffered experiments are higher than those from NNO buffered experiments. The reduced amount of iron in norbergite and the increase in hornblende suggest an increase in ferric iron. Moreover, since the Mo-MoO₂ buffer imposes an f_{O_2} several orders of magnitude lower than NNO (O'Neill, 1986), there should be an increase in ferrous iron if free oxygen can create a buffer with the Mo metal chamber. On the contrary, all unbuffered experiments, including Mo metal chamber capsules, show a higher oxygen fugacity in the runs without a buffer than those with the NNO buffer.

For this cold-sealing technique, one hypothesis is stated as the oxygen fugacity is probably buffered by the metal and the free oxygen, which is present in the gaps of the assemblies, because the oxygen can react with the metal of outer capsule, e.g. Ni, and form some oxide. Then the behavior of the capsule is similar with the capsule containing oxidized layer. However, the aims to oxidize the nickel are 1) to supply enough oxides for the buffer reaction, and 2) to separate the nickel metal and inner gold sleeve to prevent forming an alloy and contaminating the sample during anneal. It is possible to calculate the thickness of the nickel oxide layer if this hypothesis works.

After the assemblies are set up in the piston-cylinder, and at high pressure, free oxygen cannot transfer into the nickel capsule from the outside. Assume only the oxygen inside the

nickel capsule can take part in the reaction of forming nickel oxides. The inner diameter of my large capsule is 3.0 mm, and the depth of its hole is 4.0 mm. This space is occupied by air, and its volume is 28.3 mm³. The air density is 1.205 kg/mol, and the oxygen weight percent of air is 23%. The oxygen molal quantity is 2.45×10^{-7} mol, which can produce 4.9×10^{-7} mol NiO maximally. Thus, the thickness of the oxide layer can only reach 0.142 μm . Even if this thin layer can work, it will be exhausted very quickly. The result demonstrates that the free oxygen in trapped air cannot form enough oxide NiO to buffer the experiment. The experiments employing an Au-Pd tube or Ti and Mo outer chambers without oxide layers are not buffered. Shortly after the start of annealing, this free oxygen should be consumed quickly by forming H₂O.

What is the oxygen fugacity of the unbuffered experimental system, then? There are two possible controls imposed on the experimental μ_{H_2} . One is an environmental control. It is often said that a typical piston cylinder assemblage (graphite furnace, MgO spacers) fixes f_{O_2} at near to the hematite-magnetite (HM) buffer. For example, Ayers et al. (1992) describes that the f_{H_2} of the assembly with crushable alumina container is lower than HM buffer when the water activity is one. Moreover, if the graphite heater and moisture in the assembly form a buffer reaction, the environmental f_{O_2} can be around CCO-0.8 (extending arguments given in M  lard et al., 2008). However, the outer metal material, in the absence of an oxide layer, does not buffer the oxygen fugacity. This is because free oxygen, which is present between the inner tube and the outer chamber, is not abundant enough to form an effective buffer. Generally, this free oxygen would be consumed quickly to form H₂O at the start of annealing. From this point, the situation is similar to that of NNO buffer exhaustion, with hydrogen being exchanged until the inner capsule reaches f_{O_2} of the assemblage.

Alternatively, in the absence of a buffer, in a closed system, the intrinsic fugacity of water should be imposed. For example, the oxygen fugacity of pure water is more than 10^{-5} bars at 800 $^\circ\text{C}$ and 0.2 GPa (Miyashiro, 1964). Because of the increase in the fugacity coefficient from 1.737 to 10.1, at 800 $^\circ\text{C}$ and 1 GPa, the oxygen fugacity of water is significantly higher than the f_{O_2} of the NNO buffer.

It should be also noted that below 1000 $^\circ\text{C}$, oxygen cannot transfer through the gold

capsule to the outside (Truckenbrodt and Johannes, 1999). As H_2 diffuses out of the inner capsule, an increase of $f_{O_2}^{inside}$ causes a decrease of $f_{H_2}^{inside}$ and it may effectively diminish to the point at which the diffusive mass flux of H_2 is close to zero. In this case $f_{O_2}^{inside}$ remains at a certain magnitude, creating a quasi-closed system. No matter what mechanism controls $f_{O_2}^{inside}$, the oxygen fugacity of unbuffered experiments is higher than that of NNO-buffered experiments.

However, this hypothesis on the water-buffer reaction cannot explain the reduce reaction in the capsule, as his experiment hematite+ H_2O with NNO buffer. Both sides of the capsule consumes H_2 , and outside water fugacity is less than inside, so the diffusion process of hydrogen is always from inside to outside (Brooker et al., 1998). Below 1000 °C, oxygen cannot permeate through the gold layer. The consumption of H_2 leads to a high oxygen fugacity. Unless the hydrogen diffuses into the inner capsule, the buffer will not work. However, Ayers et al. put the unfired pyrophyllite in the assemblage as a water source, so it is possible for hydrogen to diffuse into the capsule. This conflict indicates some unknown details in this process, which may be quite complicated.

4.1.3 Stability of Humite Group Minerals with F

The pure OH end-member humite can be formed within the appropriate stability field. OH-chu has been found in the nature (Ferraris et al., 2000), and OH-clinohumite, OH-humite and OH-chondrodite have all been synthesized (Wunder et al., 1995; Burnley and Navrotsky, 1996; Wunder, 1998; Pawley, 2000). OH-norbergite is unstable and has not yet been reported. Whether natural samples or man-made ones, pure OH end-member humite always produces the phenomenon of intergrowths, e.g. upon the synthesis of OH-chu, intergrowths of forsterite, clinohumite and chondrodite were observed (Berry and James, 2002). F and/or Ti partition preferentially into humite in comparison to calcic amphibole and phlogopite (Rice, 1980). The starting materials of F-bearing experiments contain more F than Ti, and it is known that the amount of F controls the level of Ti that can enter the structure (Jones et al., 1969).

Clinohumite has a larger stability field at higher X_F . For example, at 1GPa, OH-chu

($X_F=0$) breaks down below 700 °C, while F-chu ($X_F=0.47$) breaks down around 1000 °C. When X_F reaches 1, F-chu will break down around 1400 °C, and it reacts to pure F-norbergite + olivine (Ulmer and Trommsdorf, 1999). Stalder and Ulmer (2001) also show that small amounts of F increase the stability field of clinohumite relative to OH-clinohumite in a pure MSH system. Because substitutions of F and Ti strengthen the structure due to the high bond strength of F and hydrogen bonding, F substitution can stabilize humite species at higher temperatures (Berry and James, 2002). Moreover, an increase in F concentration changes the humite mineral species. For instance, the amount of F relative to OH increases from clinohumite to norbergite (Jones et al., 1969). Natural chondrodite has an X_F of up to ~0.8, while all known norbergite samples have $X_F > 0.8$ (Berry and James, 2002). In contrast, the maximum structural strength for chondrodite is achieved when a hydrogen bond occurs between every O5-O5/F pair, i.e. at $X_F = 0.5$ (Berry and James, 2002).

In my experiments, F was partitioned into different humite group minerals from aqueous fluid. Essentially, high F-bearing experiments produced norbergite, of which $X_F \approx 1$, using the NNO buffer. Even if the F concentration is high enough to precipitate norbergite, OH activity is not high enough to decrease X_F in nature. Moreover, $Mg(OH)_2$ layers of humite minerals as seen from the a axis are similar, so it is possible to synthesize norbergite with X_F less than 0.8. For example, the unbuffered experiments have a high OH activity and create norbergite, of which X_F is minimally equal to 0.79, and in 3-SP2-1 experiment, its norbergite X_F reaches 0.75. The norbergite with the lowest F concentrations was formed at unbuffered conditions or at 2 GPa by far.

The OH site in humite minerals is always situated next to Mg. X_F probably relates to the ratio between the activities of F and OH, which is described from Eq. 4.1.2.1a to 4.1.2.1c. In the buffered SP2 experiments, $[F]/[OH]$ is high enough that leads to X_F nearly 1. The F concentration in SP3 bulk powder is only 40% of SP2. As a result, X_F decreases almost 1/3 of that from SP2 experiment under the same P-T conditions, but it does not decrease as the same proportion as the bulk composition. Meanwhile, SP2 experiments demonstrate that X_F decreases from 0.99 to 0.80 (from NNO buffered to unbuffered experiments, respectively), which indicates OH concentration increase at almost constant F concentrations (~0.3 wt% in fluid). If $[OH]$ increases or $[F]$ decreases, OH will eventually occupy more OH sites than F. I

got F-chondrodite with lower X_F (0.60) in SP3 unbuffered experiment.

However, the water is exhausted in some experiments, but their humite group minerals still contains the similar F concentration as other successful ones. Because the experimental temperature is not high enough to break down these F-bearing humite group minerals, the mineral compositions keep the information as they precipitate. Furthermore, X_F variations in different experiments indicate the loss of water during anneal with different diffusivities. This process will change the fugacity proportion of each gas species and influence the oxygen fugacity when water is not a dominant phase.

When the water fugacity is sufficiently low, oxygen fugacity may be higher than buffer. Following general knowledge, the water fugacity decreases will result in the lower water concentration in minerals. However, I found some inverse observations in my experiments. For example, the failed SP3 experiments have chondrodite with X_F value of 0.62, lower than 0.69 in the successful experiments. Their high OH concentrations indicate the high oxygen fugacity with the low water fugacity. Meanwhile, F will precipitate during the water loss, and its concentration in fluid will not be concentrated. After the water is exhausted totally, even if the oxygen fugacity is very high, it cannot change the X_F of the minerals which have precipitated already, unless the fluid does not distribute evenly.

Furthermore, F concentration not only constrains the X_F value in minerals, but also determines the humite species, which is essentially derived from the ratio between $n(\text{SiO}_2)$ and $n(\text{F}+\text{OH})$ in the fluid. From my results, F is shown to increase SiO_2 solubility in fluids. Furthermore, the OH concentration remains almost constant under the same P-T conditions, in the presence of an NNO buffer. Consequently, with decreasing F concentration in the bulk composition, i.e. a decrease of $n(\text{F}+\text{OH})/n(\text{SiO}_2)$, the stable humite group minerals evolve through the range norbergite, chondrodite, humite and clinohumite, which also have progressively lower X_F values. In subducting slabs, the F concentration is around several hundred ppm. Based on my results, I would expect clinohumite to exist in very small quantities in the presence of hornblende in the basaltic portion of subducting slabs.

4.2 Fluid Composition Comparison

Fluid compositions of successful experiments are calculated by mass balance. Some samples are analyzed directly by HPLC, ICP-AES and ICP-MS. The results from two methods are not exactly the same. In the first part of this section, each element concentration will be compared, and I will manage to find reasonable explanations. The second to fourth part will discuss various factors (temperature and bulk starting materials, fluorine concentrations, and pressure) influences on the element solubility in fluid. At last, I summarize the fluid compositions from my experiments.

4.2.1 Comparisons between Mass Balance and Direct Analysis

The aims of these two methods are to find the true fluid compositions during the experiments. Because of the difficulty of retrieving the fluid for direct analyses, most of researches used to calculate the fluid composition by mass-balance approach. In principle, this is a reasonable method, but in some cases, it does not work well, e.g, in SP4 or high melt proportion experiments, the F concentrations from mass-balance are zero, and with a large uncertainties. It indicates some constrains of this approach, e.g, Koga et al. (2005) discuss that the low fluid proportion results in a big error for the calculated fluid composition. My new study on the direct analyses of fluid compositions needs the confirmation from this traditional way in its suitable region. In this section, the comparisons of each element concentration are shown and investigated.

4.2.1.1 F Concentration Comparison

From mass balance calculations, F concentrations of the fluid in most of SP2 and SP3 experiments are approximately 0.3 – 0.5 wt% (Fig. 4.2.1.1a). Most of the F concentrations from HPLC measurements are plotted in the uncertainties of those from mass-balance calculations. In SP4 and high-proportion melt experiments, HPLC results are higher than mass-balance, because they are not suitable with mass balance and given as zero F

concentration. On the contrary, in SP2 and SP3 experiments, F concentrations from HPLC measurements are generally lower than those from mass balance within their uncertainties. This illustrates that most F concentrations of experiments at 1 GPa are confirmed by HPLC direct analyses. When the minerals compositions typically and reasonably represent their average values, mass balance will work perfectly and give the residual as fluid composition. Nevertheless, it is hard to say the end point of fluid retrieving procedure. Sometimes, it is impossible to collect some the residual, for they precipitated as the quench phase and did not dissolve into water again. That leads to lower F concentrations by direct analyses than mass balance calculations.

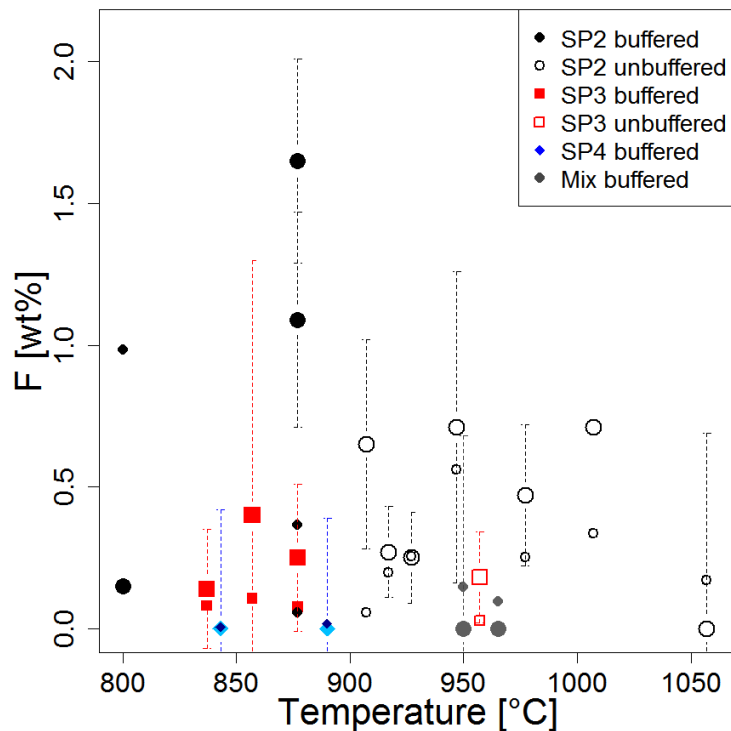


Fig. 4.2.1.1a Reasonable F concentrations from mass-balance calculation (large symbols) and HPLC analyses (small symbols) are plotted. Different symbols represent different starting materials and experimental buffer conditions. Most experiments were conducted at different temperatures, so the style symbols at the same temperature indicates that they are from the same experiment. The F concentrations from SP4 experiments by two methods are too close to distinguish from each other, so lighter blue is applied to the mass-balance date. The uncertainties (2σ) of the results from mass-balance are shown for each data, except those larger than 2 wt%. The reproducibility of HPLC measurement is good enough to ignore its error (maximum relative error is 1%), so the data of HPLC analyses are displayed without error bars.

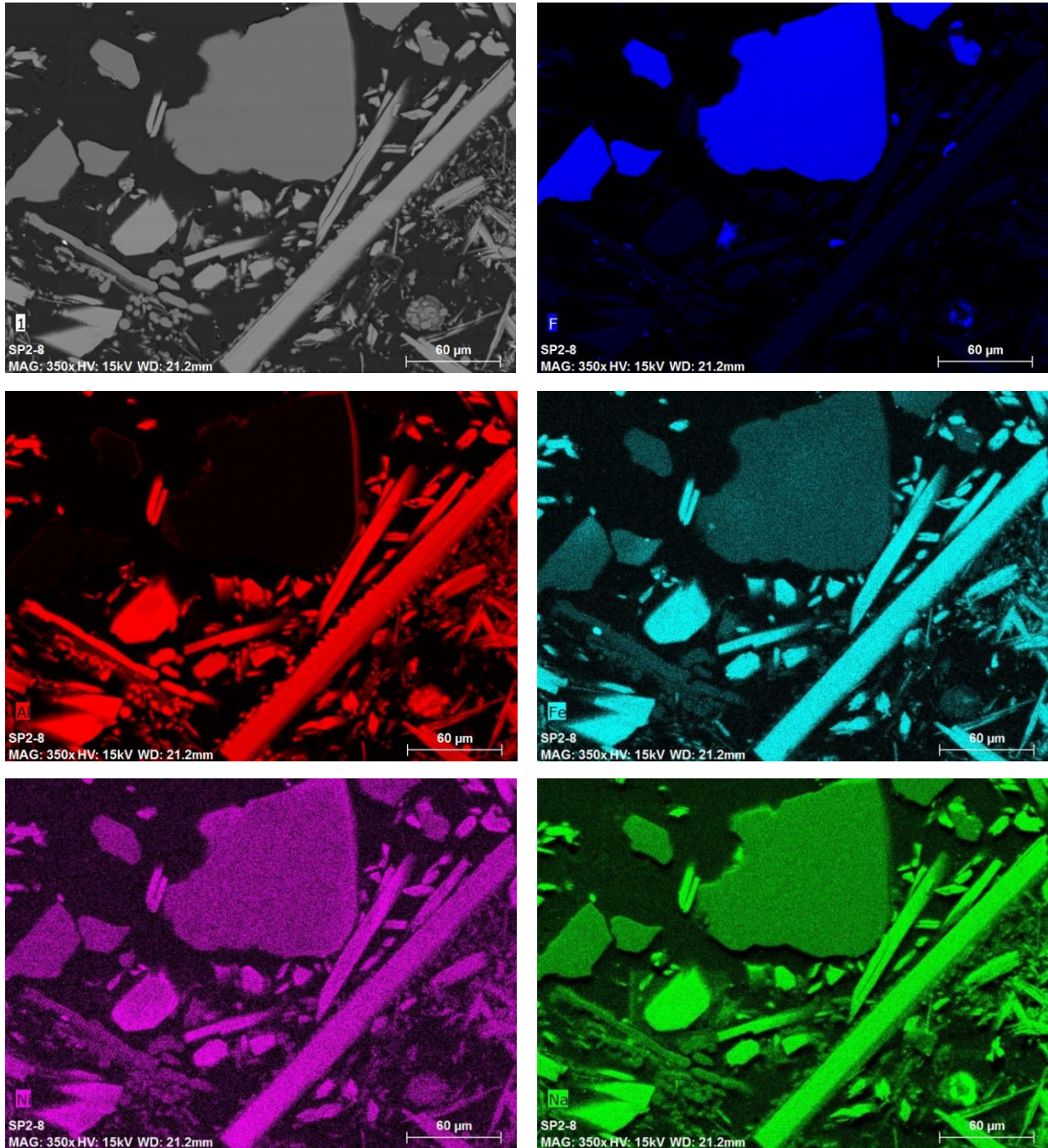


Fig. 4.2.1.1b The elements distribution maps for the experiment 1-SP2-8. The first is an SEM image, and the other five maps represent F, Al, Fe Ni, and Na, respectively. The phase assembly is introduced in Section 3.1.2.1. Some little spheres on the longest hornblende are quench phases. The distribution maps illustrate that its F and Al concentration are close to the hornblende, and its Fe, Ni and Na concentrations are similar with norbergite. The comparisons with Fig. 3.1.2.2b indicate that the proportion of the quench phases in 1-GPa experiments are much less than those conducted above 2 GPa.

However, the exceptions, of which F concentrations are not plotted in the uncertainties of the results of mass balance, should indicate some limitations for these two methods. For

example, 1-SP2-23 experiment has 1.0 wt% F by HPLC and 0.15 wt% F by mass balance in its fluid. Its fluid composition given by mass balance is abnormal, of which Al_2O_3 concentration reaches 21 wt% (Table 3.4.1.1.1e). It indicates that the abundance of Al_2O_3 is depleted in hornblende, which makes the proportion of hornblende underestimated and that of norbergite overestimated. Therefore, the F quantity in its residual should be less than the real value. On the other hand, the water lost during annealing. The small fluid proportion (0.45 mg, and the starting material mass is 4.78 mg) leads to a large uncertainty, which also suggests its result may be not precise. Moreover, the HPLC result is higher than mass balance results, which indicates that its solute precipitated as soluble phases because of the saturation as the water quantity decreases. During the post-quench procedure, the soluble phase also dissolves into the diluted fluid. The extraction fluid composition of this experiment cannot reflect the truth during anneal, but the proportion of each element should be proportional with their solubility.

Two black round symbols at 877 °C represent two experiments conducted at 2.0 and 2.5 GPa (Fig. 4.2.1.1a). Their F concentrations (1.65 wt% and 1.09 wt%) from mass balance are much higher than those (0.365 wt% and 0.055 wt%) from HPLC. The direct analytical results are out of the uncertainties of the mass balance. Obviously, the differences are derived from the component of quench phases, and this texture can be found in their SEM pictures (Fig. 3.1.2.2b, 4-SP2-1, 5-SP2-1). Generally, the solubility of mineral component increases with an increase of pressure, e.g., SiO_2 (Manning, 1994; Newton and Manning, 2002) and TiO_2 (Ayers and Watson, 1993) are well studied. Moreover, the presence of F and Cl will enhance solubility of TiO_2 (Newton and Manning, 2000; Rapp et al., 2010). Thus, these high dissolved elements are present in the fluid during the high P - T experiments. During the quench, their solubility decreases dramatically. And they cannot precipitate as crystals but quench phases. Several researches showed this texture after the large quantity water-bearing experiment above 2 GPa (Ayers et al., 1997; Koga et al., 2005). The quench phases are easy to detect in the experiments higher than 2 GPa, which indicates their larger proportion than 1-GPa experiments.

Moreover, little sphere textures are found in 1-SP2-10 (Fig. 3.1.2.1g), as well as 1-SP2-8. The elements (F, Al, Fe, Ni, and Na) EDS X-ray distribution maps of 1-SP2-8 verified the

quench phases contain these elements. The F concentration of the quench phase is close to that of hornblende (Fig. 4.2.1.1b). However, this quench phase is insoluble with water after quench, and was kept in the capsule after the post-quench procedure. This is a reason that the general HPLC results report lower F concentrations than mass balance. It is reasonable to ignore the quench phase in 1-GPa experiments, because the proportion of quench phase is too little. While, it is impossible to look over it for the experiments with significant quench phases. The results from mass balance are more reliable than HPLC at the present of high proportion quench phases. F concentrations in fluid at higher pressure are more than at 1 GPa. It may be confirmed with leaching technique (Koga et al., 2005) for more experiments.

4.2.1.2 Major Elements Concentrations Comparisons

All the extracted fluid samples were analyzed by three or four methods, mass balance calculation, HPLC, ICP-AES and ICP-MS. Some major elements, such as Na, Si, Al, Mg, and Ca were analyzed as well. These five typical cation concentrations are expressed as relative oxides form and plotted as bars from Fig. 4.2.1.2a to e. The juxtaposed bars are from the same experiments, and the bar colors indicate their analytical methods. The experiment identities are plotted under the groups of bars. In each element group, some data are missing, which indicates that it has not been determined by this approach.

Generally speaking, the direct analyses results confirm the solubility of each element from mass balance. Na and Si are soluble at high P - T conditions in aqueous fluids, and both calculated and analytical results show the significant concentrations of these two elements, which verifies that it is rational to exclude them from the conservative element set (Fig. 4.2.1.2a & b). Al solubility is rarely reported, but the studies on the solubility of albite-paragonite-quartz suggest that it is much lower than Si solubility during anneal (Manning et al., 2010; Wohlers et al., 2011). My ICP-MS analyses confirm this, and indicate some problems from mass balance, which gives abnormal high Al concentrations (Fig. 4.2.1.2c). Moreover, most Mg and Ca concentrations are given as 0 by mass balance, and direct measurements show their concentrations are very small but not zero (Fig. 4.2.1.2d & e). This is more reasonable and the results are in the uncertainties of calculated results. Even

their abnormal high concentrations are lower than Na and Si.

Except some abnormal high values from mass balance results, the concentrations of each element from different methods are close and in the same magnitude level, especially Na, Si. Because four ICP-AES analyses are for test, which is a semi-quantitative procedure, the analyses results with ICP-MS and HPLC are more reliable than ICP-AES. Therefore, the most ideal experiments are 1-SP2-15, 16, 17 & 21, and 3-SP2-1. Some experiments are partially consistent between calculated and analytical results. For example, Na, Mg and Ca concentrations from 1-SP-3, 4 & 8, and 4-SP2-2, or Na, Si and Al concentrations from 1-SP2-19 are consistent. The rest experiment results are of inconsistencies.

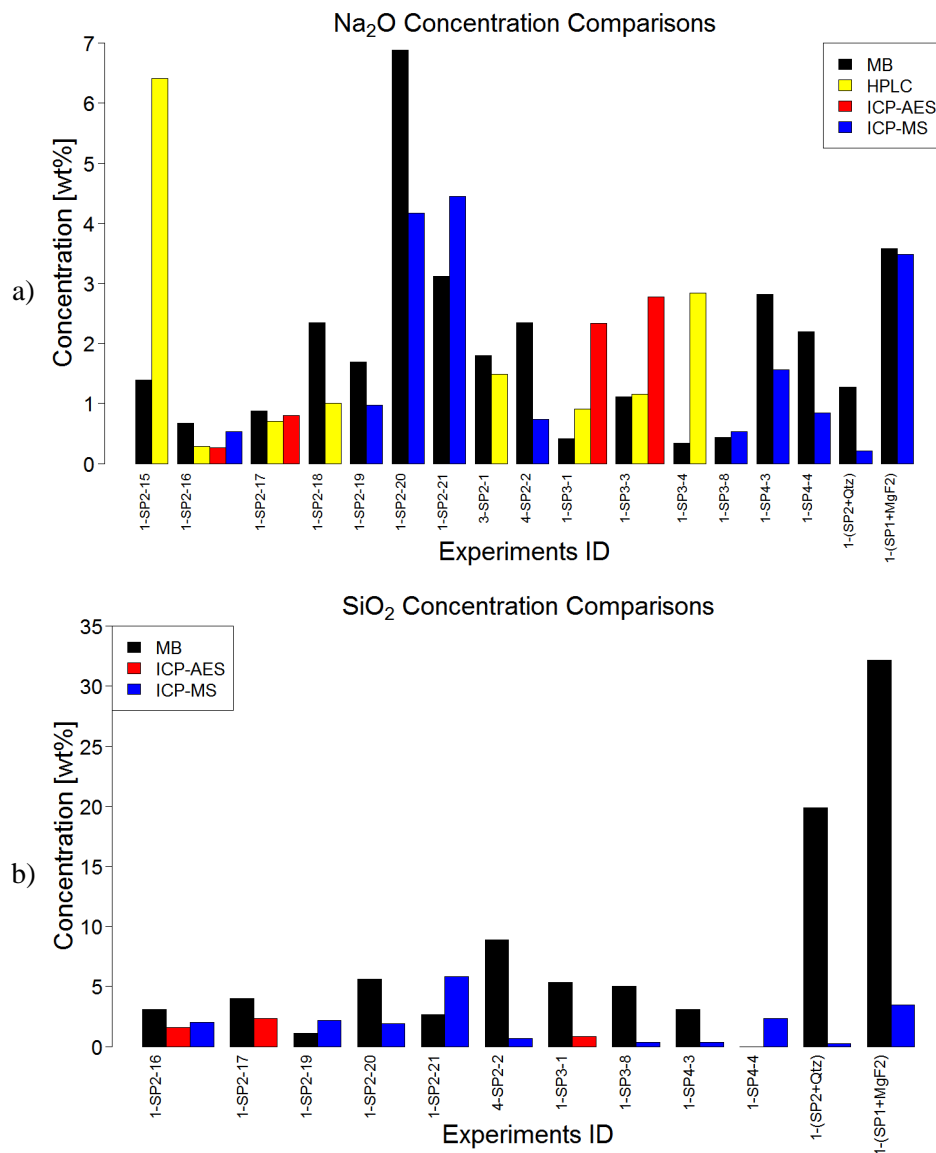


Fig. 4.2.1.2 a) Na₂O, and b) SiO₂ concentrations in fluids comparisons between different methods.

4. Discussion

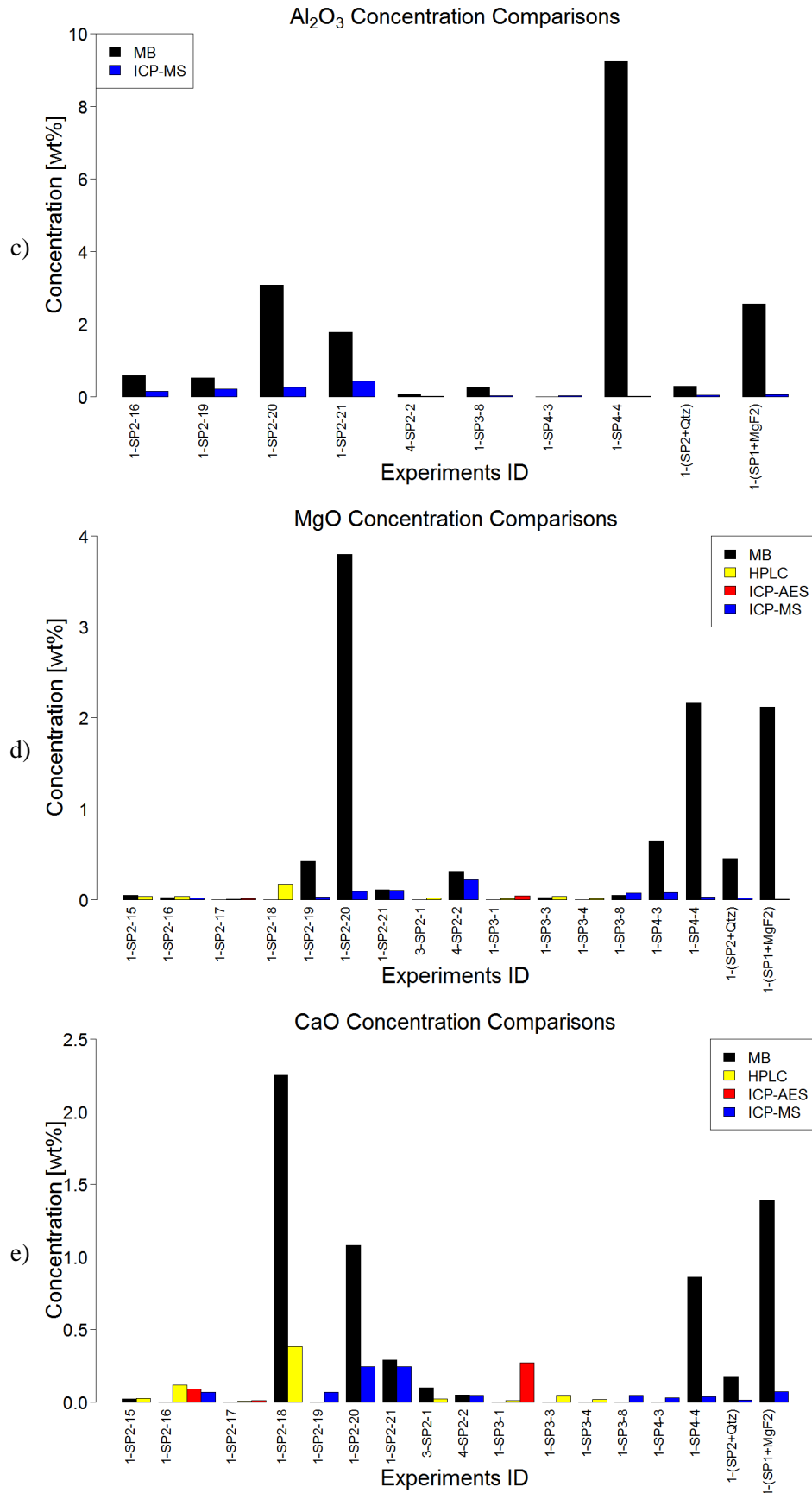


Fig. 4.2.1.2 c) Al₂O₃, d) MgO, and e) CaO concentrations in fluids comparisons between different methods.

The typical ideal experiments contain large fluid fractions ($> 40\%$), simple phase assemblies, and typically different phase compositions. The fluid proportions of 1-SP2-18 & 20, 1-SP3-3, and 1-(SP1+MgF₂) are less than 30%, which is of importance to result in their low precise calculated fluid compositions. 4-SP2-2, conducted at 2.5 GPa, has much lower concentrations of Na and Si from direct analyses than mass balance, because there are lots of quench phases in the capsule. This conclusion fits its situation of F concentration comparison.

High melt proportion experiments always get F concentration as 0, which indicates that the composition of each typical phase is not close to the true average composition or the phase assembly is complicated. For example, in experiments 1-(SP1+MgF₂) and 1-(SP2+Qtz), Si concentrations from mass balance are significantly higher than those from ICP-MS results. These experiments contain at least 3 solid phases. Mass balance does not work as well as for two solid phases experiments, such as 1-SP2-16 & 17. The more solid phases exist in the capsule, the more difficult to estimate the fluid composition by mass balance is. On the other hand, it is also hard to get a typical average composition of the degassed hydrous melt. Even if its composition can be analyzed by electron microprobe, its uncertainty is larger than minerals, and its composition cannot represent the actual component during anneal. Meanwhile, SP4 experiments also create a 3-solid-phase system without melt. The data of 1-SP4-3 & 4 show that the Si and Al concentrations of each fluid are different from mass balance result. This also suggests mass balance does not work well for these two experiments. It is possible for some close components between amphibole and pyroxene to influence the mass balance.

Because phase proportions are derived from the conservative element set, the typical mineral composition and conservative element species are crucial for the mass balance result. Confirmed by direct analytical results, those ideal experiment calculated results are reasonable within their uncertainties; those of 1-SP2-19 & 20, and 1-SP3-8 are acceptable; others, especially high melt proportion experiments, I prefer their direct analyses results to mass balance. Nevertheless, for the experiments, of which pressure is higher than 2 GPa, there is a need for more investigation on their quench phase compositions.

4.2.1.3 Indications of the Differences

Some indications from Fig. 4.2.1.1a may reveal why mass balance calculation does not work well for some experiments. In principle, the ideal calculation needs the true average composition of each mineral species, the mass of the fluid and the starting material, and suitable conservative element set. However, it is impossible to analyze all the mineral compositions to get the typical mineral composition. Instead, the normal way is to measure some biggest mineral compositions and use their average as the typical composition. It is feasible to ignore small crystals or quench phases at 1 GPa because of their little quantity. If there are significant compositional variations associated with the size of grains, the error sources from mineral compositions will make the determination of the conservative element difficult. Although it is hard to investigate which major element species are present in the fluid, the concentrations of major elements analyzed directly by ICP-MS can confirm the mass balance result. It supplies another criterion for choosing conservative elements for mass balance calculation.

The procedure of selecting conservative element set in my mass balance procedure is reasonable, because it only depends on the compositions of minerals and starting material. ICP-MS result can confirm the results, but may not correct the values completely. For example, for 1-SP2-19, I change the conservative element set by excluding Mg, Si or not, the result does not change much. And for 1-SP2-21, the concentrations of Na, Ca, Si and Al confirm their solubility and validation of its conservative element set. Therefore, it is helpful for improving the mass-balance results to form bigger crystals, which can represent the true mineral compositions.

The precondition of the mass balance calculation is the presence of the conservative elements. But all the elements solubility increase with an increase of pressure. The significant presence of quench phase, an increase number of phases and a decrease number of conservative elements can result in unreliable fluid compositions. In conclusion, the techniques for precipitating big crystals without contaminations and for the extraction of quench phases are indispensable for the high P - T condition experiments, especially when pressure is larger than 3 GPa.

4.2.2 Influences of Temperature and F concentration

Because only one F-free experiment (1-SP1-8) was analyzed by HPLC, the comparisons of major elements concentrations between F-free and F-bearing experiments are from mass balance calculation. The F-bearing experiments have similar phase assemblage (all of them contain hornblende and humite group minerals), but their fluid compositions are of subtle difference, even conducted with the same bulk powder, for their phase proportions change. For example, F concentrations are approximately 0.3 wt%, but are slightly variable in SP2 unbuffered experiments. Therefore, F concentration in different bulk composition is a leading reason to change their phase assemblage.

The concentrations of Na, Si, Al, Mg, and Ca of each experiment are shown in this section, respectively from Fig. 4.2.2.1 to 4.2.2.5. Moreover, their concentrations versus F contents are also plotted, as well as Fe concentration in Fig. 4.2.2.6. Some calculated results are far away from ideal condition for calculations, such as high melt proportion experiments ($T > 970\text{ }^{\circ}\text{C}$), low fluid proportion ones (1-SP2-23 & 24), and 1-SP2-14, which created an abnormal phase assembly. Thus, they are not compared in these figures.

4.2.2.1 Na₂O

As Fig. 4.2.2.1a shown, two experiments (1-SP3-3 and 1-SP2-18) have the highest Na₂O concentration in corresponding series experiments. Their calculated Na₂O concentrations are confirmed by HPLC analyses. Not all the sodium is incorporated by hornblende in SP1 experiments. Na concentrations in fluids of SP3 experiments are slightly higher than SP1. However, SP4 experiments have a different phase assembly system from SP2 or SP3. It is not comparable to expect Na behaviors as SP2 or SP3 experiments. SP4 are richer in MgO, and creates Na-free pyroxene. Moreover, its hornblende contains more Na than those from other three series experiments.

Na can enter A-site to balance the charge, which is led by Al substitution in T-site. This is of key point to control the Na concentration in hornblende. Na in fluid does not relate with hornblende. Furthermore, Na is easy to dissolve in fluid. Either mass balance calculations or

direct analyses show the residual Na outside the minerals. Some of the results may be over saturated, but it is hard to tell Na saturation at high $P-T$ condition. Na concentration is independent with temperature.

With the presence of F, an increase of humite group mineral proportion releases more Na from hornblende. The more F concentration of the bulk composition is, the larger humite group mineral proportion is. For example, the proportions of norbergite in SP2 experiments at 1 GPa are approximately 9 wt%, while those of chondrodite in SP3 experiments decrease to 5 wt%. Except SP4 and mixed bulk composition experiments, mass balance results show that Na_2O concentration correlates with F in fluid, especially in SP3 group and SP2 unbuffered group (Fig. 4.2.2.1c). However, Na is a soluble element under room temperature and pressure. In the silicate and water system, no reference report that other elements constrain Na solubility in aqueous fluid. Direct analytical results (Fig. 4.2.2.1d) suggest that no significant correlation between Na_2O and F concentrations, even if only selecting the hornblende bearing experiments.

In my experiments, hornblende and melt incorporate Na. F promotes hornblende breakdown and crystallization of norbergite and chondrodite, which are Na-free minerals. Consequently, Na is released into fluid, indirectly affected by F. On the other hand, hydrous melts in my experiments have less Na_2O than hornblende, so high temperature experiments create melt and release F as well. Thus, higher temperature experiments have more Na_2O concentrations. An exception is the high silica-bearing experiment (950 °C, gray point), because it crystallized hornblende in the melt.

In summary, Na_2O concentration in fluid is a result of phase assemblage and phase proportions in the system, which is indirectly influenced by F concentration in bulk composition.

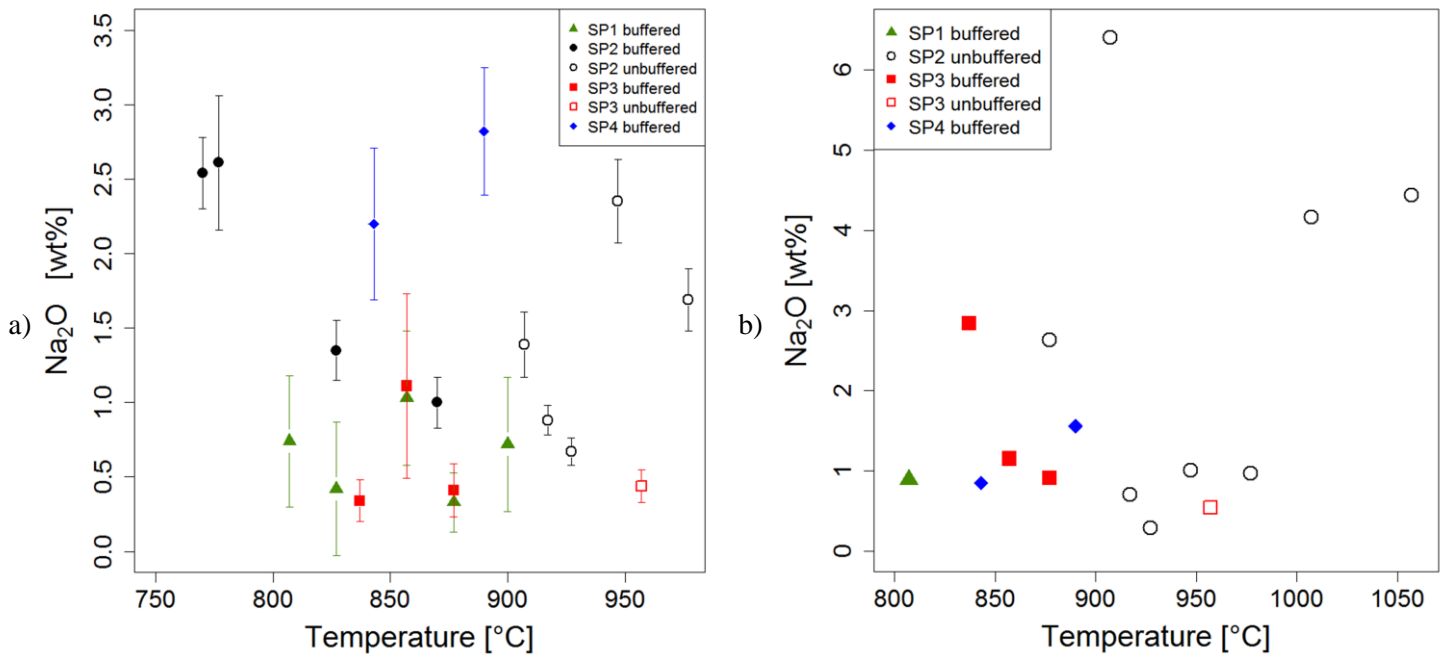


Fig. 4.2.2.1 Comparisons of Na₂O concentrations in fluids at 1 GPa. a) Mass balance results. b) Direct analytical results. The relative error bars of direct results are less than 1%.

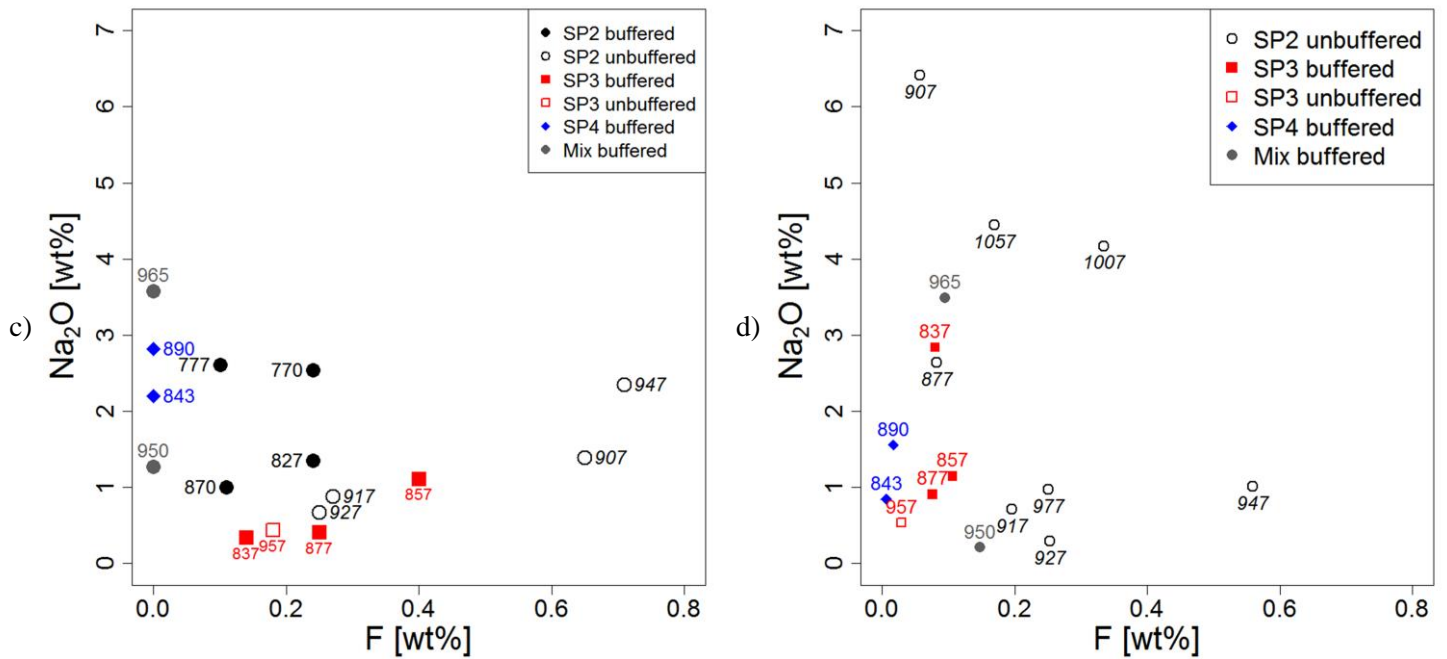


Fig. 4.2.2.1 Na₂O vs. F concentrations in fluid. The experimental temperature is shown beside each point. c) Mass balance results. d) Direct analyses results. The relative error bars of direct results are less than 1%.

4.2.2.2 SiO₂

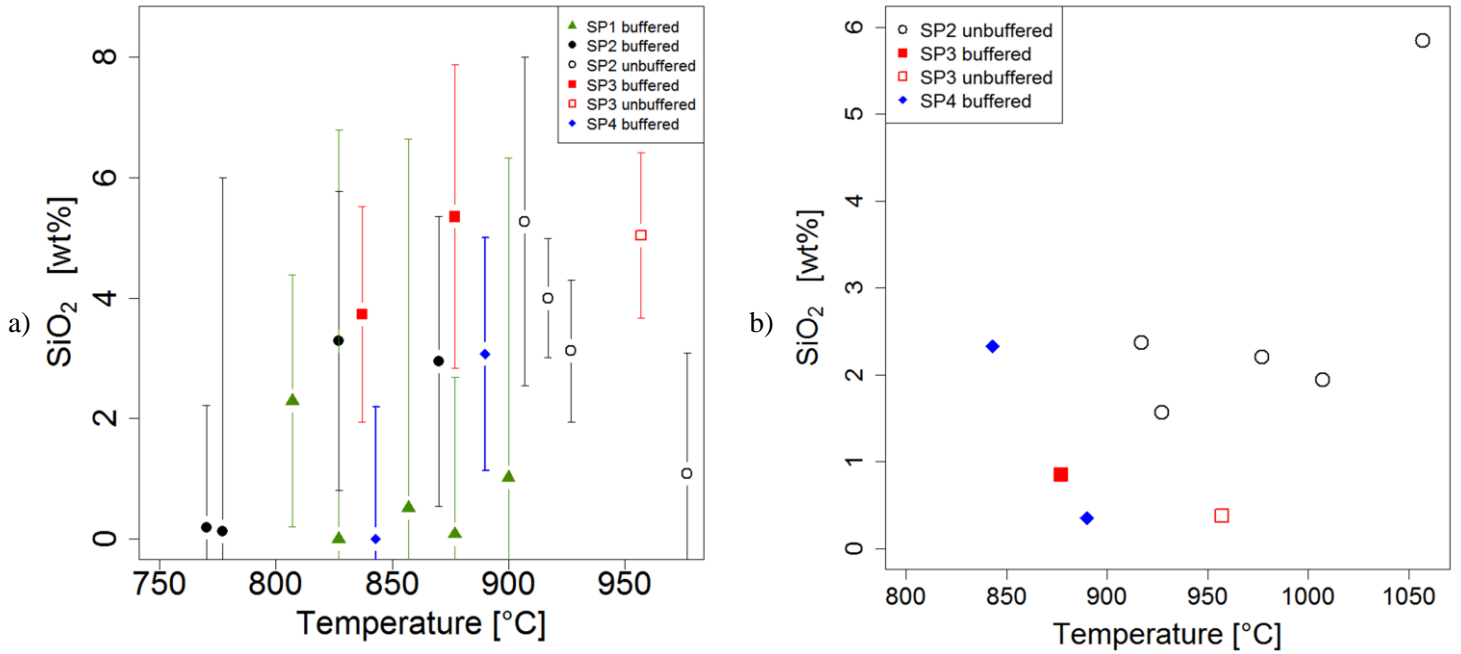


Fig. 4.2.2.2 Comparisons of SiO₂ concentrations in fluids at 1 GPa. a) Mass balance results. b) Direct analytical results. The relative error bars of direct results are less than 1%.

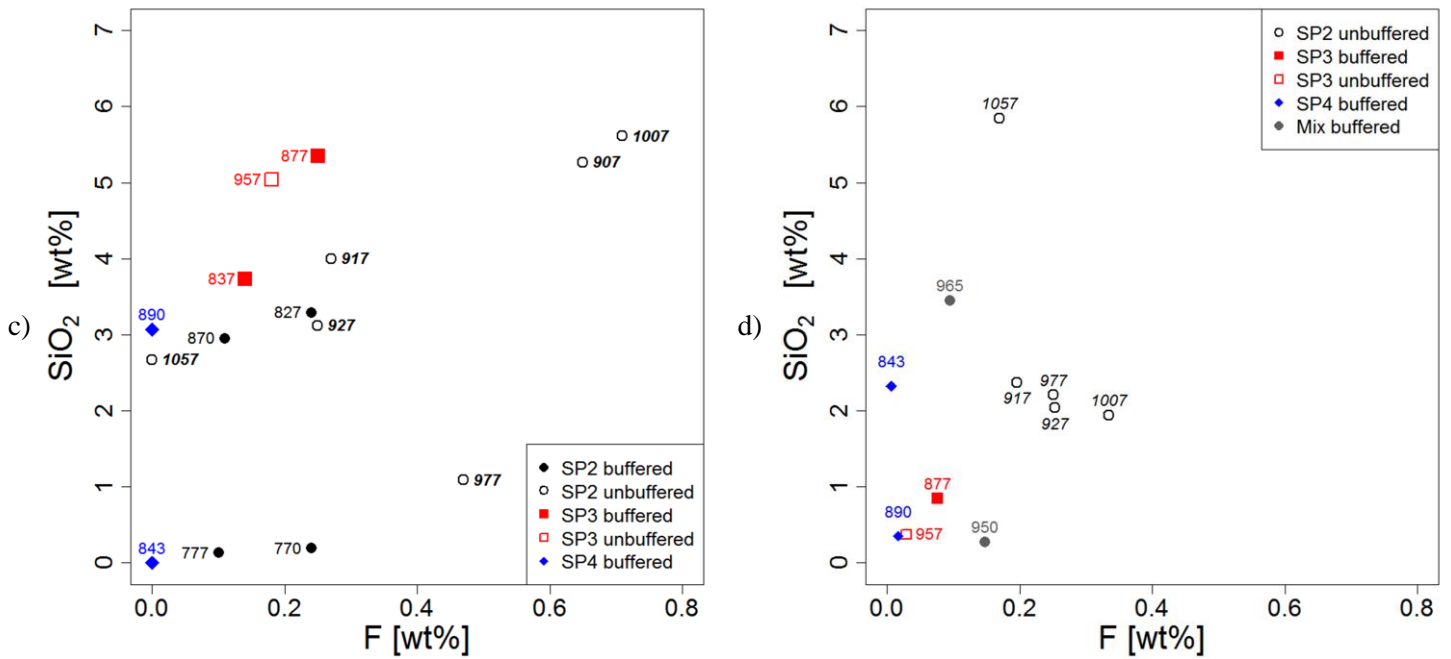


Fig. 4.2.2.2 SiO₂ vs. F concentrations in fluid. The experimental temperature is shown beside each point. Their uncertainties are not shown here. c) Mass balance results. d) Direct analyses results. The relative error bars of direct results are less than 1%.

SiO₂ can be dissolved into the fluid regardless of the presence of F from calculated results. A tendency is obvious that SiO₂ concentrations in most fluids of F-bearing experiments are higher than those in F-free experiments (Fig. 4.2.2.2a). Except for two extremely high concentration (experiments 1-SP2-18 and 1-SP3-3), all SiO₂ concentrations are less than 6%. Their fluid fractions relative to their anhydrous powder quantities are 40 % for 1-SP2-18 and 20 % for 1-SP3-3 after quench. It probably causes their abnormal calculated high concentrations. However, their fluids were not analyzed by ICP-AES or ICP-MS, so it is impossible to confirm their abnormal SiO₂ concentrations. While, the ICP-MS result for 1-SP2-23 shows that its fluid contains 7.9 wt% SiO₂ (Table 3.4.2.3d). It indicates that its fluid extracted the soluble precipitate. Na and Si could precipitate, such as sodium silicate which could be dissolved into water during extraction. The dilution factor is at least 3,000, so it is possible to dissolve all the solute into the retrieved solutions.

Generally, the solubility of SiO₂ and TiO₂ were expected to increase with temperature (Ayers and Watson, 1993; Manning, 1994). However, with an increase of pressure, the solubility of TiO₂ decreases (Ayers and Watson, 1993; Rapp et al., 2010), whereas that of SiO₂ increases (Manning, 1994; Newton and Manning, 2000). Moreover, the solubility of TiO₂ in an aqueous fluid increases in the presence of F or Cl, with TiO₂ being more soluble in 10wt% NaF solution than in 10wt% NaCl brines (Rapp et al., 2010). In contrast, an increase of Cl concentration restrains SiO₂ from dissolving in fluid under 1 GPa (Newton and Manning, 2000). Taking the F-TiO₂ relationship as an analog for an F-bearing fluid, SiO₂ should also be more soluble in the presence of F. The calculated results show that F (at less than 0.7 wt%, much lower than 10 wt% NaF) slightly increases SiO₂ solubility.

SiO₂ concentrations of F-free experiment were not analyzed. It is impossible to compare the difference with or without F. However, all the SP2 points are higher than SP3 (Fig. 4.2.2.2b), which indicates that F promotes the dissolution of Si. Moreover, SiO₂ concentration is independent of temperature with the presence of hornblende in SP2 unbuffered experiments. 1-SP2-21 (1057 °C) is hornblende-free, and its dominant phase is melt, of which the SiO₂ activity is higher than hornblende-bearing system. The SiO₂ concentrations of two SP4 experiments, which create different phase assemblies, are significantly various. Besides clinohumite and pyroxene, they yield hornblende (843 °C) and clintonite (890 °C),

respectively (Table 3.1.4). Clintonite has lower SiO_2 concentration than hornblende, which suggests that its system has lower Si activity, so its fluid has lower SiO_2 concentration.

The correlations between F and SiO_2 are weak and positive (Fig. 4.2.2.2c). It is obvious that an increase of F concentration in fluid raises the SiO_2 concentration, especially in SP2 and SP3 group, independent with buffer conditions. However, limited by the mass balance approach, the calculated results of high melt proportion or SP4 experiments are not precise. There is no reasonable explanation for three low SiO_2 concentration SP2 experiments. Thus, the data from direct analyses are plotted in Fig. 4.2.2.2d, which shows the similar tendency. Moreover, 1-SP2-21 (1057 °C) and 1-(SP1+MgF₂) (965 °C) have a similar phase assembly (spinel, melt and humite/chondrodite), which illustrates the comparable correlation between F and SiO_2 . 1-SP4-3 & 4 have different minerals – mica and hornblende. It shows a different variation on SiO_2 solubility. Therefore, SiO_2 concentration in aqueous fluid not only relates with F, but also is influenced by the mineral species which constrain the silica activity in the system. According to the proportion of hornblende in these experiments, hornblende is a dominant species and constrains the bulk SiO_2 activity in the system. On the contrary, hydrous melt have higher SiO_2 activity because of the higher temperature and less lattice energy constraint. That is why their Si concentrations drift higher within the same F concentration.

The temperature cannot determine the relationship between Si and F concentrations (Fig. 4.2.2.2d), because their concentrations in high temperature experiments are perhaps lower than in lower temperature ones. It is consistent with the fact that D_F is temperature independent in my study.

4.2.2.3 Al₂O₃

Al concentrations in fluid are totally independent with temperatures and bulk compositions from mass balance results (Fig. 4.2.2.3a). Their direct analyses data are only from ICP-MS, and most are nearly zero. It suggests that the calculated results are not precise and Al should be treated as a conservative element for the mass balance approach. In melt-bearing experiments, Al concentrations reach approximately 0.4 wt%, and are lower than the mass balance results.

Al is an important element to build the structure of hornblende and pyroxene, but it is different from Si. Mysen and Armstrong (2002) reported their experiments on solubility behavior of aluminasilicate components in fluid, of which solubility of SiO₂ is up to 25 times more than that of Al₂O₃ in aqueous fluid (in mol%, which equals to approximately 10 times in wt%). It indicates that the saturation of alumina in fluid is much lower than silicate. Wohlers et al. (2011) reports that albite solubility along with paragonite and quartz is from 0.029 – 0.053 mol/kg (0.078 – 0.143 wt%) at 500 °C and 1 GPa, while the solubility of Si is 5 to 10 times of Al (in mol/kg). Some of my experiments have spinel crystals, which states that alumina precipitates as spinel when the solution is Al-saturated. Some spinel crystals are too small to be analyzed. Consequently, Al₂O₃ concentrations from ICP-MS are probably much closer to the real values than mass balance.

SP2 experiments show Al₂O₃ solubility is dependent with temperature, which increases clearly when temperature is above 950 °C (Fig. 4.2.2.3b). Perhaps, the presence of melt helps to dissolve alumina into fluid. Moreover, the Al₂O₃ concentration of 1-SP2-23 is also plotted in Fig. 4.2.2.3b. Although its fluid composition is considered as concentrated, the result constrains an upper limitation for Al₂O₃ concentration. It shows the consistent tendency between Al₂O₃ concentration and temperature.

Furthermore, the increase of F concentration may improve the Al₂O₃ solubility. For example, Al₂O₃ solubility from SP2 experiments is higher than that from SP3 ones. While SP3 and SP4 bulk compositions are not comparable, for SP4 is Mg-richer than SP3. It is hard to compare the improvement by F in different bulk composition systems. Nevertheless, more SP3 and SP4 fluid compositions data are necessary to support this argument. However, no

matter plotted in arithmetic scale or log scale (Fig. 4.2.2.3c), Al_2O_3 concentration in fluid positively correlate with F concentration, except the highest temperature experiment (1057 °C). It is easy to understand that 1-SP2-21 at 1057 °C has a hornblende-free phase assemblage. Spinel and melt have higher alumina concentration than hornblende, so alumina activity in this experiment is higher than other SP2 experiments.

Under ambient P-T condition, alumina is insoluble; solubility of AlF_3 and $\text{Al}(\text{OH})_3$ are 0.67g/100mL and 0.0001g/100mL (20 °C), respectively, which indicates the presence of F can promote Al solubility by form different species. Moreover, solubility of AlF_3 increase from 0.56g to 1.72g as temperature rises from 0 to 100 °C. It is consistent that alumina concentration is positively correlative with temperature as well as F concentration. Moreover, AlF_3 is a covalent compound, and can form a polymer, but the low concentrations of Al and F are hard to compound as a polymer during anneal. F is detected as fluorine ion by HPLC, and some experiment HPLC results agree with their mass balance result well. Therefore, Al is present in fluid as a cation after quench. But during anneal, it is probable for F to react with Al and promote its solubility.

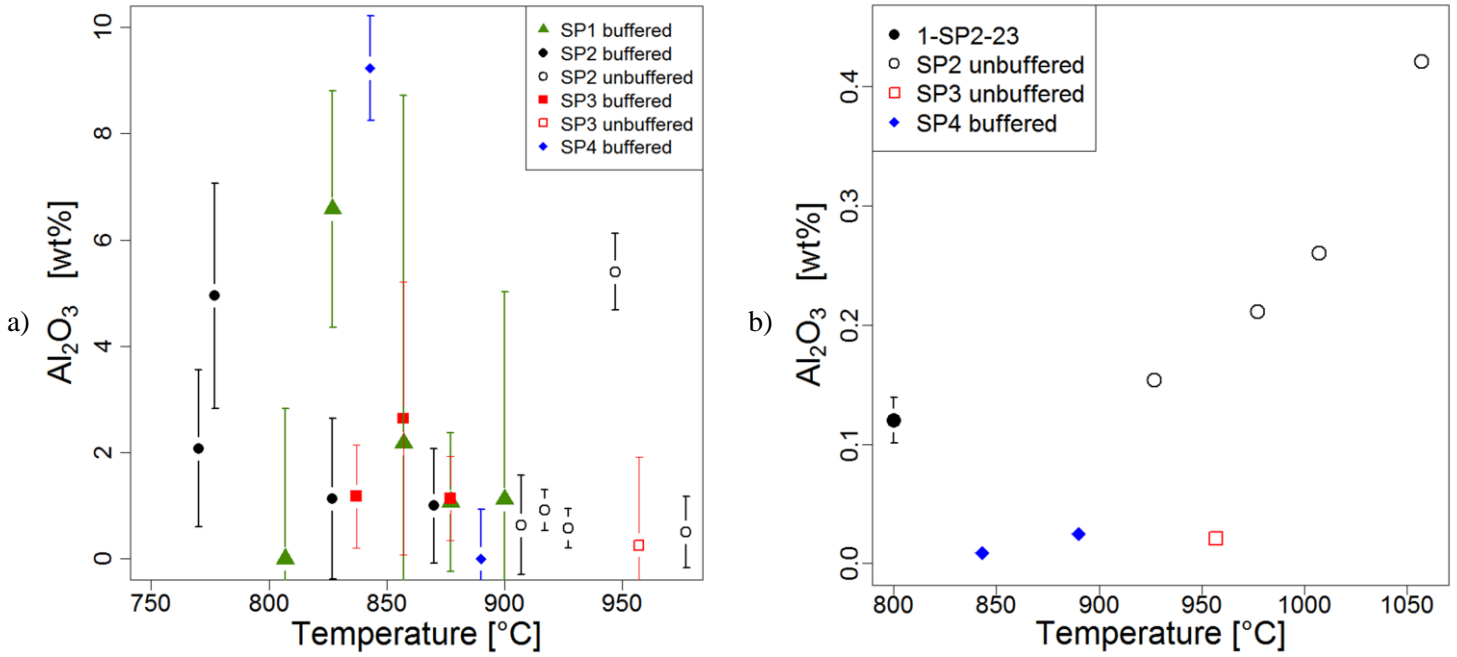


Fig. 4.2.2.3 Comparisons of Al_2O_3 concentrations in fluids at 1 GPa. a) Mass balance results. b) Direct analytical results. The relative error bars of direct results are less than 1%.

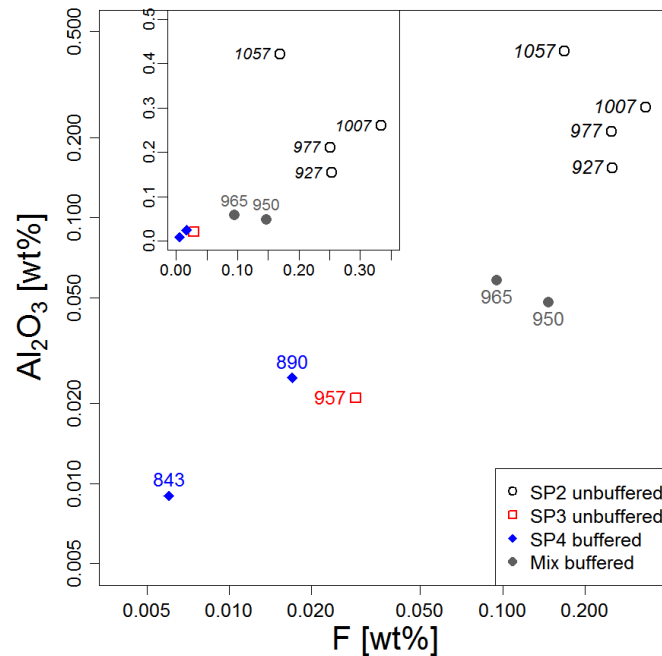


Fig. 4.2.2.3c Al_2O_3 vs. F concentrations in fluid (HPLC and ICP-MS analyses). The experimental temperature is shown beside each point. Both axes of big figure are in log scale. The relative error bars of direct results are less than 1%.

4.2.2.4 MgO

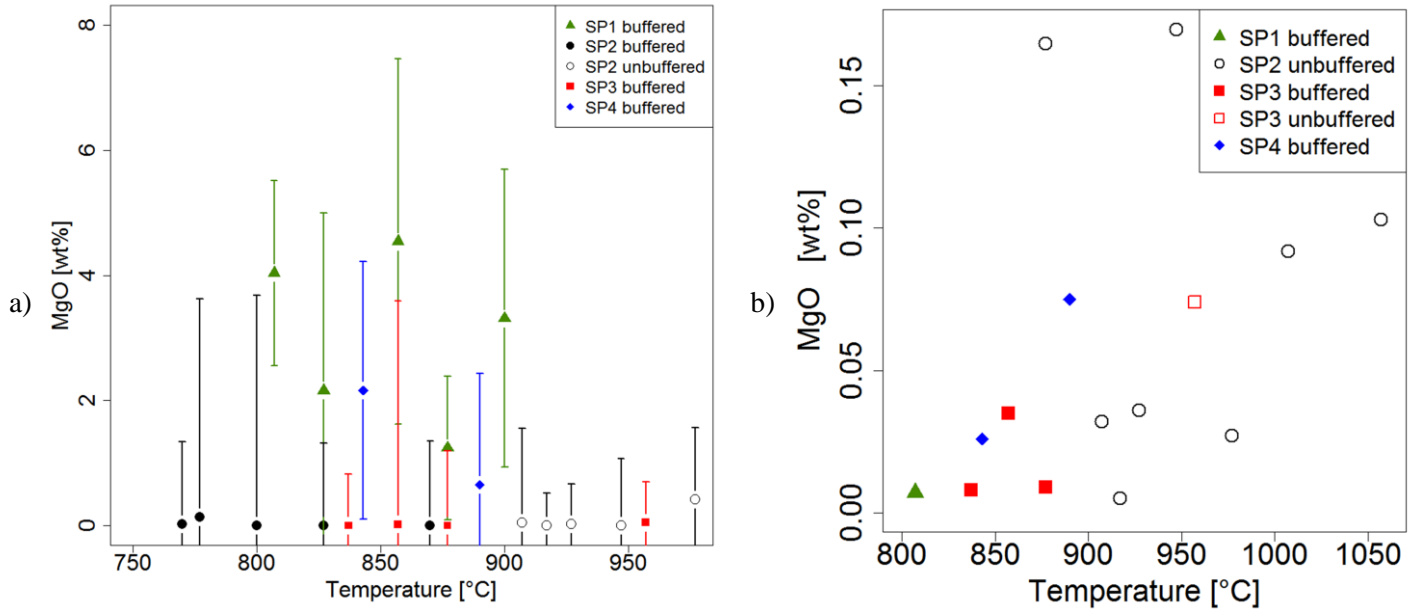


Fig. 4.2.2.4 Comparisons of MgO concentrations in fluids at 1 GPa. a) Mass balance results. b) Direct analytical results. The relative error bars of direct results are less than 1%.

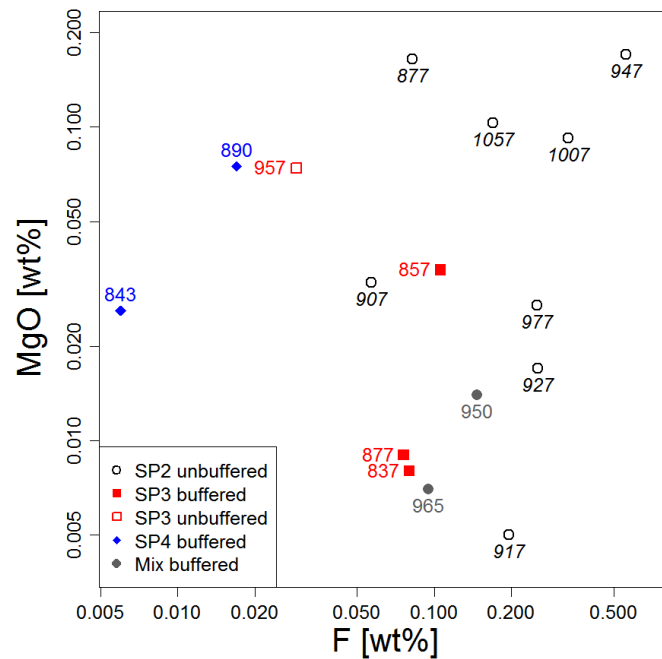


Fig. 4.2.2.4c MgO vs. F concentrations in fluid (HPLC and ICP-MS analyses). The experimental temperature is shown beside each point. Both axes of big figure are in log scale, and of small figure are in arithmetic scale.

The mass balance results show that MgO is dissolved into fluid in SP1 experiments. The introduction of MgF₂ into the solid starting powder contributes more Mg, but its solubility is nearly zero in the presence of F, since F promotes the growth of humite group minerals by associating with Mg (Fig. 4.2.2.4a). SP4 fluids have higher MgO concentrations than SP2 and SP3 (Fig. 4.2.2.4a), because of its lower bulk F concentration (0.5 wt%). However, HPLC analysis of 1-SP1-8 shows its MgO concentration is 0.007 wt%, much lower than calculated result. It indicates either the presence of another Mg-bearing mineral phase or insolubility of the residual MgO material. Moreover, ICP-MS results show that MgO concentrations of SP4 fluids are similar those of most SP2 and SP3 experiments. They demonstrate that the selection of Mg as conservative element is reasonable, but the soluble Mg species is independent with F concentration from the direct analyses, and insoluble Mg may precipitate into quench phases.

On the other hand, the mass balance calculations cannot give reasonable F concentrations for SP4 experiments, and indeed their MgO concentrations are of large uncertainties. Moreover, SP1 may precipitate pyroxene which can incorporate Mg. Therefore, the results of ICP-MS are closer to the actual values. However, it is impossible to argue the relationship between MgO concentration and temperature from mass balance results, so the direct analytical results are plotted in Fig. 4.2.2.4b. Two abnormal high concentration values at 877 (1-SP2-14) and 947 °C (1-SP2-18) are probably caused by their low fluid proportion (approximately 40% relative to the solid mass) after quench. This suggests that the low fluid proportion not only affect the mass balance results, but also influence the fluid extraction for the direct analysis. Similarly, the fluid mass of another two SP2 buffered experiments 1-SP2-23 & 24 are 10 % and 22 % relative to the anhydrous powder quantity, so their results are not discussed. Other data are less than 0.1 wt%, and illustrate that MgO concentration is slightly dependent with temperature but independent of F concentrations in bulk composition. Furthermore, the direct measurement results from HPLC and ICP-MS are plotted in Fig. 4.2.2.4c. It illustrates that MgO concentration does not change systematically with F in each series experiments, but scatter in the picture.

Humite group minerals contain Mg(OH, F)₂, as a part in their structure, which is combined just by ions. It is different from Mg₂(SiO₄), of which Si and O build the main

structure of minerals. The presence of F promoting the crystallization of norbergite is probably improved by MgF_2 precipitate. However, $K_{\text{SP}}(\text{Mg}(\text{OH})_2) = 1.5 \times 10^{-11}$, and $K_{\text{SP}}(\text{MgF}_2) = 5.16 \times 10^{-11}$ at the standard state. Their similar solubility product constants indicate that F and OH have the same ability to precipitate Mg. Assuming their K_{SP} are still close to each other at high P - T condition, the Mg solubility is controlled by OH and F concentrations. While under NNO buffer conditions, OH concentration is very low, and cannot precipitate Mg as $\text{Mg}(\text{OH})_2$. In my experiments, F promotes the Mg precipitation and constrains Mg concentrations in fluid, and F concentration can determine the equilibrium between humite group minerals and the aqueous fluid. It is reasonable to consider this problem from two aspects:

1) Mg, Si, and F concentrations are constrained by the solubility product of humite group minerals. Generally, solubility product constant is to describe the solubility behavior of ionic compound. The main structure of silicate minerals are made up by Si-O covalent bonds, and other divalent cations enter its void, so silica structure is quite different from ionic compound. However, olivine and humites are the simplest silicate minerals, and the presence of F leads to the formation of $\text{Mg}(\text{OH}, \text{F})_2$ as a part of humites. Thus, I suppose that the precipitate mechanism of humite minerals probably relates with the concept of K_{SP} . It must not be the unique constraint, since the mineral growth is an ordered process. Moreover, the solution mechanisms of silicate and silica species in aqueous fluids during high pressure and high temperature experiments have been discussed. Silicic, orthosilicic, and pyrosilicic anions are suggested to present in aqueous fluids at high P - T conditions (e.g., Newton and Manning, 2000; Mysen and Armstrong, 2002; Mysen, 2009). In my study, Mg, Si, and F are all detected in extraction fluids under room P - T condition, which indicates that they are present in fluids as ion species. Thus, it is possible to investigate the precipitate mechanism of humite group minerals from calculating the ion product of the fluid compositions.

2) Mass balance calculations do not work well for one-mineral assemblage experiment. It led to too high MgO concentration. By far, only one SP1 experiment fluid is analyzed by HPLC, and its MgO concentration has the lowest MgO concentration comparing with SP2 fluids. More direct analyses for SP1 experiment fluid compositions are necessary to compare with F-bearing experiments. Majority Mg compounds are not soluble in fluid. When silica

concentration reaches approximately 5 wt% in the fluid, it must draw down other silicate compatible elements concentrations. Mg^{2+} and SiO_4^{4-} can constrain the concentration of each other because olivine (Mg_2SiO_4) solubility in fluid is quite low.

4.2.2.5 CaO

Calculated CaO concentrations are mostly zero (Fig. 4.2.2.5a). The Ca concentrations in SP2 and SP3 experiments should be relative with that of hornblende. In SP2 experiments ($T > 940 \text{ }^\circ\text{C}$), melt incorporates more Ca than hornblende, but it does not change calcium concentrations in fluid. Either mass balance calculations or direct analyses results show that the Ca concentrations are generally less than 0.1 wt%. It can reach approximately 0.3 wt% when temperature is higher than $1000 \text{ }^\circ\text{C}$ (ignore the highest one from 1-SP2-18 with low fluid proportion). Pyroxene in SP4 experiments contains Ca, but their calculated results are not reliable. ICP-MS results show their Ca concentrations in fluids are close to zero. It verifies that Ca can be set as a conservative element for mass balance perfectly in my study. Furthermore, Ca concentration in fluid is independent with F concentration of bulk composition, but increases when temperature is higher than $950 \text{ }^\circ\text{C}$ (Fig. 4.2.2.5b).

The direct analyses results (CaO vs. F) are scattered in Fig. 4.2.2.5c. All the figures illustrate that Ca is similar with Mg in Fig. 4.2.2.4. Mg and Ca are alkaline earth elements, so they have similar chemical characters. In my experiments, it is hard to dissolve them in the fluid with the presences of fluorine ion. According to its bigger ion diameter, Ca cannot enter humite group minerals to replace Mg. The hornblende proportion decreases with an increase of F concentration, but Ca was not released into fluids and stay in hornblende in SP2 and SP3 experiments. It made the Ca concentrations in hornblende increase as the sequence of SP1, SP3 and SP2. SP4 has pyroxene as a Ca reservoir.

The abundances of Mg are larger than Ca in bulk compositions, but the direct analyses show that Mg and Ca concentrations in fluid are comparable. They do not have significant relationship with F concentrations in fluid. It indicates that Mg and Ca are indeed difficult to dissolve into the fluid, regardless of their concentrations in bulk compositions.

Most direct measurements demonstrates that Ca concentrations in the systems are less

than 0.1 wt%, only 3 high temperature experiments are above 0.2 wt%, at least twice of others. As their temperatures shown beside the points, it is clear to claim that Ca concentration in fluid is independent of temperature and F concentration.

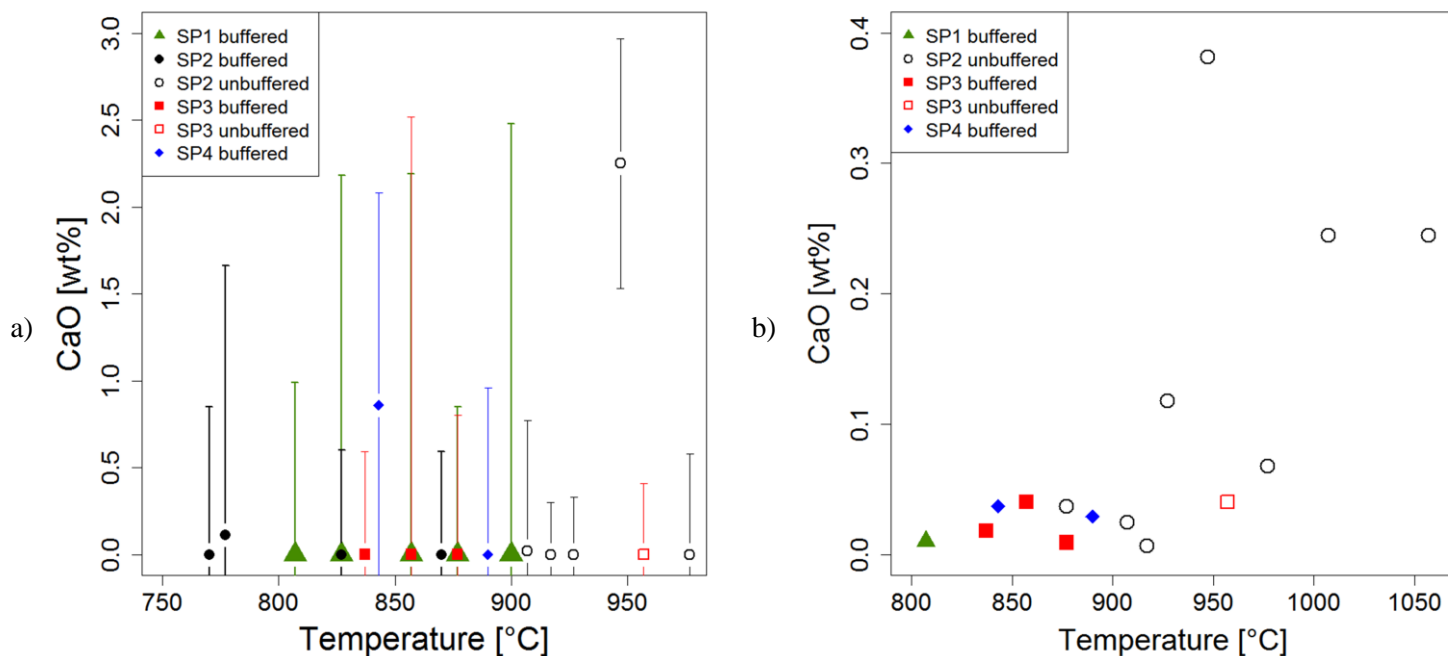


Fig. 4.2.2.5 Comparisons of CaO concentrations in fluids at 1 GPa. a) Mass balance results. b) Direct analytical results. The relative error bars of direct results are less than 1%.

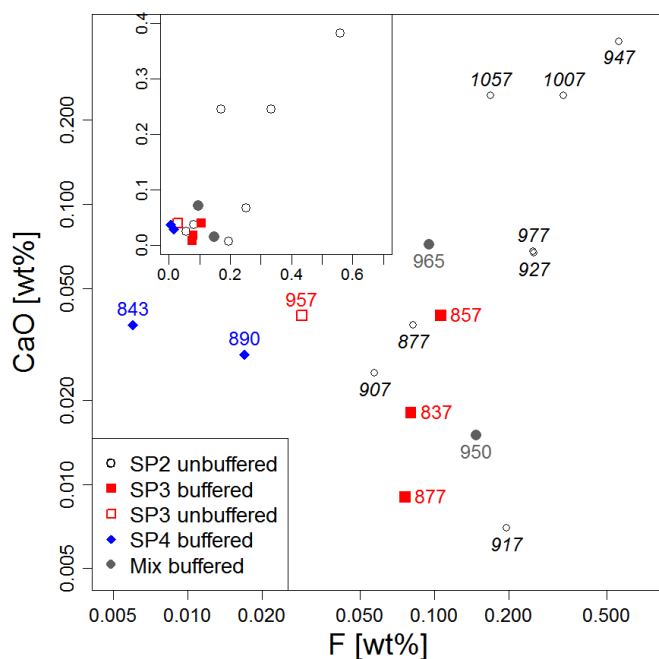


Fig. 4.2.2.5c CaO vs. F concentrations in fluid (HPLC and ICP-MS analyses). The experimental temperature is shown beside each point. Both axes of big figure are in log scale, and of small figure are in arithmetic scale. The relative error bars of direct results are less than 1%.

4.2.2.6 FeO

In bulk compositions, FeO concentrations are approximately 3 – 4 wt%. Because Fe has +2 and +3 valences, it can be present in humite group minerals and hornblende. Most mass balance calculations treated Fe as a conservative element. ICP-MS analyses confirm its low concentrations level. The highest FeO concentration is approximately 0.05 wt%.

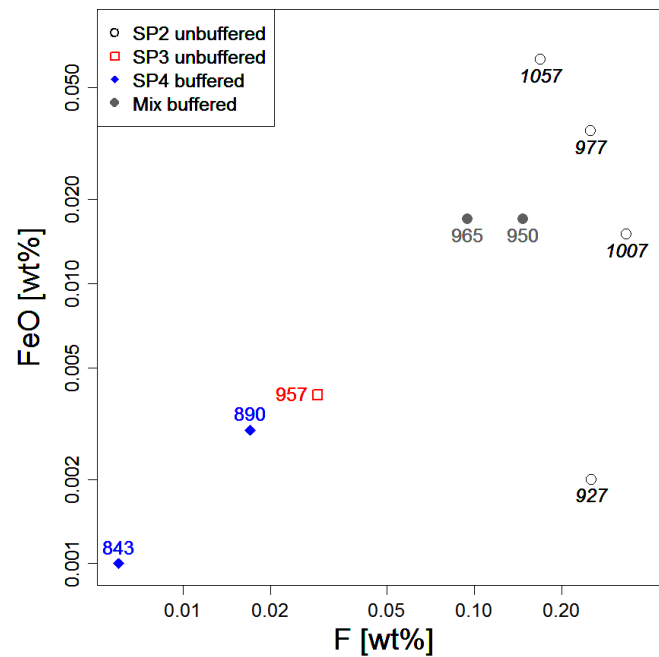


Fig. 4.2.2.6 FeO vs. F concentrations in fluid (HPLC and ICP-MS analyses). The experimental temperature is shown beside each point. Their uncertainties are not shown here. Both axes are in log scale. The relative error bars of direct results are less than 1%.

Fig. 4.2.2.6 illustrates that no obvious correlation between Fe and F concentrations of fluids or temperature. FeF_2 has a similar structure with MgF_2 , but is soluble in water. FeF_3 is similar with AlF_3 , and insoluble as well. The species of Fe ions in fluid are complicated to discuss. Under oxygen fugacity of $\Delta\text{NNO}-1$ and around 1200 °C, amphibole and co-exist melt have close $\text{Fe}^{3+}/\text{Fe}^{\text{total}}$ value (~50%) (King et al., 2000). Ayers et al. (1997) shows that NNO buffered capsule can reduce hematite to magnetite. Thus, $\text{Fe}^{3+}/\text{Fe}^{\text{total}}$ is consistent. Assuming $\text{Fe}^{3+}/\text{Fe}^{\text{total}}$ in fluid is also nearly 0.5, it indicates that the relationship between Fe and F are similar with the total effect of Al and Mg. Finally, Fe behaviors can be similar with Al or Mg, which is determined by the $\text{Fe}^{3+}/\text{Fe}^{\text{total}}$.

4.2.3 Influences of Pressure

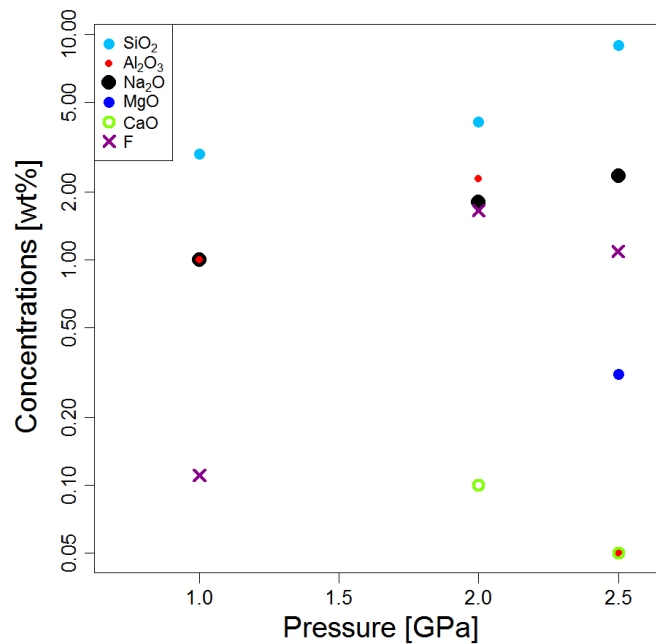


Fig. 4.2.3 Major element concentrations in fluid of SP2 experiments versus pressure (mass balance results). 1 GPa experiment (1-SP2-4) is at 870 °C, and 2 and 2.5 GPa experiments are at 877 °C. The y axis is in log scale. MgO and CaO concentrations of 1.0 GPa experiment are zero, as well as MgO at 2.0 GPa.

The researches on the major element solubility of silicate show that the increase of pressure improves their solubility, e.g. SiO₂, TiO₂, and Al₂O₃. The mineral assemblage change which indicates phase change can make solubility decrease. However, most silicate solubility increase as pressure increases. Three experiments are plotted in Fig. 4.2.3. Their experimental temperature is around 870 °C. Except CaO and Al₂O₃, other elements solubility of 2.0 and 2.5 GPa experiments are higher than those of 1 GPa experiment.

In F-bearing experiments, F stabilizes the hornblende to a larger P-T region. In SP2 experiments, hornblende breaks down between 2 to 2.5 GPa and then crystallize hydrogrossular, while if F concentration is down to hundreds ppm, hornblende will break down below 1.5 GPa. In Fig. 4.2.3, the mineral assemblage of SP2 remains from 1 to 2 GPa, and the solubility of all the elements increase, except Mg which remains zero. The phase assemblage changes to hydrogrossular-augite-norbergite at 2.5 GPa. The solubility of F and Ca decrease, but others increases. The presence of the high F concentration leads to something interesting, e.g., the substitution of Si by OH and F, or X_F value in norbergite.

4.2.4 Summary

Bulk compositions (SP1 – SP3) have similar major element concentrations, except F. They determine the mineral species and phase assemblages. Moreover, most of the cations are difficult to dissolve in water, and other element concentrations are relatively constant relative to bulk compositions.

The concentration of each element in fluid is temperature independent, except Al. ICP-MS results show Al concentrations of SP2 fluid increase with an increasing temperature (see 4.2.2.3). However, experimental determination on the quartz solubility in water suggests that it correlates with temperature (Manning, 1994). Meanwhile, it should be noted that the influence of F on solubility of TiO_2 ranges more pronounced than the influence of variations in temperature. From 700 to 1100 °C, Ti solubility ranges from 212 to 470 ppm in F-free fluid, while in systems with F-rich fluids, corresponding to the variation from 20 to 100 times the values in pure H_2O (Rapp et al., 2010). It is reasonable to treat the similar effect on silica dissolution. In my experiments, the silica activity is lower than quartz, the temperature region is small, and F concentrations in fluid are various even for the same series experiments. Thus, no significant correlation between SiO_2 concentration and temperature is shown from my results. Moreover, the mass balance results show that the presence of F in bulk compositions improves the Na and Si concentrations, and decreases Mg concentration. In summary, F appears to increase SiO_2 solubility, and decrease MgO solubility in the aqueous fluid. F-bearing fluid promotes precipitation of Si-poor, Mg-rich phases through incongruent dissolution of hornblende.

In F-bearing experiments, only SiO_2 and Al_2O_3 concentrations in fluid correlate with F concentrations, while other elements concentrations i.e., Na, Ca, Mg and Fe in fluid do not relate with F. Moreover, SiO_2 is soluble in aqueous fluid under high P-T conditions. Al_2O_3 concentrations in fluids are much less than SiO_2 . In quartz-paragonite-albite system, its fluid contains 0.17 wt% alumina and 1.68 wt% silica at 1 GPa and 500 °C (Wohlert et al., 2011). Their solubility differences are consistent with ICP-MS analyses for my experiments. There are two explanations about the solubility differences between Si/Al and other metal cations:

- 1) The minerals in my experiments are silicate. The bulk compositions have a large

proportion of silica and alumina. Their normal valences are +3 and +4. It is difficult for them to precipitate with F under high P-T conditions. Moreover, F may react with Si and Al to form complex compounds, which probably improves their solubility, and they can reach the saturations in fluid. However, F constrains Mg concentrations by precipitating humite group minerals. Perhaps, all divalent cations, i.e., Ca, Mg, Fe would be constrained by F concentrations in fluid.

2) The majority Al and Si in amphibole are in T site. They build the structure of the minerals, while other cations enter their interspace and balance the charges of oxygen, of which positions are essentially depended on their chemical characters and ion radii. For example, sodium is soluble in fluid, and its concentration in SP2 experiments reaches 5 wt%. In A site of hornblende, it only takes 30%, not 100%, because its entrances to A site is constrained by Al substitution of Si in T site in hornblende to balance the charges. If the Al abundance in hornblende increase, it is possible to increase Na abundance (e.g., the hornblende from SP4 experiments). Therefore, F does not correlate with sodium concentrations directly. For divalent cations, once they are captured by the minerals, it is hard for them to exchange with fluid, unless the mineral breaks down. For example, the researches on trace elements partitioning in the minerals usually crystallize new minerals but not utilize the diffusion method to reach the equilibrium. While the main silicate structure of Si and Al can react with the fluid directly, it is easy for them to reach the equilibrium and no constraint from the structure.

4.3 Fluorine Preferential Phase

Partition coefficients which describe the element distribution normally depend on pressure and temperature. For example, the F and OH exchange reaction happens between hornblende and norbergite: $OH_{Hb}^- + F_{Nb}^- = F_{Hb}^- + OH_{Nb}^-$. Its reaction constant (K) is a function of ΔH and temperature. $\ln K = -\frac{\Delta H}{RT} + B$. Here, B is the intercept from linear regression. However, $\ln K = \ln \gamma + \ln D_F^{Hb/Nb} - \ln D_{OH}^{Hb/Nb}$, so $\ln D_F$ should also relate with $1/T$. I have calculated the linear regression between D_F and $1/T$ for a series of isobaric experiments to determine the temperature dependence (Fig. 4.3.1.1).

I use the software OriginPro 8 for a linear fit $D_F^{Hb/Nb}$ or $D_F^{Hb/Chd}$ and $10000/T$ of each experiment with their uncertainties. For SP2 buffered experiments, $\ln D_F^{Hb/Nb} = (-0.008 \pm 0.049) \times \frac{10000}{T} + (-2.029 \pm 0.450)$, $r^2 = -0.24$. For SP2 unbuffered experiments, $\ln D_F^{Hb/Nb} = (0.033 \pm 0.115) \times \frac{10000}{T} + (-2.213 \pm 0.985)$, $r^2 = -0.22$. For SP3 buffered experiments, $\ln D_F^{Hb/Chd} = (-0.092 \pm 0.110) \times \frac{10000}{T} + (-0.844 \pm 0.967)$, $r^2 = -0.06$. Their r-squared are given as negative values, because the standard deviations of their slopes are larger than the slopes themselves. It demonstrates that $D_F^{Hb/Nb}$ and $D_F^{Hb/Chd}$ is temperature independent in the 1-GPa experiments. It is not reasonable to treat the data with linear fitting. A similar F partitioning occurs between olivine and melt (Beyer et al., 2012). With their results, the linear fitting result is $\ln D_F^{olivine/melt} = (1.69 \pm 2.77) \times \frac{10000}{T} + (-16.61 \pm 16.58)$, $r^2 = -0.46$. R-squared value also shows the temperature independence.

This also becomes visually clear from Fig. 4.3.2.1, where D_F between fluid and the different minerals are effectively temperature independent from 770 to 947 °C within the uncertainties of each experiment. I report the D_F determined by using weighted average values for sets of experiments grouped by the starting composition and by presence or absence of an oxygen buffer. The weighted average and its uncertainty will be calculated by formula 4.3a and 4.3b.

$$\widetilde{D}_F = \frac{\sum_1^n (D_F / \sigma_{D_F}^2)}{\sum_1^n (1 / \sigma_{D_F}^2)} \quad (4.3a)$$

$$\widetilde{\sigma}_{D_F} = \frac{1}{\sum_1^n (1 / \sigma_{D_F}^2)} \quad (4.3b)$$

4.3.1 Fluorine Incorporation of Minerals

Fluorine incorporation in hydrous minerals is much easier than anhydrous minerals. The hydrous species in my experiments have different fluorine incorporation ability. The D_F between minerals will reveal the fluorine preferential mineral species.

4.3.1.1 D_F between Hornblende and Humite Group Minerals

These data are plotted in Fig. 4.3.1.1 and divided in 5 groups: 1) Hb/Nb of SP2 NNO buffered experiments; 2) Hb/Nb of SP2 unbuffered experiments; 3) Hb/Chd of SP3 NNO buffered experiments; 4) Hb/Chd of SP2 unbuffered experiments and 5) Hb/Chu of SP4 buffered experiments. Their weighted average values are:

$$\ln D_F^{\frac{Hb}{Nb}}(buffered) = -2.11 \pm 0.04,$$

$$\ln D_F^{\frac{Hb}{Nb}}(unbuffered) = -1.93 \pm 0.04,$$

$$\ln D_F^{\frac{Hb}{Chd}}(SP3 buffered) = -1.62 \pm 0.08,$$

$$\ln D_F^{\frac{Hb}{Chd}}(SP2 unbuffered) = -1.45 \pm 0.07,$$

$$\text{and } \ln D_F^{\frac{Hb}{Chu}}(buffered) = -1.37 \pm 0.12.$$

Fig. 4.3.1.1 illustrates that D_F between hornblende and three humite mineral species are distinctively different in NNO buffered experiments. Notably, the F concentration of chondrodite is less than norbergite. The different partition coefficients are due to changing humite group speciation. It should be also noted that oxygen fugacity changes $D_F^{\frac{Hb}{Nb}}$ or $D_F^{\frac{Hb}{Chd}}$, caused by changing F concentration in norbergite or chondrodite. Although only four SP4 experiments were conducted, and one of them did not create hornblende but

clintonite, $D_F^{Hb/Chu}$ are consistent. Its value is close to $D_F^{Hb/Chd}$ without NNO buffer. Furthermore, the results are generally in agreement with the natural observations of an impure dolomitic limestone, in which D_F between calcic amphibole and clinohumite ranges from 0.19 to 0.33 (Rice, 1980).

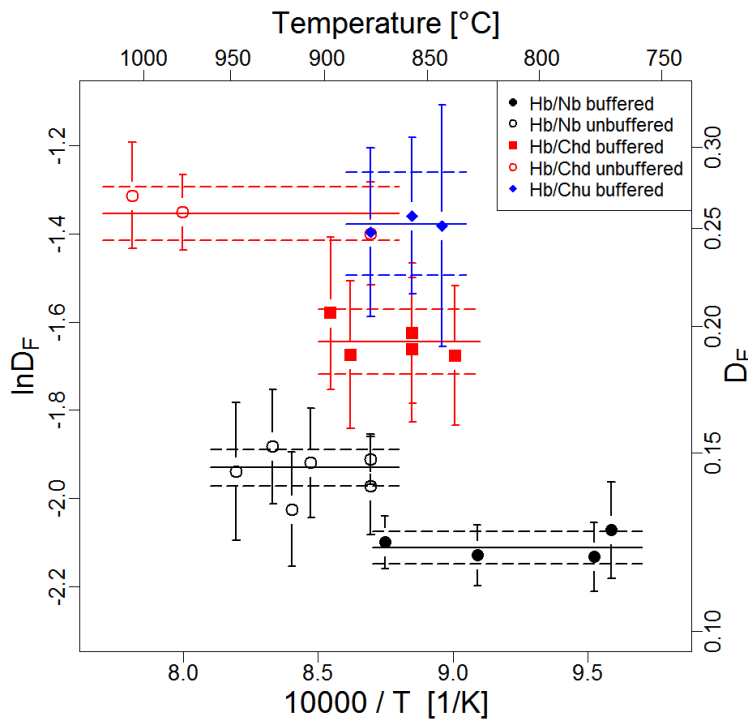


Fig. 4.3.1.1 Partition coefficients of F between hornblende and humite minerals. The solid lines are the weighted average values for each group, and dashed line pairs (above and below a solid line) indicate their uncertainties bounds (2σ). D_F between minerals appear to be temperature independent for the interval of my experiments. D_F is higher for Hb/Chd pairs, square symbol indicating hornblende-chondrodite assembly from SP3 experiments, than Hb/Nb pairs, round symbol

indicating hornblende-norbergite assembly from SP2 experiments. D_F of Hb/Chu pairs are the diamond symbol in blue. Similarly, the values of D_F are systematically larger for the experiments conducted without buffer (open symbol), than the ones with NNO-buffer (filled symbol).

The increase of pressure does not affect the D_F between hornblende and norbergite. Experiments 1-SP2-4, 2-SP2-1 and 3-SP2-1 were conducted from 1 to 2 GPa around 877 °C. Their $D_F^{Hb/Nb}$ are similar, 0.12 ± 0.02 .

4.3.1.2 D_F between Hydrogrossular and Humite Group Minerals

$D_F^{Hdg/Nb}$ are approximately 0.10 ± 0.04 , but $D_F^{Hdg/Chd}$ differ more, 0.21 ± 0.03 and 0.15 ± 0.07 . The F concentrations of norbergite and chondrodite are larger and less variable than those of hydrogrossular, so the uncertainties of $D_F^{Hdg/Chd}$ are mainly derived from

hydrogrossular. Fig. 4.3.1.2 also clearly demonstrates this discrepancy, which this can be caused by two possibilities:

1) The uncertainties of F measurements of electron microprobe are slightly high. Because either the most of hydrogrossular crystals has void, the analytical cross-section area is just enough for the measurement, or the electron microprobe analytical parameters setting is not the best. Increase current and counting time may improve the measurement.

2) The nature of hydrogrossular makes its F incorporation behavior much different from hornblende. In hornblende or humite group minerals chemical formulas, the number of OH is 2, while the OH number in hydrogrossular is depended on the number of SiO_2 replaced by H_2O . This value may not be a constant, which is from 0 – 1. This situation may cause hydrogrossular mineral composition to vary within an experiment.

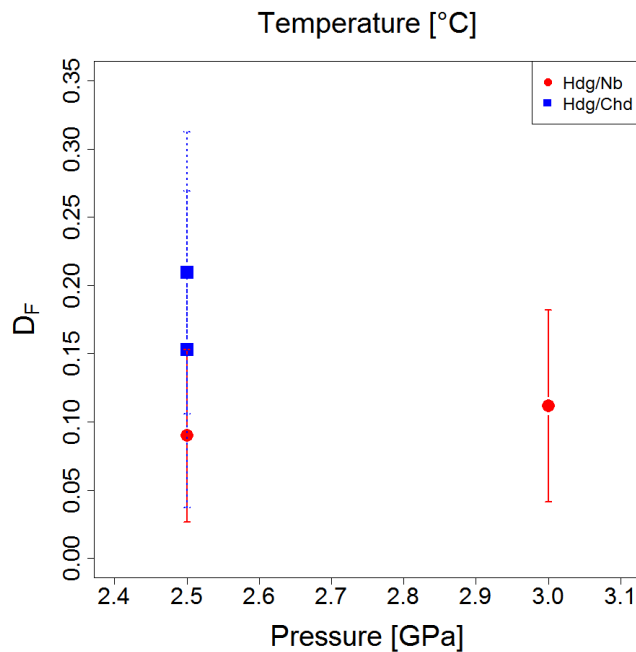


Fig. 4.3.1.2 Mineral-mineral partition coefficients of F between hydrogrossular and norbergite or chondrodite. All the experiments were conducted with NNO buffer. The blue square symbols are $D_F^{\text{Hdg/Chd}}$, and the red round symbols are $D_F^{\text{Hdg/Nb}}$. Humite group minerals and hornblende can incorporate more F than hydrogrossular, so $D_F^{\text{Hdg/Chd}}$ is lower than $D_F^{\text{Hb/Nb}}$.

In an equilibrium experiment, the same mineral have similar composition. However, in these three high pressure experiments, hydrogrossular compositions are variable. This indicates that the experiment stayed too long before reaching the conditions of hydrogrossular stability. Before the pressure reaches 2.5 GPa, and the temperature is higher than 700 °C, the rate of hornblende formation is expected to be high. When 2.5 GPa is reached, the hornblende starts to break down and nucleates hydrogrossular most likely on the surface of hornblende.

The material in the void of hydrogrossular influences the stoichiometry calculation of hydrogrossular. In fact, the number of Si is different for some points. In conclusion, these empty small spheres are not ideal for electron microprobe measurements. Two methods implementation should be employed for the future garnet-bearing experiments: 1) change the P - T path to shorten the duration for amphibole facies during the temperature increasing process; and 2) using some garnet seeds in the experiments.

4.3.1.3 Additional Results

Clintonite is present in 1-SP4-3. Two possibilities result in this: 1) Ni contamination. It will lead to the bulk composition to more ferromagnesian, for Ni and Mg have similar behaviors in mineral precipitates; and 2) the loss of the powder during anneal. Clintonite contains more Al_2O_3 and less SiO_2 than hornblende, which indicates that the depletion of SiO_2 in the capsule. With more experiments in the future, I may get the reason for this occasion.

Although the hydrous mineral transforms from hornblende to clintonite, the fluorine concentration is almost the same with hornblende, approximately 0.6 wt%. The partition coefficient of F between clintonite and clinohumite is 0.25 ± 0.07 . It is the same with D_F between hornblende and clinohumite. However, the chemical formula of clintonite contains 4OH, so it contains more water in the mineral structure. The F concentrations of clinohumite from different SP4 experiments are constant, which indicates that the F concentrations of fluids are nearly the same. It demonstrates that the incorporation of F in clintonite is less than hornblende at the same buffer condition. This difference is probably derived from the minerals species.

4.3.2 Fluorine Distribution in Minerals and Fluids

$D_F^{Fl/Min}$ are much less than 1. It suggests that fluorine is preferentially bounded to minerals, even at the high P - T conditions corresponding to upper mantle.

4.3.2.1 D_F between Fluid and Hornblende

The $D_F^{Fl/Hb}$ are determined for each group and shown in Fig. 4.3.2.1. Their weighted average values are:

$$\ln D_F^{Fl/Hb} (SP2 \text{ buffered}) = -2.33 \pm 0.97 \quad , \quad \ln D_F^{Fl/Hb} (SP2 \text{ unbuffered}) = -1.62 \pm 0.28, \text{ and } \ln D_F^{Fl/Hb} (SP3 \text{ buffered}) = -1.95 \pm 0.60.$$

Their regions of weighted standard deviation overlap with each other. Although the sample sizes are small, a Student's t-test verifies the conclusion that these three groups are not significantly different from each other. The details of the t-test are introduced in Appendix I.

Therefore, I report all the $D_F^{Fl/Hb}$ as one representative value independent of T, oxidation state and initial F abundance: 0.135 ± 0.036 .

Mass balance calculation gives a result of zero for SP4 experiments. F concentration of the fluid from 1-SP4-4 is reported with HPLC. Its $D_F^{Fl/Hb}$ is 0.011(3). It is in the same magnitude level with mass balance result.

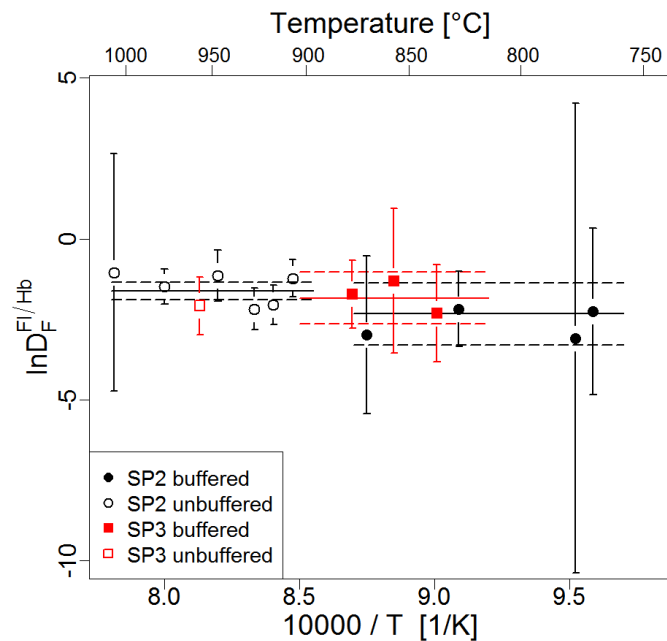


Fig. 4.3.2.1 $D_F^{Fl/Hb}$ in SP2 and SP3 experiments. X axis is $10000/T$ and its corresponding temperature axis is on the top of the figure. Y axis is $\ln D_F^{Fl/Hb}$.

4.3.2.2 D_F between Fluid and Humite Group Minerals

D_F between fluid and humite group minerals should be different, because of the variations of D_F between hornblende and humite group mineral (Fig. 4.3.1.1), but it is not obvious. The two buffered groups (Fig. 4.3.2.2) separate farther away from each other than the ones in Fig. 4.3.2.1, and t-test supports that $D_F^{Fl/Nb}$ and $D_F^{Fl/Chd}$ are significantly different. For NNO buffered experiments, the representative D_F values and their standard errors are $D_F^{Fl/Nb} = 0.010 \pm 0.010$, and $D_F^{Fl/Chd} = 0.025 \pm 0.021$. For unbuffered SP2 experiments, the mineral species transfer from norbergite to chondrodite with an increasing of temperature. Their weighted average values are quite different, $D_F^{Fl/Nb} = 0.020 \pm 0.007$, and $D_F^{Fl/Chd} = 0.059 \pm 0.032$. Even without t-test (and their sample number is too small for t-test), the values argue that $D_F^{Fl/Nb}$ is different from $D_F^{Fl/Chd}$.

The t-test cannot reject the null hypothesis that the buffer condition does not influence the partition coefficient of F, so it is feasible to classify the same D_F under different buffer conditions as one group. $D_F^{Fl/Nb} = 0.017 \pm 0.007$, and $D_F^{Fl/Chd} = 0.032 \pm 0.014$. Both $D_F^{Fl/Nb}$ and $D_F^{Fl/Hb}$ values are tested as independent with oxygen fugacity, which leads to a consistency with $D_F^{Hb/Nb}$. It demonstrates that the uncertainties of $[F]^{Fl}$ are too large to distinguish the discrepancy.

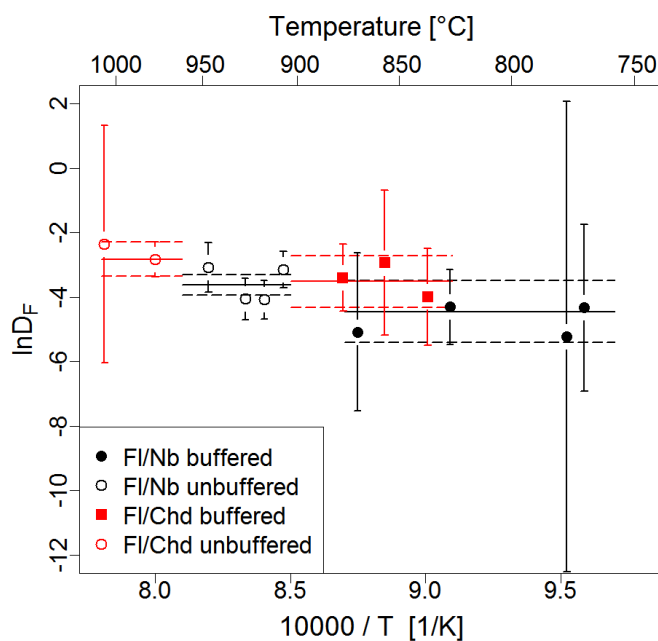


Fig. 4.3.2.2 $D_F^{Fl/Nb}$ and $D_F^{Fl/Chd}$ in SP2 and SP3 experiments. The round symbols are from SP2 experiments and the square symbols are from SP3 experiments. X axis is $10000/T$ and its relative temperature axis is on the top of the figure. Y axis is $\ln D_F$.

The fluorine concentrations of 1-SP4-3 & 4 experiments are given as 0 by mass balance calculation. HPLC results calculate the average $D_F^{Fl/Chu}$, which is 0.005. It is lower than $D_F^{Fl/Nb}$ or $D_F^{Fl/Chd}$, calculated by mass balance approach. In conclusion, humite group minerals incorporate F much more than aqueous fluid.

4.3.2.3 D_F between Fluid and Hydrogrossular

I only have one successful experiment, which contains hydrogrossular at 2.5 GPa by far. From mass balance calculation, $D_F^{Fl/Hdg}$ is 0.92(52), and from HPLC measurement, it is 0.05(2). This huge difference is expected from two reasons: 1) Partial solute precipitates into the quench phase as soon as the experiment quenched; and 2) this capsule is opened by chance when I cut its cover with a lathe, which may lead to some fluid loss during this process and an increase of the concentration of fluid by mass balance calculation. Anyway, the true D_F value probably is between 0.05 and 0.92.

4.3.2.4 D_F between Fluid and Melt

Experiments 1-SP2-18 to 21 and 1-(SP1+MgF₂) created a similar compositional melt, which has lower FeO concentration and higher F concentration than natural basalt composition (Tables in Section 3.3.5). This kind melt contains approximately 40 wt% SiO₂, 3 wt% FeO and 25 wt% MgO+CaO. Their F concentrations are from 5 to 9 wt%, and are higher than hornblende.

$D_F^{Fl/melt}$ (1-SP2-19 & 20) ranges from 0.08 to 0.11 with mass balance approach. Other experiments with high melt proportion are given F concentration as 0. From HPLC measurements, the corresponding $D_F^{Fl/melt}$ is from 0.011 to 0.053.

While in 1-SP2-20, a high silica melt is also present. It contains 84 wt% SiO₂, 7 wt% Al₂O₃ and 0.88 wt% F. Its $D_F^{Fl/silica\ melt}$ is 0.81, and is higher than other $D_F^{Fl/melt}$. In 1-(SP2+Qtz) experiment, the melts have a similar composition with the former one, but with a little higher CaO and lower Al₂O₃ concentration. This subtle difference leads to the F concentration increase to 2 wt%. With HPLC measurement result, its $D_F^{Fl/melt}$ is 0.072(18). All above

indicate that the F concentration is quite relative with the melt composition. It is easy to find that high silica melt with little MgO and CaO is difficult to incorporate F. The more MgO and CaO in the melt promote its F incorporation.

4.3.3 Summary

With the F distribution information of my experiments, it is obvious to get a general sequence that fluorine preferential incorporation: Mg/Ca-rich silicate melt, hydrous minerals (humite group minerals, amphibole, mica, and hydrogrossular), aqueous fluids, and anhydrous minerals. Therefore, it is difficult for aqueous fluid to dissolve fluorine with the presence of the amphibole or humite group minerals. In the following section, I will qualify the F budget transport via aqueous fluids with the constraints of my experiments.

4.4 F Transport Budget from Subducting Slab at Amphibolite Facies

The aim of this study is to estimate how much F can be transferred from subducting slab to subarc mantle. Most of my experimental conditions are limited in amphibolite facies, where amphibole minerals are stable. From this study, $D_F^{Fl/Hb}$ is the most important for modeling the F partitioning in subducting slab. Before the temperature and pressure start to break down the amphibole, the D_F value is useful for the model calculation of their dehydrated process. Typical amphibole with trace level fluorine concentrations will break down at pressure of less than 2 GPa. In this section, I will use three methods from the study results to estimate the quantity of F that can be transferred from an amphibole slab by aqueous flux.

4.4.1 F Saturation Constraint in Fluid

From the mass balance calculations, the weighted average concentrations of fluids are $[F]_{SP2}^{Fl} = 0.27\%$, $[F]_{SP3}^{Fl} = 0.19\%$, and hornblendes are $[F]_{SP2}^{Hb} = 2.20\%$ and $[F]_{SP3}^{Hb} =$

1.43%. The presence of F will co-precipitate humite group minerals with hornblende. Norbergite of which X_F is nearly 1 is saturated by F in that system. Moreover, in an excess doped experiment 1-(SP2+MgF₂), pure MgF₂ phase was found. It suggests that the system is saturated with F. Hornblende disappears and norbergite remains. Because their norbergite compositions are similar, the Hb-Nb-F1 paragenesis of SP2 experiments indicates F saturation at a maximum of 2700 ppm F, limited by solubility. The model calculation by Eiler et al. (2000) show that 0.5 – 1.0 wt% of slab-derived material is added to the sources of mantle-derived arc magmas. Then the F concentration in sub-arc magma sources increase 14-27 ppm from typical depleted mantle values (14 ppm, Le Voyer et al., 2010). This would lead to a maximum F increase by a factor of 2 in the region of magma genesis. Norbergite is rarely observed in metamorphic rocks derived from a subducting slab, whereas clinohumite has been reported (Yang, 2003; Garrido et al., 2005). Therefore, this value can be considered as a theoretical maximum; slab-derived fluid must carry less F to sub-arc mantle than the estimate above.

4.4.2 Constraint with X_F Model

In Eq. 4.1.2.1c, R value (ratio between F and OH concentration) of the NNO buffered capsules is higher than that in unbuffered capsules. The parameter b is a constant. Assuming arbitrary values for b , the black curve in Fig. 4.4.2.1a illustrates the evolution of X_F in norbergite, with two X_F norbergite values (>0.99 and ~ 0.80) shown on the curve. It should be noted that the sigmoidal shape of the function (Eq. 4.1.2.1c) is constant regardless of the b value. Because the F concentration in SP3 is approximately 40 % of SP2, the ratio of [F]/[OH] decreases under the same experimental conditions, and the X_F of chondrodite decreases to 0.69. Assuming $X_F^{Nb} = 0.993$, $X_F^{Chd} = 0.69$, [OH] is a constant at the same $P-T$ conditions, and $[F]_{SP3}^{Flu}(1900ppm) = 0.7 \cdot [F]_{SP2}^{Flu}(2700ppm)$, then $b^{Chd} = 45b^{Nb}$. For example, I set $b=25$ in Fig. 4.4.2.1a to illustrate the Eq. 4.1.2.1c. The red curve in Fig. 4.4.2.1a represents the X_F of chondrodite. The exchange reaction 4.1.2.1b leads to a simple relationship between X_F and the ratio of [F]/[OH] in the fluid.

4.4.2.1 X_F Model Suitability

This curve is similar with traditional chemical titration curve. The significant X_F variation takes place within a three orders of magnitude variation, which I call it the X_F **sensitive area** to $[F]/[OH]$ ratio. Depending on the difference between the constant b of minerals, the X_F sensitive areas for different minerals vary. X_F of norbergite is sensitive to the increasing of oxygen fugacity, while hornblende not. In principle, the X_F value of hornblende should be influenced by oxygen fugacity, or essentially by the $[F]/[OH]$ ratio changes. However, X_F^{Hb} is constant within the uncertainties regardless of presence or absence of the NNO buffer in this temperature region. It shows that X_F^{Hb} is less sensitive than norbergite to changes in the oxygen fugacity. Three possibilities can affect this:

1) The structure and chemistry of hornblende are more complex than norbergite. Its OH site proportion is less than humite group minerals. F and OH exchange reactions between hornblende and fluid are more difficult. Moreover, hornblende can accommodate both Fe^{2+} and Fe^{3+} ions in its structure. While Fe concentration in hornblende increase slightly in unbuffered experiments, Fe charge compensation perhaps influence selective attraction of F and OH in hornblende, maintaining a relatively unchanging equilibrium constant between fluid and hornblende.

2) The decrease of the ratio between the activity of F and OH in SP2 experiments does not reach the X_F sensitive area, which can change X_F^{Hb} significantly. Nevertheless, X_F^{Hb} decreases slightly when the melt is present in the capsule. It demonstrates that X_F^{Hb} is stable just around the temperature region of 750 to 950 °C at 1 GPa.

When the temperature is above 940 °C, X_F^{Hb} of SP2 experiments show a decreasing trend in Fig. 4.1.1.1. Meanwhile, humite species transform from norbergite to humite, which is also accompanied with a decrease of X_F (Fig. 4.1.1.2.1). As a whole, their X_F also decreases slowly with an increasing of temperature, especially after 940 °C. Because of the presence of melt of which F concentration is approximately 6 – 8 wt%, $[F]^{Fl}$ decreases. When temperature is higher, the oxygen fugacity of NNO buffer and the fugacity coefficient of water will increase as well. Therefore, their R values obviously decreases, which leads to X_F^{Hb} decrease. This observation states that X_F^{Hb} also accord with Eq. 4.1.2.1a & c. The difference between

hornblende and norbergite is the value of b . When the oxygen fugacity increases, R decreases. This change plots in the X_F sensitive area of norbergite, but not hornblende. It is probably the reason that X_F^{Hb} is constant when the oxygen fugacity changes from 750 to 950 °C. It also indicates hornblende is close to its F saturation in SP2 experiments.

3) The F concentration in hornblende is less than norbergite. I do not have amphibole standard for electron microprobe calibration, so its F concentration (~2 wt%) may suffer a large uncertainty, which leads to the insensitivity of the X_F^{Hb} . X_F^{Hb} changes cannot be recognized within their uncertainties.

X_F^{Hb} from SP3 and SP4 buffered experiments are relatively constant in each group. Similar with the occasions of SP2 experiments, although their oxygen fugacity should increase with the increase of temperature, the R of each group does not change enough to reach the sensitive area. However, with the F concentration decrease of bulk compositions, X_F^{Hb} decrease obviously from SP2 (5 wt% F) to SP4 (0.5 wt% F). A similar conclusion happened to the X_F values of humite group minerals. Although the species of humite changes from SP2 to SP4 in buffered experiments, their X_F values decrease as the F concentration decreases.

Fig. 4.1.1.2.1 show a decrease trend of X_F when temperature increases except some abnormal results. For example, 1-SP2-14 experiment created norbergite and chondrodite, which was explained as the loss of bulk composition. 1-SP4-3 experiment created a different phase assembly. In order to excluding this disruption, the ratios of X_F between hornblende and humite group minerals are plotted in Fig. 4.4.2.1b.

In NNO buffered SP2 and SP3 experiments, $D(X_F)^{\text{Hb/Nb}}$ (~0.5) is higher than $D(X_F)^{\text{Hb/Chd}}$ (~0.47). While, $D(X_F)^{\text{Hb/Chu}}$ is approximately 0.33 in SP4 experiments. Because these minerals are belonged to two mineral groups, and the compositions are similar, their X_F values are comparable. It indicates the decreasing extent of X_F^{Hb} is larger than humite group minerals, of which species is varied with F concentration changes. For reaction 4.1.2.1b, if the mineral species is the same, its equilibrium constant should be the same. The compositions of hornblende from SP2 and SP3 experiments demonstrate their similarity, so their constant b (Eq. 4.1.2.1c) are the same. Moreover, the experiment 1-(SP2+Qtz) also gives the same conclusion for amphibole minerals. Two amphibole minerals (hornblende and anthophyllite),

and they have similar F concentrations (2.20 wt%) and X_F values (0.47 – 0.48). Although the minerals are in the melt phase, it also indicates that the X_F value relates with $[F]/[OH]$ ratio in the surrounding environment.

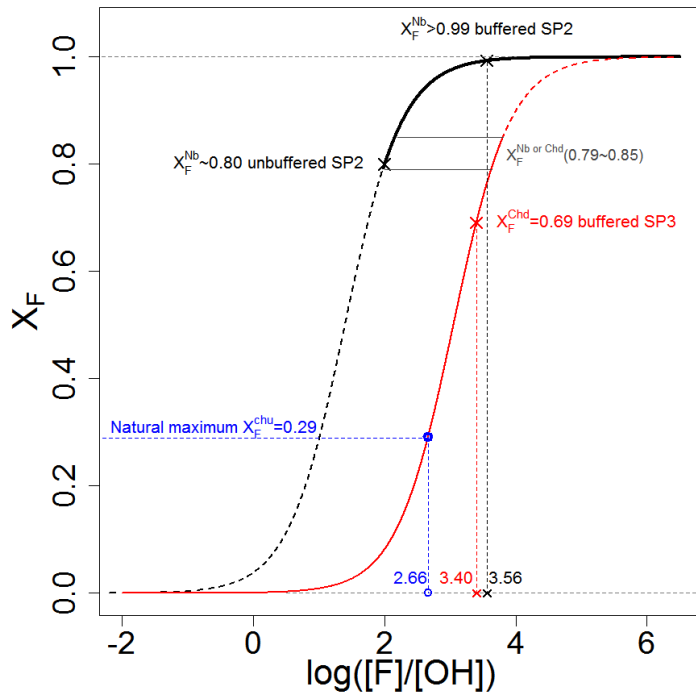


Fig. 4.4.2.1a The relationship between X_F and $\log([F]/[OH])$ for norbergite and chondrodite. Although the parameter b is unknown (Eq. 4.1.2.1c), it is possible to estimate the relative $[F]^{Fl}$ in a similar phase assemblage. The black curve is plotted to illustrate X_F^{Nb} , assuming $b^{Nb}=25$, and the red curve is for X_F^{Chd} , where b^{Chd} is 1125 ($45b^{Nb}$), estimated from data in this study. X_F decreases from 0.99 to 0.10 over a 3 orders of magnitude change in $[F]/[OH]$. The solid parts of the curves represent the stability regions

of norbergite and chondrodite. X_F^{Nb} changes significantly with oxygen fugacity, as shown by the black curve: the $[F]/[OH]$ ratio decreases by approximately 40 times. The maximum X_F of natural clinohumite is 0.29 (blue dashed line). The chondrodite curve is used to estimate $[F]^{Fl}$ in equilibrium with clinohumite ($X_F^{Chd}=0.29$) for the same chondrodite X_F , based on this model.

For humite group minerals which are different from the hornblende, their structures change with the species change. The estimated values of b^{Nb} and b^{Chd} are different. However, the X_F^{Nb} (0.81) and X_F^{Chd} (0.77) in experiment 1-SP2-14 are close, and the X_F^{Nb} (0.72) and X_F^{Chd} (0.73) in experiment 4-SP2-2 are also similar. Within their uncertainties, they are the same. If only consider these two experiment results, it seems to indicate the same value of b for norbergite and chondrodite. This inconsistency demonstrates the complicated process of the crystal formation and F equilibrium in these two experiments.

With Eq. 4.1.2.1c, the ratio of X_F between two minerals (e.g. hornblende and norbergite) can be expressed as below:

$$D(X_F^{Hb/Nb}) = \frac{X_F^{Hb}}{X_F^{Nb}} = \frac{\frac{1}{1 + b^{Hb}/R}}{\frac{1}{1 + b^{Nb}/R}} = 1 - \frac{b^{Hb} - b^{Nb}}{R + b^{Hb}} \quad (4.4.2.1)$$

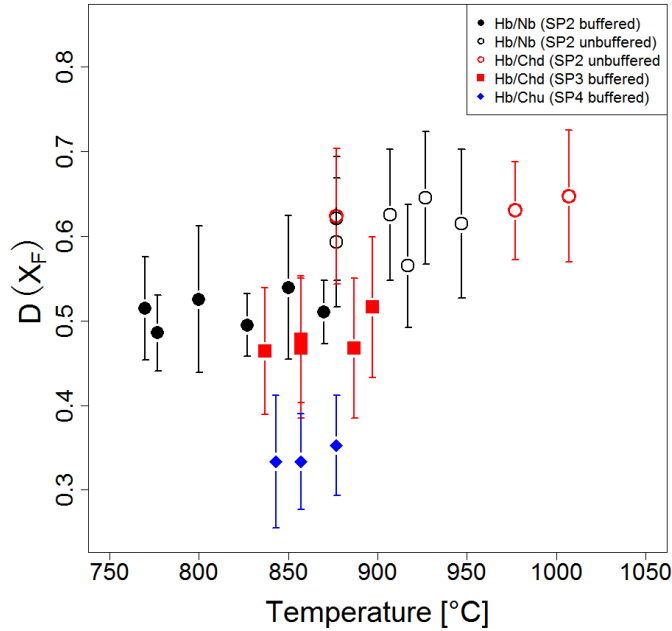


Fig. 4.4.2.1b The ratio of X_F between hornblende and humite group minerals.

Because $X_F^{Nb} > X_F^{Hb}$, $b^{Hb} > b^{Nb}$. At the same temperature, the value of b is constant, so $D(X_F)$ will decrease with a decrease of R value. As shown in Fig. 4.4.2.1b, $D(X_F)$ decrease from SP2 to SP4 around 850 °C. However, both b and R are functions of P - T condition, because OH concentration and the equilibrium constant of equation 4.1.2.1b will change at different conditions. It is too complicated to discuss the changes of $D(X_F)$ with temperature increasing. Nevertheless, Fig. 4.4.2.1b illustrates that $D(X_F)$ is slightly dependent with temperature. This trend for SP3 experiments is the most obvious, while the data of unbuffered SP2 experiments fluctuate more than other groups. This could be explained with two reasons: 1) SP2 experiments are F-saturated systems. The measurements for high F concentration have larger uncertainties; and 2) the oxygen fugacity was not controlled by the buffer, so it is difficult to determine their actual oxygen fugacity inside, and they perhaps differ much. This similar fluctuation even happened to SP2 buffered group. In summary, Fig. 4.4.2.1b indicates a relationship between oxygen fugacity and $D(X_F)$, if ignored the complicated process and parameters, because oxygen fugacity of NNO buffer increases with an increase of temperature (O'Neill and Pownceby, 1993).

It is possible to interpret the decrease of X_F at 877 °C and from 1 to 2 GPa with this X_F model. Assuming H_2 , O_2 , and H_2O in the system is ideal mixing, and the oxygen fugacity is controlled by NNO buffer. Their proportions are fixed at the same temperature when the system reaches the equilibrium. As the total pressure increases, the partial pressures of H_2 and H_2O increase as well as OH fugacity increases, so X_F^{Hb} and X_F^{Nb} become lower (Fig. 4.1.1.3). OH concentration is proportional with $f_{O_2}^{\frac{1}{4}}$ and $f_{H_2O}^{\frac{1}{2}}$ from Eq. 4.1.2.1a, where f_{O_2} is fixed by NNO buffer at the same temperature. Thus, OH concentration only relates with $f_{H_2O}^{\frac{1}{2}}$. Moreover, X_F^{Hb} and X_F^{Nb} decrease in different rate. X_F^{Hb} decreases linearly with the increase of pressure, but X_F^{Nb} decreases as a curve. Because R values for hornblende and norbergite reach their own sensitive areas, and $b^{Hb} > b^{Nb}$, the same extent of R decreasing resulted in more decrease for norbergite than hornblende. $D(X_F)$ between hornblende and norbergite are nearly constant around 0.5 (Fig. 4.1.1.3), which also reflects their constant oxygen fugacity. In conclusion, this [F]/[OH] ratio model can explain X_F behaviors in my experiments.

4.4.2.2 Equilibrium with Clinohumite

With the researches on the relationship between X_F of humite group minerals and F concentrations in the co-exist fluid, it is possible to estimate the maximum F solubility in slab fluid in the presence of clinohumite. For example, clinohumite is common in natural subduction zones (Garrido et al., 2005), where the X_F of titanium-rich clinohumite (Ti-chu) in metaharzburgite is 0.19 (Sanchez-Vizcaino et al., 2005). In another study on natural samples, the maximum X_F of clinohumite from Cima di Gagnone was as high as 0.29 (Evans and Trommsdorf, 1983). In experimental studies, X_F of clinohumite reaches up to 1 (Ulmer and Trommsdorf, 1999). F take-up by humite group minerals is controlled by an F-OH exchange reaction. NNO-buffered experiments' results can be used to estimate the relative F concentration in a fluid, since the oxygen fugacity of the upper mantle is close to that of the NNO buffer (Parkinson and Arculus, 1999). However, this model calculation does not account for the exchange reaction present in Ti-rich clinohumite, $TiO_2 \leftrightarrow Mg(OH,F)_2$.

As shown in Fig. 4.4.2.1a, the values of the F concentration are determined by the value

of X_F and the OH concentration in fluid, which is independent of the F concentration in the fluid. First, with known X_F values, the value of R can be deduced from Eq. (4.1.2.1c) and Fig. 4.4.2.1a. In SP3 experiments, $X_F^{Chd} = 0.69$, and then $R_{SP3} = 10^{3.40}$. I use a clinohumite X_F^{Chu} of 0.29 (Evans and Trommsdorf, 1983) to estimate the F concentration in the equilibrium fluid. The calculated value of R is $10^{2.66}$, which is smaller by a factor of 0.18 than the R of the SP3 fluid (blue circle in Fig. 4.4.2.1a). Since $[F]_{SP3}^{Fl} = 0.19\%$, $[F]^{Fl}$ is therefore 342 ppm. Because this estimate is based on the chondrodite exchange equilibrium, $[F]^{Fl}$ in equilibrium with clinohumite must be smaller. For instance, the decrease of bulk F abundance changes the humite group speciation, which suggests anticorrelation between F abundance and $n(\text{Si})/n(\text{F}, \text{OH})$ in a humite mineral. The estimate of $[F]^{Fl}$ in equilibrium with clinohumite can be as little as half that of $[F]^{Fl}$ in equilibrium with chondrodite for the same X_F . Therefore, the maximum $[F]^{Fl}$ coexisting with clinohumite is 171 ppm.

Furthermore, this result is confirmed by the direct analyses of SP4 series experiments. With the presence of clinohumite ($X_F = 0.39$), their F concentrations range from 60 to 170 ppm. It is reasonable to deduce that if X_F^{Chu} is 0.29, its equilibrium fluid will contain less F than 126 ($170 \times 0.29/0.39$) ppm. In consequence, this fluid can only increase 2 ppm to the subarc magma sources, and the slab-derived fluid does not enrich the F abundance in sub-arc mantle.

4.4.3 Non-modal Melting Model

In subducting slabs, it is possible that amphibole is the only major mineral phase that carries F, in the absence of humite group minerals. In this case, when the subducting slab descends deeper into the upper mantle, amphibole will break down and release fluid. This process will fractionate F between fluid and the remaining minerals. With the trace element fractionation equation (batch equilibrium, Shaw, 1970), I obtain the function below to calculate F concentrations in the released aqueous fluid,

$$[F]^{Fl} = \frac{[F]^{bulk}}{D^{bulk/Fl} + p_{Fl}^{bulk}(1 - P)},$$

where $[F]^{Fl}$ is F concentration in fluid, $[F]^{bulk}$ is the initial F concentration in the rock,

p_{Fl}^{bulk} is fluid fraction, $D^{bulk/Fl}$ and P are functions of initial amphibole proportion, φ^{Amp} , in amphibolite. Typically D is defined as:

$$D^{Rock/Fl} = \varphi^{Amp} \cdot D_F^{Amp/Fl} + \varphi^{Plag} \cdot D_F^{Plag/Fl} + \varphi^{Qtz} \cdot D_F^{Qtz/Fl}.$$

The dehydration reaction parameter, P , is expressed as $P = p_{Hb}^{Fl} \cdot D_F^{Hb/Fl} = \frac{1}{2.1\%} \times 7.1 = 338.1$, because the OH end-member amphibole is the only dehydrating phase in this model and it contains 2.1 wt% water. p_{Fl}^{bulk} varies from 0 to $\varphi^{Amp} \cdot 2.1\%$.

Quartz and plagioclase are nominally anhydrous minerals. The solubility of hydrogen in quartz is less than 100H/10⁶Si at 1.5 GPa, or less than 15 ppm of water can exist in quartz (Kronenberg et al., 1986; Gerretsen et al., 1989). At around 1 GPa, few OH sites are available for F substitution in these nominally anhydrous minerals. In natural spinel lherzolites, the F concentrations in olivine are less than 10 ppm (Beyer et al., 2012). The F concentrations in quartz and plagioclase are so low that the partition coefficients of F between quartz or plagioclase and fluid can be considered as 0 in comparison to that of hornblende. Thus, using the D_F values of this study, and assuming amphibole is hornblende, the equation is simplified to $D^{bulk/Fl} \approx \varphi^{Hb} \cdot D_F^{Hb/Fl} = 7.1 \cdot \varphi^{Hb}$.

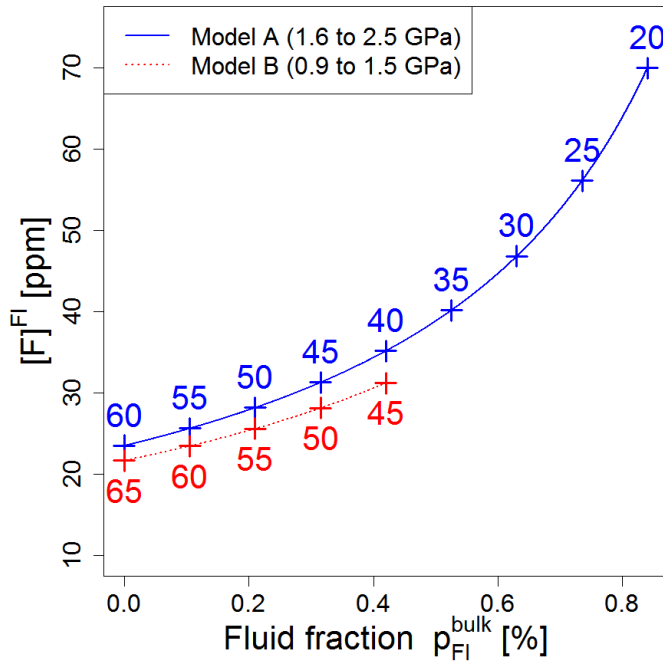


Fig. 4.4.3 Fluorine concentration of an aqueous fluid in equilibrium with dehydrating amphibolite. The bulk F concentration of the rock is assumed to be 100 ppm (a typical MORB value). Fluid is derived only from the amphibole breakdown. Thus, the production of 1 wt% water requires approximately 48 wt% amphibole. As amphibole dehydrates progressively, F concentration in the aqueous fluid increases proportionally. The proportions of remaining amphibole are shown by two curves, A and B. Model A (blue) and model B (red) represent

the differences in initial amphibole abundance, and the extent of dehydration; the proportion of amphibole decreases from 60 to 20 % (blue), and from 65 to 45 % (red), respectively (Poli, 1993).

Fig. 4.4.3 shows the modeled F concentrations in the fluid from the amphibole breakdown process. The proportion of amphibole in dehydrating amphibolite is based on experimental results; it decreases from 65 to 45 wt% with an increase of pressure from 0.9 to 1.5 GPa, and decreases from 60 to 20 wt% within a pressure from 1.6 to 2.5 GPa (at constant $T=650\text{ }^{\circ}\text{C}$, Poli, 1993). I assume that the average F concentration in amphibolite is 100 ppm, and that no other mineral retains F, which is thus released solely by amphibole breakdown. As the extent of amphibole breakdown increases, the F concentration in the fluid increases, ranging from 20 to 70 ppm. As long as amphibole remains in dehydrating rock, no significant quantity of F is transferred. In this scenario, an aqueous fluid from partially dehydrated amphibolite can remove a maximum of 0.5 % of the initial F budget. Therefore, no significant quantity of F is transferred into sub-arc mantle by aqueous fluids from an amphibole-bearing slab. This model presents one example of a diverse range of slab dehydration processes. Here, the amphibole breaks down continuously with increasing depth, instead of episodic dehydration at single pressure-temperature conditions. The bulk water content is 1.2%, while some models predict 5.4% water (e.g. Hacker et al., 2003).

As amphibole progressively breaks down, F concentration in the fluid increases. It would seem likely complete amphibole break down would supply more F into the sub-arc mantle. However, the total concentration of fluorine in the fluid cannot exceed the clinohumite saturation concentration (F saturation in clinohumite is 5.93 wt%, and the average D_F between fluid and clinohumite is 0.00513, so I can estimate 304 ppm F co-exist with hornblende). Therefore, in any case, the aqueous fluid derived from amphibolite does not significantly enrich F in sub-arc mantle.

Lastly, the partition coefficient for F between basaltic melt and F-pargasitic hornblende is 1.59 – 2.78 (Dalou et al., 2010 Fall Meeting, AGU, San Francisco, Calif.). D_F between hastingsite and rhyolite is around 1.4 (Van den Bleeken and Koga, 2012 EMPG conference, Kiel, Germany). D_F between the co-existing melt composition and K-richterite ranges from 0.71 to 1.43 (Edgar and Pizzolato, 1995), and between kakortokite and amphibole it is 0.83 – 2.86 (Kohler et al., 2009). Comparing these values with our results indicates that F probably transfers from slab to mantle via melt when amphibole is present. Furthermore, the slab flux is F concentrated than subarc magma zone. In F-bearing amphibolite, micro clinohumite

4. Discussion

crystals may exist. During the dehydration and breakdown process of amphibole, the amphibolite perhaps crack and release some small minerals. If the flux has enough kinetic energy, it will carry away parts of the minerals. By far, there is no technique can observe the normal slab flux behaviors, so it is hard to tell the possibilities for my guess. But earthquakes in the subduction zone occur frequently, the energy release perhaps improve the slab flux carries more substances, like big rivers can carry lots of sands.

4. Discussion

5. Technical Problems

The large quantity water bearing experiment is difficult to perform, and the quantitative analysis of the composition of high pressure aqueous fluids remains challenging. Two main reasons are: 1) the low success rate of the experiments and 2) the determination of the fluid composition after experiments. This is an aspect that experimental geochemistry groups on fluid experiments are less than anhydrous experiment groups, but scientists still managed to improve the techniques for these two points. Ayers' cold sealing technique is an improvement for the setup of piston cylinder assemblage and the oxygen fugacity control. For fluid compositions analyses, Kessel et al. (2004) developed the diamond aggregate technique with a combination of a freezing stage, LA-ICPMS and Cs internal standard. Koga et al., (2005), Manning et al. (2010) and this study managed to analyses the fluid composition (major and trace cations) with ICPMS. More and more convenient and precise technique will be developed. Although this study managed advancement for an understanding of the behavior of volatile elements in hydrothermal/magmatic systems, the data remains limited. In this section, I will address some technique problems in this study and some potential solutions.

5.1 Sealing Technique for High P - T Experiments

Successfully sealing the capsules for the fluid-bearing experiments is the most important step to keep fluid during anneal. I used both arc welding sealing technique and cold sealing technique to conduct my experiments. They have obvious differences, and their advantages and disadvantages are complementary. For arc welding technique, the capsule is sealed before loading into the piston cylinder. After sealing, it is feasible to ensure its sealing with drying in the oven. According to the presence of large water quantity, it is necessary to leave enough space in the capsule to avoid heating the water during welding. Otherwise, the melt point of metal will decrease, and the boiling water vapor can cause some micro gaps in the metal. It probably leads to the failure of sealing. Moreover, its wired wedge shape makes it

unconvenient to load into the piston cylinder. A double capsule technique is indispensable to control the oxygen fugacity, and meanwhile it leads to a larger volume of the capsule. On the contrary, the cold sealing technique avoids the disadvantages of arc welding capsules, but the sealing process is not under control, and I cannot make sure the sealing of the capsule before the quench. If the sealing is failed, it will lead to the water leaking, even bulk composition loss. The losses of fluids also bring some potential problems:

1) In those experiments, of which most fluid was lost during anneal, the solute in fluid may precipitate as some soluble materials. When I retrieve them into flask, they may re-dissolve into water. In this occasion, the measured solute concentration is larger than the actual concentration and HPLC analysis will not be precise.

2) The small fluid proportion leads to the large uncertainty of mass balance result.

3) Sometimes the fluid loss indicates partial loss of bulk composition. In this case, the mass balance result cannot be reliable.

In my experiments, I classified the experiments with fluid left as successful ones. In summary, the success rate of experiments at 1 GPa is approximately 60%. When pressure increases to 3 GPa, the rate decreases to 30%. Because all the charges after quench are sealed well, I list some potential reasons for fluid loss and corresponding solutions for them:

1) Failed sealing. Although I do not encounter this situation, I can image that the lid and the capsule cannot fuse together. Polish the osculant surfaces of the lid and the capsule. Make sure the surface is clean before setup. This improves the cold sealing.

2) Capillary action. If the water is filled in the capsule, it will leak as soon as the lid covers, because of the capillary action. Press the lid on the top of the capsule, and then uncover it to see if there is any water left on the gold surface. Generally, 1 mm deep space should be left in the capsule to avoid this leaking.

3) Capsule deformation. Before heating, the initial pressure reaches 0.5 GPa to cold seal the capsule. The deformation of capsules will compress the space of inner capsule and lead to the leakage, which must happen to some failed experiments with no space left. When all the inner assemblage was made by crushable MgO, the deformations happened to almost all the capsules, especially for larger volume capsule or higher pressure experiments. Using anhydrate pyrophyllite as the capsule holder, the capsule deformations occur much less. But

for 3 GPa experiments, the success rate are not improved.

4) Hydrogen diffusion. High P - T condition leads to water thermolysis. The hydrogen diffusion makes the buffer effective during the experiment, but it is unavoidable to lose water in this manner. (Ayers et al., 1992) describe this rapid consumption of water, and suggest increasing the ambient hydrogen fugacity or to using capsule materials with lower H_2 diffusivities to decrease the hydrogen diffusion. In my experiments, Ti or Mo capsule experiments have higher success rates, which indicates they lower the water loss during anneal. The presence of unfired pyrophyllite in the piston-cylinder assemblage supplies the water source to increase the hydrogen fugacity outside the capsule (Ayers et al., 1997).

Although these problems can be improved with corresponding solutions, the success rate is still low. Probably, it will be perfect to combine the advantages of two sealing technique together. As the development of pulsed arc welding technique (e.g., "PUK 3s Pro Plus", made by the company "Lampert"), it is possible to weld the lid and the capsule on the foundation of cold sealing capsules design without heating the samples.

5.2 Crystal Growth

Large crystals (width $> 100 \mu\text{m}$) in the capsules are helpful for analyses. First, the mineral compositions are represented more precisely, because the large crystals have larger weight. It leads to accurate phase proportions with mass balance and precise fluid composition. Second, large crystals are feasible for ion probe analyses. According to the limitations of the image detect, crystal dimension is important for this measurement. Generally, the mineral size should be larger than $50 \mu\text{m}$.

In the experiments, of which temperature are lower than $800 \text{ }^\circ\text{C}$, the crystals are always small. As the temperature increases, the crystals, especially norbergite and chondrodite, significantly grow bigger. However, it is easy for hornblende to precipitate longer but not wider. It is not wide enough for the ion probe analysis. It is important to find a technique on increasing the width of hornblende for the future study. I have tried two potential solutions:

1) Introduction of amphibole seeds. The nucleation process needs much more energy

than crystal growth. The seed-free system nucleate crystal nucleus everywhere almost the same time, so the crystals are small and distribute evenly. Although higher temperature and good convection improve the minerals growth, it is useless to increase the dimension of the crystals at lower temperature. Therefore, crystal seeds can help the mineral growth, because the new overgrowth can precipitate on the seeds without waiting the new nucleation. I managed some experiments with amphibole seeds at 750 °C. Significant overgrowth was found surrounding the seeds, and their sizes are wider than 50 µm. Larger seed crystals can product larger minerals. However, before the overgrowths start to precipitate on the seeds, the seed rims probably are dissolved into fluid. If the seed composition is much different from the bulk composition, it may introduce some contamination and affect the mass balance results. Therefore, the ideal seeds are of similar composition crystals. I tried the crystals from SP1 experiment as seeds. It did not work, because the crystal sizes are too small. Before the precipitation on seed, they are perhaps dissolved into fluid.

2) Another potential idea from Ken Koga is a combination of the ultrasonic technique and piston-cylinder. Ultrasonic is useful in dissolving materials, breaking down crystals, and improving the fluid mixture and convection. Its characters are all helpful to precipitate large crystal. However, it reveals a technical problem that transmitting the ultrasonic into the charges during the experiments. Many tests are needs before the technique is mature.

5.3 Advantages and Limitations of Mass Balance and Direct Analysis

It is a challenge to determine the fluid compositions in fluid bearing experiments. Mass balance is a common method for the determination of phase proportions and fluid compositions. Diamond trap is also a technique for small quantity fluid proportion experiments. Recently, Manning et al. (2010) conducted some fluid-extraction experiments and analyzed with ICP-AES for Na, Al, and Si concentrations. Scientists employed these techniques to confirm the calculation's results. However, their disadvantages constrain to collect and analyze the fluid compositions perfectly.

5.3.1 Differences and Similarities of Fluid Components of Different Methods

In my fluid-bearing experiments, the phases in the capsules after quenching are minerals, aqueous fluid and quench phases, perhaps besides melts and saturated precipitations. With electron microprobe or SEM, it is easy to distinguish minerals, melt and quench phases. Hydrous melt degassed and exsolved during quench, so it is hard to determine their precise compositions, but only an average with large beam size. Most quench phases are too small to analyze and rarely present in 1-GPa experiments. After experiments, melt and quench phases are solid. They cannot dissolve into deionized water during the post-quench procedure.

However, two failed experiments 1-SP2-22 and 2-SP2-1 were found their fluid masses are below the detection limit (0.01 mg) after the fluid extraction process. The direct analyses show that the retrieved solutions have significant Na, F, and trace Mg, Ca concentrations. Comparing with K_{SP} of MgF_2 (5.16×10^{-11}) and CaF_2 (3.9×10^{-11}), their Mg/Ca and F concentration products are much smaller than the corresponding K_{SP} . This certifies that the presences of solid soluble substances in their capsules and ion concentrations are lower than their saturations. When the fluid proportion decreases, they may precipitate on the minerals surfaces during the experiments because of the saturation, e.g., Na^+ or F^- . This part is not counted by minerals, so both direct analyses and mass balance will count this content into fluid compositions. Nevertheless, this happened in experiments with small fluid proportion left after quench. Their fluids larger than 40 wt% probably are not saturated with solute. On the other hand, it is not necessary to worry about this case in Na, K-free systems, because other elements are difficult to precipitate as soluble substances. In consequence, if the fluid weight fraction of an experiment is less than 30 wt%, it is probably saturated with the solute and precipitate during anneal. And the excess solute will be dissolved into the extraction fluid by diluting.

In summary, the fluid compositions by mass balance approach contain all the residual part (aqueous fluid, quench phases, and saturated precipitations), while post-quench procedure can only extract and transfer the aqueous fluid and saturated precipitations into a volumetric flask. Therefore, neither of methods can separate the saturated precipitations

independently. By far the unique way to solve this problem is to enlarge the ratio between fluid and solid in the capsule.

5.3.2 Limitations of Mass Balance

The ideal mass balance needs exact compositions of starting materials and representable crystals, and precise phase proportions, which is from mass balance as well. However, these conditions will not be perfect for general experiments. Therefore, mass balance approach suffers some obvious limitations.

First, it is primary to search the mineral species carefully. Once some phases missed, the calculated phase proportion will be changed. Their compositions perhaps are counted as residuals to the fluid, and lead to higher result than true value. It is easy to find all the mineral species in a capsule, so the fluid composition is close to the true value. Occasionally, the absence of minerals is abnormal. For example, chondrodite is failed to sample in 1-SP3-1 experiment. While I compare with the phase assemblage and F concentrations in hornblende, the presence of chondrodite should be more reasonable.

Second, it is important to determine the representative mineral compositions, because correct phase compositions can work out the precise phase proportions. The compositions of big crystals in the capsule are typical to represent their species, so a normal strategy is using an average composition of 3 – 5 biggest crystals. However, the low temperature experiments only create small crystals and distribute evenly. No typical minerals are present, so the unique way is to get an average composition with more crystals. This brings larger uncertainties of Al and Si concentrations for hornblende, but the averages are not far from the true value.

Third, an obvious loss of bulk compositions will make the fluid composition totally unreliable. For example, the abnormal phase assemblage of 1-SP2-14 indicates a significant loss during anneal. Its calculated fluid composition contains approximately 1 wt% F, which is much higher than other SP2 experiments. It is hard to distinguish the bulk composition loss without F, if the phase assemblage remains the same.

Forth, similar mineral compositions get wired phase proportions. It constrains the mass

balance performance. Some experiments have F-free fluid by mass balance calculations, e.g., SP4 series, and high melt-bearing experiments. However, HPLC analyses detect fluorine ion peak, which indicates that the mass balance fails to estimate the phase proportion and leads to an unreliable result. If there are minerals have partial similar concentrations of the conservative elements, the calculated proportion will have big uncertainties. For these occasions, the direct measurements bring preferable results.

Fifth, fluid proportion directly affects the precision of fluid compositions. Koga et al. (2005) argue that the more compatible elements in mineral phases and the less fluid proportion in fluid-bearing experiments lead to the higher uncertainties of the partition coefficient. Their calculations about the error propagations are consistent with this study. As F is preferably incorporated by hydrous minerals, the lower the fluid fraction results in the larger uncertainties of the fluid compositions with mass balance calculations. However, I express the partition coefficient of F with the weighted average. The weight from small fluid proportion experiment is too little to influence the result. On the other hand, regardless of D_F uncertainties, D_F values are close with each other.

In summary, mass balance works well when the fluid fraction higher than 50%, significant solid phase proportions, and their typical average compositions. However, its obvious disadvantages push people to look for valid direct analytical techniques. This study on the tests on HPLC, ICP-AES and ICP-MS is a new contribution on this exploration.

5.3.3 Post-Quench Procedure

The fluid extraction is an important step for preparing the diluted solutions for direct analyses. Beside its procedure for avoiding contaminations, some details should be paid enough attention as well to prevent fluid loss or extraction incompletely.

1) Bubbles in the capsules perhaps block the convections of the fluid between inside and outside the capsules. It is helpful for retrieving the fluid into the beaker to deflate the bubbles with a vacuum pump.

2) Micro crystals can be agitated to the outside of the capsule during the extraction in

ultrasonic water bath. It probably increases the fluid mass value for calculation. I tried to measure their total mass when this situation happened, but their quantity is under the detection limit of the balance. It states that the error from this part can be ignored.

3) Opening the capsule totally improves the fluid extraction process, but easily loses micro crystals. On the contrary, stopping piercing the capsules as soon as the fluid comes out may result in partial residual fluid in the capsule. Therefore, it is vital and experientially dependent to open the capsule suitably.

After the fluid extraction, the capsule was filled with the diluted solution. Because the dilute factor is at least 3000, it is reasonable to ignore the part left in the capsule. Apparently, the extraction solution dissolved the original aqueous fluid and the saturation precipitation. No matter mass balance or fluid extraction for direct analyses cannot separate the saturation precipitation from the fluid compositions.

Up to now, my fluid extraction technique cannot transfer the quench phases into fluid, because they are solid after anneal. For high pressure experiments, which form quench phase after the experiments, some approaches are needed to get its composition. Two methods have been reported. Ayers et al. (1997) designed a special two-layer capsule with a perforated membrane to prevent most of the solid powder convection into the capsule. After quench, the solute quench phase was collected and was melt to a homogeneous phase for analysis. The other is done by Koga et al. (2005). They managed to dissolve the quench phase by a suitable acid, and all the quench phases were transport into fluid for analysis. Fortunately, the majority of my experiments were conducted at 1 GPa. Their quench phases are too little to be found, so I looked over this part normally. While in 2.5 and 3 GPa experiments, it is apparent to find abundance of quench phase in their capsules. In the future, for the experiments at the pressure higher than 2 GPa, this technique problem for the extraction of quench phases should be considered.

5.3.4 Limitations of Direct Analytical Techniques

HPLC, ICP-AES and ICP-MS were applied to analyze the dilute solutions. Because the principle of each technique is different, their analyzable species are different.

Fluorine ion can only be analyzed by HPLC with specific column. The detection limit is approximately 1 ppb. By far, the lowest F concentration of my extracted solution is 6 ppb. The reproducibility is excellent. However, if some F is present in the fluid as other compound (HF, or F complex), HPLC cannot detect them. Fluorine cannot be present as HF, because the pH value of the eluent is approximately 12 (0.9 mmol/L Na₂CO₃). Moreover, F can react with Si, Al, Fe, and Mg to form complex compounds. For example, SiF₄ was detected by remote FT-IR observation in volcanic plume (Mori et al., 2002). No studies suggest the Si-F formations under high *P-T* conditions, but the formation of SiF₆²⁻ has been reported at low pH (Aigueperse et al., 2000). The Si solubility improvements with the presence of F also indicates the reaction between Si and F. However, it is possible to dissociate SiF₆²⁻ completely under ambient *P-T* conditions when pH is approximately 7. If diluting the solution, the concentration of SiF₆²⁻ in the same system will decrease at least two magnitude orders more than the concentrations of F and Si (Finney et al., 2006). Because the pH of the deionized water is approximately 4 and the extraction solution is diluted as 3600 times, it is possible for most of the fluoride complexes to dissociate. This undetected species can be studied by *in-situ* observation technique in the future.

On the other hand, it is feasible to calculate the concentrations of the fluoride complexes with Mg, Ca, and Fe with the direct analysis results. HPLC analyses detect fluorine ion concentration, and ICP-MS report the total concentration of each cation element. With the complex constant between F and various metal cations, it is possible to estimate the complexed fluorine concentrations. For example, the calculated complexed relative fluorine concentration to the free fluorine ion concentration of 1-SP2-16 is shown in the table below. The total of the compound fluorine quantities of Al, Fe, and Mg is relatively less than 1 %. The relative uncertainty of HPLC measurement is approximately 1 %, so the difference of fluorine concentrations caused by complex compound can be ignored. However, it is feasible to dissociate F from other compounds with chemical way (e.g, EDTA solution) to confirm this

difference by HPLC measurement.

Table 5.3.4 Calculated complexed fluorine concentrations

Element	Concentration		lgK ₁	lgK ₂	lgK ₃	relative [F ⁻] _{complexed} / %
	ppb	10 ⁻⁹ mol/L				
F	142	7470				
Fe	0.264	4.74	5.28	9.30	12.06	0.04
Al	4.74	87.8	6.10	11.15	15.00	0.2
Mg	0.618	25.4	1.30			<10 ⁻⁵

The other two techniques are suitable for analyzing cations concentrations. With ICP technique, all the species of each detectable element can be counted into its total concentration. Actually, these two techniques have many differences besides principle. In LMV, ICP-AES is normally used to analyze 5 major elements, and the detection limit only reaches ppm level. One of its advantages is to analyze the unknown solutions directly without any pretreatment. ICP-MS has a much lower detection limit than ICP-AES, and can analyze almost all the isotopes because of its high resolution. Although it is calibrated by 3 different level standard solutions, an internal standard should be mixed into the unknown solutions. Furthermore, nitric acid is needed to control the pH value of solutions. For my samples, this ICP-MS pretreatment created some problems. During the post-quench procedure, some micro crystals or fragments may be present in the dilute solution. With the nitric acid pretreatment, these micro solid phases can be dissolved into the fluid, and contaminate the solution. For example, in the fluid of 1-SP2-24, Fe, Mg, Ca, Ni and Al concentrations are much higher than other experiments, while other elements are similar. The difference is probably caused by the acidification pretreatment. However, it is enough to conclude this without comparing results from other techniques. Even if ICP-MS is the best for analyzing the solutions, it is still necessary to confirm some major element concentrations with other techniques. Otherwise, a filter process should be developed in the post-quench procedure.

5.4 Standards for High F-bearing Minerals

The major element concentrations are measured with electron microprobe. In principle, chemical composition is determined by comparing the intensities of characteristic X-rays with the sample material with intensities from known composition (standards). The count numbers from the sample must be corrected for matrix effects (absorption and secondary fluorescence) to yield quantitative chemical compositions. Therefore, the ideal standards for the target minerals are the same specie minerals.

Although I managed to measure the compositions of high concentration F-bearing minerals, there are some subtle difficulties. In hydrous minerals and melt, hydrogen concentrations cannot be detected. Therefore, stoichiometric calculations or direct oxygen measurements are two feasible methods with electron microprobe to estimate the hydrogen concentrations. The former can work well on minerals, while for degassed hydrous melt, only the latter can work. However, when I analyzed norbergite crystals with estimating the oxygen concentration with oxides formula (the difference mode of the EMP software), the F concentration will be 1 wt% higher than that measuring oxygen concentration directly. Although for norbergite, this difference is less than the uncertainty of F, it indicates somewhat that using CaF_2 as the standard sample for high F-bearing minerals are not strict enough to calculate the oxygen matrix effects to fluorine. In the future, it will be perfect to find a humite group mineral and an amphibole with high F concentrations as standards for electron microprobe measurement.

5. Technical Problems

6. Outlooks

This experimental study reveals not only a new constraint on slab flux with volatile elements and the importance of the new tracer in the subduction zone, but also some disadvantages on the previous experimental techniques. Although my strategy did not solve the technique problems, this study made some advancement. In this section, I will describe my outlooks for future work.

6.1 Oxygen Fugacity In and Out of Capsules

Oxygen fugacity is a fundamental intensive variable in mantle processes. It is important in determining such features as sub- and super-solidus phase relationships, the nature of volatile species, and trace element partitioning (Arculus, 1985). Different from other parameters (such as P , T , and compositions), oxygen fugacity varies by nine orders of magnitude in the terrestrial rocks. Hence, it is necessary to determine the oxygen fugacity in the high P - T experimental studies.

Generally, in high temperature furnace at ambient pressure experiments, the oxygen fugacity is controlled by hydrogen and carbon dioxide gas mixture. While in piston cylinder or multi-anvil, the oxygen fugacity is controlled by solid buffer powder. The solid mixture with different valent states of elements can work as buffer, such as Ni/NiO (NNO), Fe/FeO (IW), $\text{Fe}_3\text{O}_4/\text{Fe}_2\text{O}_3$ (MH), and Co/CoO (CoCO). The estimated oxygen fugacity values of solid buffers were investigated, and some empirical equations were found to determine the oxygen fugacity at high temperature (Chou, 1978; O'Neill, 1986; Chou, 1987; O'Neill and Pownceby, 1993). Therefore, scientists utilize these equations to determine the oxygen fugacity at experimental conditions.

In some references, the verifications of buffers are reported. For example, NNO buffer can oxidize pure nickel powder to NiO, or reduce hematite to magnetite (Ayers et al, 1997). However, it only indicates that NNO buffer controls the oxygen fugacity at an approximate

state. The true oxygen fugacity inside the capsule probably is different from that is imposed by buffer. Jakobsson (2012) calculates that the variations of hydrogen fugacity in the outer capsule with an increase of carbon activity can lead to the oxygen fugacity changes in the inner capsules. Moreover, King et al. (2000) demonstrate that the oxygen fugacity difference between inside and outside the inner capsule is twice of the water activity of melt in the inner capsule. Essentially, the effect of buffer is derived from the hydrogen equilibrium, and hydrogen is dissociated from water. In principle, if the water activities in the inner and outer capsules are dominant and close to 1, then the oxygen fugacity inside the inner capsule should be equal to that of buffer. In fact, the two references mentioned above realize this difference and calculate the precise oxygen fugacity for their experiments (King et al., 2000; Jakobsson, 2012). Different from these mineral-melt systems, the oxygen fugacity of the inner capsule in large fluid quantity experiments should be less different than fluid-free experiments.

Inner and outer capsules are two relatively isolated systems. Only hydrogen can transfer between them, and the hydrogen fugacity are in equilibrium when buffer works. However, the continual diffusion of hydrogen during the anneal leads to the water loss. If the water loss mass is significant, the oxygen fugacity will be higher than the buffer. As King et al. (2000) discuss, when water is not dominant, it is unreliable to set water activity as 1, but it is possible to calculate the water activity of melt following Burnham (1979) and the water contents. Jakobsson (2012) find that the effect of the presence of carbon cannot be ignored, and hydrogen fugacity also increases if oxygen fugacity of buffer is lower than FMQ and the carbon permeation is present. Even for the hydrous-free melt experiments, if the graphite heater and moisture in the assembly form a buffer reaction, the environmental f_{O_2} can be around CCO-0.8 (extending arguments given in Médard et al 2008), which indicates that the ambient influence of experimental assemblies cannot be ignored.

On the other side, it is feasible to utilize water dissociation equilibrium to calculate the oxygen fugacity with known hydrogen fugacity and water activity, according to the presence of aqueous fluid. However, silicate is soluble at high $P-T$ conditions. In my experiments, the average fluid of 1-GPa experiment has 6 wt% SiO_2 , 1 wt% NaO and 0.3 wt% F, so the water molar fraction is approximately 97.3 %. It is acceptable to assume its water activity as one. Moreover, if each SiO_2 is combined with at least 2 H_2O molecules (Newton and Manning,

2000), the free water molar fraction will decrease to 93.5 %. Then it is more reasonable to estimate the water fugacity with water molar fraction in the solution.

Above is a comprehension from thermodynamic equilibrium of buffer. While from dynamic aspect, there are some confusing details during the process of reaching equilibrium. First of all, the knowledge on the consumption of oxygen is of limitation. Oxygen and hydrogen are both from the dissociation of water, and their concentration ratio is 1:2. Moreover, their fugacity coefficients are in the same magnitude, so their initial fugacity are close. But, oxygen cannot diffuse to the outside of the gold capsule below 1000 °C. However, the hydrogen fugacity is much higher than oxygen fugacity for most of buffers with theoretical calculations. It is easy to understand that pure nickel powder is oxidized to NiO, but it is hard to image that hematite is reduced to magnetite (section 4.1.2.2). Second, the process of the buffer increasing the hydrogen fugacity inside the inner capsule is not clear. If no oxygen is consumed in the inner capsule, then another possibility of decreasing the oxygen fugacity is hydrogen diffusion from outside to inside. It is quite feasible if there is large quantity of water present outside the capsule. However, in the design of cold sealing technique, there is no large space to contain water except some hydrous parts. Moreover, even no pyrophyllite is present as a water source in the assemblage, the buffer can work well. Third, the oxygen fugacity will change with a decrease of water proportion in the capsule, because the molar fraction of oxygen may increase. In NNO buffered SP3 experiments, the X_F values of chondrodite are different between successful and failed experiments (section 4.1.1.2.1). All the capsules have obvious empty space among the minerals. It indicates the presence of water at beginning, but some of them exhausted water during anneal. This demonstrates that water proportion in the experiment is an important parameter for the oxygen fugacity control. Forth, the air sealed into the capsule increase the initial oxygen fugacity. There is 20 % oxygen in the air. If volume ratio between air and water is 1:1, then the fractional pressure of the air oxygen at 1 GPa is 1.53 bar. This indicates that the oxygen fugacity in the capsule is higher than hydrogen fugacity at the initial state, and perhaps influences the oxygen fugacity during the experiments.

6.2 F and Cl Partitioning between Other Minerals and Fluid

The partition coefficient of F between amphibole and aqueous fluid is investigated in this study. The experimental conditions are mostly at 1 GPa, which is corresponding the shallow layer of the upper mantle. The P - T range is constrained at the amphibolite facies in the subducting crust. However, the amphibole as a hydrous mineral is present in amphibolite of the oceanic crust in the subduction zone. Some hydrous minerals (lawsonite, zoisite, chloritoid, and talc) can be present at the pressure after the breakdown of amphibole in subducting oceanic crust (Schmidt and Poli, 1998). Furthermore, hydrous phases are important to bring the volatile elements down to the depth, but most anhydrous minerals form beyond the stabilities of the hydrous phases. Thus, the F and Cl incorporations in the anhydrous minerals (e.g, garnet, pyroxene, or olivine) are also crucial to understanding the volatile elements transport behaviors.

In other parts of a subduction zone, i.e, mantle wedge, subducting sediment, and the upper mantle of the subducting plate, some different hydrous minerals exist. They also transfer the water into the depth. For example, the dehydration of oceanic crust in the lower depth (~50 km) will flow into the mantle wedge. The enrichment of water leads to the formation of chlorite, which goes deeper with the convection of the mantle wedge. Moreover, serpentine in the peridotitic lithosphere may reach the depth of 200 km, so it is also necessary to investigate the distribution of the volatile elements in subducting lithosphere. With the knowledges of these basic thermodynamics parameters, it will be feasible for people to understand the F and Cl cycle budget in the subduction factory.

6.3 Improvements on Determination of Fluid Compositions

Although the direct analysis methods have some problems, most of them have yield consistent fluid compositions. A few aspects should be noted and improved in the future.

First, develop Ayers' technique to increase the success rate and the fluid fraction in the capsule after quench. It will be helpful for mass balance calculations and to prevent the saturation precipitation.

Second, it is possible for direct analyses to employ the leaching technique (Koga et al., 2005) to dissolve the quench phase without damage the minerals. In order to avoid the contaminations from the acidification procedure, it is necessary to separate the aqueous fluid and quench phase extractions as two steps. It also needs more attentions on how to determine the end point of dissolving the quench phase.

Third, filter out the micro solid crystals or fragments from the retrieved dilute solutions. Two details should be paid attentions: 1) sufficient leaching to avoid the solute kept on the filter, but be sure dilution of the solution above the detect limitation; 2) this procedure should be finished before ICP-MS analyses, while for other analyses, it is not necessary.

Forth, total F concentration analyses. Because only HPLC can analyze fluorine ion in the fluid, it is helpful to use a chemical process (e.g, mix with EDTA) to release all the F as fluorine ion.

6.4 F Incorporation and Melt Compositions

From this study, the partition coefficient of F between aqueous fluid and hydrous minerals are far less than 1. Therefore, it is reasonable to express that aqueous fluid cannot transfer F significantly from subducting slab to subarc mantle at amphibolite facies. The potential transport way is melt. However, the partition coefficients between melt and amphibole can be larger or less than 1 (section 4.4.3), while those between melt and anhydrous minerals are much larger than 1. Therefore, the melt and amphibole compositions are important for determining the F partitioning between them. By far, there is no evidence on the F incorporation influenced by amphibole composition variation in this study. Therefore, systematical investigations of the F incorporation by different melt species are expected.

The SP2 experiments ($T > 950$ °C) display some information on this aspect, because two kinds of hydrous melts are present. Most melt contains 6 – 9 wt% F, and they were suffered degassing and exsolution after quenching the experiments. Their texture is of porosity, and it is rich in Ca and Mg. While F concentration of one high-silica melt is much lower (~1 wt% F and ~89 wt% SiO₂). Therefore, the comparison between them suggests that F incorporation is

preferential into Ca/Mg-rich melt.

This investigation on F partitioning in melts contains a large composition range, so it is a complicated and useful work. Like traditional trace elements were studied by many groups, more and more researches on F partitioning between melt and minerals will start. In order to avoid the effects from the composition changes for distinguishing the F preferential cations, I suppose that either conducting the experiments with the same bulk composition, or using a standard mineral as a reference, because F concentration should relate to bulk compositions and phase assembly during anneal.

References

- Abe, N., Arai, S., Yurimoto, H., 1998. Geochemical characteristics of the uppermost mantle beneath the Japan island arcs: implications for upper mantle evolution. *Physics of the Earth and Planetary Interiors*, 107(1-3): 233-248.
- Aigueperse, J. et al., 2000. Fluorine Compounds, Inorganic, Ullmann's Encyclopedia of Industrial Chemistry. Wiley-VCH Verlag GmbH & Co. KGaA.
- Albarede, F., Provost, A., 1977. Petrological and geochemical mass-balance equations - an algorithm for least-square fitting and general error analysis. *Computers & Geosciences*, 3(2): 309-326.
- Amstutz, A., 1951. Sur l'évolution des structures alpines. *Archives des sciences.*, 4(5): 7.
- Anderson, A.T., 1975. Some basaltic and andesitic gases. *Reviews of Geophysics*, 13(1): 37-55.
- Anderson, D.L., 1995. Lithosphere, asthenosphere, and perisphere. *Reviews of Geophysics*, 33(1): 125-149.
- Anderson, R.N., DeLong, S.E., Schwarz, W.M., 1978. Thermal Model for Subduction with Dehydration in the Downgoing Slab. *The Journal of Geology*, 86(6): 731-739.
- Anderson, R.N., DeLong, S.E., Schwarz, W.M., 1980. Dehydration, Asthenospheric Convection and Seismicity in Subduction Zones. *The Journal of Geology*, 88(4): 445-451.
- Arculus, R.J., 1985. Oxidation status of the mantle: past and present. *Annual Review of Earth and Planetary Sciences*, 13: 75-95.
- Atherton, M.P., Petford, N., 1993. Generation of sodium-rich magmas from newly underplated basaltic crust. *Nature*, 362(6416): 144-146.
- Ayers, J.C., Brenan, J.B., Watson, E.B., Wark, D.A., Minarik, W.G., 1992. A new capsule technique for hydrothermal experiments using the piston-cylinder apparatus. *American Mineralogist*, 77(9-10): 1080-1086.
- Ayers, J.C., Dittmer, S.K., Layne, G.D., 1997. Partitioning of elements between peridotite and H₂O at 2.0–3.0 GPa and 900–1100 °C, and application to models of subduction zone processes. *Earth and Planetary Science Letters*, 150(3–4): 381-398.
- Ayers, J.C., Watson, E.B., 1993. Rutile solubility and mobility in supercritical aqueous fluids. *Contributions to Mineralogy and Petrology*, 114(3): 321-330.
- Bai, Q., Kohlstedt, D.L., 1992. Substantial hydrogen solubility in olivine and implications for

- water storage in the mantle. *Nature*, 357(6380): 672-674.
- Baker, D.R., Balcone-Boissard, H., 2009. Halogen diffusion in magmatic systems: Our current state of knowledge. *Chemical Geology*, 263(1-4): 82-88.
- Baker, M., Grove, T., Price, R., 1994. Primitive basalts and andesites from the Mt. Shasta region, N. California: products of varying melt fraction and water content. *Contributions to Mineralogy and Petrology*, 118(2): 111-129.
- Berry, A.J., James, M., 2002. Refinement of hydrogen positions in natural chondrodite by powder neutron diffraction: implications for the stability of humite minerals. *Mineralogical Magazine*, 66(3): 441-449.
- Beyer, C., Klemme, S., Wiedenbeck, M., Stracke, A., Vollmer, C., 2012. Fluorine in nominally fluorine-free mantle minerals: Experimental partitioning of F between olivine, orthopyroxene and silicate melts with implications for magmatic processes. *Earth and Planetary Science Letters*, 337: 1-9.
- Bouvier, A.S., Metrich, N., Deloule, E., 2008. Slab-derived fluids in the magma sources of St. Vincent (Lesser Antilles arc): Volatile and light element imprints. *Journal of Petrology*, 49(8): 1427-1448.
- Boyd, F.R., England, J.L., 1960. Apparatus for phase-equilibrium measurements at pressures up to 50 kilobars and temperatures up to 1750 °C. *Journal of Geophysical Research*, 65(2): 741-748.
- Brooker, R., Holloway, J.R., Hervig, R., 1998. Reduction in piston-cylinder experiments; the detection of carbon infiltration into platinum capsules. *American Mineralogist*, 83(9-10): 985-994.
- Burnham, C.W., 1979. Magmas and hydrothermal fluids. In: Barnes, H.L. (Ed.), *Geochemistry of Hydrothermal Ore Deposits*. John Wiley and Sons, New York, pp. 71-136.
- Burnley, P.C., Navrotsky, A., 1996. Synthesis of high-pressure hydrous magnesium silicates: Observations and analysis. *American Mineralogist*, 81(3-4): 317-326.
- Carroll, M.R., Webster, J.D., 1994. Solubilities of sulfur, noble gases, nitrogen, chlorine, and fluorine in magmas, Volatiles in Magmas. *Reviews in mineralogy*. Mineralogical Soc America, Washington, DC, pp. 231-279.
- Chen, Y., Provost, A., Schiano, P., Cluzel, N., 2011. The rate of water loss from olivine-hosted melt inclusions. *Contributions to Mineralogy and Petrology*, 162(3): 625-636.
- Chou, I.M., 1978. Calibration of oxygen buffers at elevated P and T using the hydrogen fugacity sensor. *American Mineralogist*, 63(7-8): 690-703.
- Chou, I.M., 1987. Calibration of the graphite-methane buffer using the f_{H_2} sensors at 2-kbar

- pressure. *American Mineralogist*, 72(1-2): 76-81.
- Dalou, C., 2011. Fluorine and chlorine fractionation in the sub-arc mantle: An experimental investigation, Université Blaise Pascal, Clermont-Ferrand, France.
- Dalou, C., Koga, K., Shimizu, N., Boulon, J., Devidal, J.-L., 2012. Experimental determination of F and Cl partitioning between lherzolite and basaltic melt. *Contributions to Mineralogy and Petrology*, 163(4): 591-609.
- Defant, M.J., Drummond, M.S., 1990. Derivation of some modern arc magmas by melting of young subducted lithosphere. *Nature*, 347(6294): 662-665.
- Dixon, J.E., Clague, D.A., Stolper, E.M., 1991. Degassing history of water, sulfur and carbon in submarine lavas from Kilauea volcano, Hawaii. *Journal of Geology*, 99(3): 371-394.
- Dixon, J.E., Stolper, E.M., 1995. An experimental study of water and carbon dioxide solubilities in mid-ocean ridge basaltic liquids .2. Applications to degassing. *Journal of Petrology*, 36(6): 1633-1646.
- Edgar, A.D., Pizzolato, L.A., 1995. An experimental study of partitioning of fluorine between K-richrichterite, apatite, phlogopite, and melt at 20 kbar. *Contributions to Mineralogy and Petrology*, 121(3): 247-257.
- Eiler, J.M. et al., 2000. Oxygen isotope geochemistry of oceanic-arc lavas. *Journal of Petrology*, 41(2): 229-256.
- Elliott, T., Plank, T., Zindler, A., White, W., Bourdon, B., 1997. Element transport from slab to volcanic front at the Mariana arc. *Journal of Geophysical Research-Solid Earth*, 102(B7): 14991-15019.
- Evans, B.W., Trommsdorf, V., 1983. Fluorine hydroxyl titanian clinohumite in a pline recrystallized garnet peridotite: compositional controls and petrologic significance. *American Journal of Science*, 283A: 355-369.
- Ferraris, G., Prencipe, M., Sokolova, E.V., Gekimiyants, V.M., Spiridonov, E.M., 2000. Hydroxylclinohumite, a new member of the humite group: Twinning, crystal structure and crystal chemistry of the clinohumite subgroup. *Zeitschrift Fur Kristallographie*, 215(3): 169-173.
- Finney, W.F., Wilson, E., Callender, A., Morris, M.D., Beck, L.W., 2006. Reexamination of Hexafluorosilicate Hydrolysis by ¹⁹F NMR and pH Measurement. *Environmental Science & Technology*, 40(8): 2572-2577.
- Garrido, C.J. et al., 2005. Enrichment of HFSE in chlorite-harzburgite produced by high-pressure dehydration of antigorite-serpentinite: Implications for subduction magmatism. *Geochem. Geophys. Geosyst.*, 6(1): Q01J15.

- Gerretsen, J., Paterson, M.S., McLaren, A.C., 1989. The uptake and solubility of water in quartz at elevated pressure and temperature. *Physics and Chemistry of Minerals*, 16(4): 334-342.
- Gill, J.B., 1981. Orogenic andesites and plate tectonics. *Minerals, Rocks and Inorganic Materials*. Springer Berlin Heidelberg, New York, 390 pp.
- Grove, T.L., Till, C.B., Lev, E., Chatterjee, N., Medard, E., 2009. Kinematic variables and water transport control the formation and location of arc volcanoes. *Nature*, 459(7247): 694-697.
- Hacker, B.R., Abers, G.A., Peacock, S.M., 2003. Subduction factory - 1. Theoretical mineralogy, densities, seismic wave speeds, and H₂O contents. *Journal of Geophysical Research*, 108(B1).
- Hirth, G., Kohlstedt, D.L., 1996. Water in the oceanic upper mantle: implications for rheology, melt extraction and the evolution of the lithosphere. *Earth and Planetary Science Letters*, 144(1-2): 93-108.
- Holloway, J.R., Wood, B.J., 1988. *Simulating the Earth: Experimental geochemistry*. Springer, Boston, Massachusetts.
- Honda, S., Saito, M., Nakakuki, T., 2002. Possible existence of small-scale convection under the back arc. *Geophysical Research Letters*, 29(21): 2043.
- Ionov, D.A., 2010. Petrology of Mantle Wedge Lithosphere: New Data on Supra-Subduction Zone Peridotite Xenoliths from the Andesitic Avacha Volcano, Kamchatka. *Journal of Petrology*, 51(1-2): 327-361.
- Iwamori, H., 1998. Transportation of H₂O and melting in subduction zones. *Earth and Planetary Science Letters*, 160(1-2): 65-80.
- Jakobsson, S., 2012. Oxygen fugacity control in piston-cylinder experiments. *Contributions to Mineralogy and Petrology*, 164(3): 397-406.
- Jones, N.W., Ribbe, P.H., Gibbs, G.V., 1969. Crystal chemistry of humite minerals. *American Mineralogist*, 54(3-4): 391-411.
- Kay, R.W., Kay, S.M., 1993. Delamination and delamination magmatism. *Tectonophysics*, 219(1-3): 177-189.
- King, P.L., Hervig, R.L., Holloway, J.R., Delaney, J.S., Dyar, M.D., 2000. Partitioning of Fe³⁺/Fe_{total} between amphibole and basanitic melt as a function of oxygen fugacity. *Earth and Planetary Science Letters*, 178(1-2): 97-112.
- Koga, K.T., Daniel, I., Reynard, B., 2005. Determination of trace element partition coefficients between water and minerals by high-pressure and high-temperature

- experiments: Leaching technique. *Geochemistry Geophysics Geosystems*, 6.
- Kohler, J., Schonenberger, J., Upton, B., Markl, G., 2009. Halogen and trace-element chemistry in the Gardar Province, South Greenland: Subduction-related mantle metasomatism and fluid exsolution from alkalic melts. *Lithos*, 113(3-4): 731-747.
- Kohlstedt, D.L., Keppler, H., Rubie, D.C., 1996. Solubility of water in the α , β and γ phases of $(\text{Mg,Fe})_2\text{SiO}_4$. *Contributions to Mineralogy and Petrology*, 123(4): 345-357.
- Kronenberg, A.K., Kirby, S.H., Aines, R.D., Rossman, G.R., 1986. Solubility and Diffusional Uptake of Hydrogen in Quartz at High Water Pressures: Implications for Hydrolytic Weakening. *Journal of Geophysical Research*, 91(B12): 12723-12744.
- Lange, N.A., Speight, J.G., 2005. Lange's handbook of chemistry. McGraw-Hill standard handbooks. McGRAW-HILL, New York.
- Laporte, D., Toplis, M., Seyler, M., Devidal, J.-L., 2004. A new experimental technique for extracting liquids from peridotite at very low degrees of melting: application to partial melting of depleted peridotite. *Contributions to Mineralogy and Petrology*, 146(4): 463-484.
- Le Voyer, M., Rose-Koga, E.F., Shimizu, N., Grove, T.L., Schiano, P., 2010. Two Contrasting H_2O -rich Components in Primary Melt Inclusions from Mount Shasta. *Journal of Petrology*, 51(7): 1571-1595.
- Méclard, E., McCammon, C.A., Barr, J.A., Grove, T.L., 2008. Oxygen fugacity, temperature reproducibility, and H_2O contents of nominally anhydrous piston-cylinder experiments using graphite capsules. *American Mineralogist*, 93(11-12): 1838-1844.
- Manning, C.E., 1994. The solubility of quartz in H_2O in the lower crust and upper-mantle. *Geochimica Et Cosmochimica Acta*, 58(22): 4831-4839.
- Manning, C.E., Antignano, A., Lin, H.A., 2010. Premelting polymerization of crustal and mantle fluids, as indicated by the solubility of albite+paragonite+quartz in H_2O at 1 GPa and 350–620 °C. *Earth and Planetary Science Letters*, 292(3–4): 325-336.
- McMillan, P.F., 1994. Water solubility and speciation models. In: Carroll, M.R., H., J.R. (Eds.), Volatiles in Magmas. Reviews in mineralogy. Mineralogical soc america, Washington, pp. 131-156.
- Mével, C., Caby, R., Kienast, J.R., 1978. Amphibolite facies conditions in oceanic-crust - example of amphibolitized flaser-gabbro and amphibolites from Chenaillet ophiolite massif (Hautes Alpes, France). *Earth and Planetary Science Letters*, 39(1): 98-108.
- Miyashiro, A., 1964. Oxidation and reduction in the Earth's crust with special reference to the role of graphite. *Geochimica Et Cosmochimica Acta*, 28(5): 717-729.

- Molina, J.F., Poli, S., 2000. Carbonate stability and fluid composition in subducted oceanic crust: an experimental study on H₂O-CO₂-bearing basalts. *Earth and Planetary Science Letters*, 176(3-4): 295-310.
- Mori, T., Sato, M., Shimoike, Y., Notsu, K., 2002. High SiF₄/HF ratio detected in Satsuma-Iwojima volcano's plume by remote FT-IR observation. *Earth Planets and Space*, 54(3): 249-256.
- Moune, S., Sigmarsson, O., Thordarson, T., Gauthier, P.J., 2007. Recent volatile evolution in the magmatic system of Hekla volcano, Iceland. *Earth and Planetary Science Letters*, 255(3-4): 373-389.
- Mysen, B.O., 2009. Solution mechanisms of silicate in aqueous fluid and H₂O in coexisting silicate melts determined in-situ at high pressure and high temperature. *Geochimica Et Cosmochimica Acta*, 73(19): 5748-5763.
- Mysen, B.O., Armstrong, L., 2002. Solubility behavior of alkali aluminosilicate components in aqueous fluids and silicate melts at high pressure and temperature. *Geochimica Et Cosmochimica Acta*, 66(12): 2287-2297.
- Newton, R.C., Manning, C.E., 2000. Quartz solubility in H₂O-NaCl and H₂O-CO₂ solutions at deep crust-upper mantle pressures and temperatures: 2–15 kbar and 500–900 °C. *Geochimica Et Cosmochimica Acta*, 64(17): 2993-3005.
- Newton, R.C., Manning, C.E., 2002. Solubility of enstatite + forsterite in H₂O at deep crust/upper mantle conditions: 4 to 15 kbar and 700 to 900 °C. *Geochimica Et Cosmochimica Acta*, 66(23): 4165-4176.
- O'Neill, H.C., Pownceby, M., 1993. Thermodynamic data from redox reactions at high temperatures. I. An experimental and theoretical assessment of the electrochemical method using stabilized zirconia electrolytes, with revised values for the Fe-“FeO”, Co-CoO, Ni-NiO and Cu-Cu₂O oxygen buffers, and new data for the W-WO₂ buffer. *Contributions to Mineralogy and Petrology*, 114(3): 296-314.
- O'Neill, H.S.C., 1986. Mo-MoO₂ (MOM) oxygen buffer and the free energy of formation of MoO₂. *American Mineralogist*, 71: 1007-1010.
- Otsuka, K., Karato, S.-i., 2011. Control of the water fugacity at high pressures and temperatures: Applications to the incorporation mechanisms of water in olivine. *Physics of the Earth and Planetary Interiors*, 189(1–2): 27-33.
- Parkinson, I.J., Arculus, R.J., 1999. The redox state of subduction zones: insights from arc-peridotites. *Chemical Geology*, 160(4): 409-423.
- Parsons, B., 1982. Causes and consequences of the relation between area and age of the ocean floor. *Journal of Geophysical Research: Solid Earth*, 87(B1): 289-302.

- Parsons, B., Sclater, J.G., 1977. An analysis of the variation of ocean floor bathymetry and heat flow with age. *Journal of Geophysical Research*, 82(5): 803-827.
- Pawley, A., 2000. Stability of clinohumite in the system MgO-SiO₂-H₂O. *Contributions to Mineralogy and Petrology*, 138(3): 284-291.
- Peacock, S.M., 1996. Thermal and petrologic structure of subduction zones. In: Bebout, G.E., Scholl, D.W., Kirby, S.H., Platt, J.P. (Eds.), *Subduction Top to Bottom*. Geophys. Monogr. Ser. AGU, Washington, DC, pp. 119-133.
- Peacock, S.M., 2003. Thermal structure and metamorphic evolution of subducting slabs, Inside the Subduction Factory. Geophys. Monogr. Ser. AGU, Washington, DC, pp. 7-22.
- Peacock, S.M., Rushmer, T., Thompson, A.B., 1994. Partial melting of subducting oceanic crust. *Earth and Planetary Science Letters*, 121(1-2): 227-244.
- Plank, T., Langmuir, C.H., 1998. The chemical composition of subducting sediment and its consequences for the crust and mantle. *Chemical Geology*, 145(3-4): 325-394.
- Poli, S., 1993. The amphibolite-eclogite transformation: an experimental study on basalt. *American Journal of Science*, 293(10): 1061-1107.
- Poli, S., Schmidt, M.W., 2002. Petrology of subducted slabs. *Annual Review of Earth and Planetary Sciences*, 30(1): 207-235.
- Rapp, J.F., Klemme, S., Butler, I.B., Harley, S.L., 2010. Extremely high solubility of rutile in chloride and fluoride-bearing metamorphic fluids: An experimental investigation. *Geology*, 38(4): 323-326.
- Rapp, R.P., Watson, E.B., 1995. Dehydration Melting of Metabasalt at 8–32 kbar: Implications for Continental Growth and Crust-Mantle Recycling. *Journal of Petrology*, 36(4): 891-931.
- Rapp, R.P., Watson, E.B., Miller, C.F., 1991. Partial melting of amphibolite/eclogite and the origin of Archean trondhjemites and tonalites. *Precambrian Research*, 51(1-4): 1-25.
- Rauch, M., Keppler, H., 2002. Water solubility in orthopyroxene. *Contributions to Mineralogy and Petrology*, 143(5): 525-536.
- Reynard, B., in press. Serpentine in active subduction zones. *Lithos*(0).
- Rice, J., 1980. Phase equilibria involving humite minerals in impure dolomitic limestones. *Contributions to Mineralogy and Petrology*, 71(3): 219-235.
- Ringwood, A.E., 1974. The petrological evolution of island arc systems: Twenty-seventh William Smith Lecture. *Journal of the Geological Society*, 130(3): 183-204.
- Roeder, D.H., 2009. American and Tethyan fold-thrust belts. Gebr. Borntraeger.

- Rose-Koga, E.F. et al., 2012. Mantle source heterogeneity for South Tyrrhenian magmas revealed by Pb isotopes and halogen contents of olivine-hosted melt inclusions. *Chemical Geology*, 334(0): 266-279.
- Saal, A.E., Hauri, E.H., Langmuir, C.H., Perfit, M.R., 2002. Vapour undersaturation in primitive mid-ocean-ridge basalt and the volatile content of Earth's upper mantle. *Nature*, 419(6906): 451-455.
- Sanchez-Vizcaino, V.L. et al., 2005. Petrology of titanian clinohumite and olivine at the high-pressure breakdown of antigorite serpentinite to chlorite harzburgite (Almirez Massif, S. Spain). *Contributions to Mineralogy and Petrology*, 149(6): 627-646.
- Schmidt, M.W., Poli, S., 1998. Experimentally based water budgets for dehydrating slabs and consequences for arc magma generation. *Earth and Planetary Science Letters*, 163(1-4): 361-379.
- Sen, C., Dunn, T., 1994. Dehydration melting of a basaltic composition amphibolite at 1.5 and 2.0 GPa: implications for the origin of adakites. *Contributions to Mineralogy and Petrology*, 117(4): 394-409.
- Shaw, D.M., 1970. Trace element fractionation during anatexis. *Geochimica Et Cosmochimica Acta*, 34(2): 237-243.
- Sparks, R.S.J., 2003. Forecasting volcanic eruptions. *Earth and Planetary Science Letters*, 210(1-2): 1-15.
- Spilliaert, N., Mérich, N., Allard, P., 2006. S-Cl-F degassing pattern of water-rich alkali basalt: Modelling and relationship with eruption styles on Mount Etna volcano. *Earth and Planetary Science Letters*, 248(3-4): 772-786.
- Stalder, R., Ulmer, P., 2001. Phase relations of a serpentine composition between 5 and 14 GPa: significance of clinohumite and phase E as water carriers into the transition zone. *Contributions to Mineralogy and Petrology*, 140(6): 670-679.
- Stern, C.R., Saul, S., Skewes, M.A., Futa, K., 1986. Garnet peridotite xenoliths from the Pali-Aike alkali basalts of southernmost South America. In: Ross, J. (Editor), Fourth International Kimberlite Conference. Geological Society of Australia, Perth, Australia, pp. 735-744.
- Straub, S.M., Layne, G.D., 2003. The systematics of chlorine, fluorine, and water in Izu arc front volcanic rocks: Implications for volatile recycling in subduction zones. *Geochimica Et Cosmochimica Acta*, 67(21): 4179-4203.
- Straub, S.M., Layne, G.D., Schmidt, A., Langmuir, C.H., 2004. Volcanic glasses at the Izu arc volcanic front: New perspectives on fluid and sediment melt recycling in subduction zones. *Geochem. Geophys. Geosyst.*, 5(1): Q01007.

- Symonds, R.B., Rose, W.I., Bluth, G.J.S., Gerlach, T.M., 1994. Volcanic-gas studies; methods, results, and applications. *Reviews in Mineralogy and Geochemistry*, 30(1): 1-66.
- Syracuse, E.M., Abers, G.A., 2006. Global compilation of variations in slab depth beneath arc volcanoes and implications. *Geochemistry Geophysics Geosystems*, 7.
- Tait, S., Thomas, R., Gardner, J., Jaupart, C., 1998. Constraints on cooling rates and permeabilities of pumice in an explosive eruption jet from colour and magnetic mineralogy. *Journal of Volcanology and Geothermal Research*, 86(1-4): 79-91.
- Tatsumi, Y., Eggins, S., 1995. Subduction Zone Magmatism. *Frontiers in earth science*. Blackwell Science, Cambridge, Mass., United States, 224 pp.
- Turcotte, D.L., Schubert, G., 1982. *Geodynamics: Applications of Continuum Physics to Geological Problems*. John Wiley & Sons, Incorporated.
- Ulmer, P., Trommsdorf, V., 1999. Phase relations of hydrous mantle subducting to 300km. In: Fei, Y., Bertka, C., Mysen, B. (Eds.), *Mantle Petrology: Field observations and high pressure experimentation: A tribute to Francis R. (Joe) Boyd*. The Geochemical Society, pp. 259-281.
- Villemant, B.t., Boudon, G., 1999. H₂O and halogen (F, Cl, Br) behaviour during shallow magma degassing processes. *Earth and Planetary Science Letters*, 168(3-4): 271-286.
- von Huene, R., Scholl, D.W., 1991. Observations at convergent margins concerning sediment subduction, subduction erosion, and the growth of continental crust. *Reviews of Geophysics*, 29(3): 279-316.
- Wallace, P.J., 2005. Volatiles in subduction zone magmas: concentrations and fluxes based on melt inclusion and volcanic gas data. *Journal of Volcanology and Geothermal Research*, 140(1-3): 217-240.
- Wallace, P.J., Anderson, A.T., 1998. Effects of eruption and lava drainback on the H₂O contents of basaltic magmas at Kilauea Volcano. *Bulletin of Volcanology*, 59(5): 327-344.
- Watson, E., Wark, D., Price, J., Van Orman, J., 2002. Mapping the thermal structure of solid-media pressure assemblies. *Contributions to Mineralogy and Petrology*, 142(6): 640-652.
- White, D.A., Roeder, D.H., Nelson, T.H., Crowell, J.C., 1970. Subduction. *Geological Society of America Bulletin*, 81(11): 3431-3432.
- White, R.S., McKenzie, D., O'Nions, R.K., 1992. Oceanic crustal thickness from seismic measurements and rare earth element inversions. *Journal of Geophysical Research: Solid Earth*, 97(B13): 19683-19715.
- Wirth, E.A., Korenaga, J., 2012. Small-scale convection in the subduction zone mantle wedge.

- Earth and Planetary Science Letters*, 357: 111-118.
- Witter, J.B., Kuehner, S.M., 2004. A simple empirical method for high-quality electron microprobe analysis of fluorine at trace levels in Fe-bearing minerals and glasses. *American Mineralogist*, 89(1): 57-63.
- Wohlert, A., Manning, C.E., Thompson, A.B., 2011. Experimental investigation of the solubility of albite and jadeite in H₂O, with paragonite + quartz at 500 and 600 °C, and 1–2.25 GPa. *Geochimica Et Cosmochimica Acta*, 75(10): 2924-2939.
- Wunder, B., 1998. Equilibrium experiments in the system MgO–SiO₂–H₂O (MSH): stability fields of clinohumite-OH [Mg₉Si₄O₁₆(OH)₂], chondrodite-OH [Mg₅Si₂O₈(OH)₂] and phase A (Mg₇Si₂O₈(OH)₆). *Contributions to Mineralogy and Petrology*, 132(2): 111-120.
- Wunder, B., Medenbach, O., Daniels, P., Schreyer, W., 1995. First synthesis of the hydroxyl end-member of humite, Mg₇Si₃O₁₂(OH)₂. *American Mineralogist*, 80(5-6): 638-640.
- Wyllie, P., Sekine, T., 1982. The formation of mantle phlogopite in subduction zone hybridization. *Contributions to Mineralogy and Petrology*, 79(4): 375-380.
- Wyllie, P.J., 1988. Magma genesis, plate tectonics, and chemical differentiation of the Earth. *Reviews of Geophysics*, 26(3): 370-404.
- Yang, J.J., 2003. Titanian clinohumite-gamet-pyroxene rock from the Su-Lu UHP metamorphic terrane, China: chemical evolution and tectonic implications. *Lithos*, 70(3-4): 359-379.
- Yang, X.Z., 2012. An experimental study of H solubility in feldspars: Effect of composition, oxygen fugacity, temperature and pressure and implications for crustal processes. *Geochimica Et Cosmochimica Acta*, 97: 46-57.
- Zhang, Y., 2000. Energetics of gas-driven limnic and volcanic eruptions. *Journal of Volcanology and Geothermal Research*, 97(1–4): 215-231.

Appendixes

Appendix I Student's t-test for Grouping D_F

In order to distinguish the partition coefficient of F from different experimental conditions can be classified as one group or not, a Student's t-test is employed for this procedure. Generally, this statistic method needs to input every valid value of each group, and then most software, such as Excel, R, Origin, can give the result directly. However, this way is assumed the weight for each datum is the same, which is different from my situation. In my experiments, each D_F value has its own uncertainty, which is derived from the error propagation of each measurements and calculations. And I used their weighted average values to express the results, so they are different from the former situation. Here, I have to employ these weighted average values, weighted standard errors and number of participants for the t-test.

Another assumption is that the two group D_F values have the same variance. Because the D_F values are temperature independent in my experimental temperature region, and they are calculated with the same method, as long as their sample size is big enough, their distributions should have the same variance. Consequently, the t-test equations are:

$$t = \frac{|\bar{X}_1 - \bar{X}_2|}{S_{X_1 X_2} \cdot \sqrt{\frac{1}{n_1} + \frac{1}{n_2}}}$$

where

$$S_{X_1 X_2} = \sqrt{\frac{(n_1 - 1)S_{X_1}^2 + (n_2 - 1)S_{X_2}^2}{n_1 + n_2 - 2}}$$

After calculating out the t value, compare the relative p value in Table App. 1. If the t value is greater than the value in the cell, the difference between two groups is significant, and can reject the null hypothesis.

For example, the partition coefficient of F between fluid and hornblende of SP2 experiments, $\ln D_F^{Fl-Hb} (SP2 \text{ buffered}) = -2.33 \pm 0.97$ and $n_1 = 5$,

$$\ln D_F^{Fl-Hb} (SP2 \text{ no buffer}) = -1.62 \pm 0.28 \text{ and } n_2 = 6.$$

So $t=1.570$, and its degree of freedom is 9. At the 0.05 level, $t < 2.26$, which cannot reject the null hypothesis, and It is possible to classify these two group as the same one. This t-test can help us to justify my grouping strategy when the weighted average and standard errors overlaps with each other. If they are totally separated, it is unnecessary to do this test.

Table App. 1 Critical values of t-test (two-tailed)

Degrees of Freedom	Probability, p			
	0.1	0.05	0.01	0.001
1	6.31	12.71	63.66	636.62
2	2.92	4.30	9.93	31.60
3	2.35	3.18	5.84	12.92
4	2.13	2.78	4.60	8.61
5	2.02	2.57	4.03	6.87
6	1.94	2.45	3.71	5.96
7	1.89	2.37	3.50	5.41
8	1.86	2.31	3.36	5.04
9	1.83	2.26	3.25	4.78
10	1.81	2.23	3.17	4.59
11	1.80	2.20	3.11	4.44
12	1.78	2.18	3.06	4.32
13	1.77	2.16	3.01	4.22
14	1.76	2.14	2.98	4.14
15	1.75	2.13	2.95	4.07
16	1.75	2.12	2.92	4.02
17	1.74	2.11	2.90	3.97
18	1.73	2.10	2.88	3.92
19	1.73	2.09	2.86	3.88
20	1.72	2.09	2.85	3.85
21	1.72	2.08	2.83	3.82
22	1.72	2.07	2.82	3.79
23	1.71	2.07	2.82	3.77
24	1.71	2.06	2.80	3.75
25	1.71	2.06	2.79	3.73
26	1.71	2.06	2.78	3.71
27	1.70	2.05	2.77	3.69
28	1.70	2.05	2.76	3.67
29	1.70	2.05	2.76	3.66
30	1.70	2.04	2.75	3.65
40	1.68	2.02	2.70	3.55
60	1.67	2.00	2.66	3.46
120	1.66	1.98	2.62	3.37
infinity	1.65	1.96	2.58	3.29

Appendix II Expansion Coefficient of Pyrophyllite

Pyrophyllite is a phyllosilicate mineral composed of aluminium silicate hydroxide: $\text{Al}_4[\text{Si}_8\text{O}_{20}](\text{OH})_4$. It is widely used in high-pressure experiments, both as a gasket material and as a pressure-transmitting medium. Because it is a hydrous mineral and begin to lose water under high temperature (450-850 °C), it can be treated as a water source during the experiment as well.

Pyrophyllite is very soft (hardness of 1 to 1.5) and are greasy to the touch, so it is easily machineable and has excellent thermal stability. While, after heating at 1100 °C, pyrophyllite dehydrates and becomes very hard. Its hardness is comparable with alumina. Because of both characters of pyrophyllite, it is usually used to machining as parts of assemblage for high pressure and temperature experiments. To avoid the bulk composition loss by the deformation of the capsule, it is necessary to make a hard material surround the capsule. So pyrophyllite is suitable for this aim. However, it should be noted that its dimension will expand. Hence, it is important to know the expansion coefficient of pyrophyllite, and this will be helpful to design the parts size before heating.

Table Appendix II Investigation of pyrophyllite expansion coefficient

No.	1	2	3	4	5	Average
Before/mm	5.90	5.86	9.10	9.17	9.19	
After/mm	6.00	5.97	9.28	9.34	9.36	
Coefficient	1.017	1.019	1.020	1.019	1.018	1.019

In my latest experiments, I utilized the pyrophyllite to make rings to hold my capsules. I managed to make 5 different diameters for both 1/2 and 3/4 inch piston cylinder assemblage. And they showed the consistency of the expansion, of which average is 1.019.

Appendix III Original Data of ICP-MS Analyses

Table App.III.a Undiluted fluid concentrations (July. 24, 2012, unit: ppb)

Expt. ID	1-SP2-16	RSD	1-SP2-19	RSD	1-SP2-21	RSD	1-SP2-20	RSD	4-SP2-2	RSD
Si	-----		-----		-----		-----		-----	
Ti	0.5176	24.6	0.3723	10.9	3.677	4.0	0.3454	9.4	0.1632	7.7
Al	44.36	1.5	102.8	1.8	175.9	2.0	38.08	3.7	10.25	1.0
Cr	0.0252	9.6	0.02998	17.7	0.9018	7.6	0.03084	31.9	0.0145	35.6
Fe	0.7646	4.8	24.76	1.6	38.86	6.7	3.132	4.6	2.779	2.4
Mg	5.592	1.6	14.81	1.9	48.99	5.5	15.3	2.4	204.7	1.9
Ca	26.01	1.3	44.81	2.6	137.9	1.8	48.53	4.4	43.52	3.3
Mn	0.1192	4.1	0.4631	1.4	0.9598	5.1	0.1807	4.0	0.3716	7.4
Ni	0.6919	1.9	6.629	1.0	0.6683	4.8	18.34	2.1	1514	0.7
Na	-----		-----		-----		-----		-----	
K	54.38	1.8	43.3	2.2	92.87	4.4	74.15	9.2	84.71	2.6
Expt. ID	1-SP3-8	RSD	1-SP4-3	RSD	1-SP4-4	RSD	1-(SP2+Qtz)	RSD	1-(SP1+MgF2)	RSD
Si	-----		-----		-----		-----		-----	
Ti	0.4184	30.4	0.2154	8.8	0.1621	5.7	0.7562	2.2	0.4499	4.5
Al	18.56	9.5	17.52	3.8	3.741	3.2	101.9	1.2	14.73	2.5
Cr	1.109	72.3	0.4954	73.3	0.1605	11.9	0.2587	3.4	0.4493	100
Mg	74.93	39.6	60	5.6	12.13	0.6	34.7	0.7	1.963	0.9
Ca	48.61	1.3	27.66	6.2	20.35	0.4	42.9	2.2	24.77	4.2
Fe	5.105	6.7	3.469	70.3	0.43	10.4	52.91	0.2	6.409	20.9
Mn	0.2185	8.2	0.1825	4.4	0.07205	3.3	1.299	1.1	0.1896	3.3
Ni	94.33	6.8	150.5	1.0	2.943	1.3	404.8	0.6	27.14	4.0
Na	-----		-----		-----		-----		-----	
K	82	2.0	65.81	2.0	40.11	2.9	77.45	1.8	77.36	3.7
Expt. ID	1-(SP1+CaF2)	RSD	1-SP2-23	RSD	1-SP2-24	RSD				
Si	-----		-----		-----					
Ti	1.408	7.9	0.7822	26.0	5.708	6.3				
Al	61.85	15.7	11.13	16.0	226.8	27.1				
Cr	0.5315	53.3	1.644	63.1	14.6	6.4				
Mg	31.91	2.7	19.59	26.1	351.5	27.6				
Ca	667.2	0.7	32.78	27.5	163	14.0				
Fe	7.13	5.8	9.476	17.3	81.34	2.5				
Mn	0.908	12.8	0.4114	31.7	2.728	7.3				
Ni	206.8	2.2	57.7	0.2	241.2	1.9				
Na	-----		-----		-----					
K	137.5	0.9	80.19	0.6	94.98	1.6				

RSD indicates relative standard deviation.

Table App.III.b Diluted fluid concentrations (July, 19, 2012, unit: ppb)

Expt. ID	1-SP2-16	RSD	1-SP2-19	RSD	1-SP2-21	RSD	1-SP2-20	RSD	4-SP2-2	RSD
Si	61.08	2.6	180.2	8.7	245.3	2.6	21.12	21.0	75.66	6.1
Ti	0.05337	88.6	0.09407	13.3	0.5159	5.6	0.04083	17.1	0.03037	21.1
Al	4.739	2.3	21.78	6.9	23.25	2.2	4.573	3.0	1.801	1.6
Cr	0.01103	18.0	0.06721	25.7	0.2358	96.3	0.01493	44.5	0.005103	83.0
Fe	0.2645	6.6	9.424	6.6	11.33	1.6	1.718	2.8	0.2375	11.3
Mg	0.6183	1.4	3.187	5.2	6.313	15.5	1.345	9.7	31.86	0.3
Ca	5.564	5.5	13.84	10.6	17.47	2.5	6.204	1.5	7.583	5.0
Mn	0.01781	5.7	0.1149	9.9	0.1352	5.8	0.02455	8.1	0.053	34.0
Ni	0.117	8.2	1.68	5.3	0.1165	3.5	0.1458	8.2	172.3	0.6
Na	25.3	1.8	125.9	4.6	295.9	2.6	72.1	1.0	126.8	1.1
K	16.23	4.0	44.99	16.1	20.95	9.6	18.63	2.0	23.19	5.7
Expt. ID	1-SP3-8	RSD	1-SP4-3	RSD	1-SP4-4	RSD	1-(SP2+Qtz)	RSD	1-(SP1+MgF ₂)	RSD
Si	37.4	18.6	27.63	2.7	95.97	0.4	102.7	16.8	100.6	1.5
Ti	0.04181	40.2	0.02662	61.4	0.02438	23.0	0.1424	20.9	0.05268	9.7
Al	1.681	17.8	2.783	4.6	0.41	2.2	16.65	0.1	1.193	6.4
Cr	0.04669	76.2	-0.003336	37.3	-0.005959	33.4	0.03977	61.3	-0.007887	6.3
Mg	0.8036	34.5	0.2293	13.3	0.1059	27.0	9.321	2.9	0.4757	9.1
Ca	6.35	2.1	2.916	1.3	1.411	1.4	5.302	9.6	0.09425	5.8
Fe	5.453	4.5	4.526	8.5	1.766	28.0	7.423	5.7	2.958	10.9
Mn	0.02254	41.1	0.01292	13.6	0.01311	9.8	0.2284	8.1	0.01377	13.6
Ni	17.94	0.3	8.191	0.3	22.76	0.9	50.02	4.5	0.9492	7.3
Na	85.01	1.3	194	1.4	55.59	1.8	126.7	1.3	161.4	0.9
K	20.47	5.4	17.29	2.7	12.12	9.3	23.53	2.9	18.04	3.3
Expt. ID	1-(SP1+CaF ₂)	RSD	1-SP2-23	RSD	1-SP2-24	RSD				
Si	35.36	3.2	132.4	11.2	184.8	8.1				
Ti	0.2782	8.2	0.2164	53.0	0.8763	3.6				
Al	11.04	0.5	2.613	25.3	20	15.9				
Cr	0.04061	4.6	0.5022	52.0	2.077	38.4				
Mg	1.976	8.4	2.66	95.3	19.91	13.4				
Ca	6.062	4.8	6.646	67.7	39.71	41.1				
Fe	129.4	0.4	6.593	42.3	25.89	5.1				
Mn	0.2303	3.8	0.07064	78.3	0.9383	7.7				
Ni	51.01	0.1	3.96	43.5	627.1	0.6				
Na	101.2	2.1	229.8	1.1	223.5	1.5				
K	35.1	2.2	23.29	4.3	23.73	8.6				

RSD indicates relative standard deviation.